



NASA-TM-78622 19800012802

An Experimental Evaluation of a Helicopter Rotor Section Designed By Numerical Optimization

R. M. Hicks and W. J. McCroskey

March 1980

LIBRARY COPY

APR 29 1980

LANGLEY RESEARCH CENTER
NASA
HAMPTON, VIRGINIA



An Experimental Evaluation of a Helicopter Rotor Section Designed By Numerical Optimization

R. M. Hicks, Ames Research Center, Moffett Field, California
W. J. McCroskey, Aeromechanics Laboratory, AVRADCOM Research and Technology Laboratories



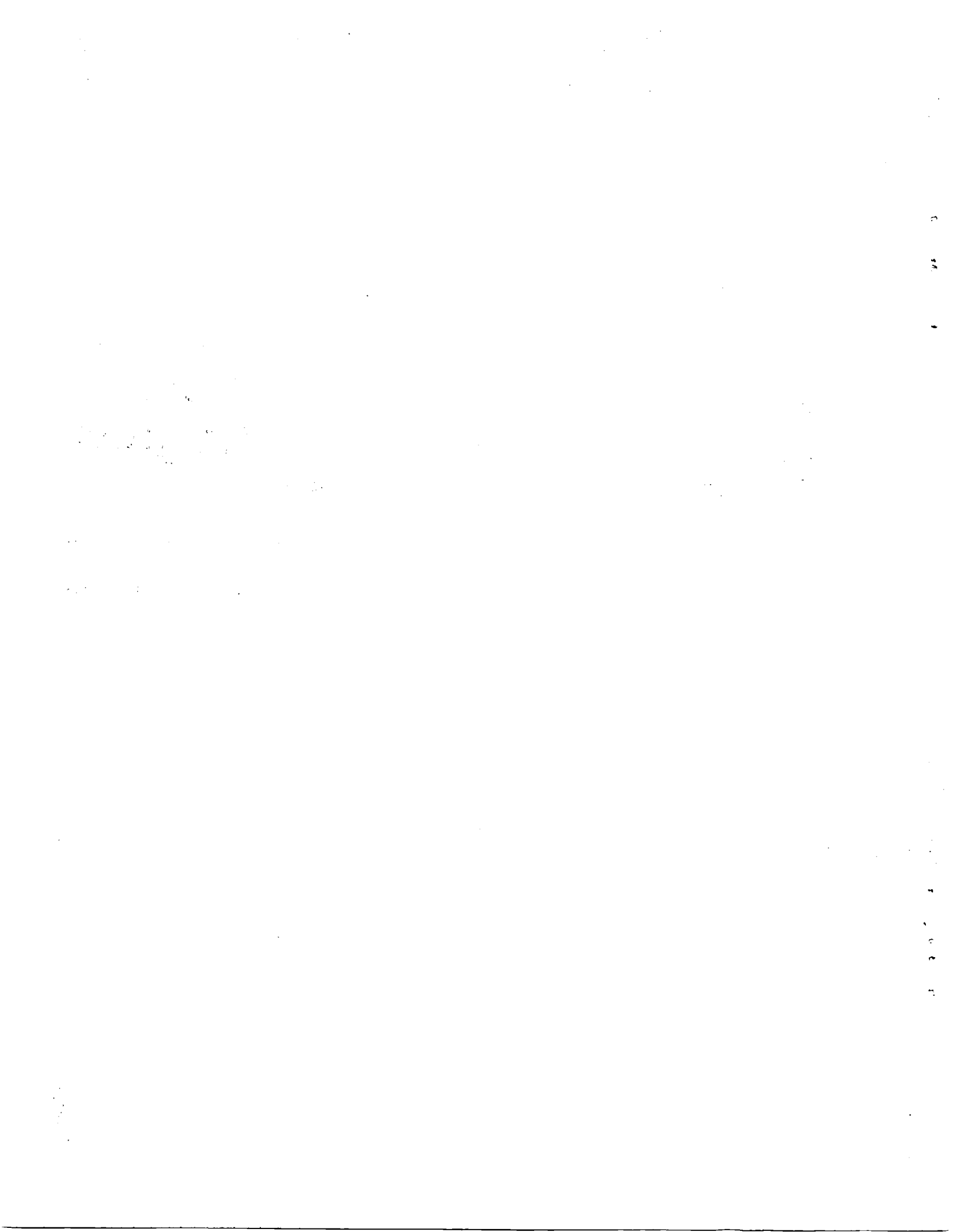
National Aeronautics and
Space Administration

Ames Research Center
Moffett Field, California 94035

N80-21287 #

United States Army
Aviation Research and
Development Command
St. Louis, Missouri 63166





NOMENCLATURE

a	design variables, eqs. (1)
b	design variables, eqs. (1)
c	airfoil chord, m (ft)
c_d	section drag coefficient
c_l	section lift coefficient
c_m	section pitching-moment coefficient referenced to quarter chord
C_p	pressure coefficient $\frac{P_1 - P_\infty}{q_\infty}$
C_p^*	pressure coefficient for $M_l = 1$
f	shape function, eqs. (1)
g	shape function, eqs. (1)
h	tunnel height, m(ft)
M	free-stream Mach number
m	shape function exponent, eqs. (2)
n	shape function exponent, eqs. (2)
p	static pressure, N/m ² (lb/ft ²)
q	dynamic pressure, N/m ² (lb/ft ²)
R	Reynolds number based on free-stream conditions and airfoil chord
r	shape function exponent, eqs. (2)
s	shape function exponent, eqs. (2)
x	airfoil abscissa, m (ft)
y	airfoil ordinate, m (ft)

Subscripts:

max maximum

l local

- ∞ free stream
- δ wall correction factor
- α angle of attack

AN EXPERIMENTAL EVALUATION OF A HELICOPTER ROTOR

SECTION DESIGNED BY NUMERICAL OPTIMIZATION

R. M. Hicks
Ames Research Center

and

W. J. McCroskey
Aeromechanics Laboratory
AVRADCOM Research and Technology Laboratories

SUMMARY

A 10-percent thick helicopter rotor section designed by numerical optimization has been tested at Mach numbers of 0.2, 0.3, 0.4, 0.5, 0.6, 0.7, 0.75, 0.77, 0.79, 0.8, 0.81, 0.82, 0.83, and 0.84 with Reynolds numbers ranging from 1.9×10^6 at Mach 0.2 to 4×10^6 at Mach numbers above 0.5. During the design process, emphasis was placed upon achieving acceptable maximum lift coefficients at Mach numbers below 0.6, a drag divergence Mach number of at least 0.8 at lift coefficients near 0 and low pitching-moment coefficients.

Test results have shown that the maximum lift coefficient decreased from approximately 1.33 at Mach numbers of 0.2, 0.3, and 0.4 to below 1 at Mach 0.7. A drag divergence Mach number of 0.82 at lift coefficients near 0 was achieved with some "drag creep" at Mach numbers above 0.6. Pitching-moment coefficients at zero lift decreased from approximately -0.01 at Mach 0.2 to -0.03 at Mach 0.8.

INTRODUCTION

An automated airfoil section design program utilizing a conjugate gradient numerical optimization algorithm (ref. 1) coupled with an aerodynamic analysis program (ref. 2) has been used successfully in the past to design advanced airfoil sections at low to transonic speeds (refs. 3-5). A major advantage of design by numerical optimization is that the designer may consider multiple design points simultaneously during the design process. For example, "drag creep" was eliminated during the design of an advanced supercritical airfoil section for Mach 0.78 by imposing a drag constraint at Mach 0.76 (ref. 3). The constraint prevented the optimization code from seeking a profile which was highly design-point optimized without regard to off-design performance. Such direct consideration of two design conditions would be difficult, if not impossible, with inverse design methods. This feature of design by numerical optimization makes it useful in the design of rotor sections since several design conditions must be considered simultaneously during the design process. Some of these design conditions are high maximum-lift coefficients and good stall characteristics from Mach 0.3 to 0.5, a high

lift/drag ratio at Mach 0.6 and $c_d \sim 0.6$, a drag divergence Mach number of at least 0.8, no "drag creep", and low pitching moments over most of the Mach number range. To achieve all these conditions the optimization code must monitor and constrain certain aerodynamic parameters at five or six different combinations of Mach number and angle of attack. Such a design problem inevitably means compromise and would normally be carried out by trial and error with the designer making all decisions and providing all computer manipulations. With numerical optimization, the computer makes many of the design decisions thus reducing the time and manpower required during the design process. While there are no fundamental limits on the number of design points that can be considered, there are cost limitations. For example, a typical five-design-point problem would use approximately 8 hr of CPU time on a CDC 7600 computer. During the study reported here, three design conditions were considered. Two conditions addressed the high-lift performance of the retreat-ing blade while the third considered advancing blade performance. "Drag-creep" and hover performance were not considered in order to reduce computing time and cost. As will be shown later, omitting "drag creep" from consideration compromised airfoil performance above Mach 0.7.

DESIGN METHOD

Only a brief description of numerical optimization will be given here since a complete discussion of the technique can be found in reference 6.

Airfoil design by numerical optimization starts with a baseline profile provided by the designer. The baseline profile can be somewhat arbitrary but is usually chosen from a family of airfoils which exhibit some of the characteristics desired by the designer. Such a choice reduces the time and cost required to finalize the design.

The airfoil geometry is represented in the design program by the following equations

$$\left. \begin{aligned} y_{us} &= y_{us, \text{baseline}} + \sum_i a_i f_i \\ y_{ls} &= y_{ls, \text{baseline}} + \sum_i b_i g_i \end{aligned} \right\} \quad (1)$$

where $y_{us, \text{baseline}}$ and $y_{ls, \text{baseline}}$ are the ordinates of the upper and lower surfaces of the baseline airfoil, a_i and b_i are the participation coefficients (design variables) and f_i and g_i are the shape functions which are added linearly to the baseline profile by the optimization program to achieve the desired design improvement. The contribution of each function, f_i or g_i , is determined by the value of the participation coefficients a_i and b_i . The shape functions, f_i and g_i , can be any smooth function defined over the airfoil chord, but experience has shown that the following functions give acceptable results from most design problems:

$$\left. \begin{aligned}
 f_i \text{ or } g_i &= \sin[\pi(x/c)^n]^m \\
 f_i \text{ or } g_i &= \frac{(x/c)^s [1 - (x/c)]}{e^{r(x/c)}}
 \end{aligned} \right\} \quad (2)$$

where n , m , s , and r are exponents which determine the chordwise locations and/or magnitude of each shape function. Such functions are well suited to airfoil design because the effect of each function can be concentrated over a limited region of the airfoil.

The optimization design process begins by setting all participation coefficients to zero so the first computation gives the aerodynamic characteristics of the baseline profile. After computation of the characteristics of the baseline profile the optimization program changes the participation coefficients, one by one, from the initial value of 0 to a small number $\epsilon \ll 1$. The aerodynamic analysis of each perturbed airfoil was obtained and used to calculate the gradient of the aerodynamic coefficients with respect to each design variable. The importance of each shape function in achieving the design goals can be ascertained at any step during the optimization process by observing the value of the participation coefficient associated with each function at that step.

The optimization design program used during this study permits the designer to designate one or more of the aerodynamic quantities to be minimized or maximized as the objective function. All other aerodynamic and geometric quantities pertinent to the design are treated as constraints. The designer must decide which parameters will be treated as constraints and which will be the objective function. If the choice is not obvious it will be necessary to use trial and error to determine which combination of objective function and constraints gives the best overall result.

During the present study, the shock-drag coefficient at $M = 0.82$, $\alpha = 0^\circ$ was chosen to be the objective function. Constraints were imposed on the shock-drag coefficients ($c_d \leq 0.001$) at $M = 0.4$, $\alpha = 12^\circ$, and $M = 0.5$, $\alpha = 10^\circ$ to delay retreating blade shock-stall. The shock-drag objective function forced the optimization program to seek a shock-free airfoil at $M = 0.82$, $\alpha = 0^\circ$. As the optimization process proceeded it became clear that the profile required for good advancing blade performance would not necessarily produce good retreating blade performance. Hence, the designer had to decide if the drag constraints imposed at $M = 0.4$ and 0.5 were too restrictive and whether or not to require a shock-free profile for $M = 0.82$. In other words, the design required a compromise and it was decided that the design process should not be completely automated for this first application of numerical optimization to the design of a rotor section. Hence, the designer remained in the "loop" for the entire optimization process monitoring design progress, adjusting shape functions, altering constraints, and changing design conditions in an effort to find the most suitable compromise.

The aerodynamic analysis code contained in the design program does not consider the effect of viscosity. Hence, several intermediate airfoils were selected during the design process for boundary layer and stall analysis. If boundary-layer growth appeared excessive or premature separation was indicated, adjustments were made to the shape functions and/or constraints to guide the optimization process to a more efficient airfoil.

The airfoil selected as the initial profile to start the optimization process for this design problem was a Wortman airfoil designed for helicopter applications. This profile was chosen since it already exhibited some of the desired characteristics of a rotor section and hence would require less computer time to achieve the final design. The profile resulting from this demonstration of design by numerical optimization is designated the A-1 airfoil since it is the first rotor section designed by numerical optimization at Ames Research Center.

APPARATUS AND TEST PROCEDURE

Model

An airfoil model of the A-1 airfoil (shown in fig. 1) was machined from a stainless-steel billet (the profile coordinates are given in table 1). The model had a chord of 15.24 cm (6 in.) and a span of 60.96 cm (24 in.). The model was equipped with 24 upper-surface orifices and 23 lower-surface orifices drilled normal to the surface to determine the pressure distribution on the model surfaces.

Wind Tunnel

The test was conducted in the Ames 2- by 2-Foot Transonic Wind Tunnel, a variable-speed, continuous-flow, ventilated-wall, variable-pressure facility. The tunnel can be used for two-dimensional testing by replacing the ventilated side walls with solid walls where model-supporting thick glass windows are mounted. The windows are rotated by a motorized drive system to change the angle of attack. A 82-tube drag rake located 1.75 chords behind the model trailing edge was used to survey the model wake. Airfoil models are mounted spanning the horizontal dimension of the tunnel test section so that the center of rotation is near the 25-percent chord station on the model. The gaps between the side walls and the end of the model were sealed.

Instrumentation

Measurements of the model surface pressures and the wake-rake pressures were made by an automatic pressure-scanning system that utilizes precision pressure transducers. Basic tunnel pressures were measured with precision mercury manometers. Angle of attack was measured with a potentiometer operated by the drive gear for the rotating side windows. Data were obtained by a high-speed, data-acquisition system and recorded on paper tape.

Tests

The section aerodynamic coefficients of the A-1 airfoil model were obtained at the following nominal test conditions:

<u>M</u>	<u>R×10⁻⁶</u>
0.20	1.9
.30	2.5
.40	3.5
.50	3.5
.60	4.0
.70	4.0
.75	4.0
.77	4.0
.79	4.0
.80	4.0
.81	4.0
.82	4.0
.83	4.0
.84	4.0

The angles of attack ranged from approximately -2° to stall. At the higher Mach numbers it was not possible to obtain data for a fully-stalled condition because of severe vibration of the wake rake due to the unsteady loads induced by total flow separation over the upper surface of the model. Data were obtained for all test conditions with free transition only.

Pressure coefficients were determined from surface pressure measurements. Section normal-force coefficients, chord-force coefficients, and pitching-moment coefficients were obtained from an integration of the pressure coefficients. The pitching-moment coefficients were referenced to the quarter-chord point. Section profile drag was calculated from the wake-rake total and static-pressure measurements.

The model angle of attack was corrected for the presence of the tunnel walls by the following equation:

$$\Delta\alpha = \delta(c/h)c_l$$

where $\Delta\alpha$, δ , c/h , and c_l are the angle-of-attack correction, correction factor, model chord/tunnel height ratio, and section lift coefficient, respectively. The angle-of-attack correction factor δ is a function of Mach number. The following values were used and the corresponding $\Delta\alpha$ was added algebraically to the model geometric angle of attack expressed in degrees:

<u>M</u>	<u>δ^1</u>
0.2	5.4
.3	8.5
.4	10.6
.5	11.9
.6	12.5
.7	12.8
.75	12.9
.77	12.9
.79	12.9
.80	13.0
.81	13.0
.82	13.0
.83	13.1
.84	13.1

RESULT AND DISCUSSION

The basic aerodynamic force coefficients for the A-1 airfoil are shown in figures 2(a) through 2(n). The lift curves indicate that the stall characteristics are fairly abrupt at Mach numbers 0.2, 0.3, and 0.4 but become much more gradual at Mach numbers greater than 0.4 (compare fig. 2(a) and 2(e)). The stall characteristics were difficult to determine at the higher Mach numbers due to severe vibration of the wake rake under conditions of massive flow separation. The lift curves exhibit some nonlinearity at the lower Mach numbers which may be due to variations in transition location.

The drag polars at Mach numbers below 0.7 show a minimum drag point at lift coefficients above 0.3 due to an increase in laminar flow over the lower surface which is caused by the pressure gradient changing from adverse to favorable near the leading edge (compare the pressure distributions in figs. 3(a) and 3(d)).

The pitching-moment curves exhibit some nonlinearity with increasing lift coefficient which may be attributed to variation in the transition location. The pitching-moment coefficient at zero lift decreased from approximately -0.01 at Mach 0.2 to -0.03 at Mach 0.8. Pitching moments of this magnitude are somewhat greater than desired and are due primarily to the inability of the aerodynamic theory contained within the design program to predict the pressure distribution accurately near the trailing edge.

Pressure distributions for all test conditions are shown in figures 3 through 16. Of particular interest is the pressure "peak" appearing near the leading edge on the lower surface at low lift coefficients for all test Mach numbers. This pressure "peak" is due to the flow accelerating too rapidly around the leading edge of the lower surface and is a result of too much

¹The correction factors, δ , were determined during a tunnel calibration conducted by L. S. Stirers, Jr.

forward curvature. The pressure "peak" could have been minimized during design by imposing a constraint on shock drag at a Mach number slightly less than 0.8 to avoid "drag creep." Such a constraint would have forced the optimization code to seek a curvature distribution which would accelerate the flow more gradually along the lower surface, thereby delaying shock development until after "drag rise." The pressure distributions along with the drag curves clearly show that the lower surface pressure "peak" was the main contributor to the "drag creep" of the A-1 airfoil. Further work is needed to assess the effect of changing the leading-edge contour on the overall performance of the profile.

The upper surface pressure distribution exhibits a slight pressure "hump" over the forward region of the profile at low lift coefficients which gives rise to a weak shock at transonic conditions. The moderate adverse pressure gradient following this "hump" would cause transition to occur near the leading edge at low Mach numbers but would not cause separation for typical flight Reynolds numbers as indicated by the good trailing-edge pressure recovery.

Summary curves of drag coefficient vs Mach number for lift coefficients from 0 to 0.5 are shown in figure 17. The "drag creep" due to the pressure "peak" near the leading edge on the lower surface discussed earlier is clearly evident above Mach 0.6 at $c_l = 0$. As the lift coefficient increases, the pressure "peak" on the lower surface decreases and the "drag creep" is replaced by an early "drag rise" due to increasing shock strength on the upper surface.

Summary curves of pitching-moment coefficient vs Mach number for lift coefficients from 0 to 0.5 are shown in figure 18. The desired range of $-0.01 \leq c_m \leq 0.01$ was achieved only at Mach 0.2 for all lift coefficients but was attained at Mach numbers to 0.7 at lift coefficients of 0.4 and 0.5. The difficulty in achieving low pitching moments was due primarily to two factors: first, the aerodynamic theory contained in the design program did not predict the pressures near the trailing edge well enough, and second, the magnitude of the pressure "peak" near the leading edge on the lower surface was under-predicted by the theory for some flight conditions causing the importance of the "peak" to be underestimated. If the "peak" were eliminated the suction pressures over the forward lower surface would be minimized thereby reducing the nosedown pitching moment.

A summary plot of maximum lift coefficient vs Mach number is shown in figure 19. The maximum lift coefficient remains nearly constant from Mach 0.2 to Mach 0.4 at a value of approximately 1.33 and falls rapidly thereafter. The constancy of maximum lift coefficient at lower Mach numbers is due in part to increasing Reynolds number with increasing Mach number, but it also reflects the favorable pressure distributions generated by the design method at $M = 0.4$,

Some typical experiment-theory comparisons are shown in figure 20. In general, the theory predicts the basic character of the flow fairly accurately. However, there are discrepancies between experiment and theory in some areas. First, the trailing-edge pressure recovery is consistently overestimated by

theory, even for attached flow. Second, the shock location shown by the experimental data is somewhat further aft than indicated by theory (figs. 20(g) and 20(h)). Finally the theory tends to give poor drag prediction. A rather surprising feature of the experiment-theory comparison is the good agreement for the low Mach number, high lift condition (e.g., fig. 20(b)). This agreement was not anticipated because the Nash-McDonald, integral, boundary-layer method used to correct the potential aerodynamic theory was developed for flattop transonic pressure distributions with concave pressure recoveries. The fact that the theory reproduces the main features of the flow reasonably well makes a redesign effort of the A-1 airfoil possible. A complete description of the theoretical aerodynamic analysis program used for the experiment-theory comparison can be found in reference 7.

CONCLUDING REMARKS

An advanced helicopter rotor airfoil section has been designed by numerical optimization. The section is intended for use on rotor blades of constant profile and therefore was designed to exhibit acceptable aerodynamic characteristics over a wide range of Mach number, angle-of-attack conditions. Such a section would be expected to be less than optimum at each condition.

Wind-tunnel test results have shown that a drag divergence Mach number of 0.82 at zero lift was achieved with a maximum lift coefficient of approximately 1.33 at Mach numbers of 0.2, 0.3, and 0.4. Test Reynolds numbers varied from 1.9×10^6 at Mach 0.2 to 4×10^6 for Mach numbers greater than or equal to 0.6. A modest amount of "drag creep" occurred at low lift coefficients at Mach numbers above 0.6 due to rapid acceleration of the flow to supersonic speed along the lower surface. The leading-edge bluntness which caused the acceleration was developed to promote acceptable stall characteristics and $c_{l_{max}}$ at intermediate Mach numbers. More work is needed to find a better compromise profile which will exhibit good "drag-rise" characteristics, acceptable $c_{l_{max}}$, and no "drag creep."

In spite of the deficiencies found with the A-1 airfoil, numerical optimization has been found to be a good technique for rotor section design; the main advantage being the ability to consider multiple design conditions simultaneously during the design process.

The test results validated the basic approach for the multiple design point problem of rotor blades with conflicting requirements.

REFERENCES

1. Vanderplaats, Garret N.: CONMIN-A Fortran Program for Constrained Function Minimization. NASA TM X-62,282, 1973.
2. Jameson, A.: Iterative Solution of Transonic Flows Over Airfoils and Wings Including Flows at Mach 1. Comm. Pure Appl. Math., vol. 27, 1974, pp. 283-309.
3. Johnson, Raymond R.; and Hicks, Raymond M.: Application of Numerical Optimization to the Design of Advanced Supercritical Airfoils. NASA CP-2045, Part 1, Advanced Technology Airfoil Research, vol. 1, presented at Langley Research Center, March 7-9, 1978, pp. 315-320.
4. Hicks, Raymond M.; and Schairrer, Edward T.: Effects of Upper Surface Modification on the Aerodynamic Characteristics of the NACA 63₂-215 Airfoil Section. NASA TM-78503, 1979.
5. Lores, M. E.; Smith, P. R.; and Hicks, R. M.: Supercritical Wing Design Using Numerical Optimization and Comparisons with Experiment. AIAA paper 79-0065 presented at the 17th Aerospace Sciences Meeting, New Orleans, La., Jan. 15-17, 1979.
6. Hicks, Raymond M; and Vanderplaats, Garret N.: Application of Numerical Optimization to the Design of Low-Speed Airfoils. NASA TM X-3213, 1975.
7. Bauer, F.; Garabedian, P.; Korn, D.; and Jameson, A.: Supercritical Wing Sections II. Lecture Notes in Economics and Mathematical Systems, vol. 108, Springer-Verlag, 1975.

TABLE 1.- COORDINATES FOR THE
A-1 AIRFOIL

0.00000	0.00000	0.00000
.00020	.00238	-.00233
.00050	.00377	-.00338
.00100	.00541	-.00472
.00200	.00766	-.00651
.00350	.01013	-.00844
.00500	.01214	-.00995
.00650	.01388	-.01120
.00800	.01543	-.01227
.01000	.01732	-.01350
.01250	.01945	-.01482
.01600	.02214	-.01634
.02000	.02490	-.01777
.02500	.02801	-.01922
.03500	.03335	-.02137
.05000	.03991	-.02365
.06500	.04523	-.02549
.08000	.04961	-.02710
.10000	.05421	-.02902
.12500	.05829	-.03104
.15000	.06098	-.03277
.20000	.06344	-.03551
.25000	.06431	-.03727
.30000	.06446	-.03828
.35000	.06409	-.03866
.40000	.06316	-.03848
.45000	.06154	-.03782
.50000	.05924	-.03665
.55000	.05623	-.03501
.60000	.05249	-.03297
.65000	.04792	-.03056
.70000	.04246	-.02785
.75000	.03600	-.02486
.80000	.02860	-.02153
.85000	.02064	-.01786
.90000	.01260	-.01374
.92500	.00899	-.01144
.95000	.00598	-.00888
.97500	.00392	-.00603
.99000	.00322	-.00421
1.00000	.00299	-.00300

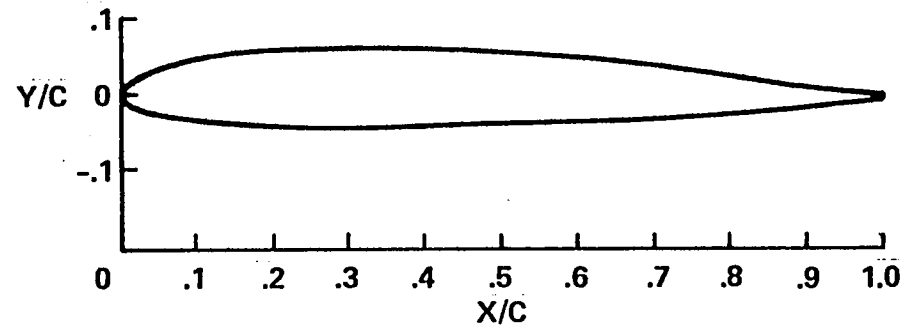
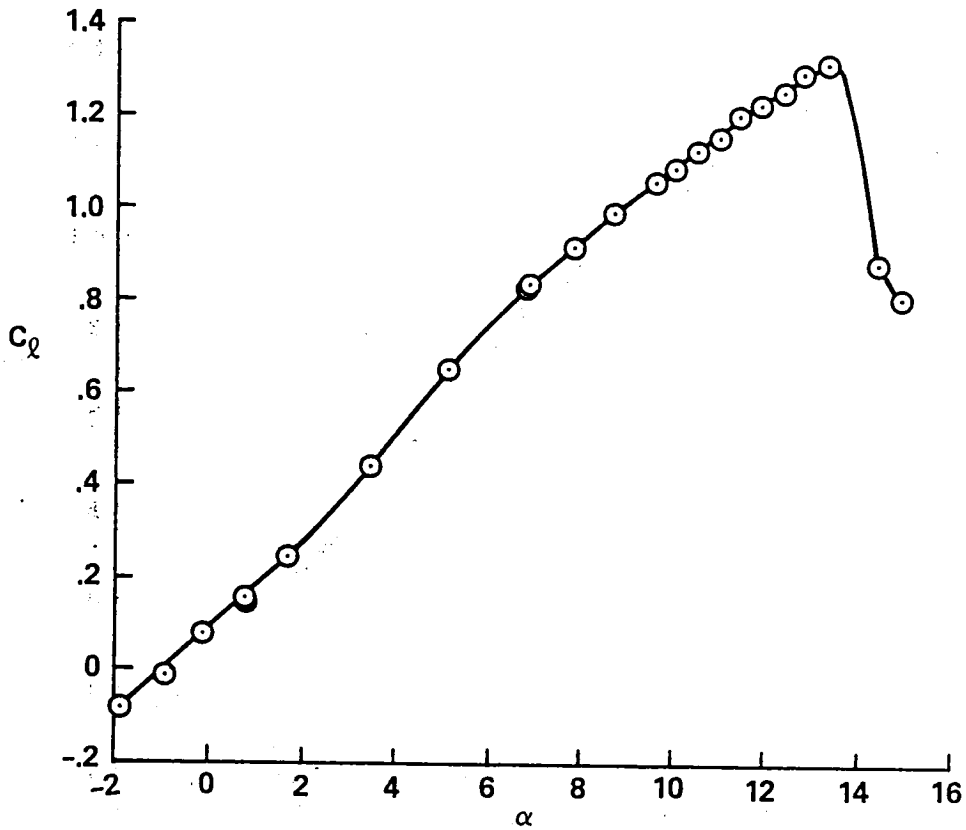
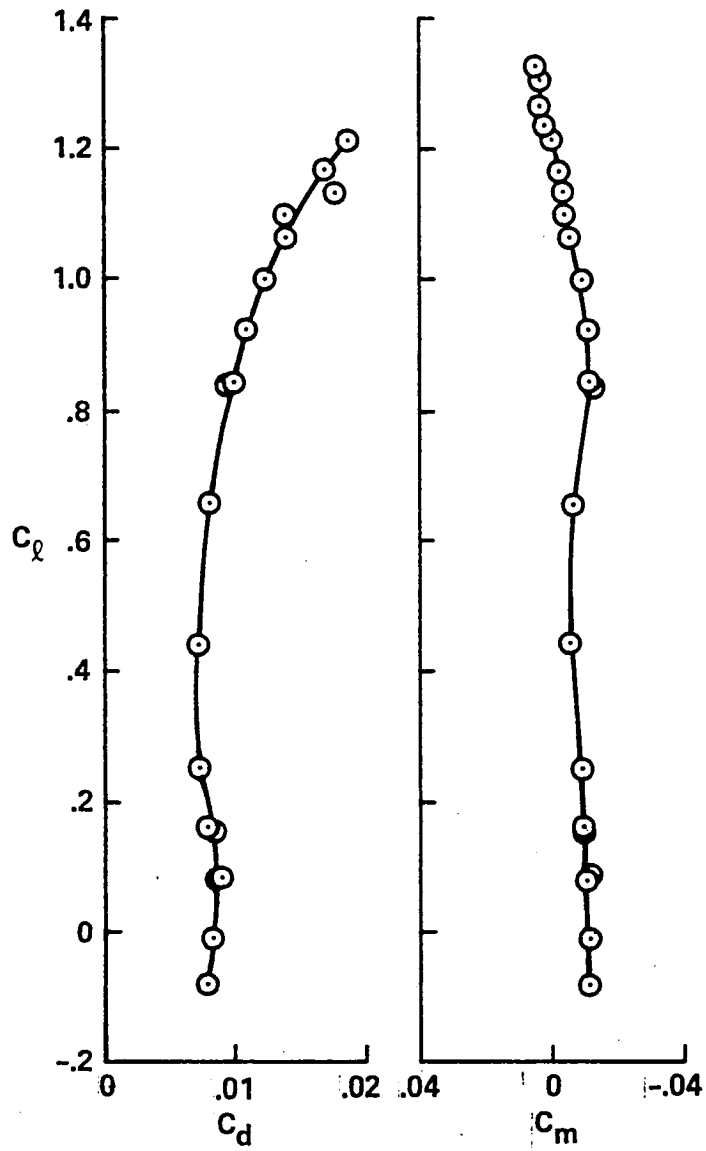


Figure 1.- Helicopter rotor section A-1.



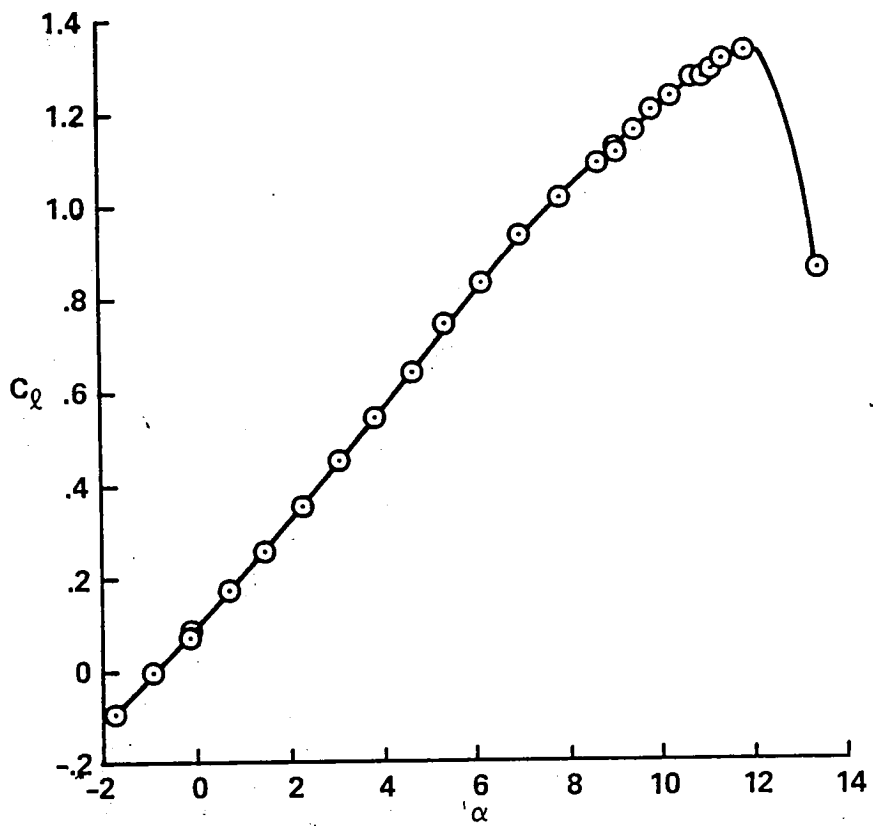
(a) $M_{set} = 0.2$, $Re_{set} = 1.9 \times 10^6$.

Figure 2.- Aerodynamic characteristics of airfoil A-1; transition free.



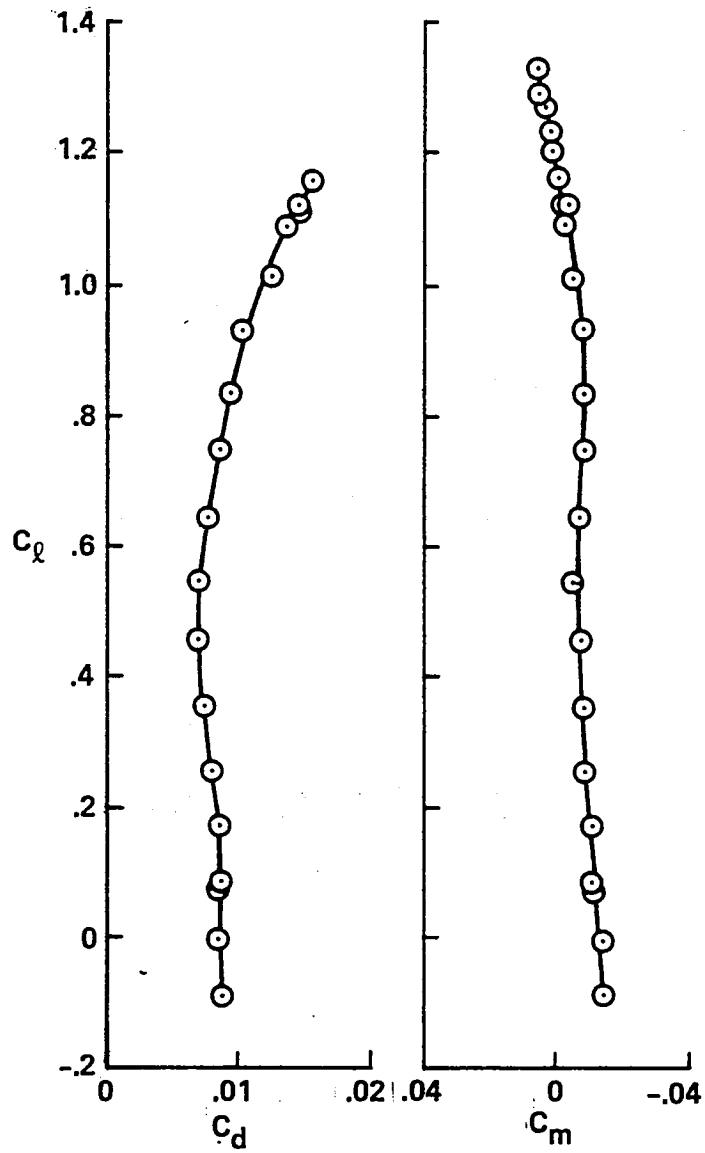
(a) Concluded.

Figure 2.- Continued.



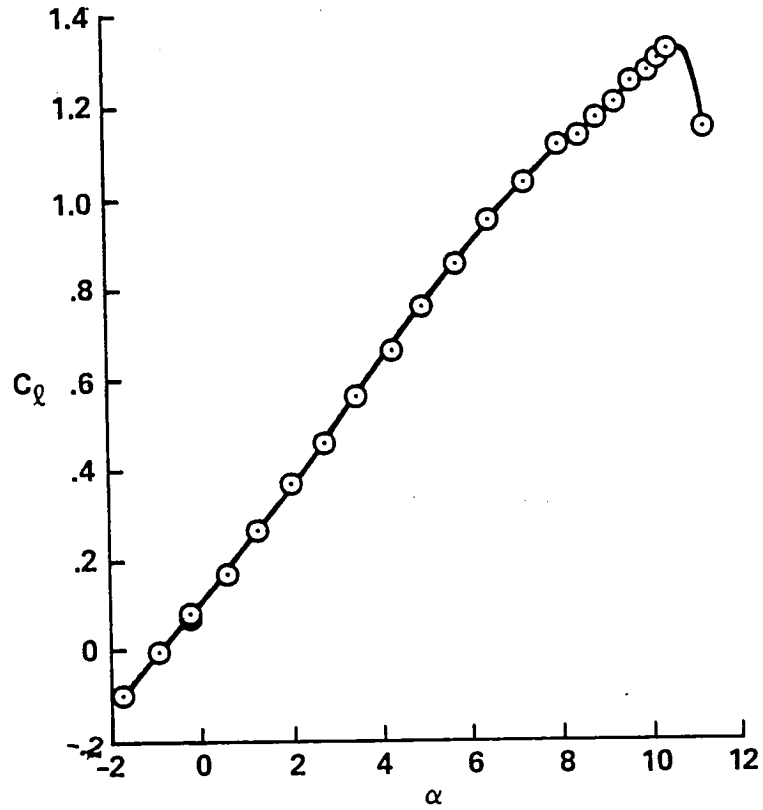
(b) $M_{\text{set}} = 0.3$, $Re_{\text{set}} = 2.5 \times 10^6$.

Figure 2.- Continued.



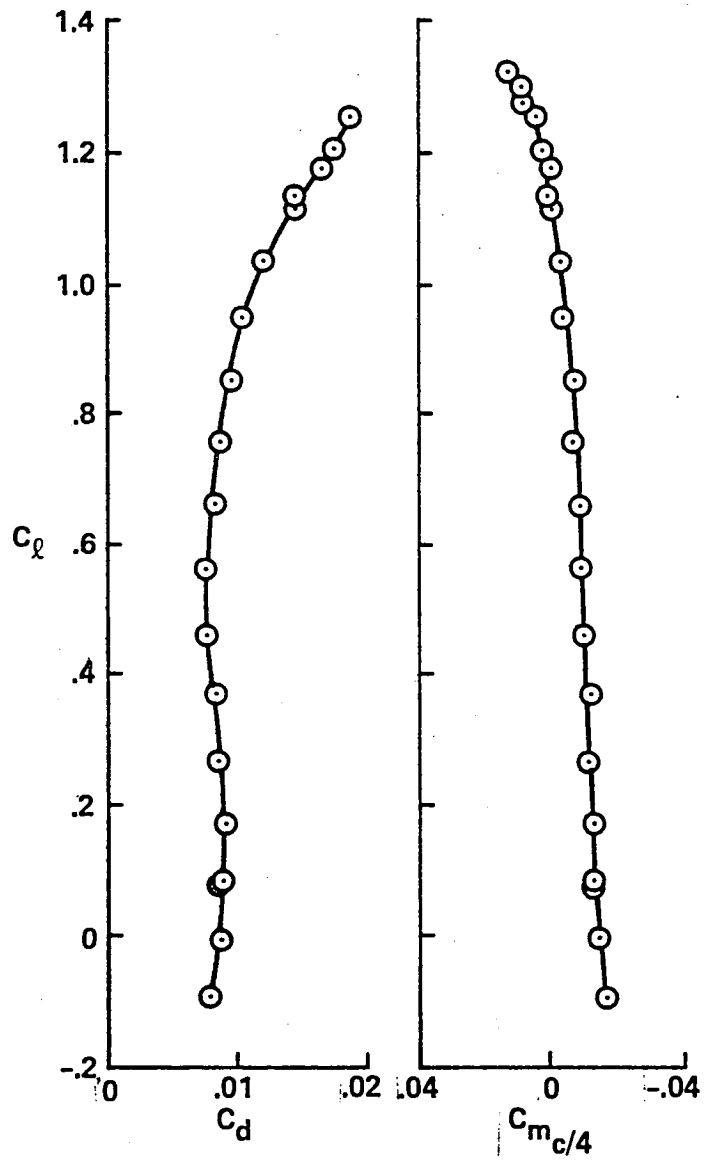
(b) Concluded.

Figure 2.- Continued.



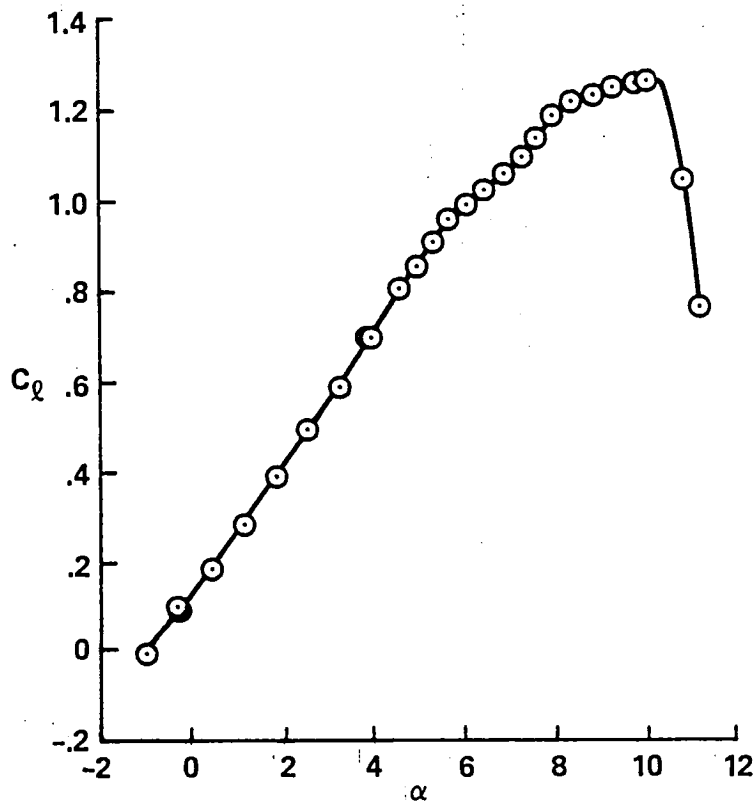
(c) $M_{\text{set}} = 0.4$, $Re_{\text{set}} = 3.5 \times 10^6$.

Figured 2.- Continued.



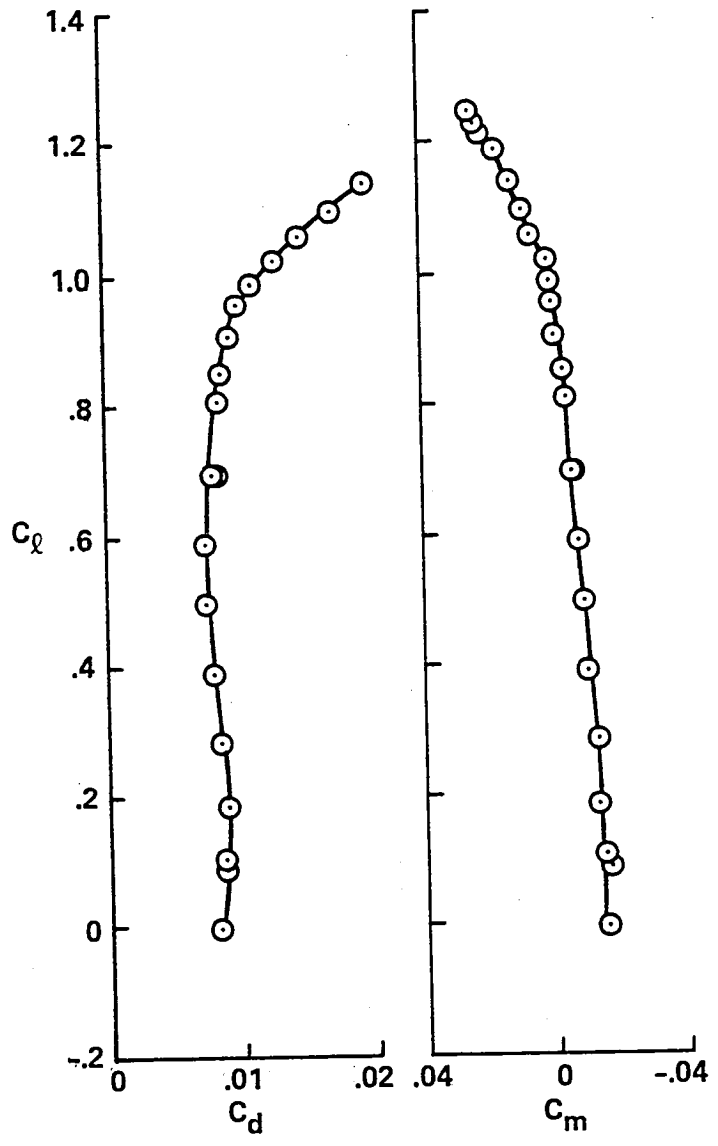
(c) Concluded.

Figure 2.- Continued.



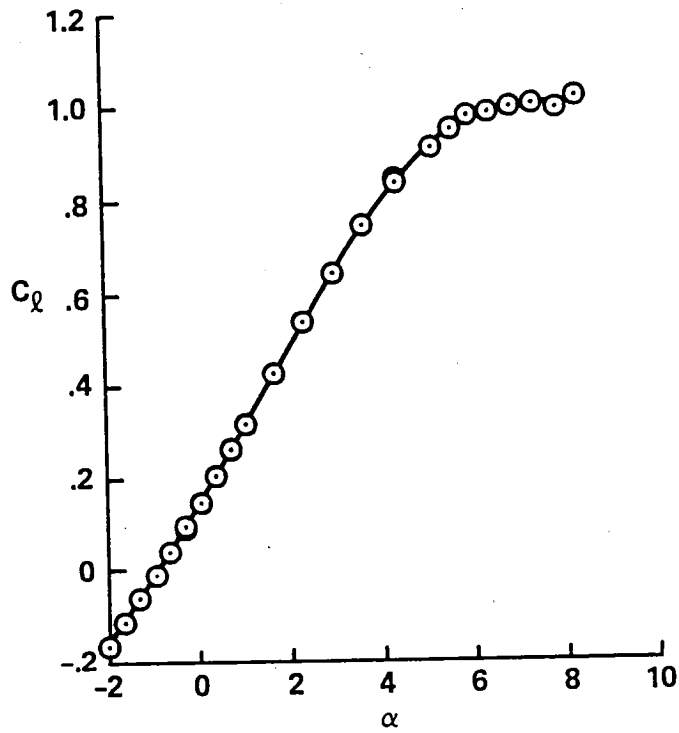
(d) $M_{\text{set}} = 0.5$, $Re_{\text{set}} = 3.5 \times 10^6$.

Figure 2.- Continued.



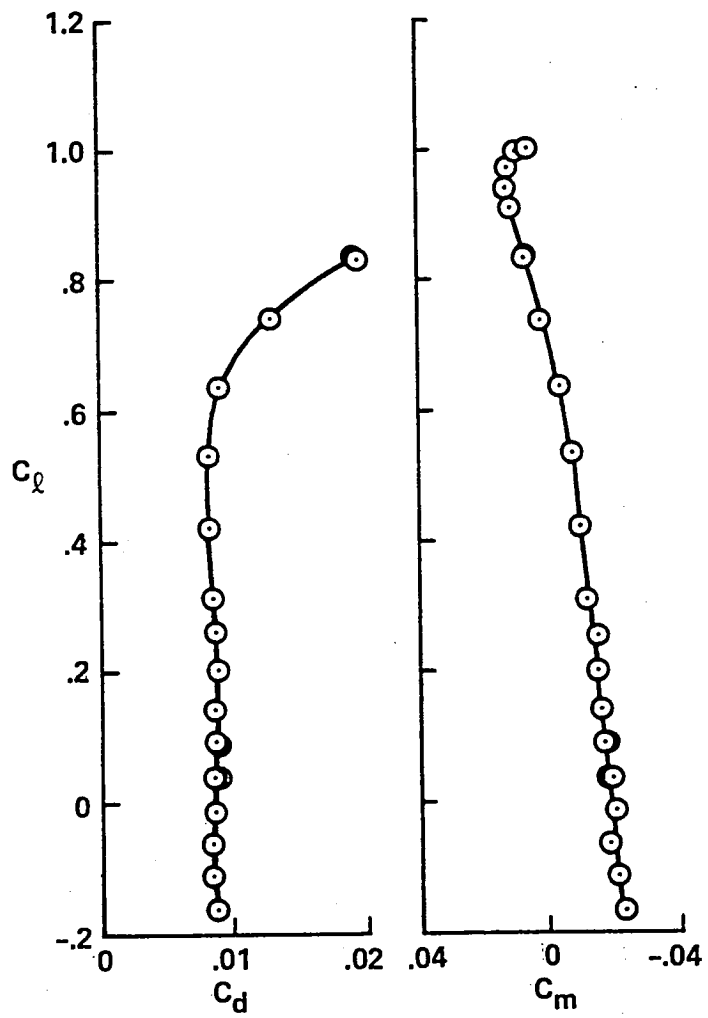
(d) Concluded.

Figure 2.- Continued.



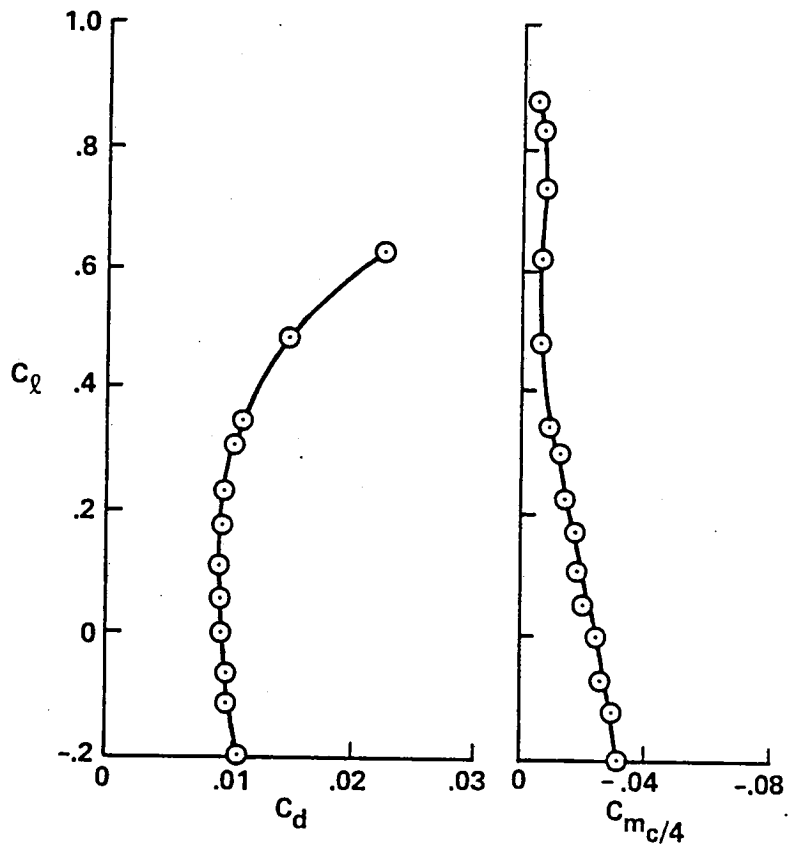
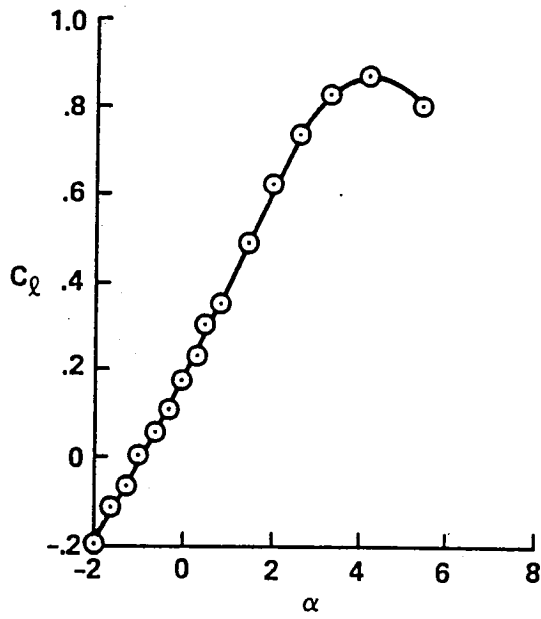
(e) $M_{\text{set}} = 0.6$, $Re_{\text{set}} = 4 \times 10^6$.

Figure 2.- Continued.



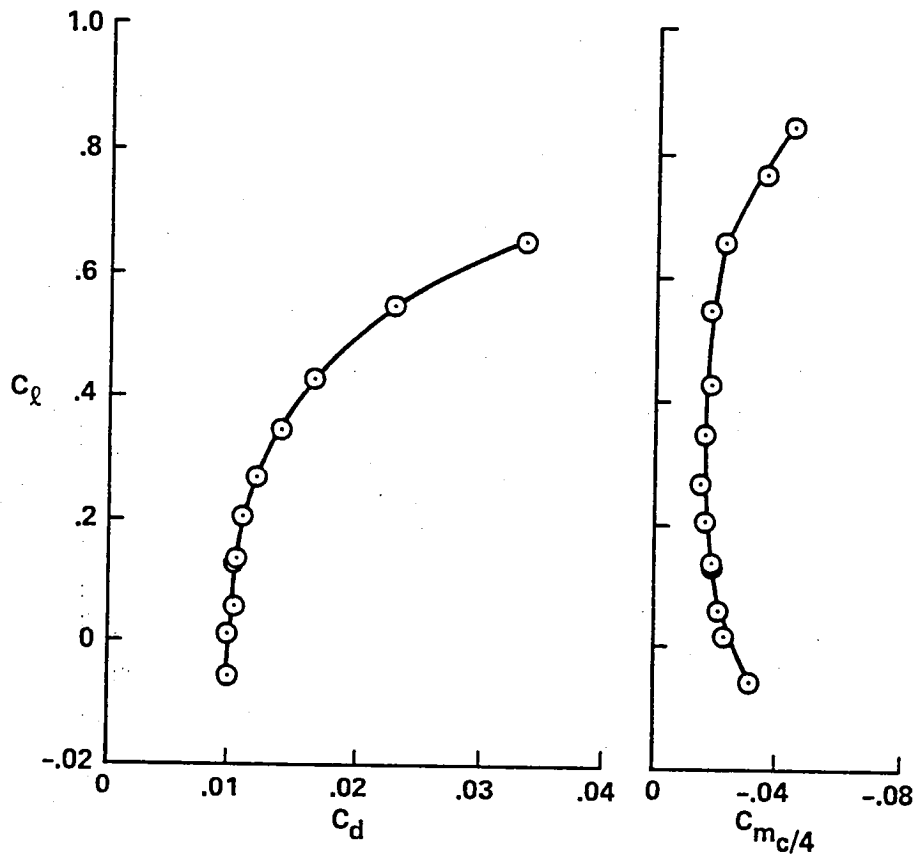
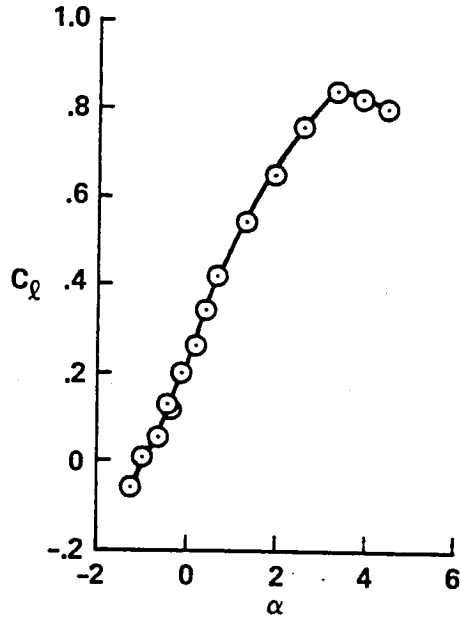
(e) Concluded.

Figure 2.- Continued.



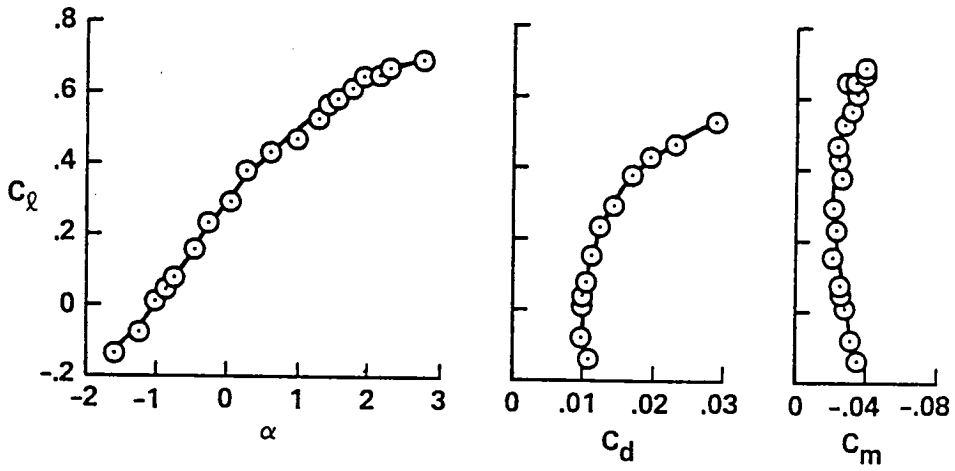
(f) $M_{set} = 0.7$, $Re_{set} = 4 \times 10^6$.

Figure 2.- Continued.

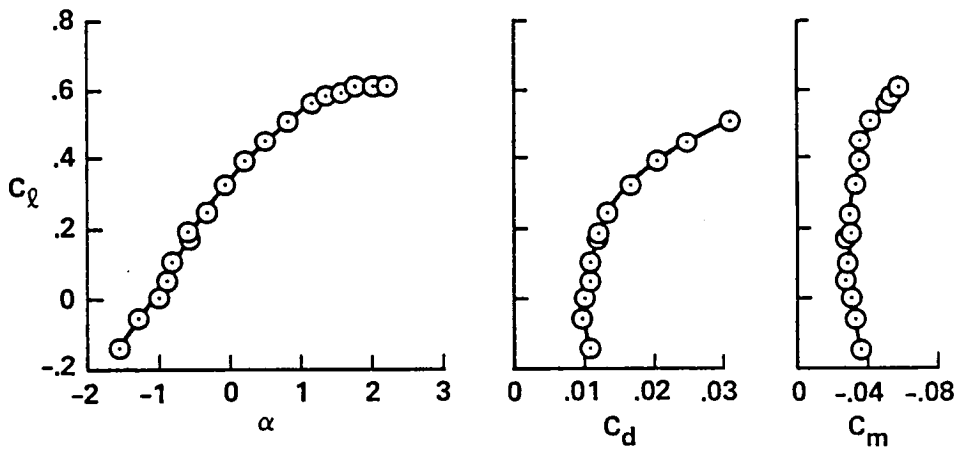


(g) $M_{set} = 0.75, Re_{set} = 4 \times 10^6$.

Figure 2.- Continued.

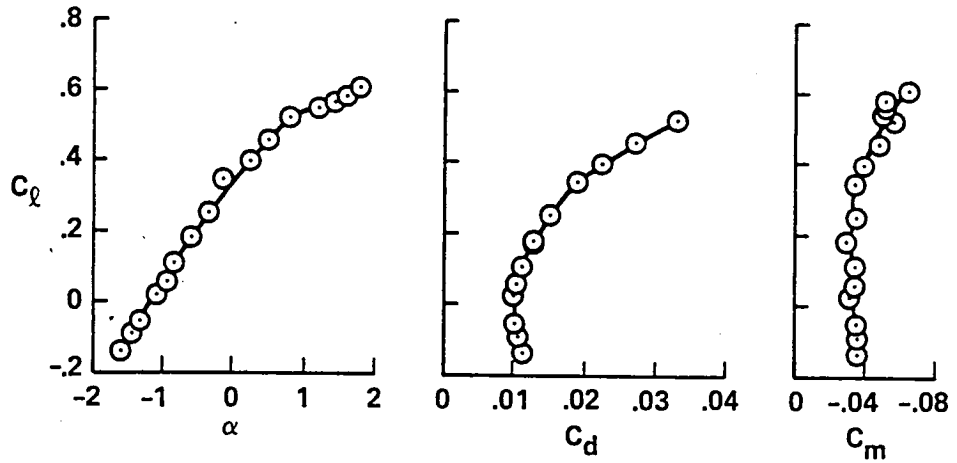


(h) $M_{set} = 0.77$, $Re_{set} = 4 \times 10^6$.

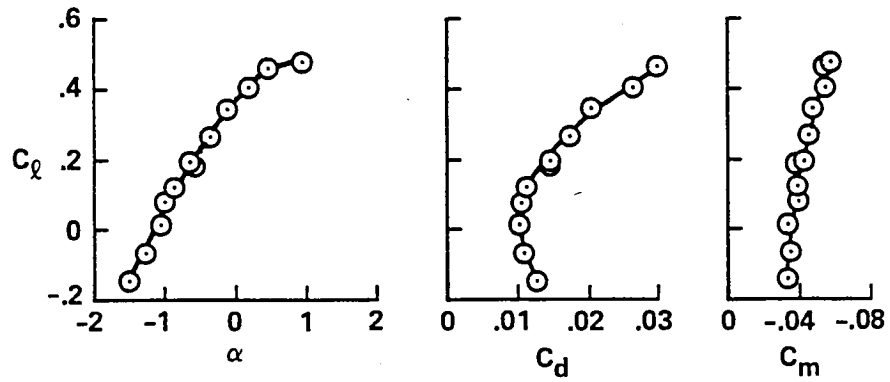


(i) $M_{set} = 0.79$, $Re_{set} = 4 \times 10^6$.

Figure 2.- Continued.

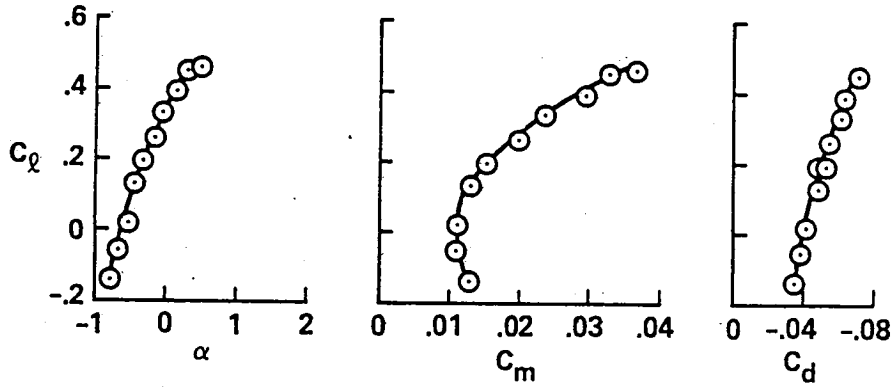


(j) $M_{set} = 0.8$, $Re_{set} = 4 \times 10^6$.

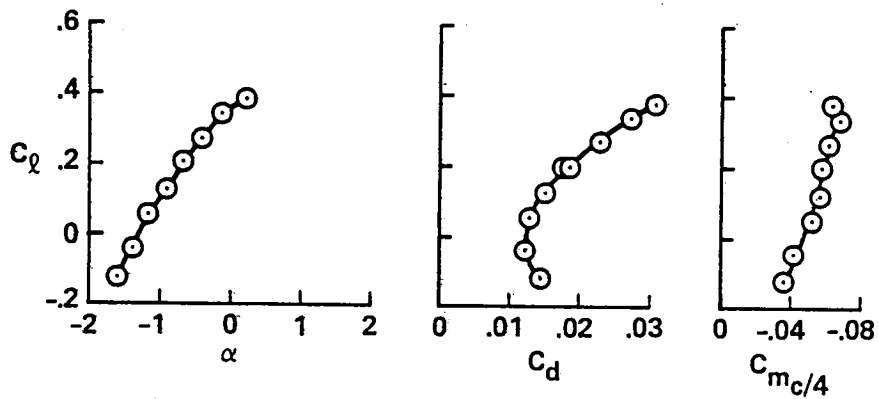


(k) $M_{set} = 0.81$, $Re_{set} = 4 \times 10^6$.

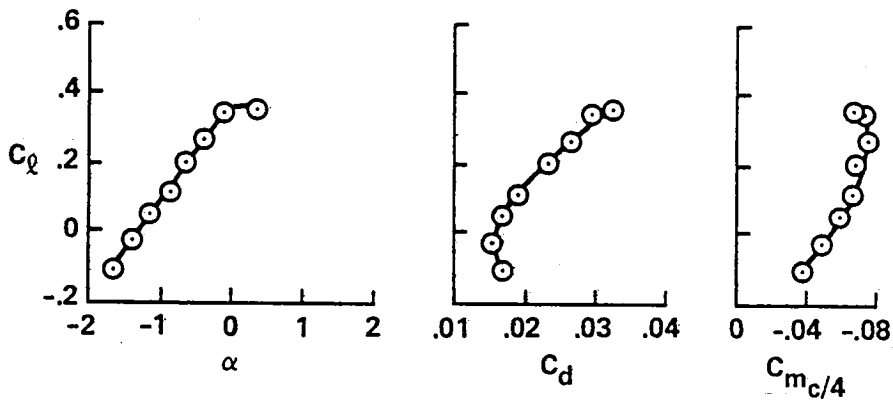
Figure 2.- Continued.



(l) $M_{set} = 0.82$, $Re_{set} = 4 \times 10^6$.



(m) $M_{set} = 0.83$, $Re_{set} = 4 \times 10^6$.



(n) $M_{set} = 0.84$, $Re_{set} = 4 \times 10^6$.

Figure 2.- Concluded.

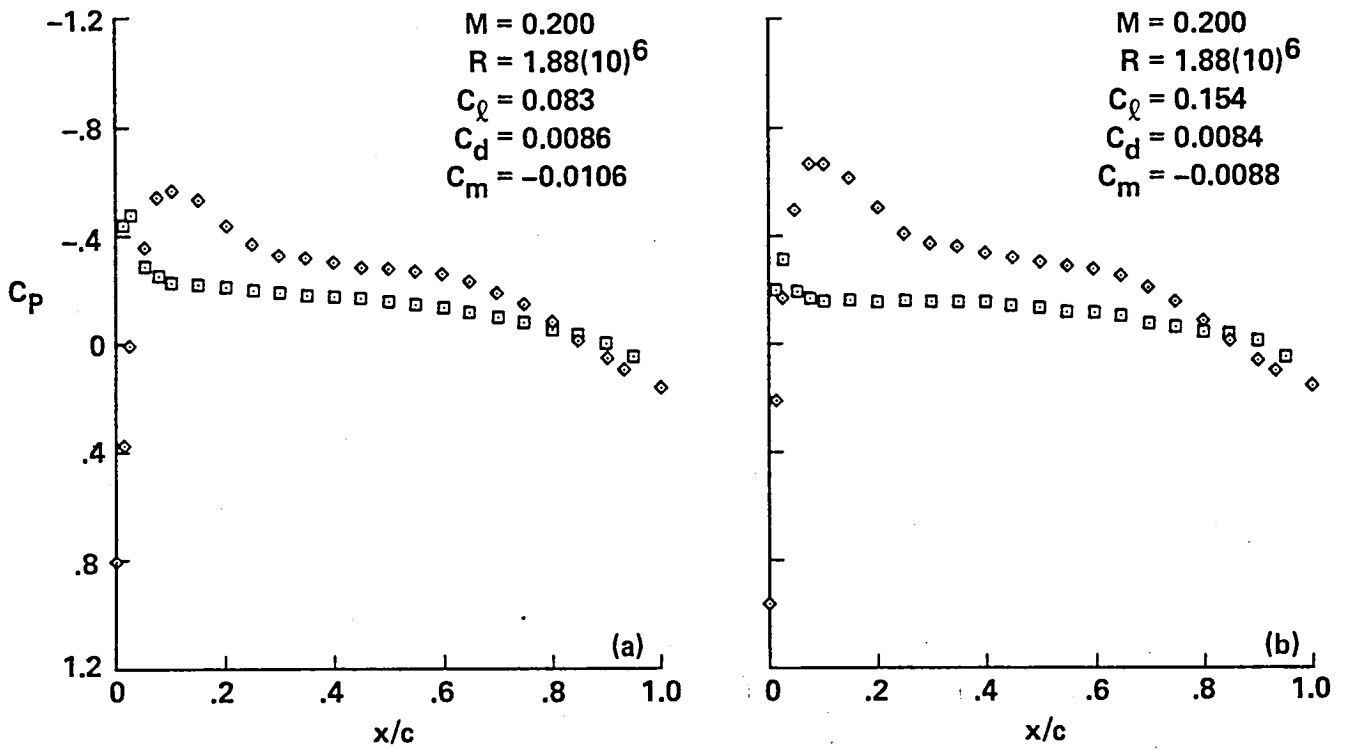


Figure 3.- Pressure distributions for A-1 airfoil, $M_{set} = 0.2$.

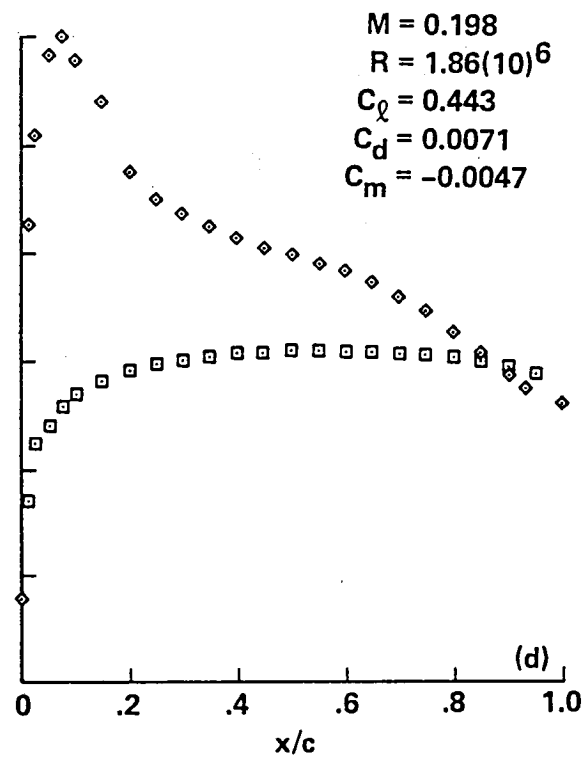
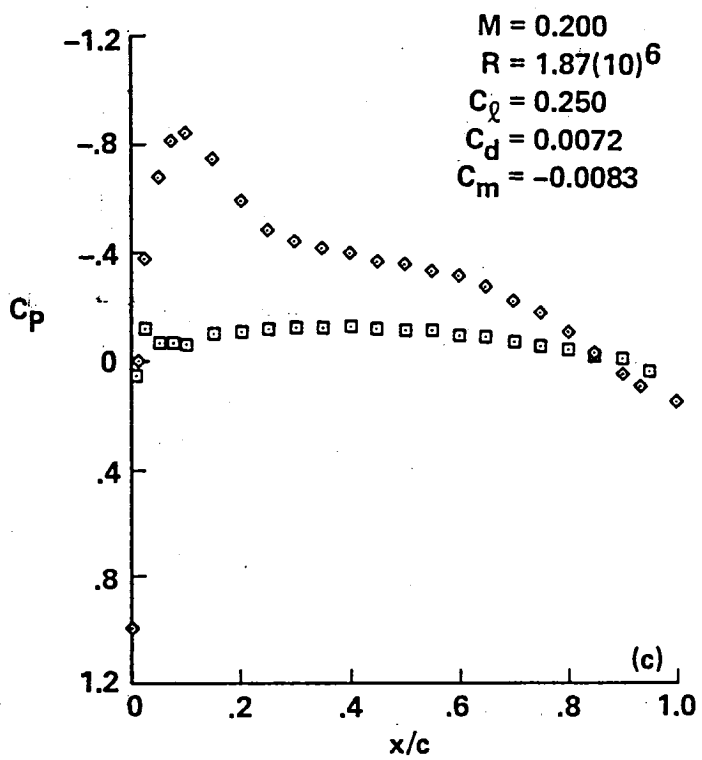


Figure 3.- Continued.

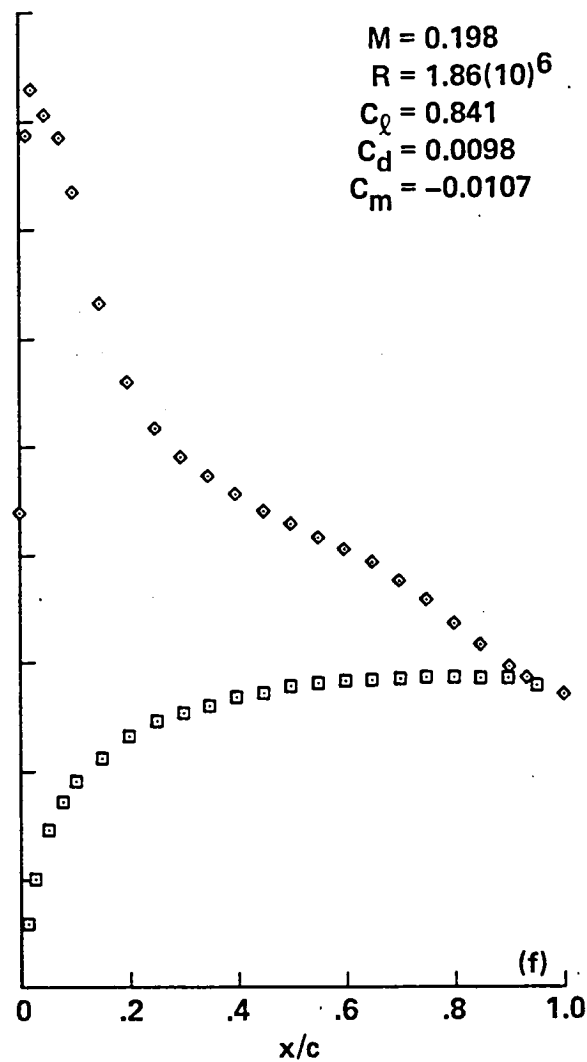
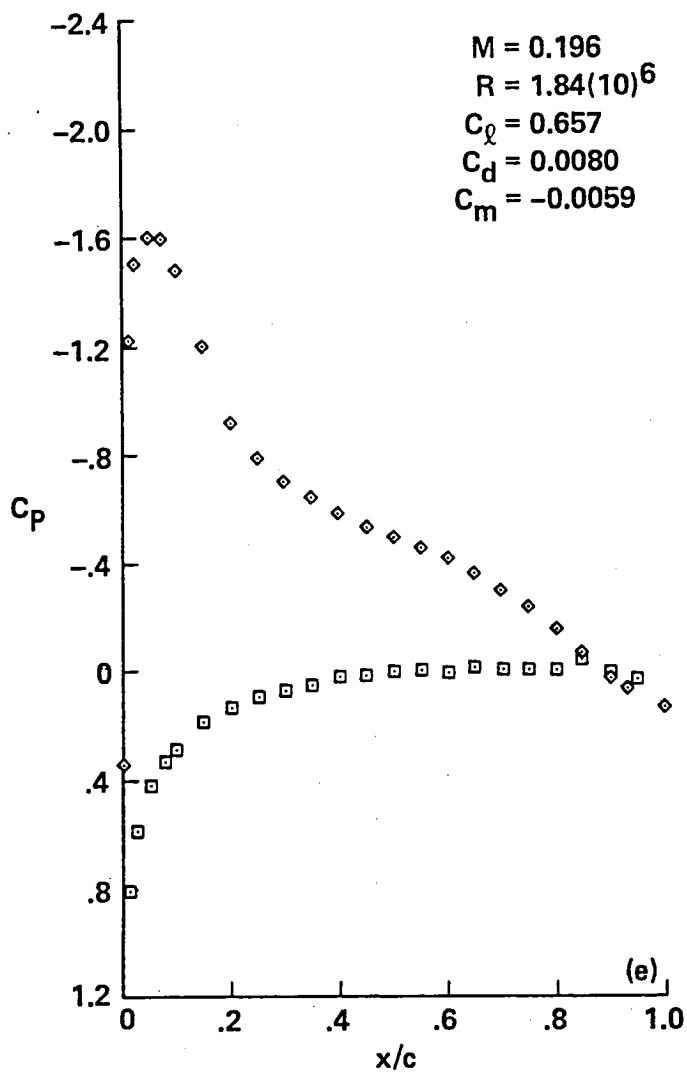


Figure 3.- Continued.

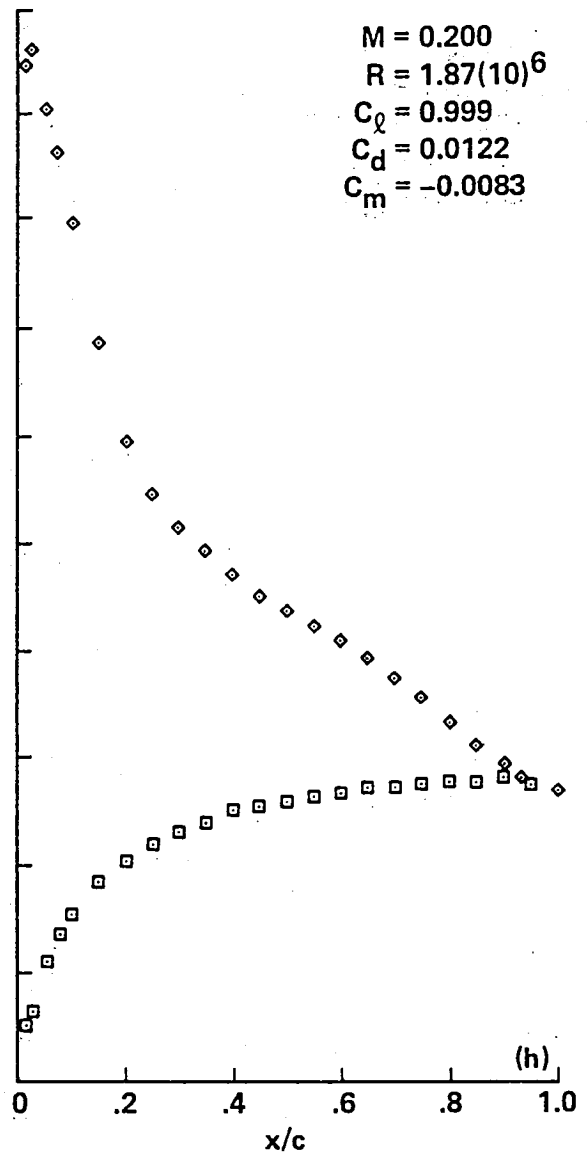
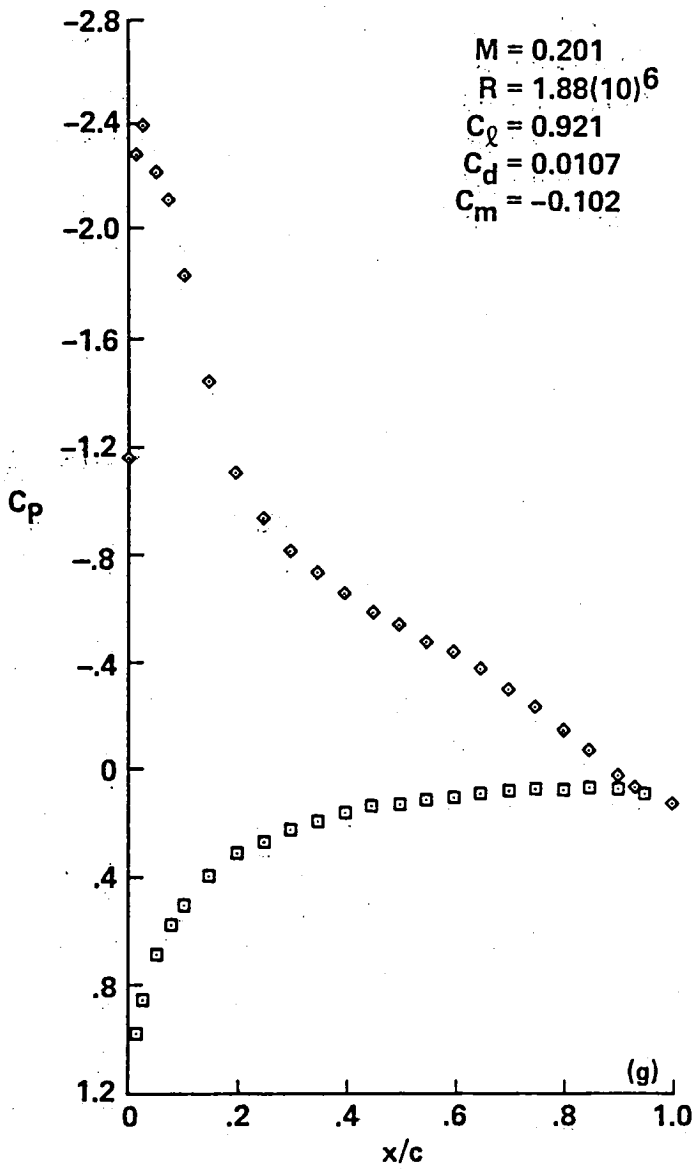


Figure 3.- Continued.

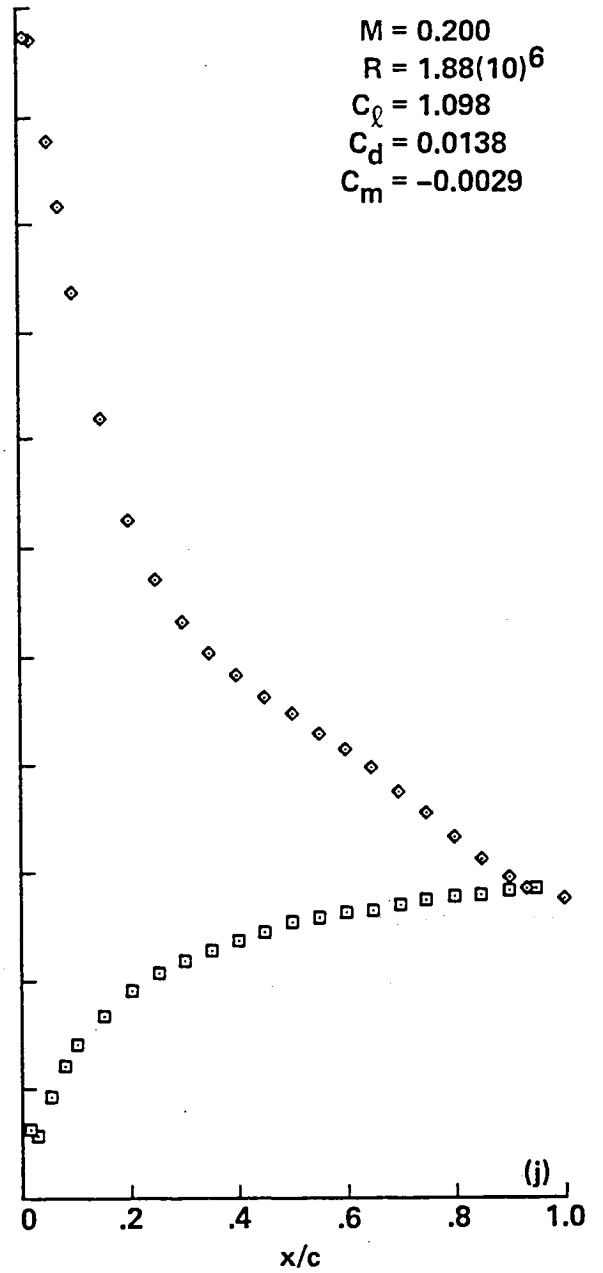
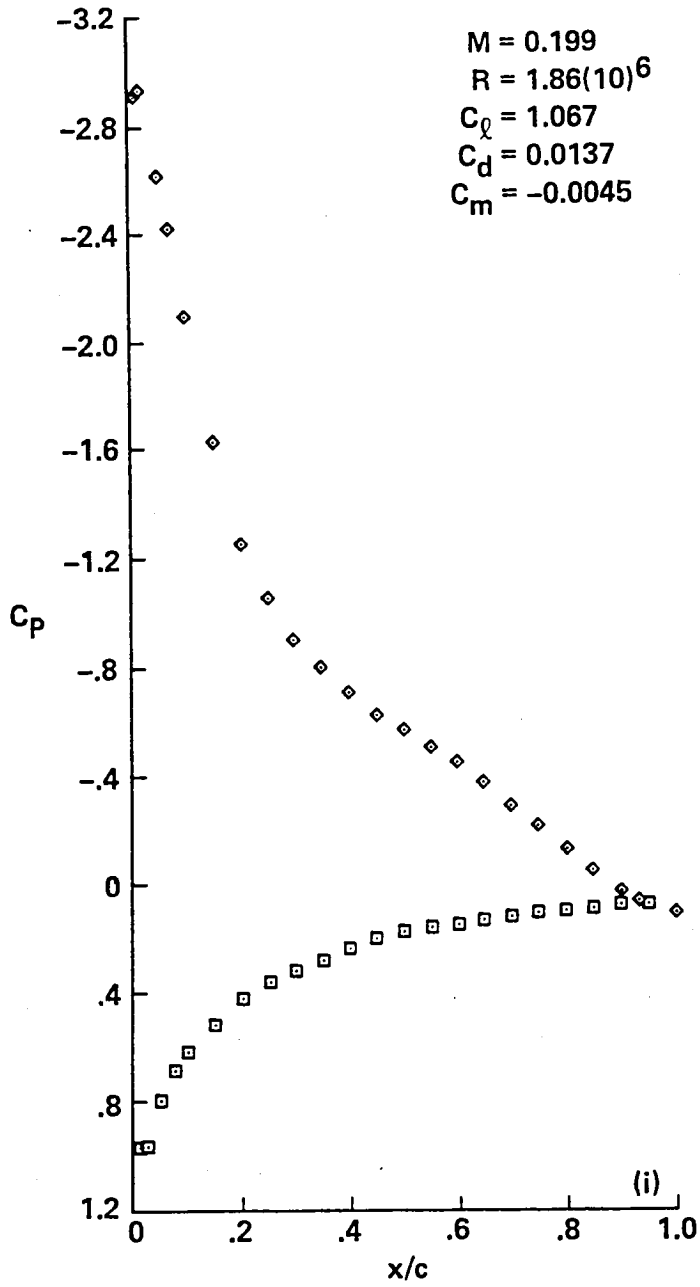


Figure 3.- Continued.

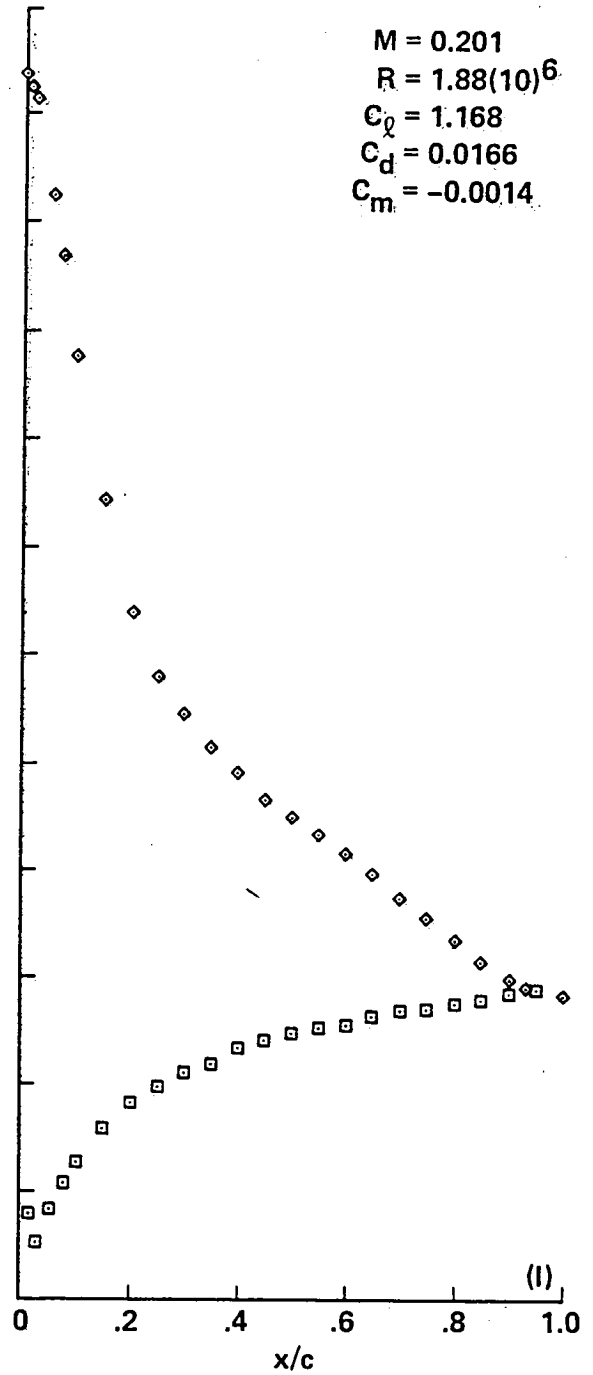
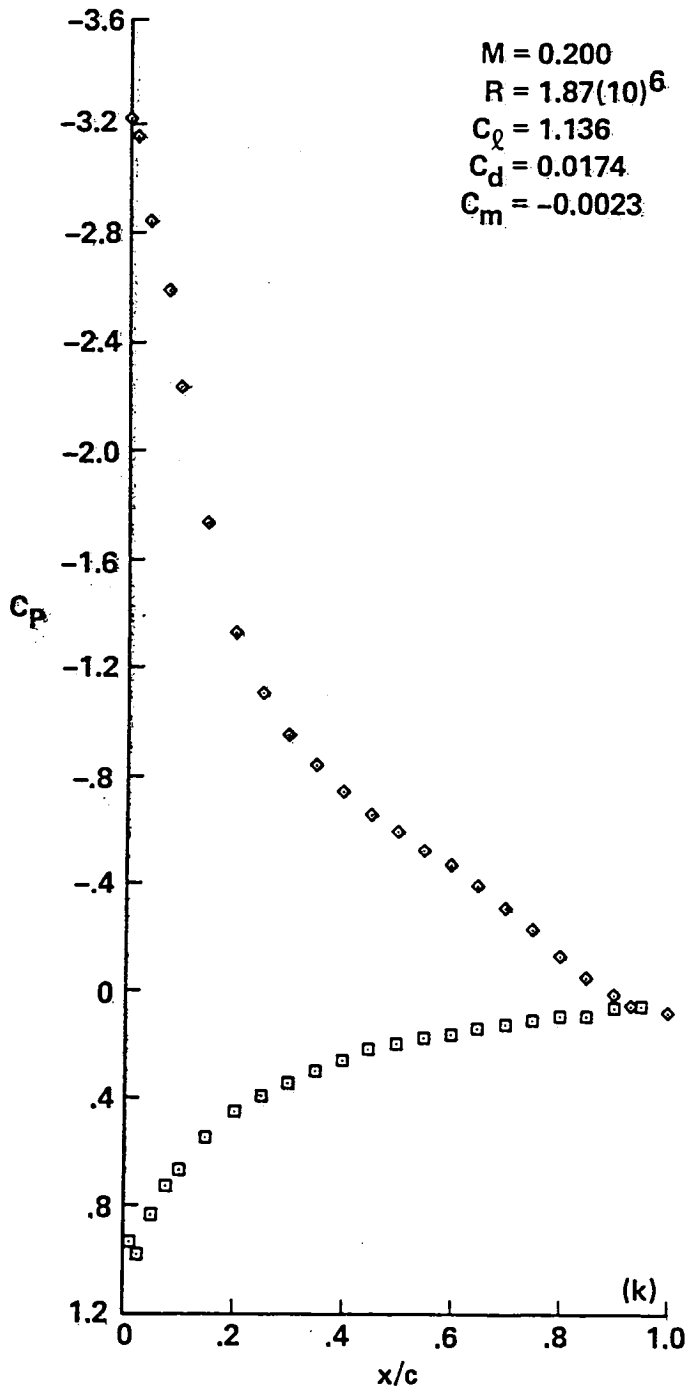


Figure 3.- Continued.

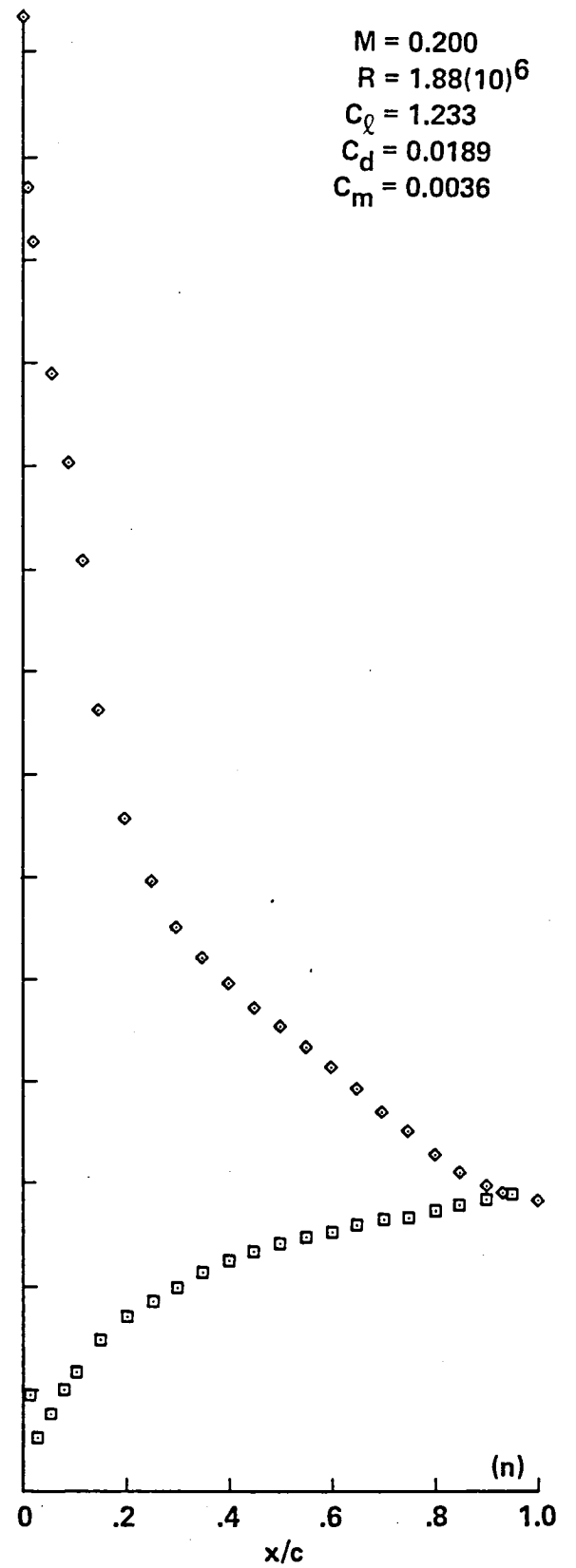
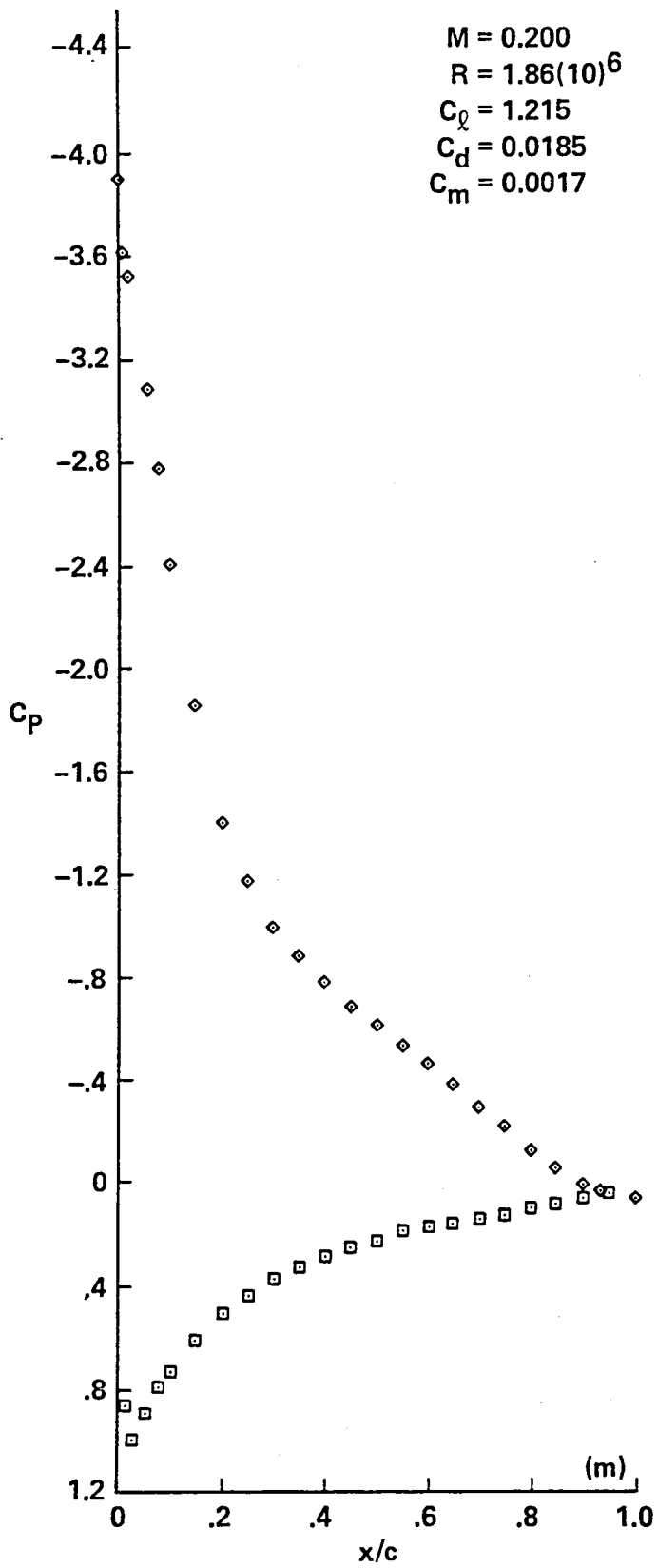


Figure 3.- Continued.

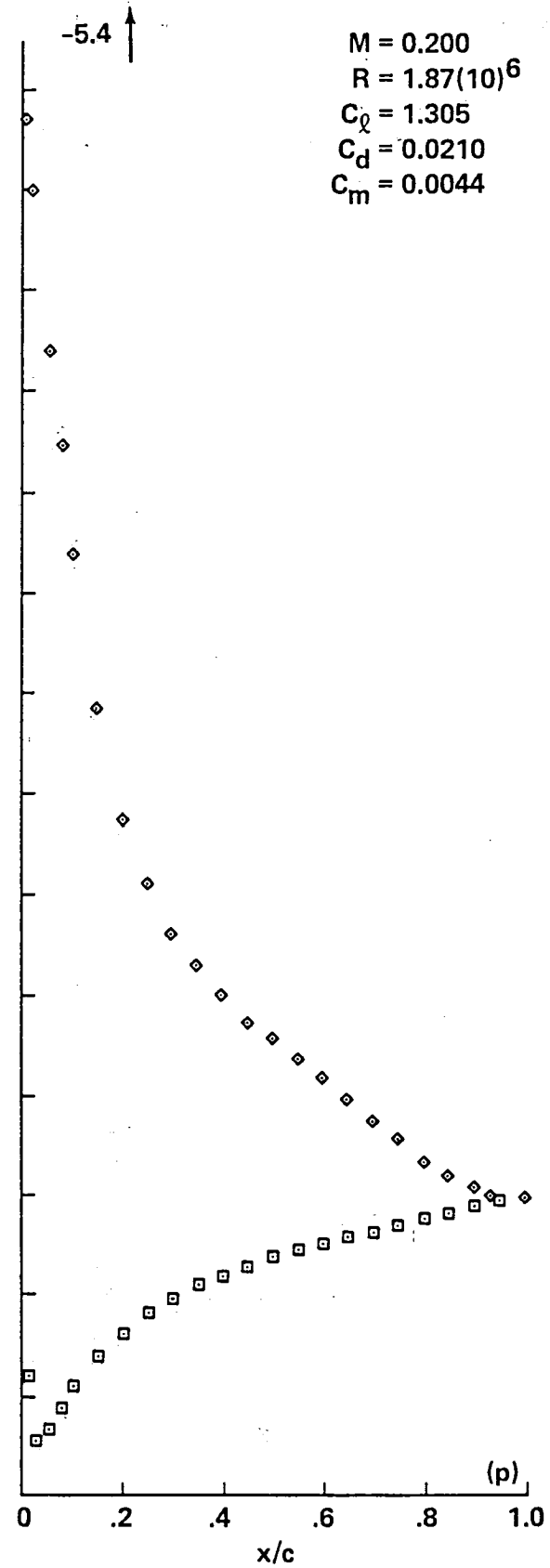
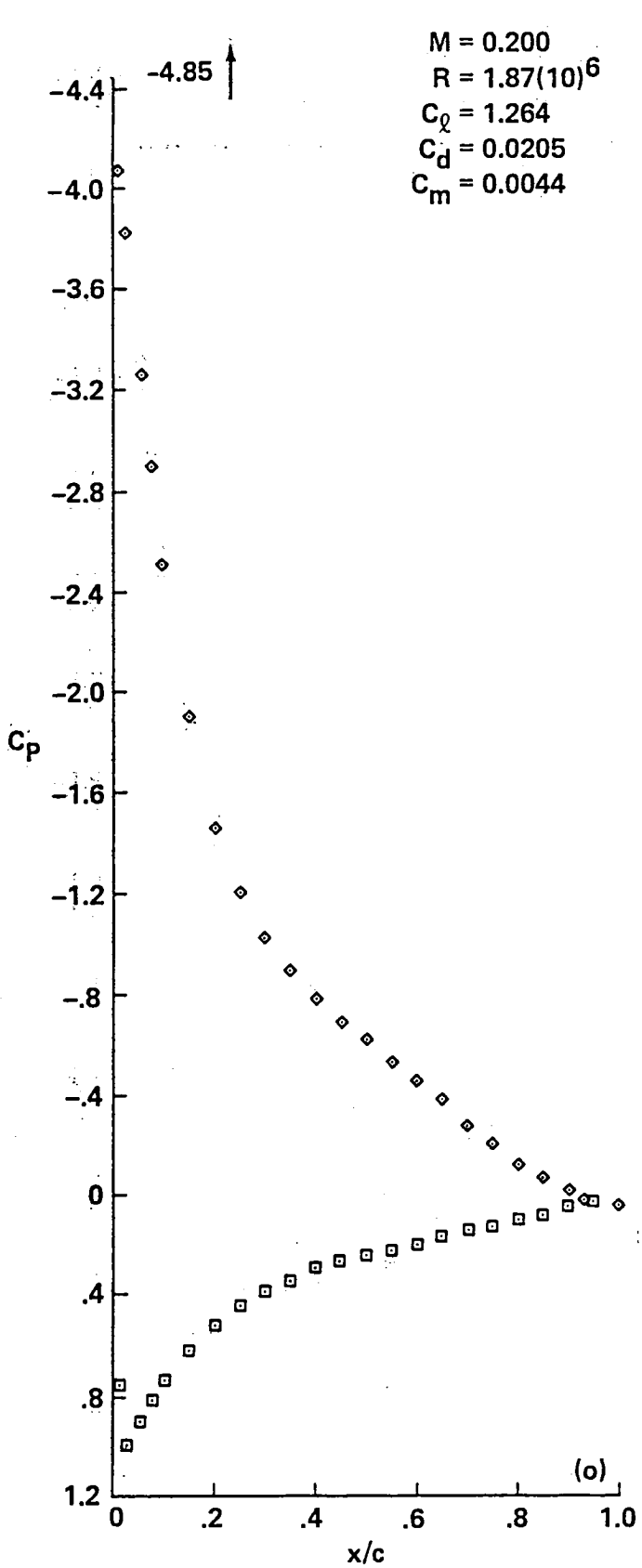


Figure 3.- Continued.

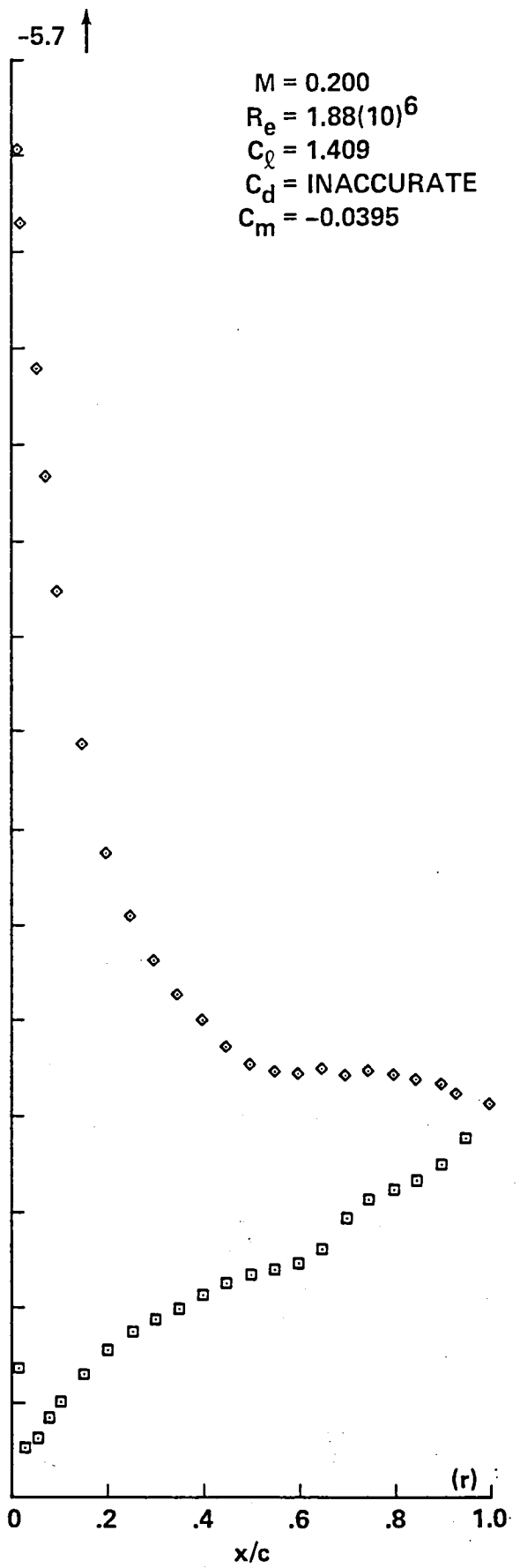
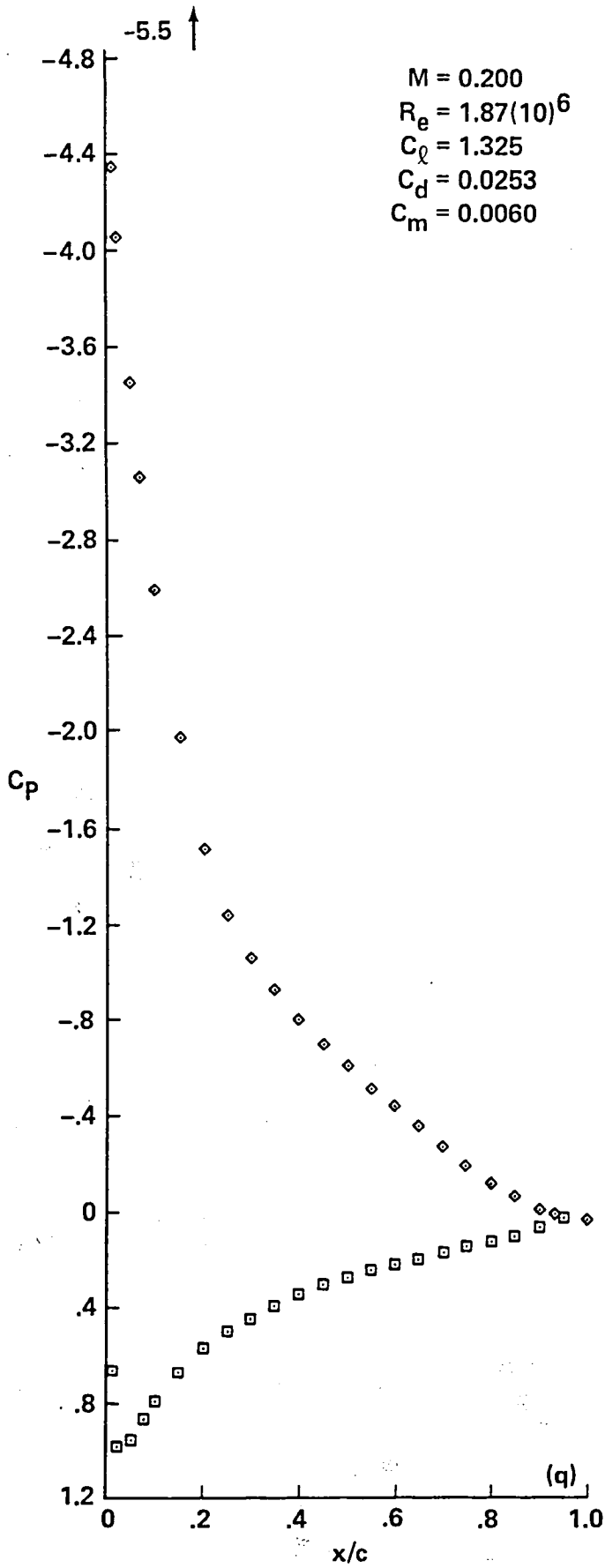


Figure 3.- Continued.

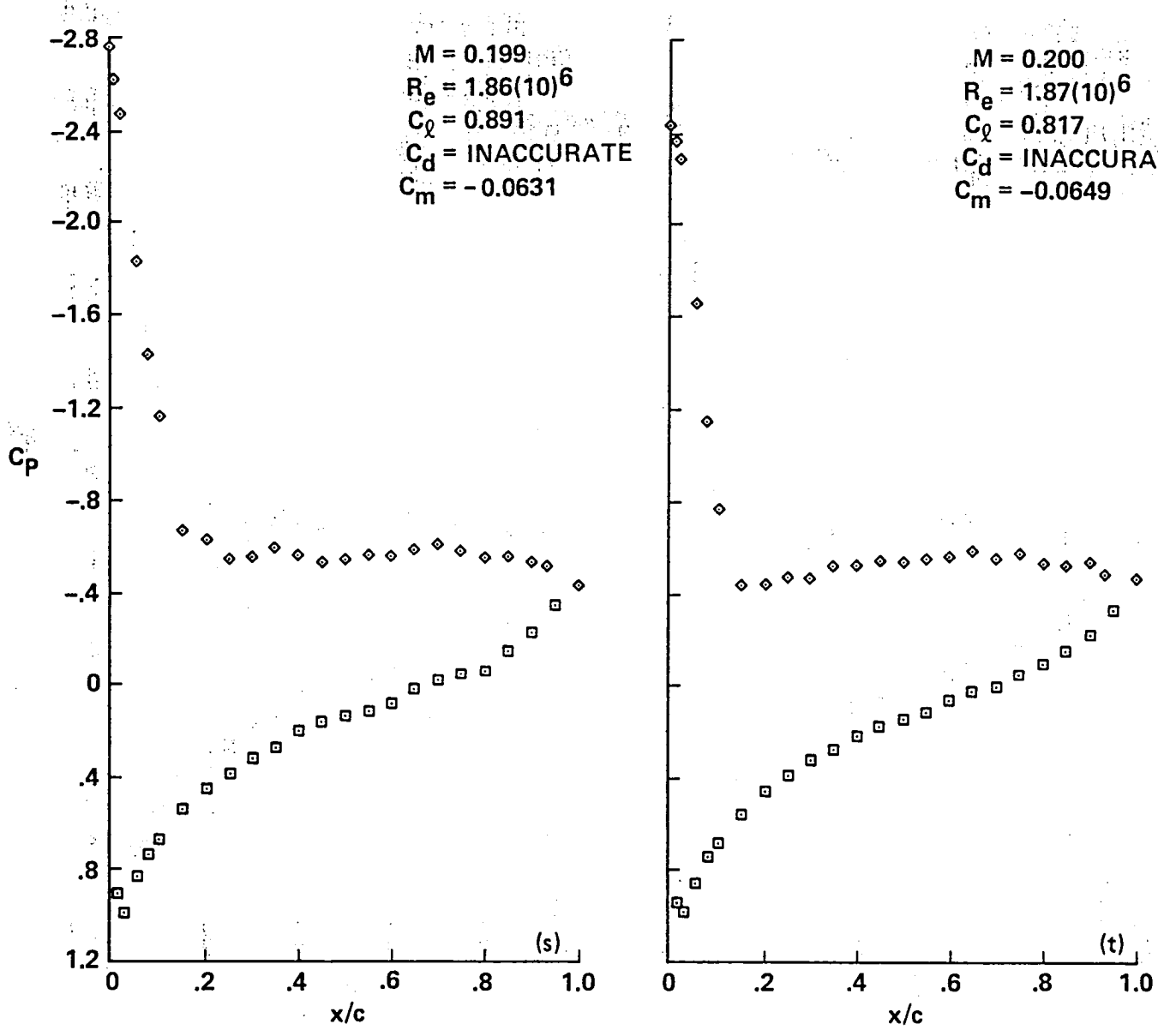


Figure 3.- Concluded.

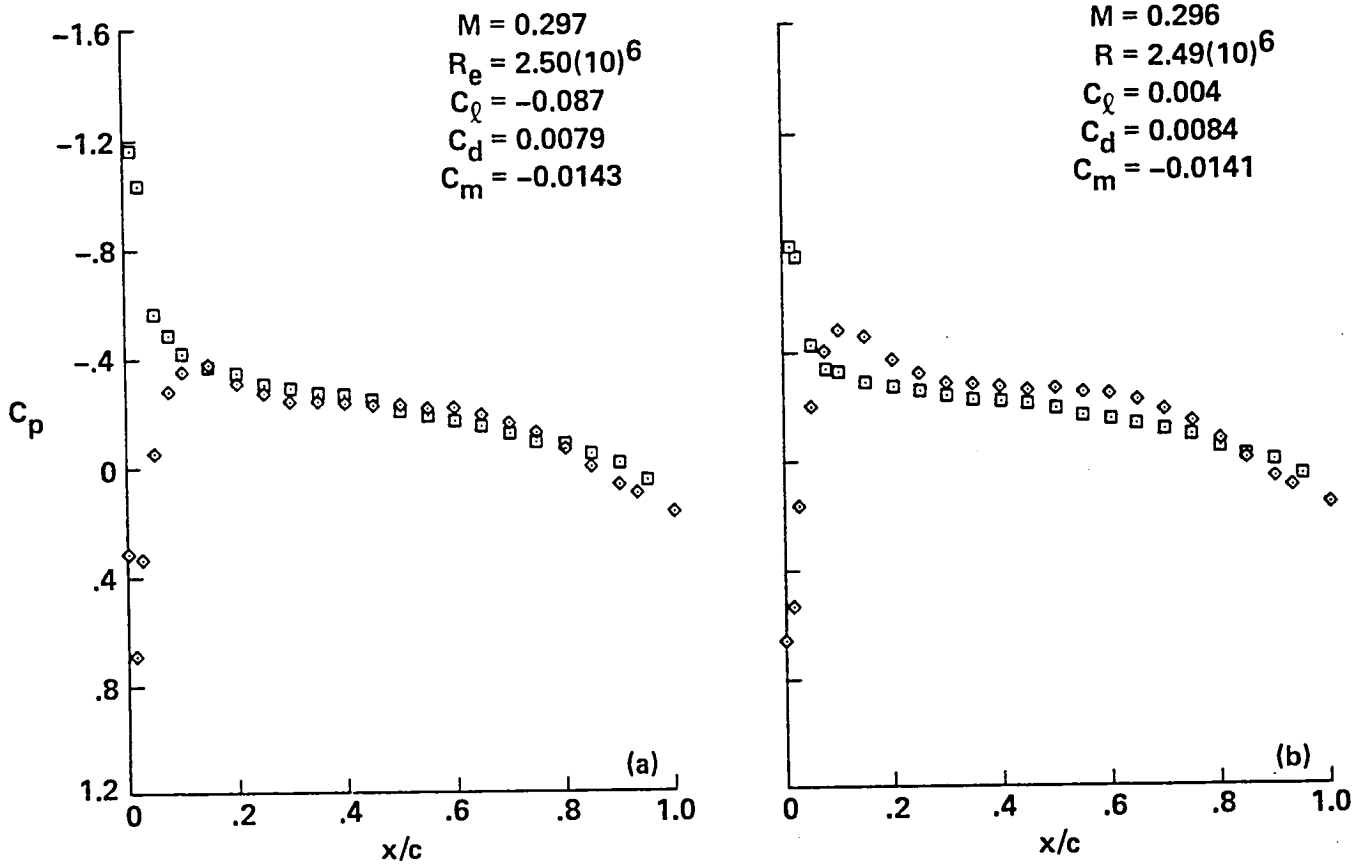


Figure 4.- Pressure distributions for A-1 airfoil, $M_{set} = 0.3$.

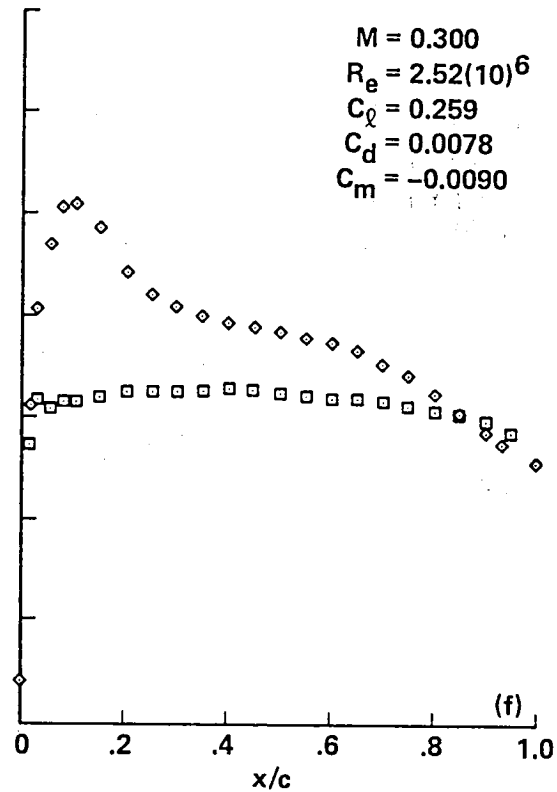
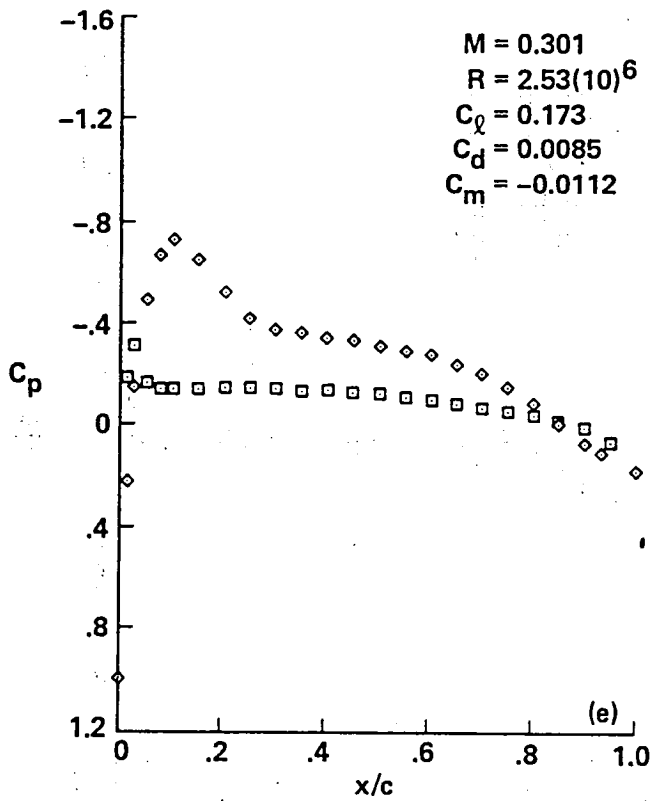
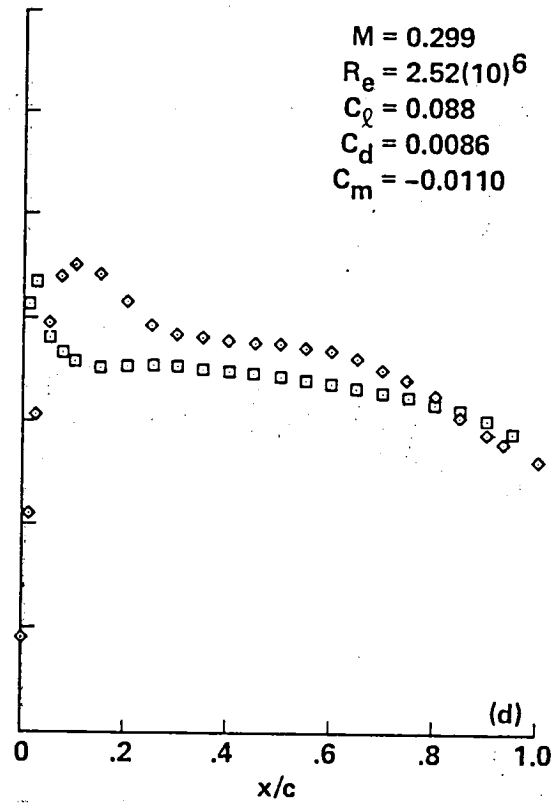
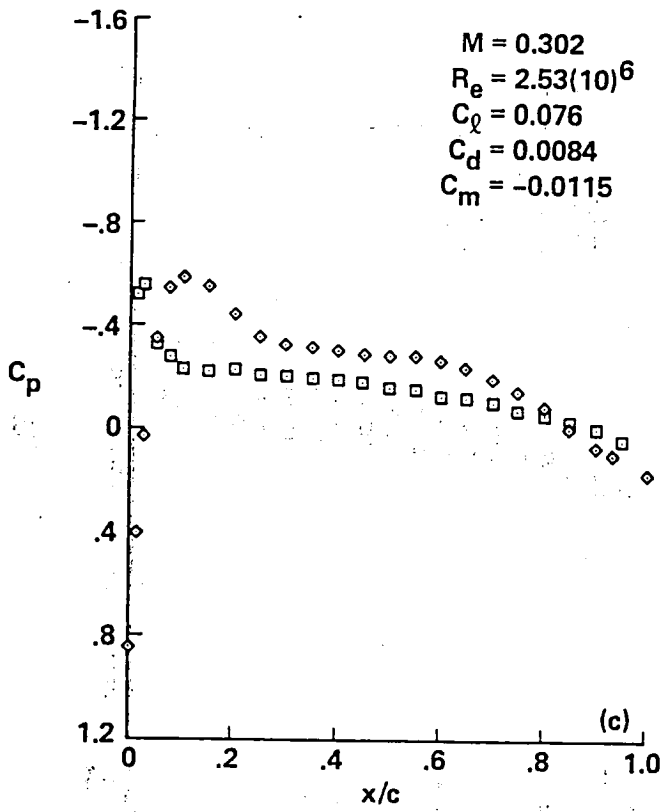


Figure 4.- Continued.

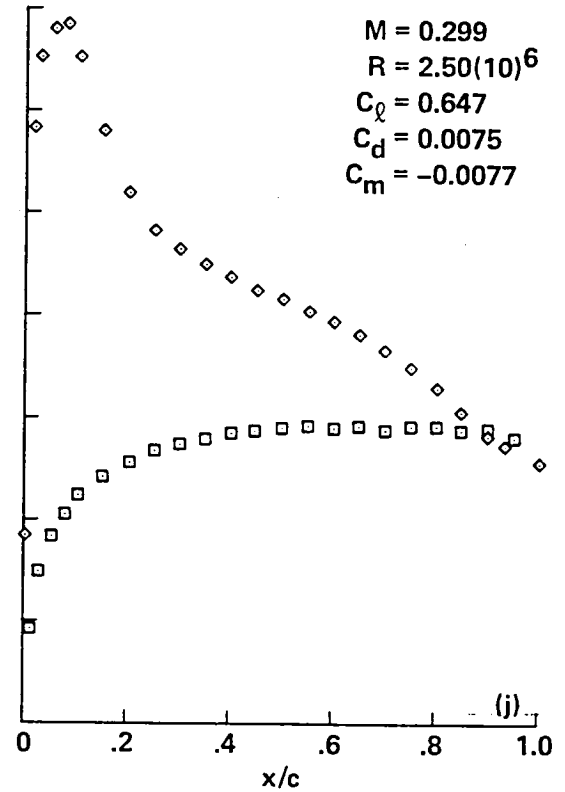
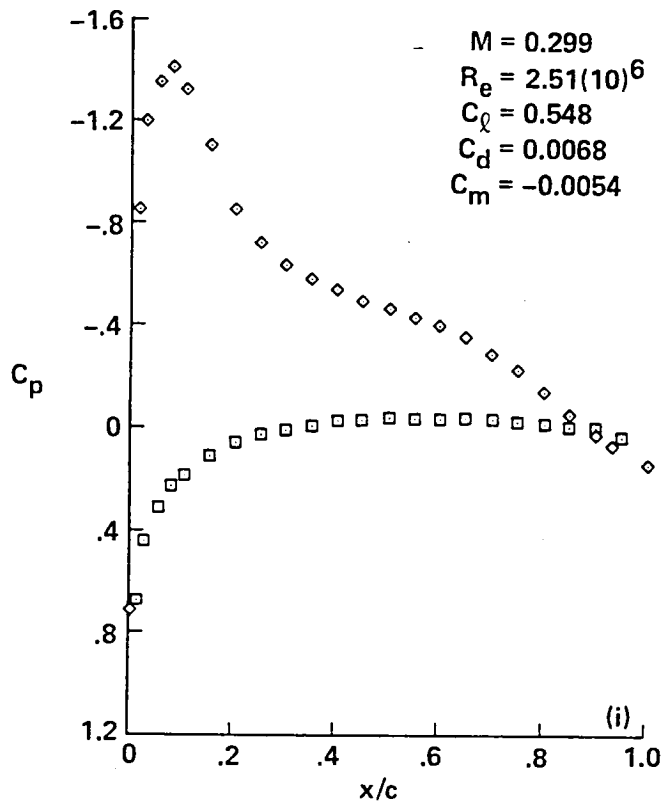
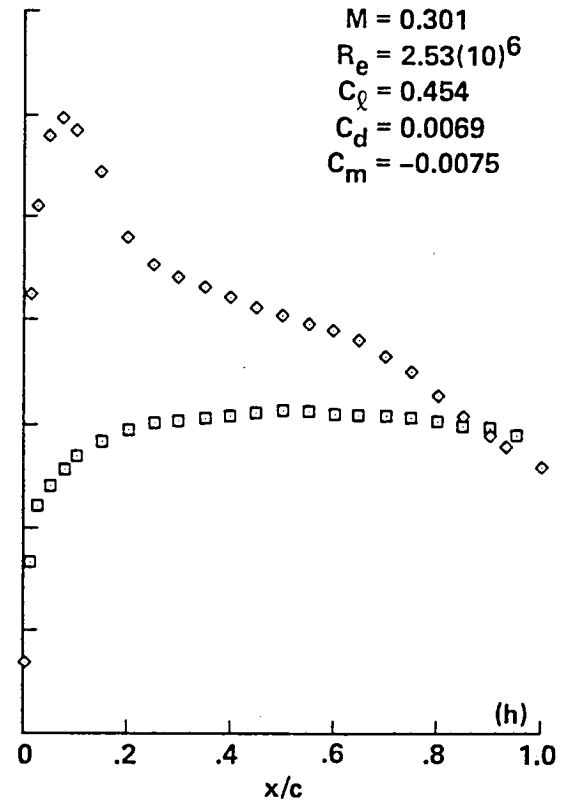
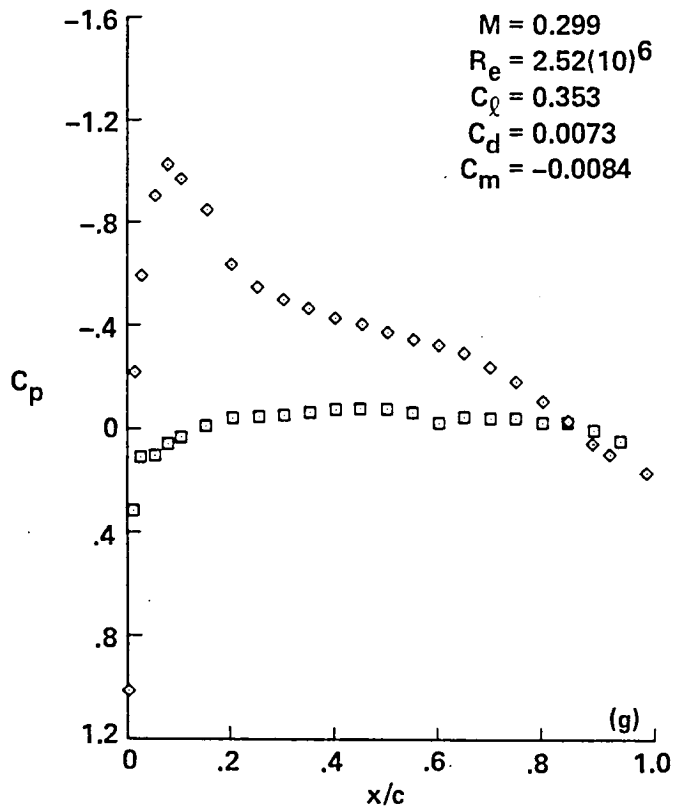


Figure 4.- Continued.

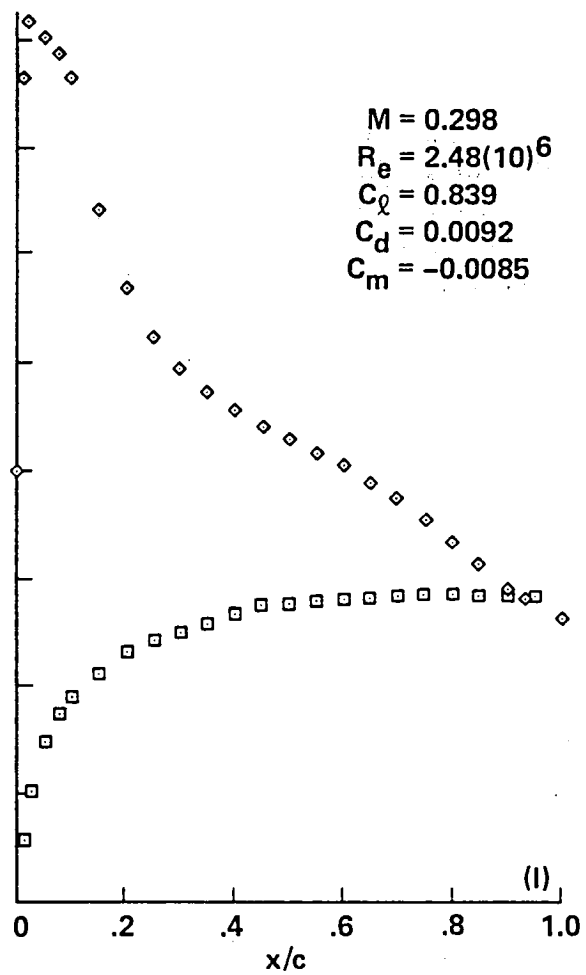
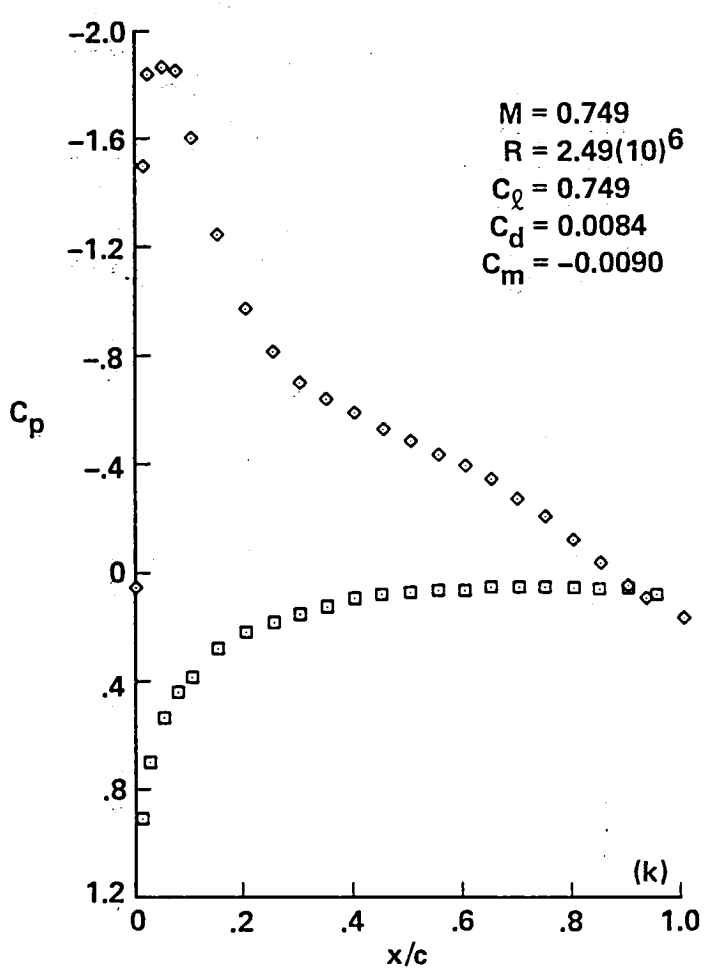


Figure 4.- Continued.

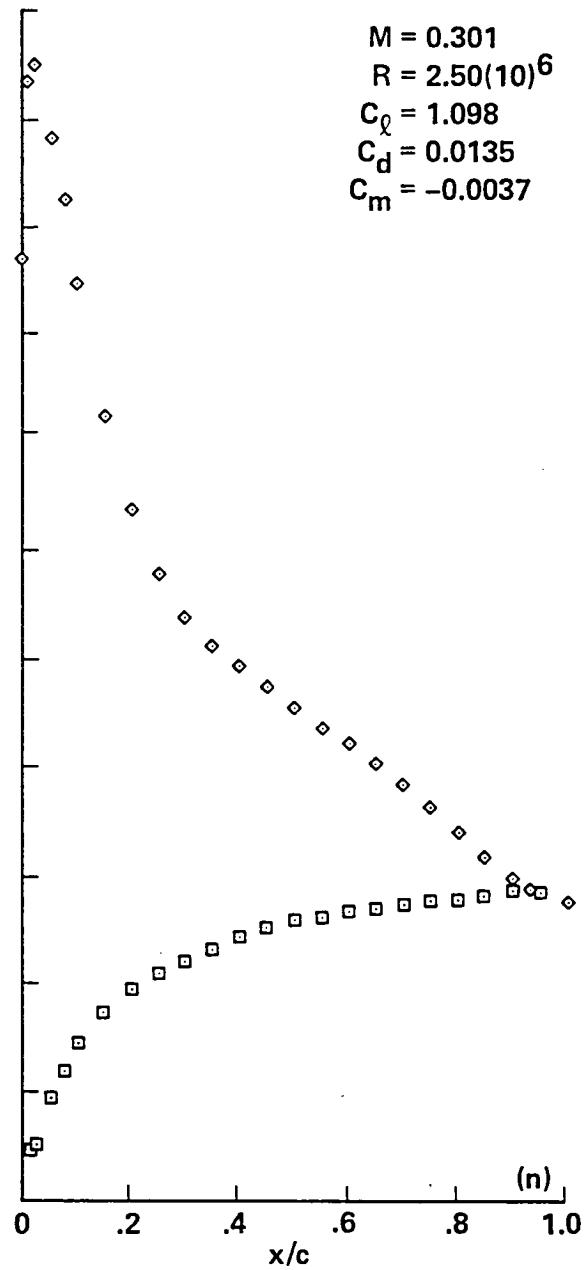
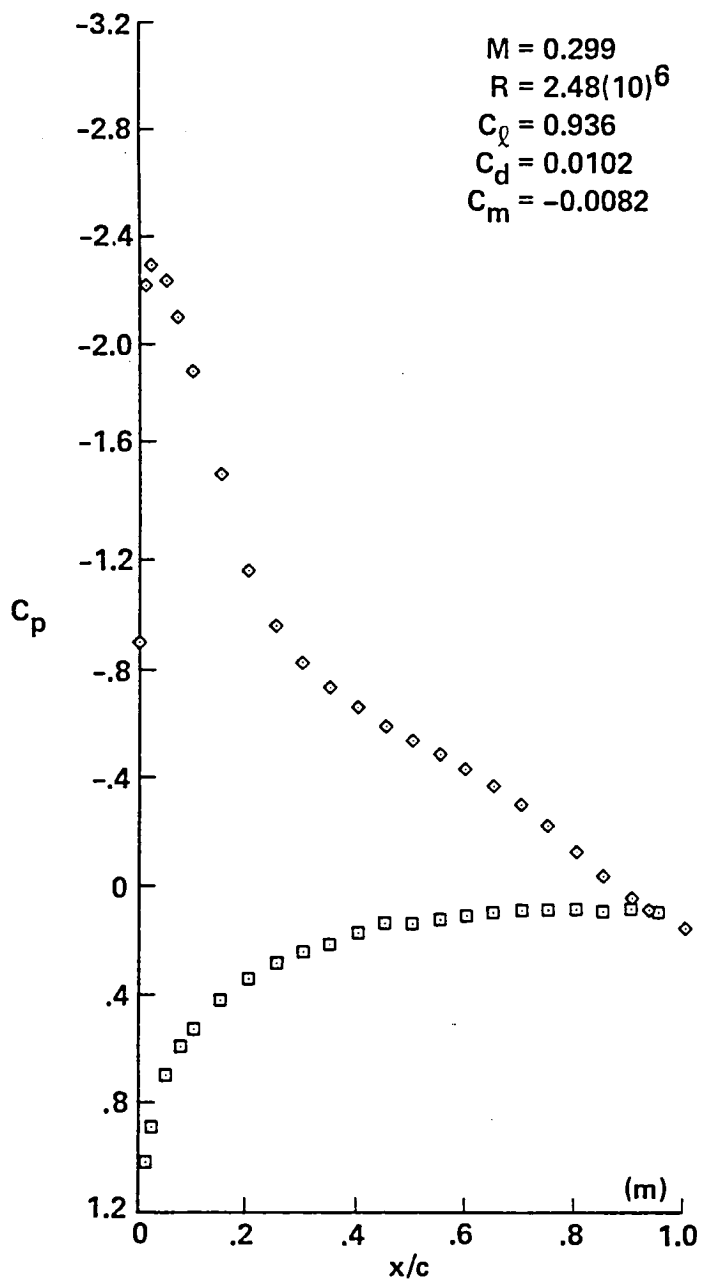


Figure 4.- Continued.

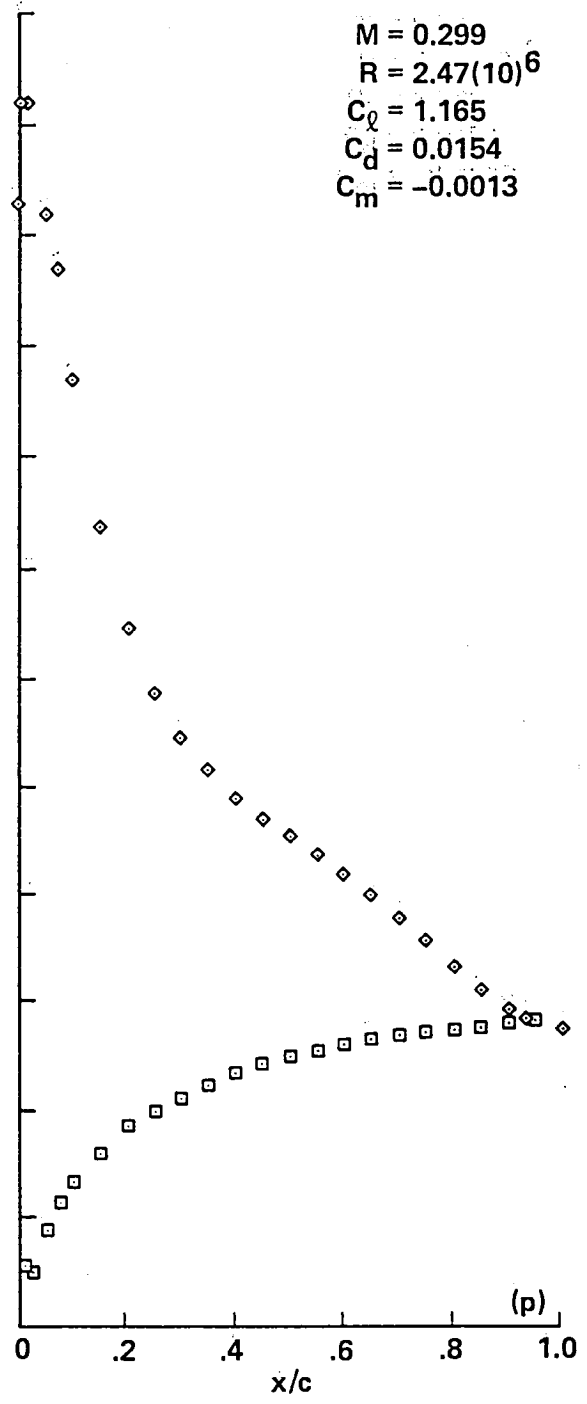
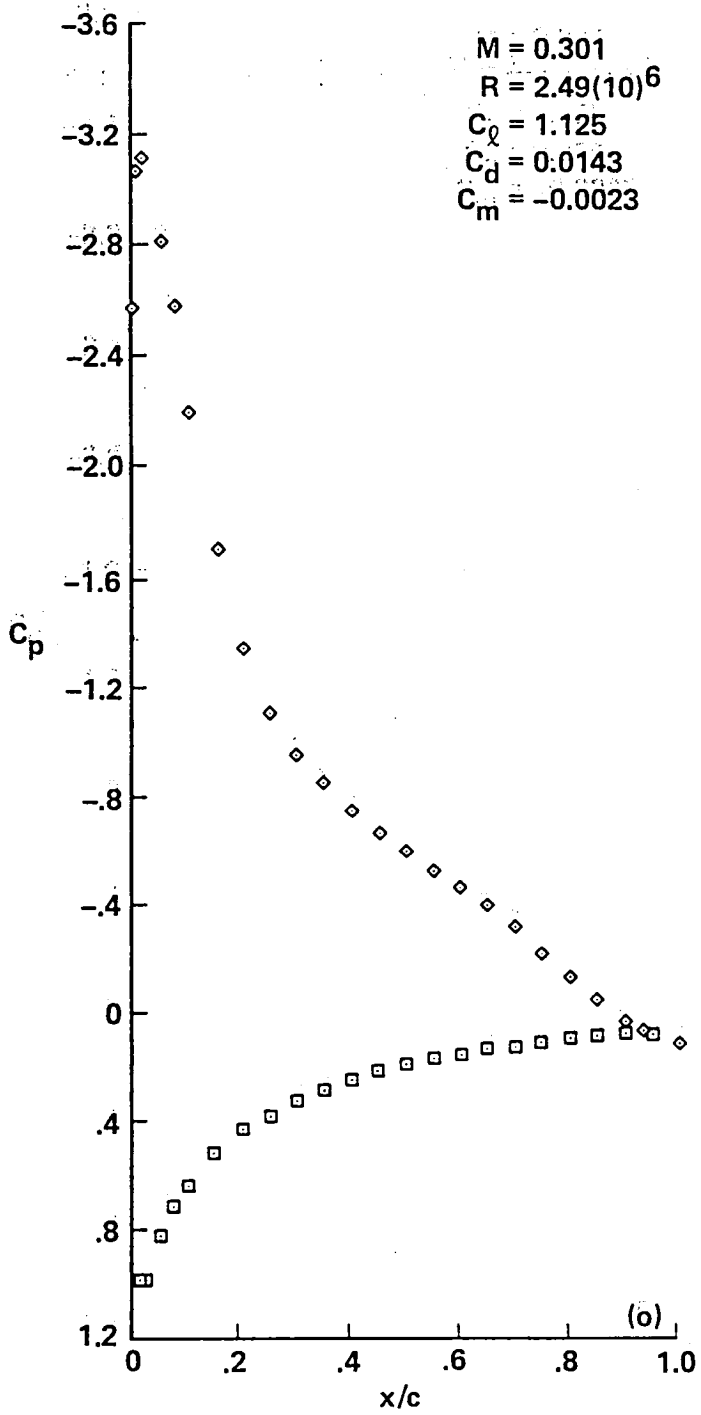


Figure 4.- Continued.

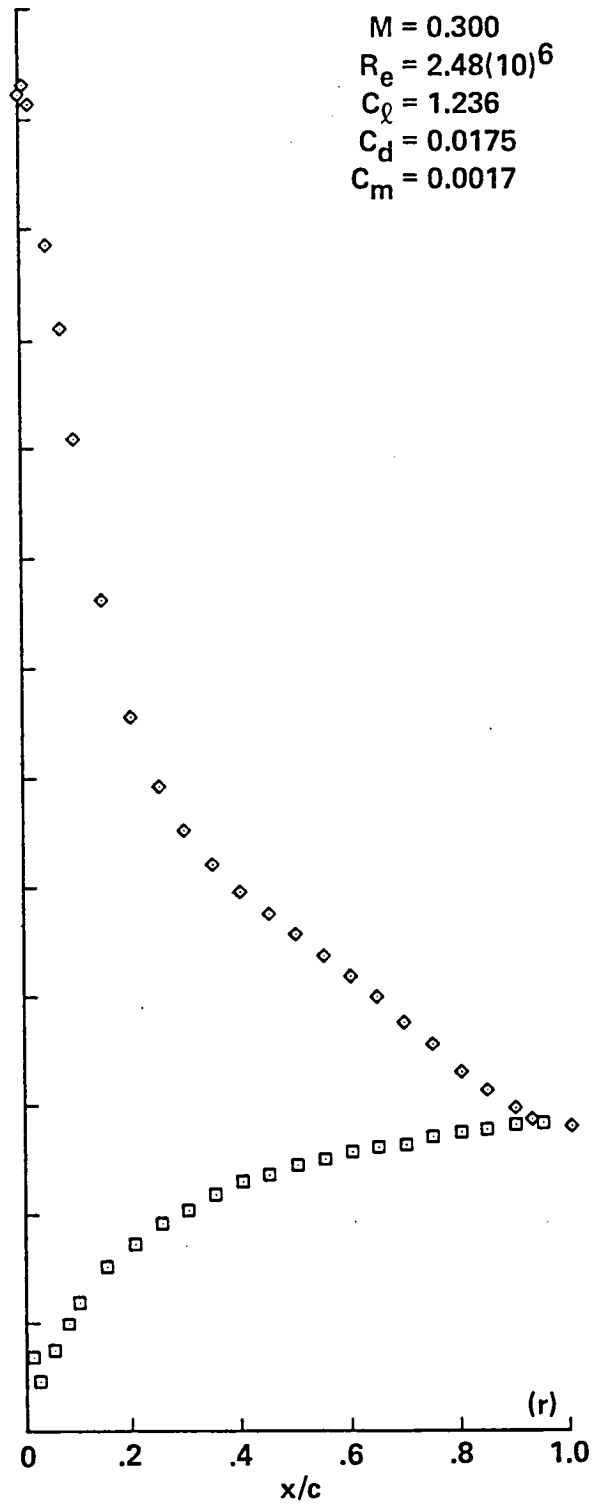
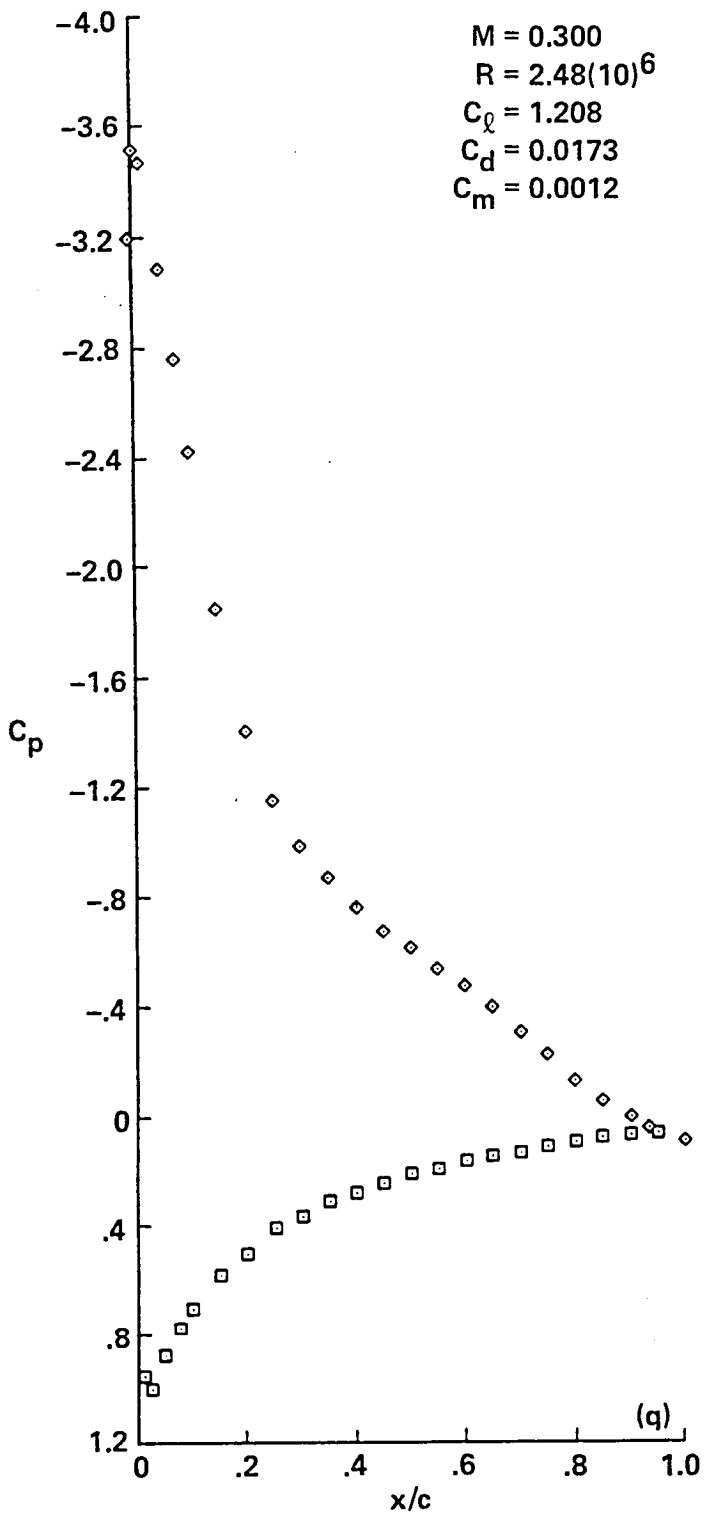


Figure 4.- Continued.

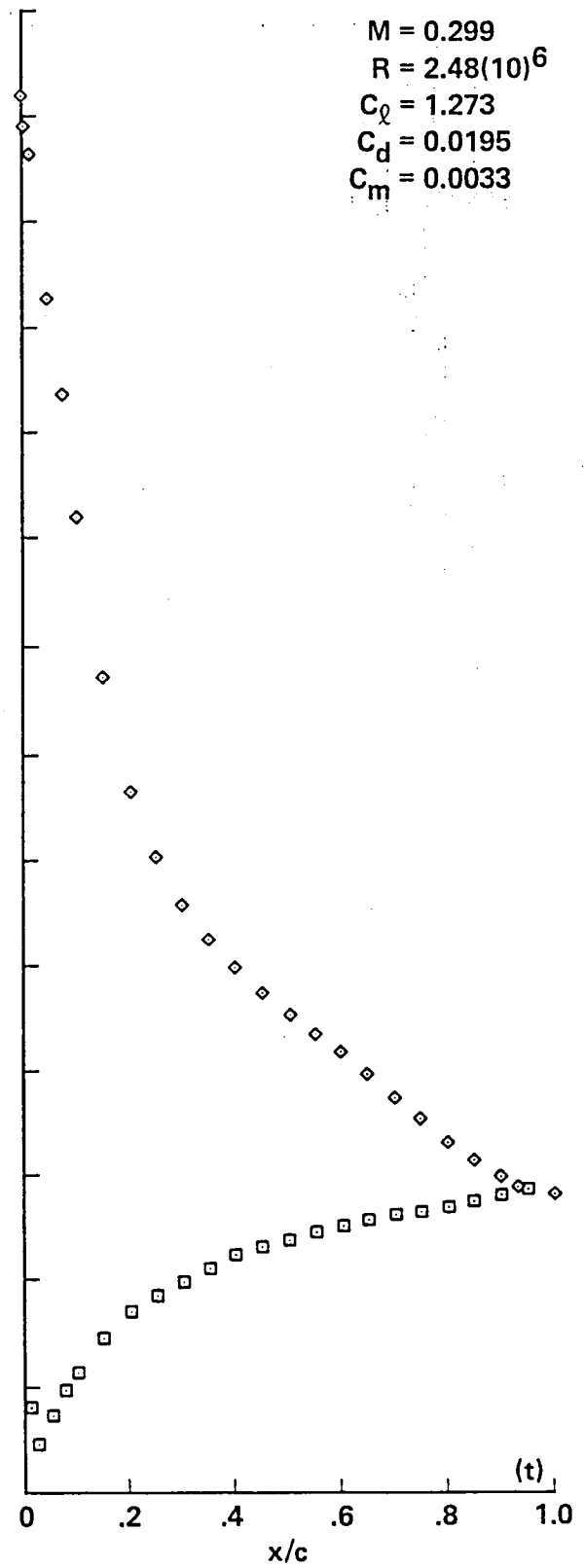
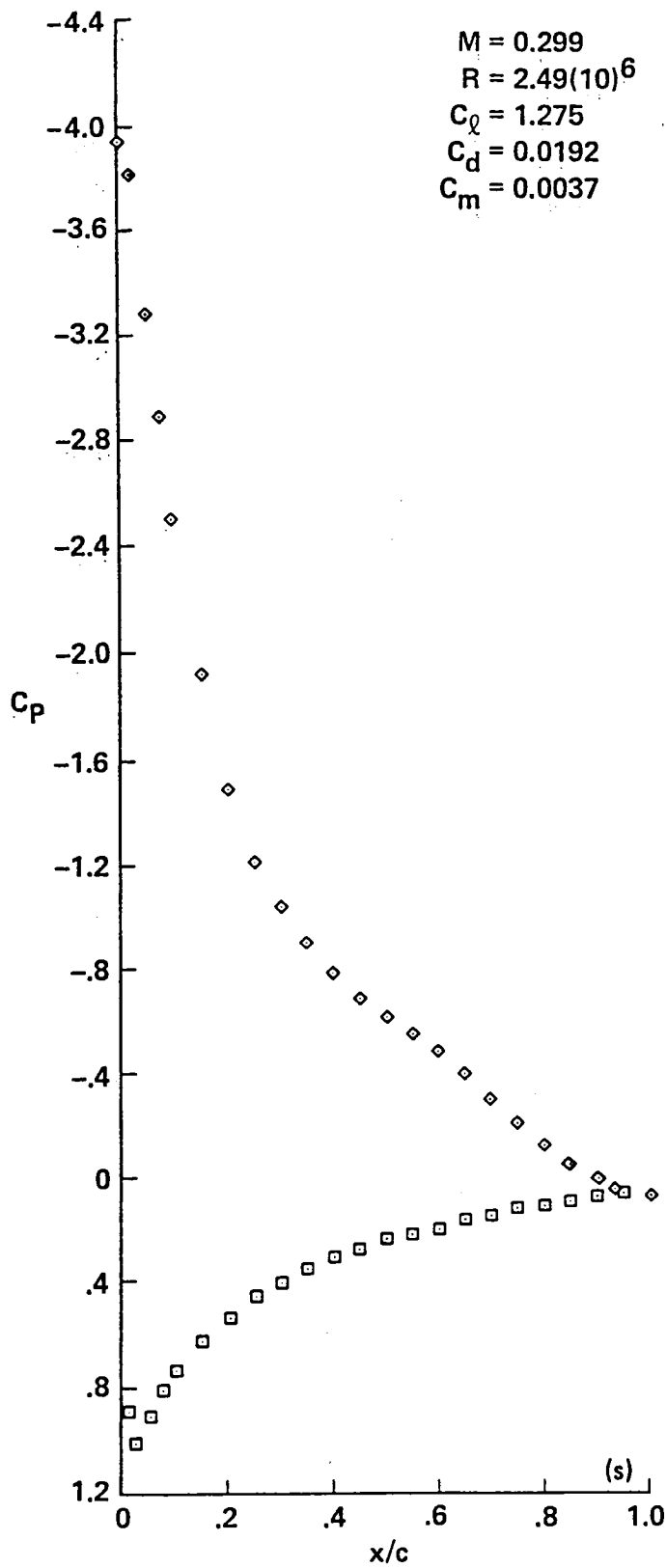


Figure 4.- Continued.

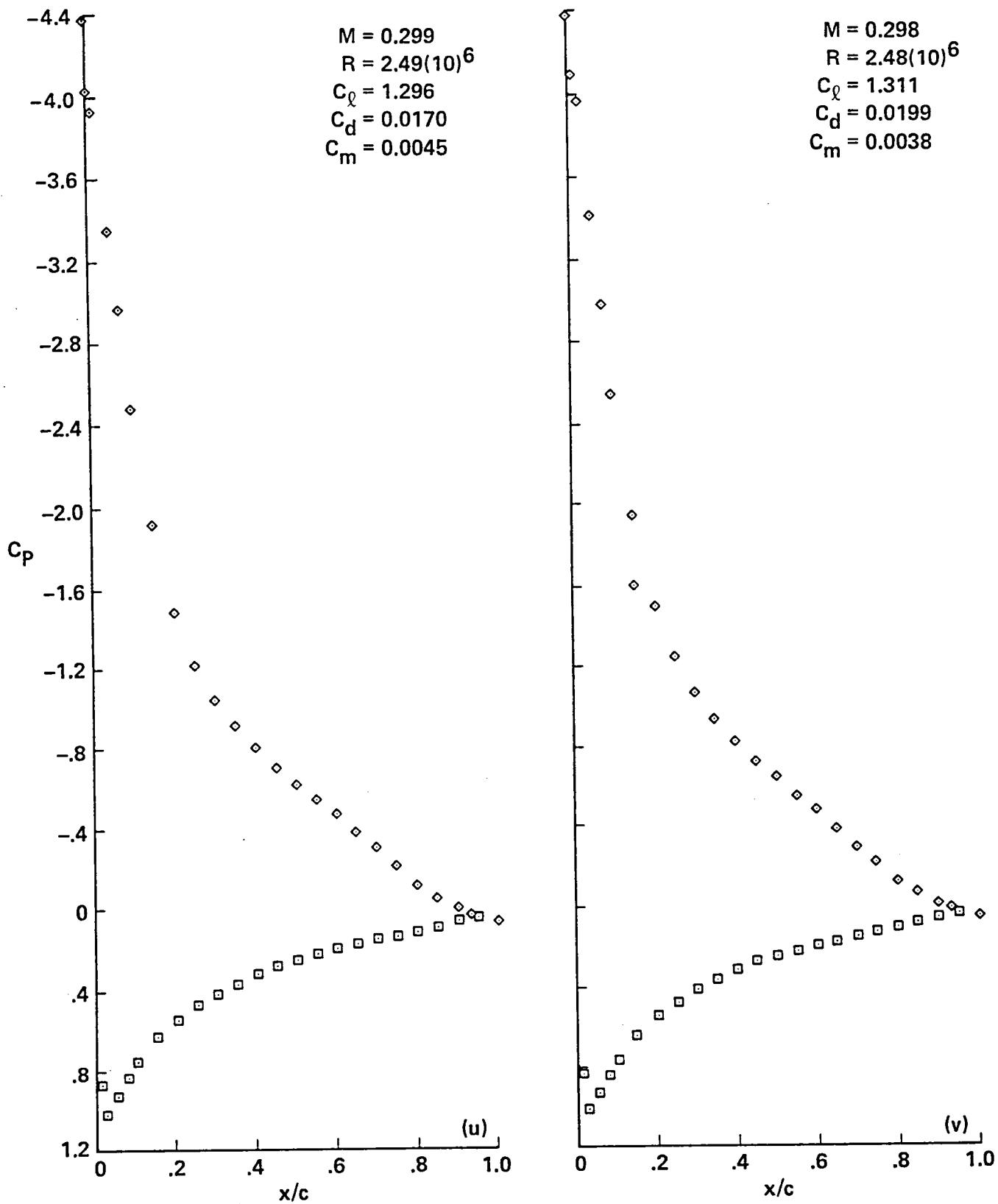


Figure 4.- Continued.

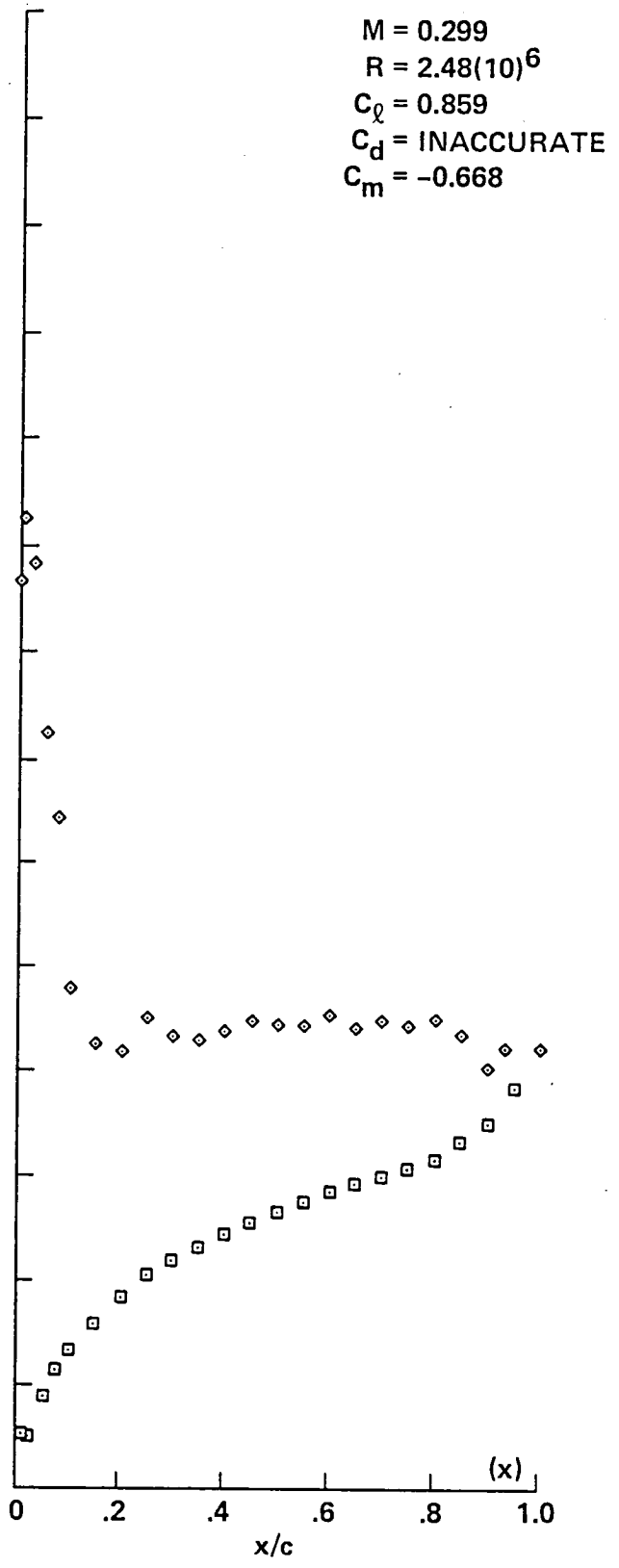
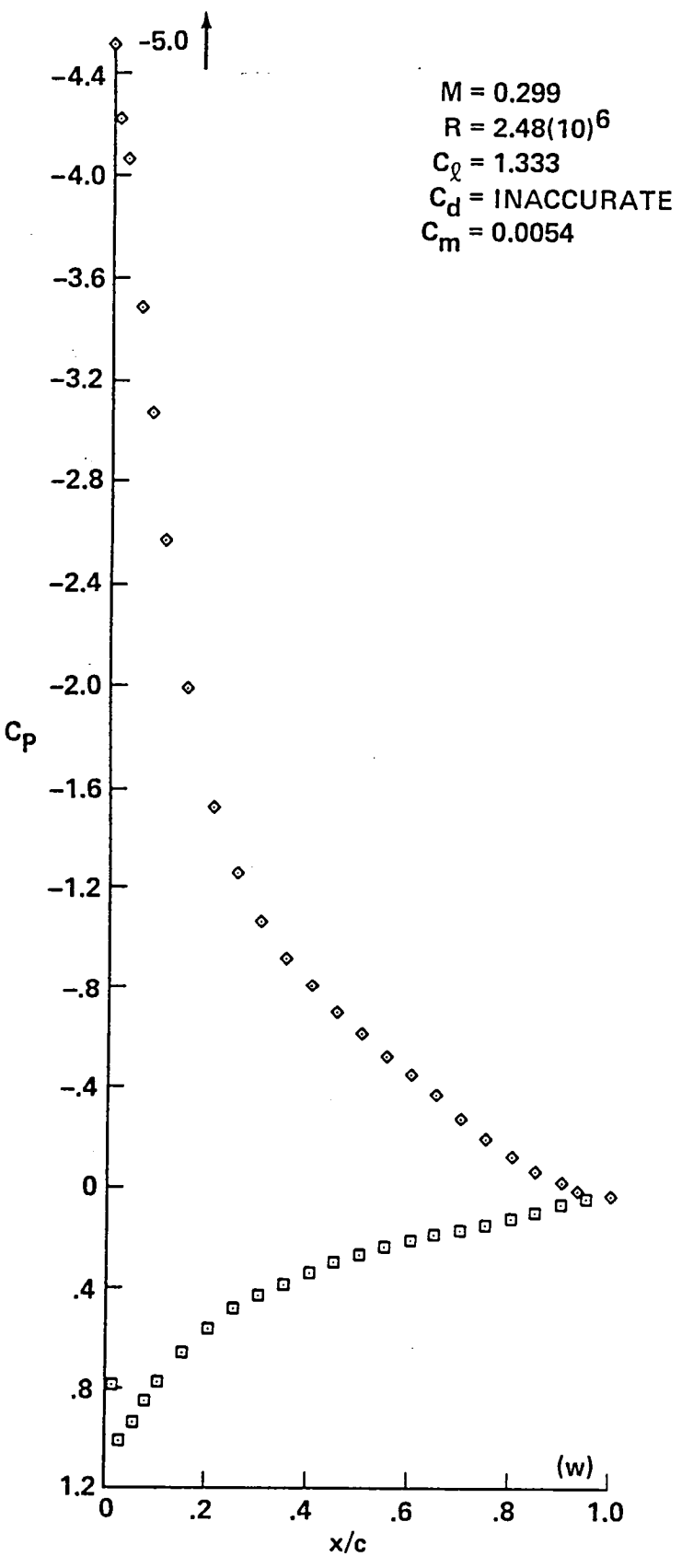


Figure 4.- Concluded.

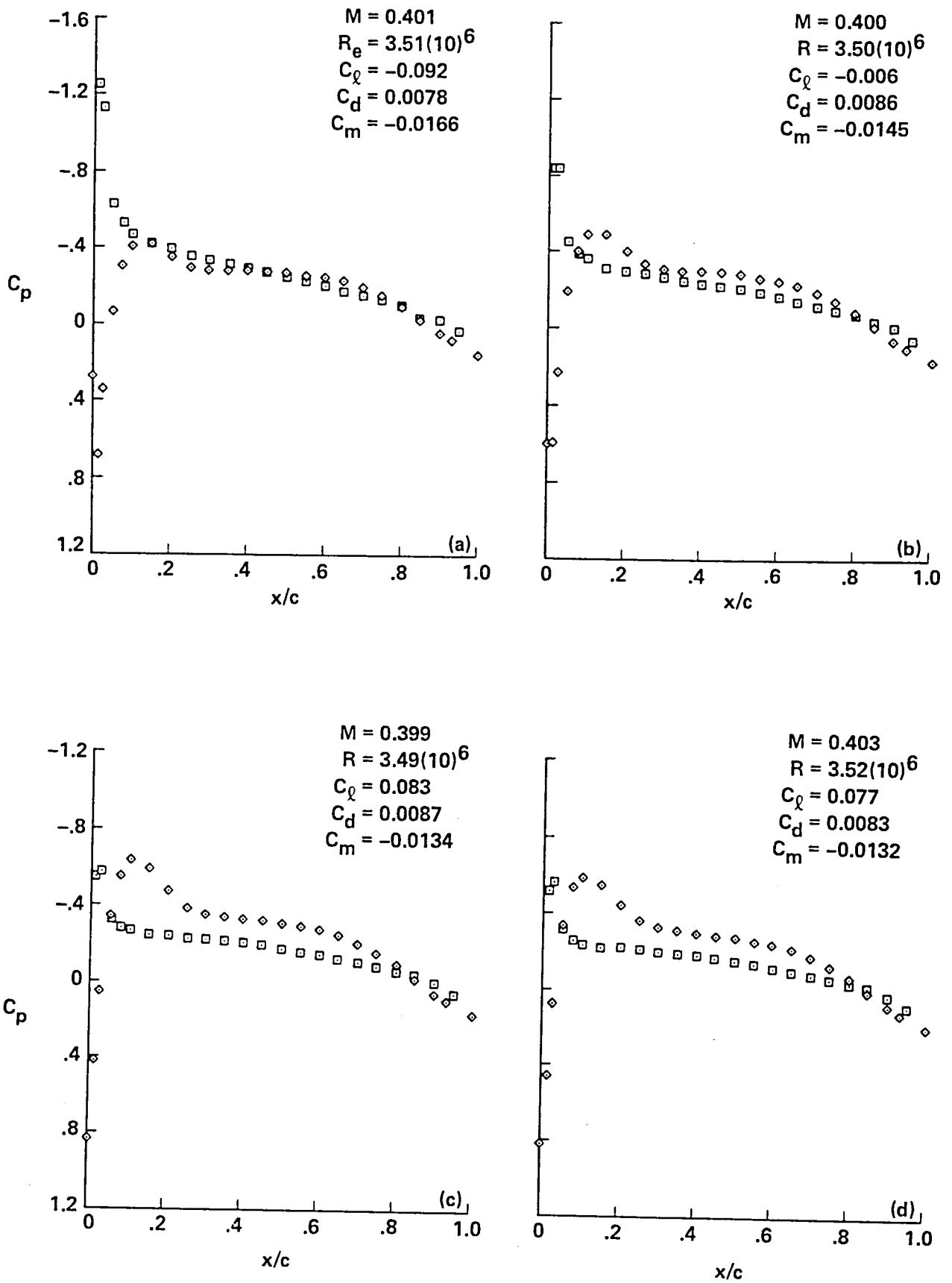


Figure 5.- Pressure distributors for A-1 airfoil, $M_{set} = 0.4$.

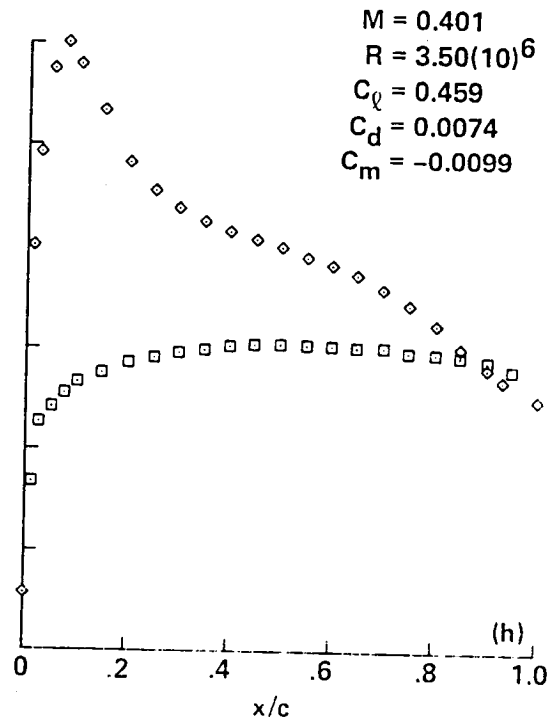
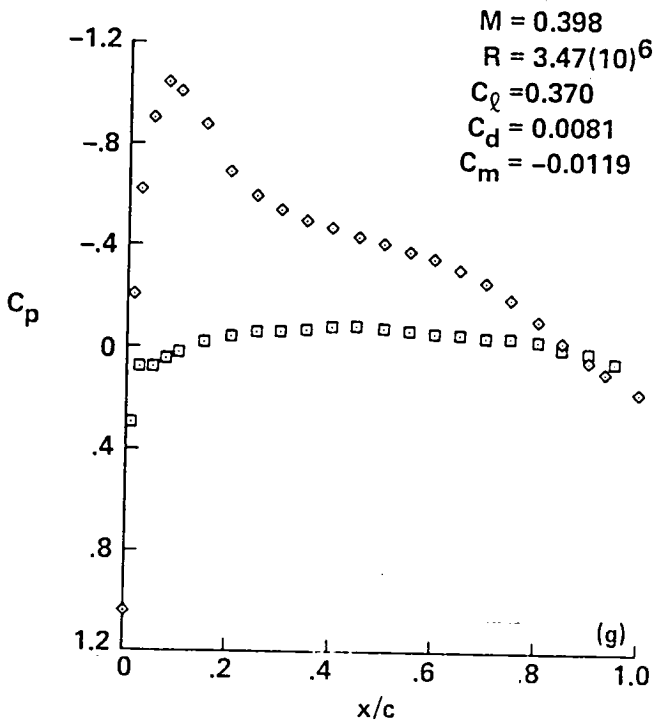
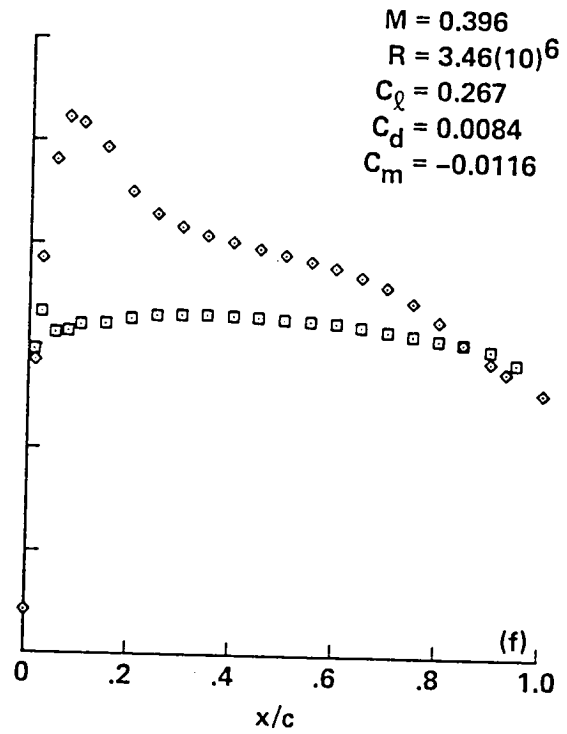
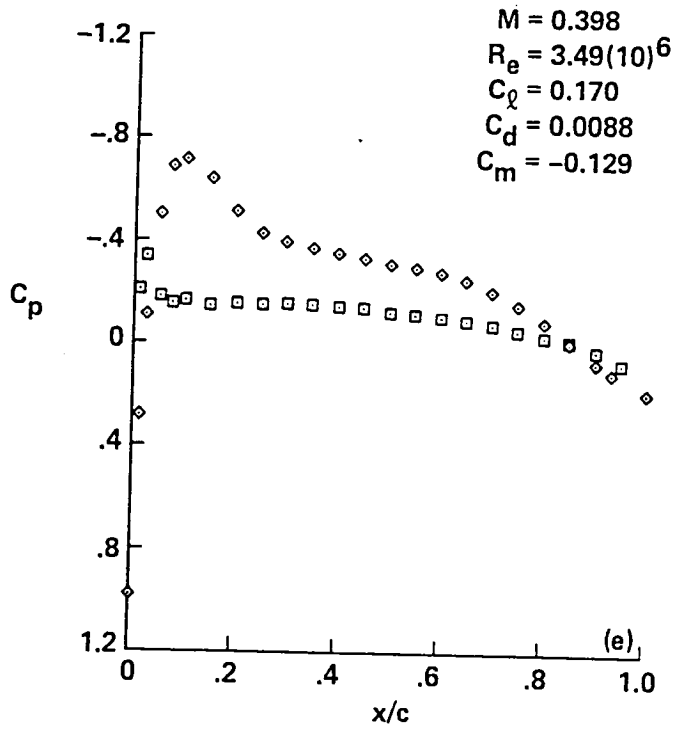


Figure 5.- Continued.

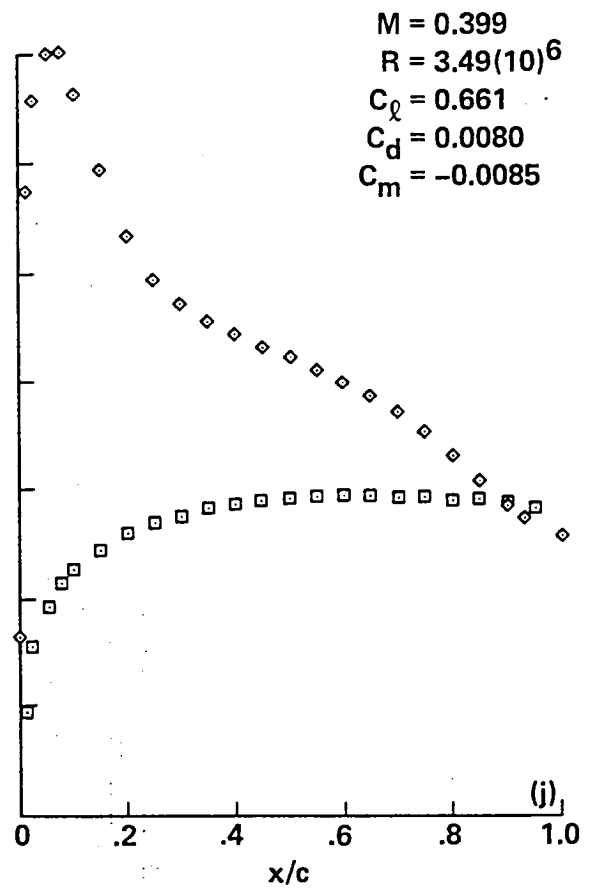
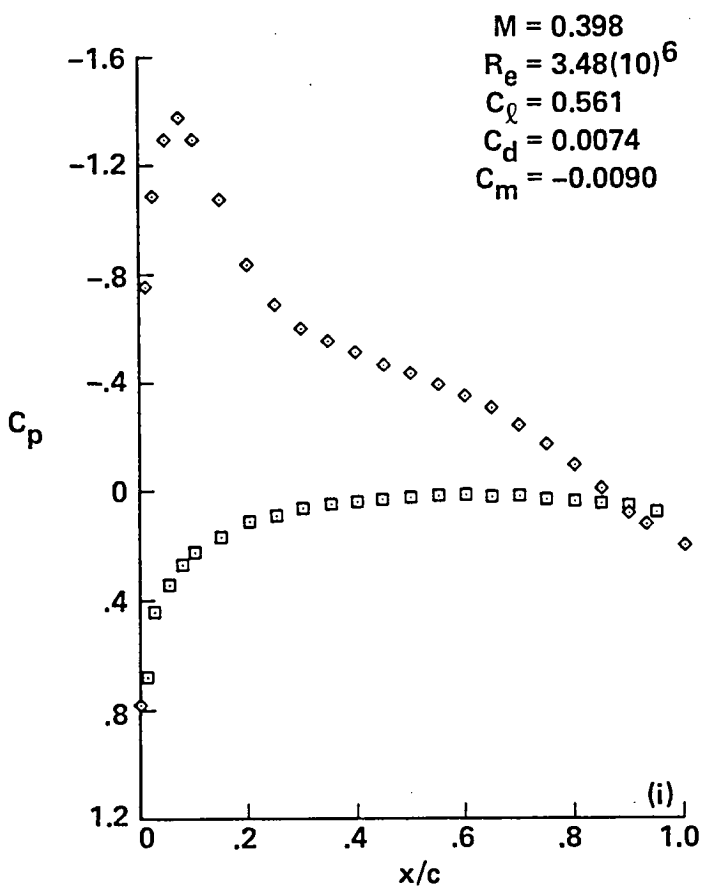


Figure 5.- Continued.

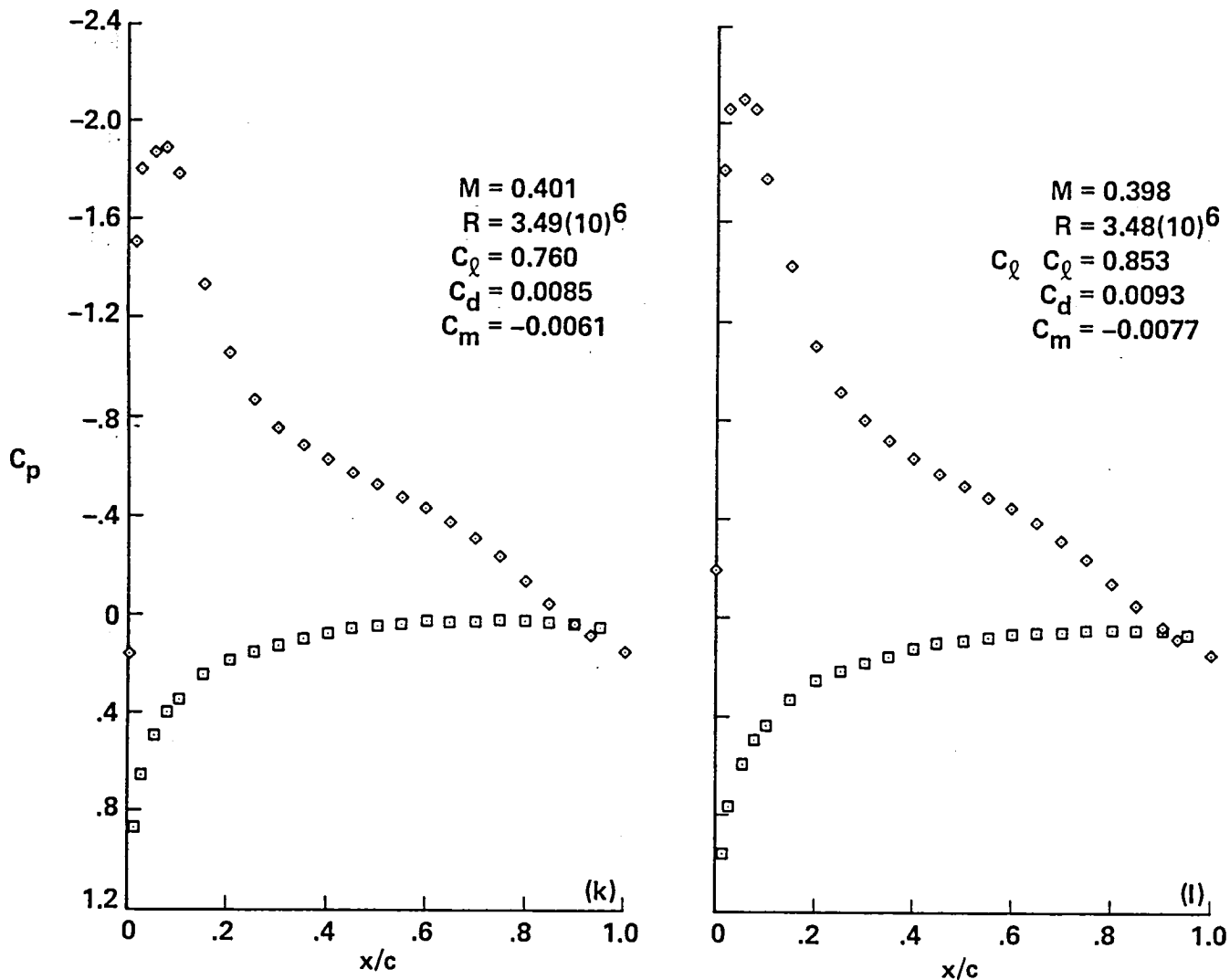


Figure 5.- Continued.

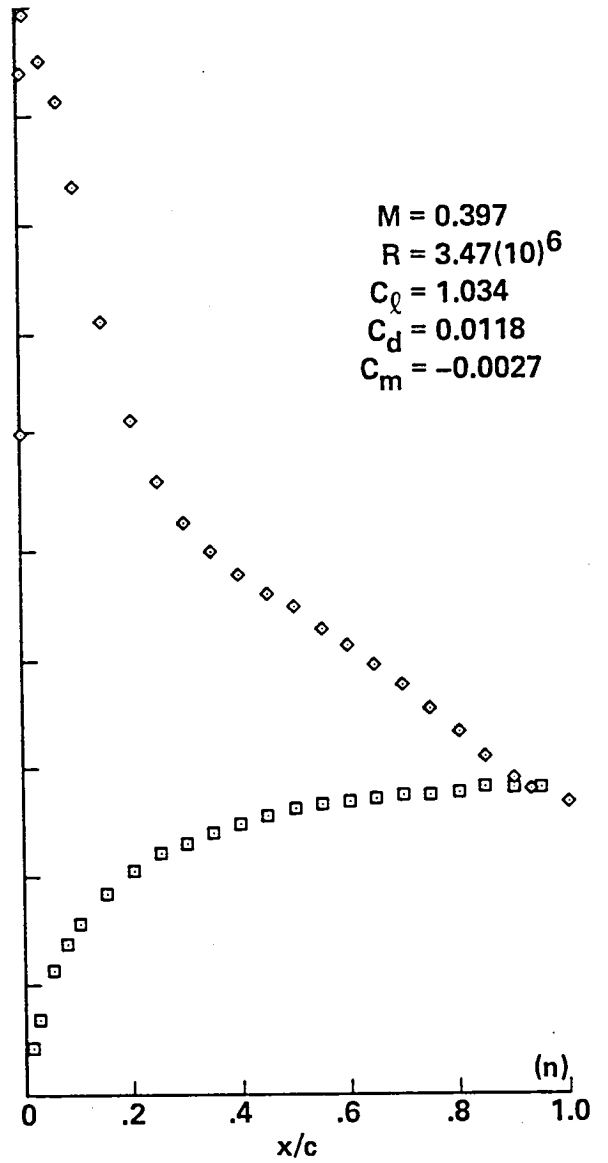
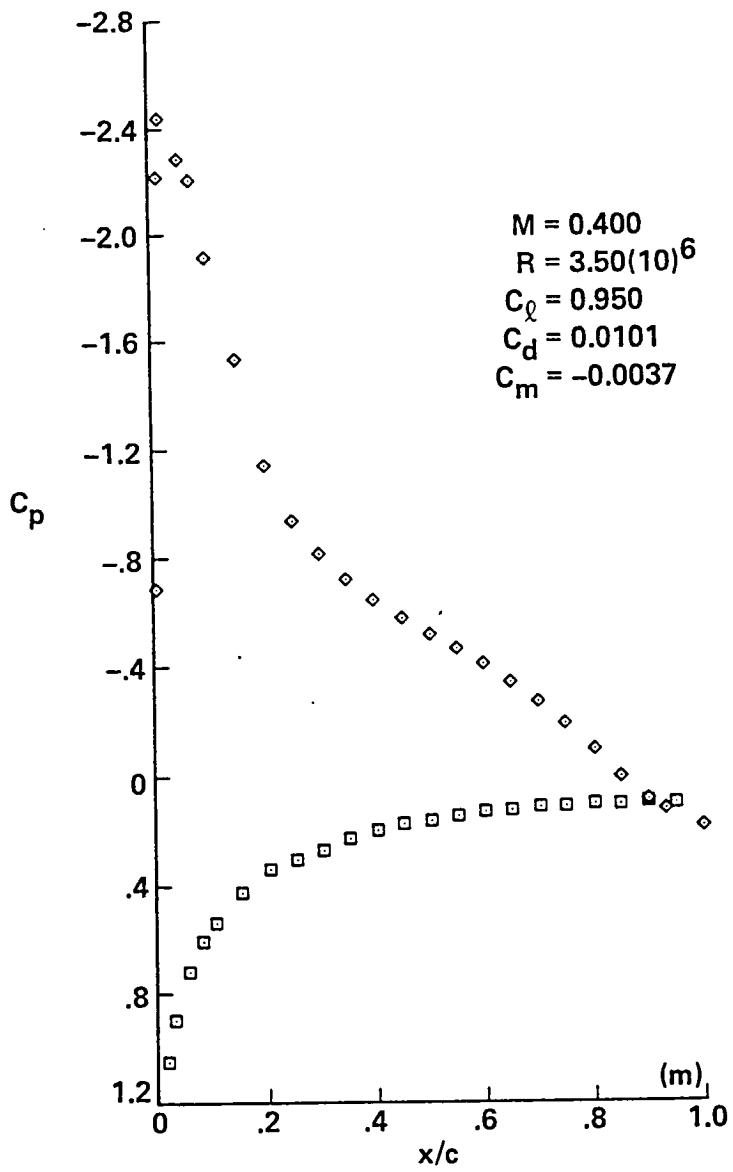


Figure 5.- Continued.

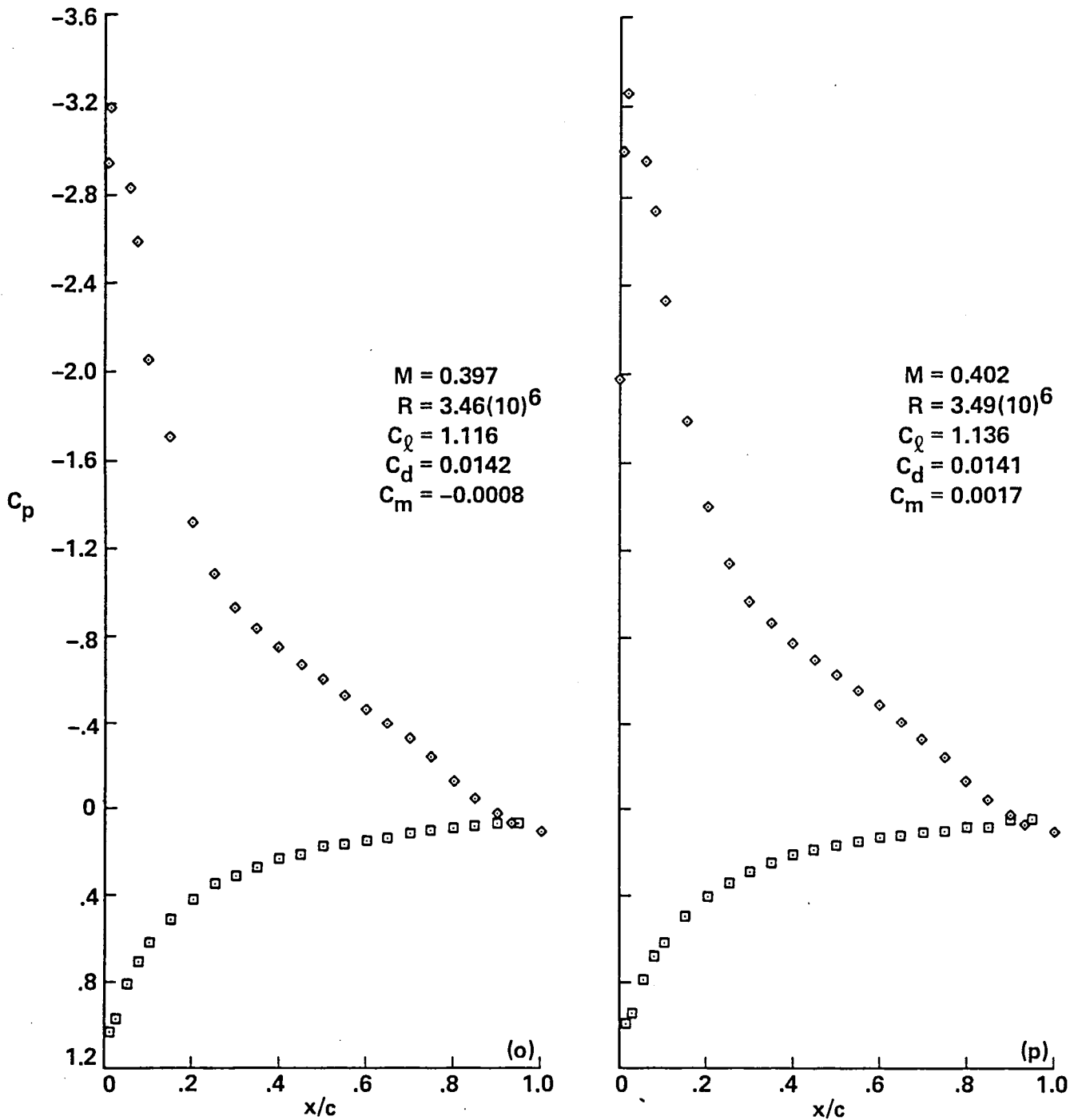


Figure 5.- Continued.

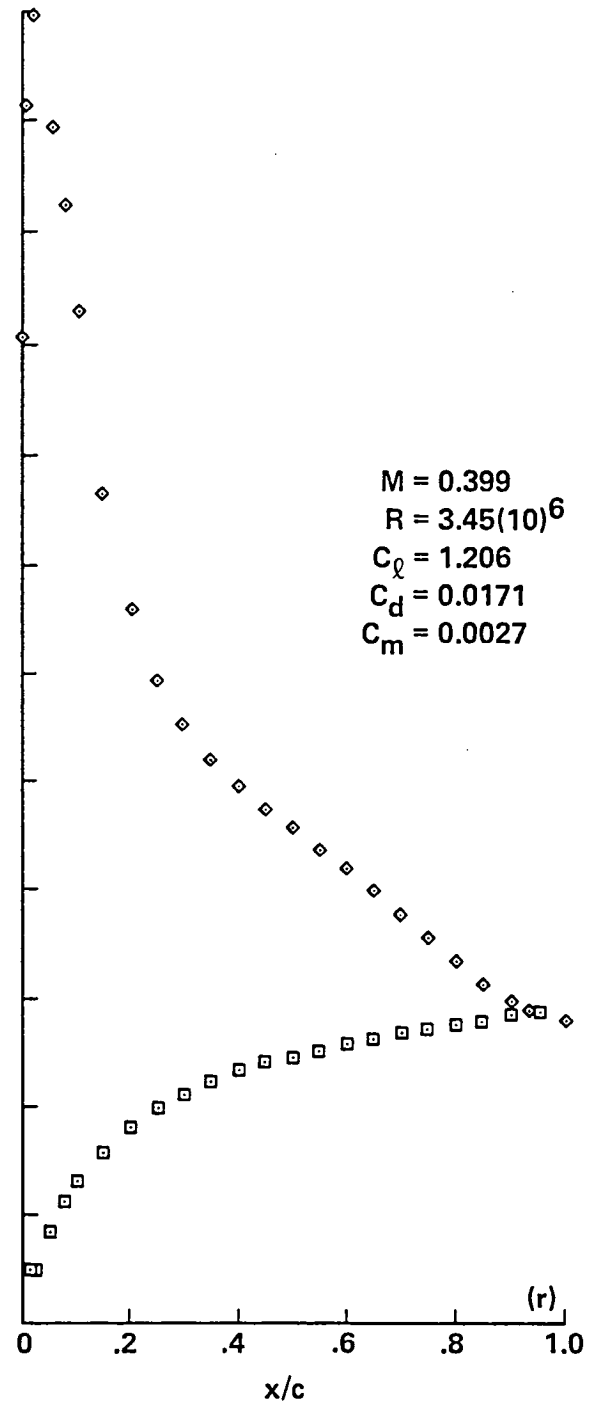
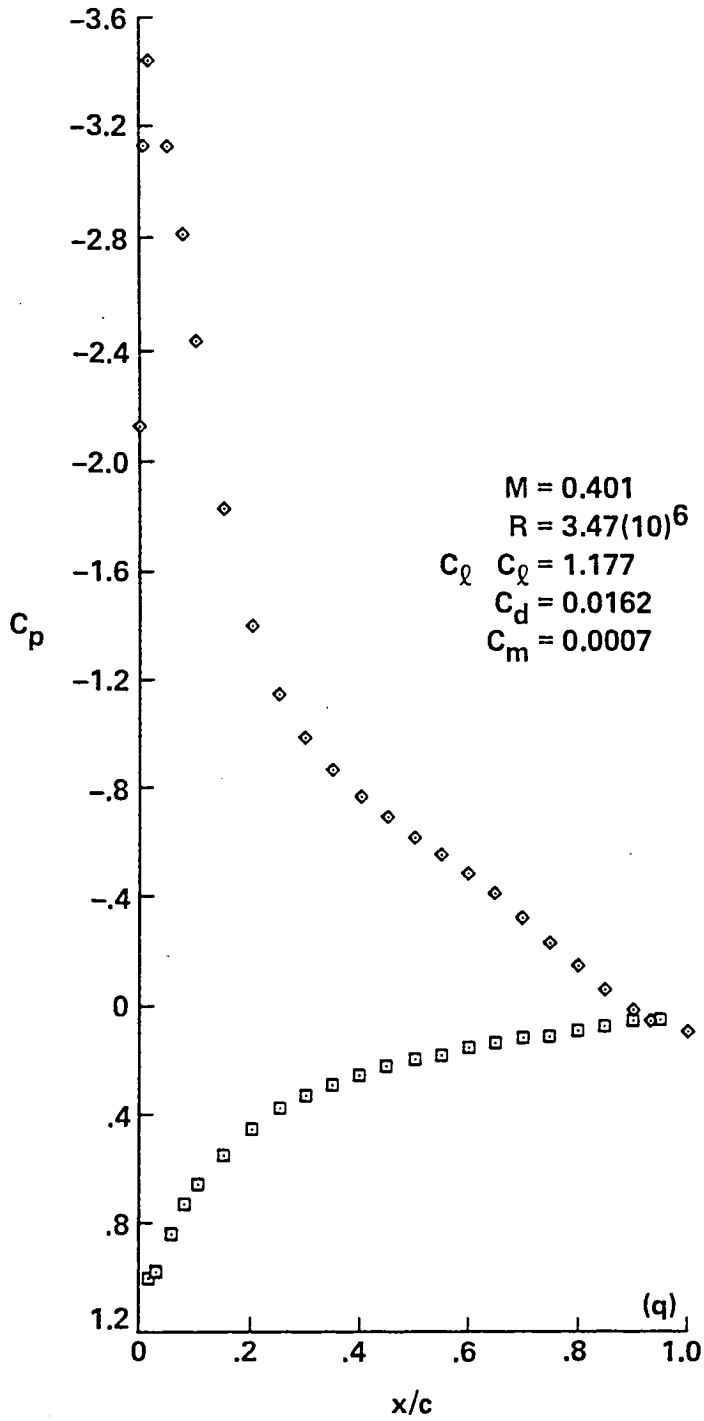


Figure 5.- Continued.

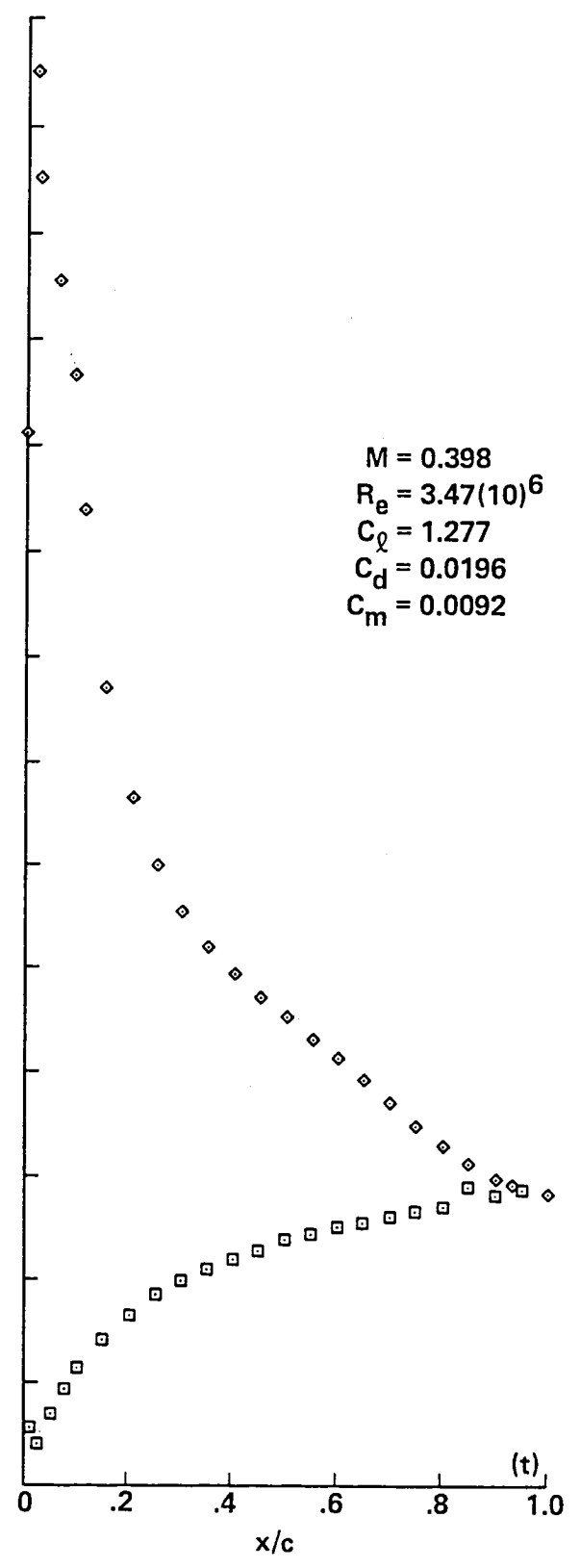
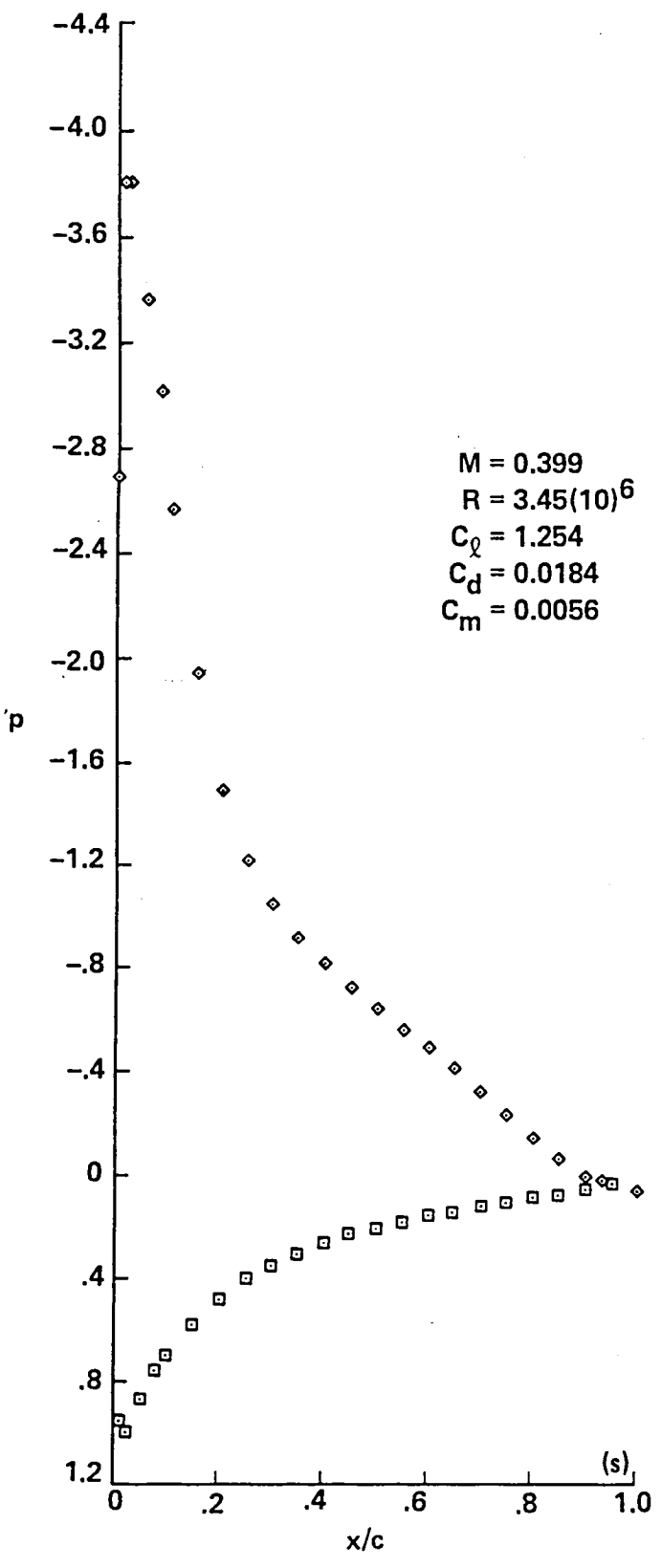


Figure 5.- Continued.

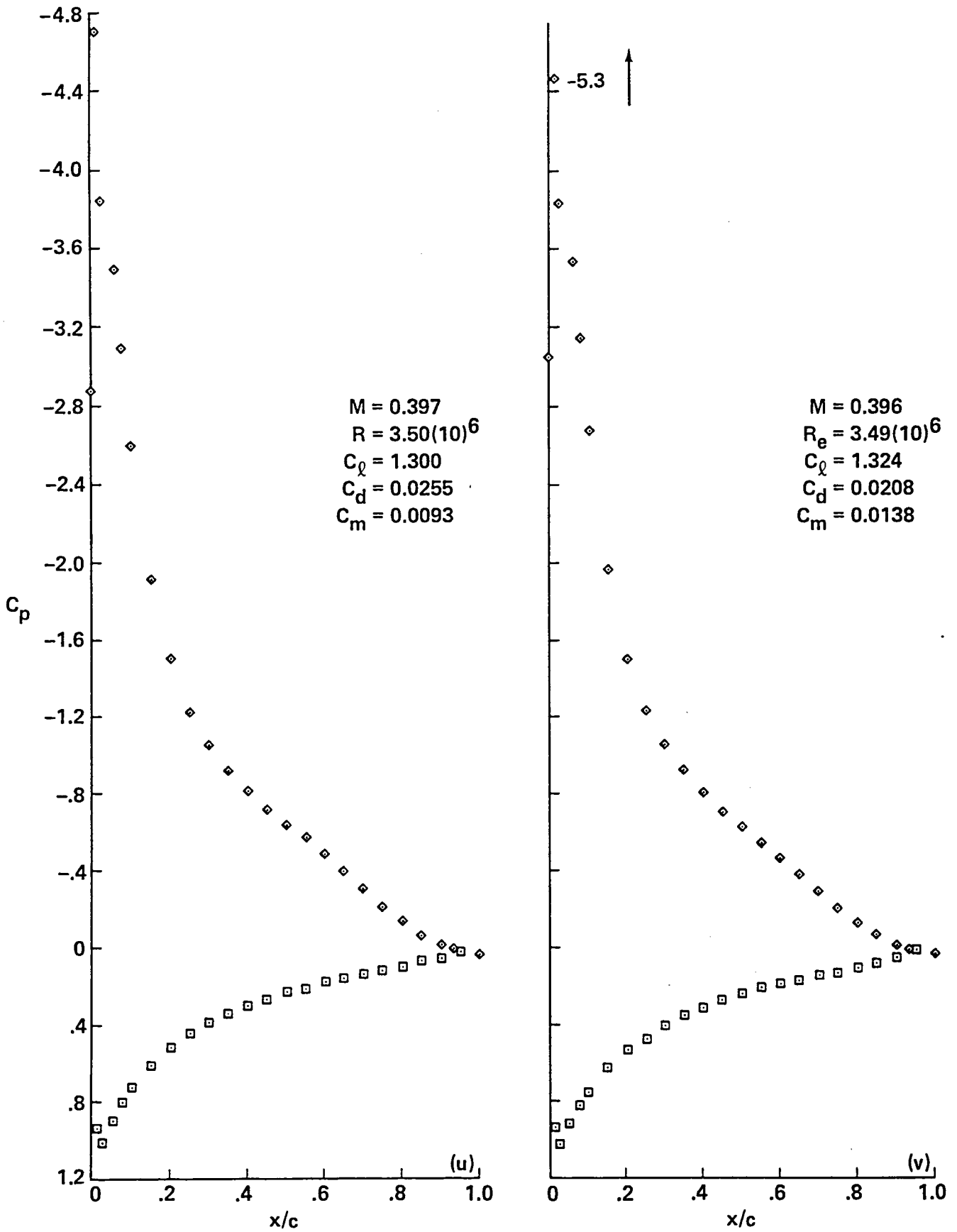


Figure 5.- Concluded.

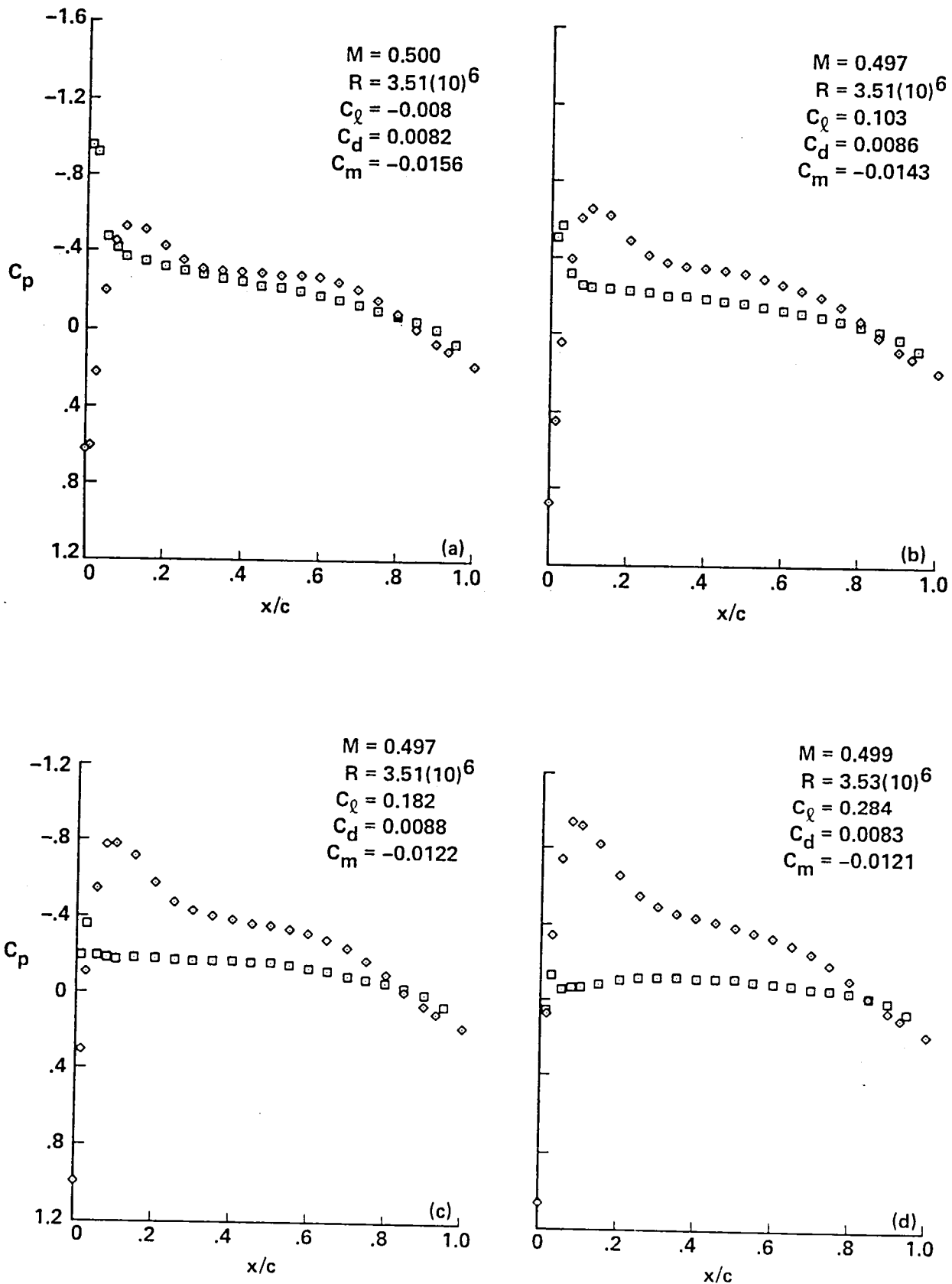


Figure 6.- Pressure distributions for A-1 airfoil, $M_{set} = 0.5$.

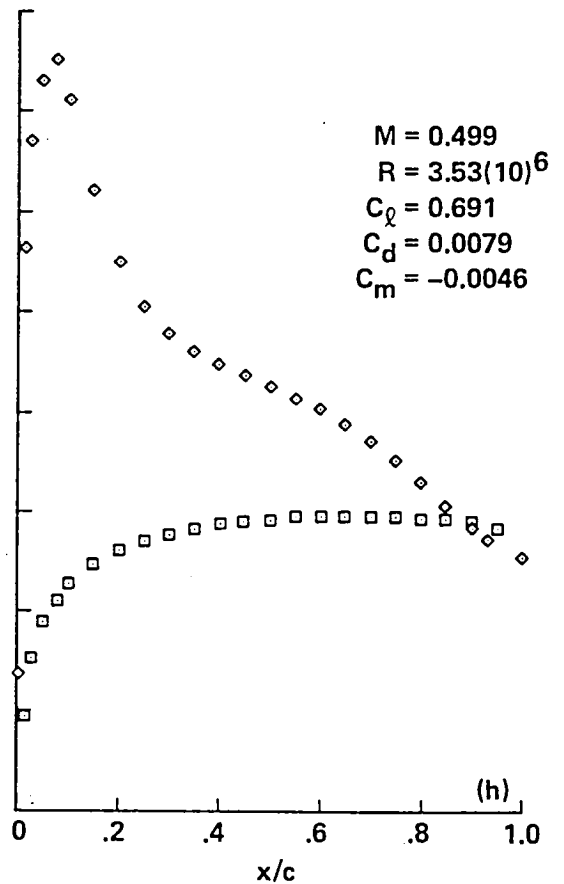
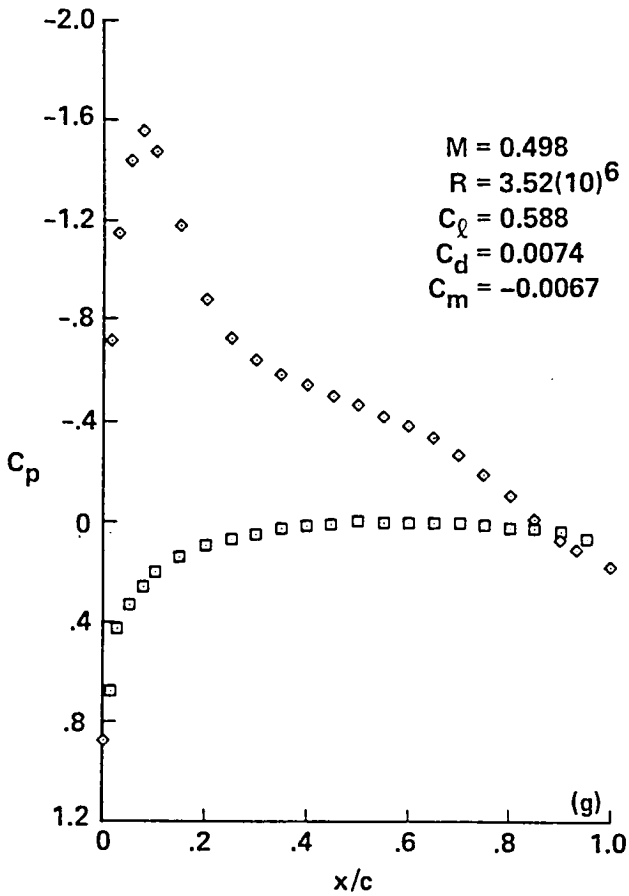
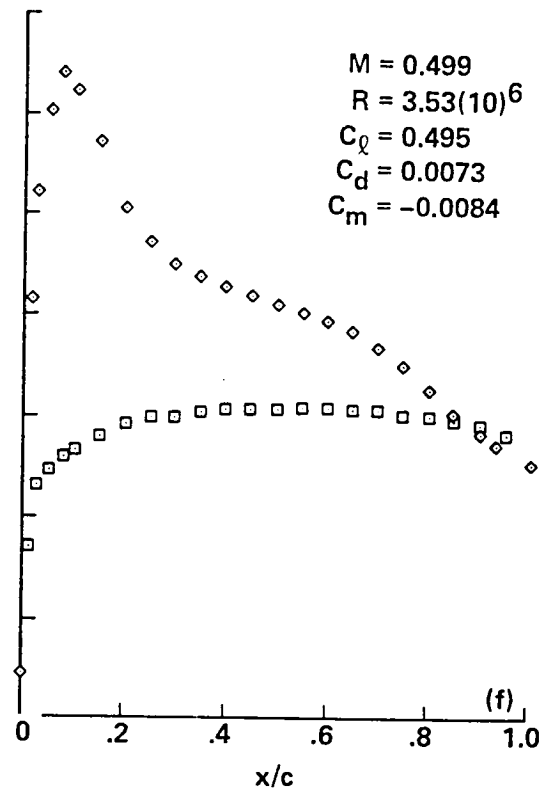
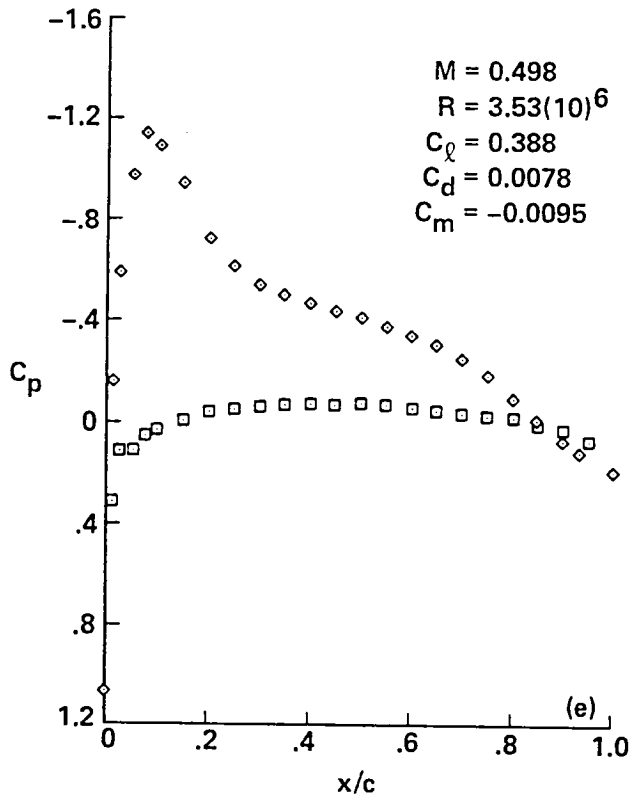


Figure 6.- Continued.

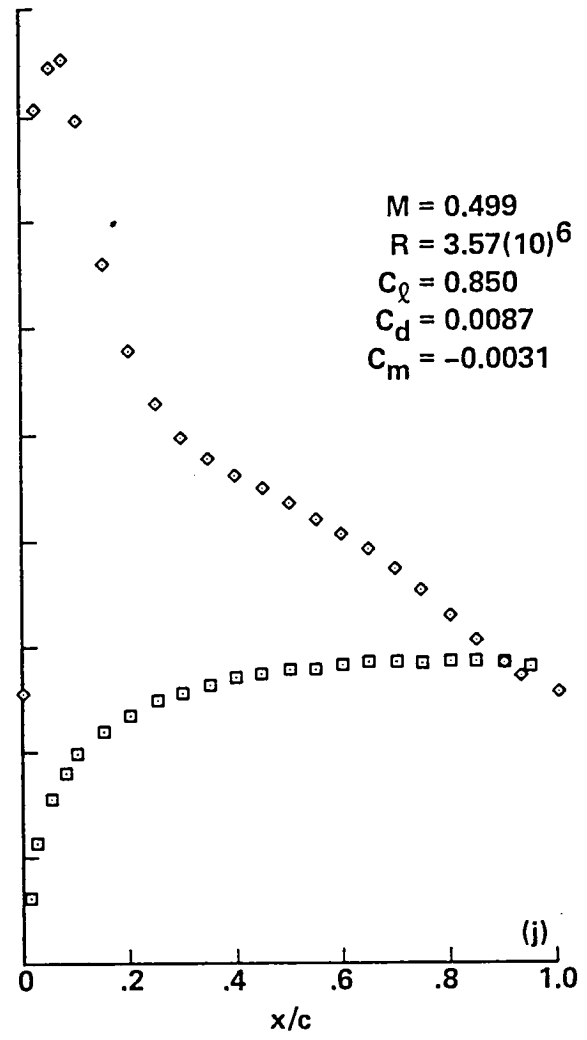
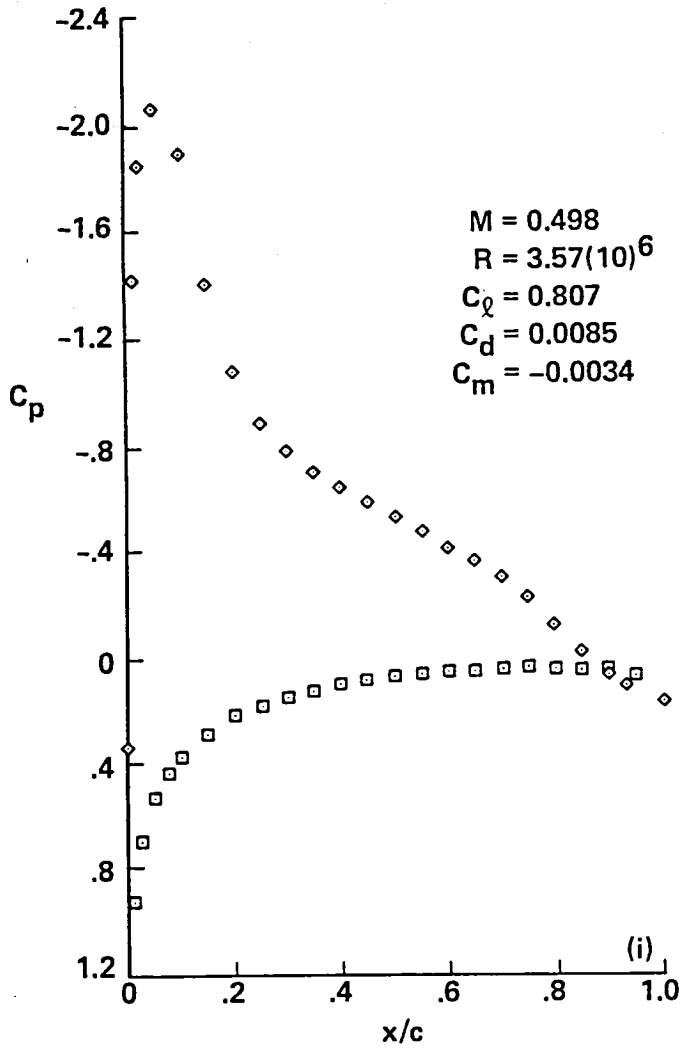


Figure 6.- Continued.

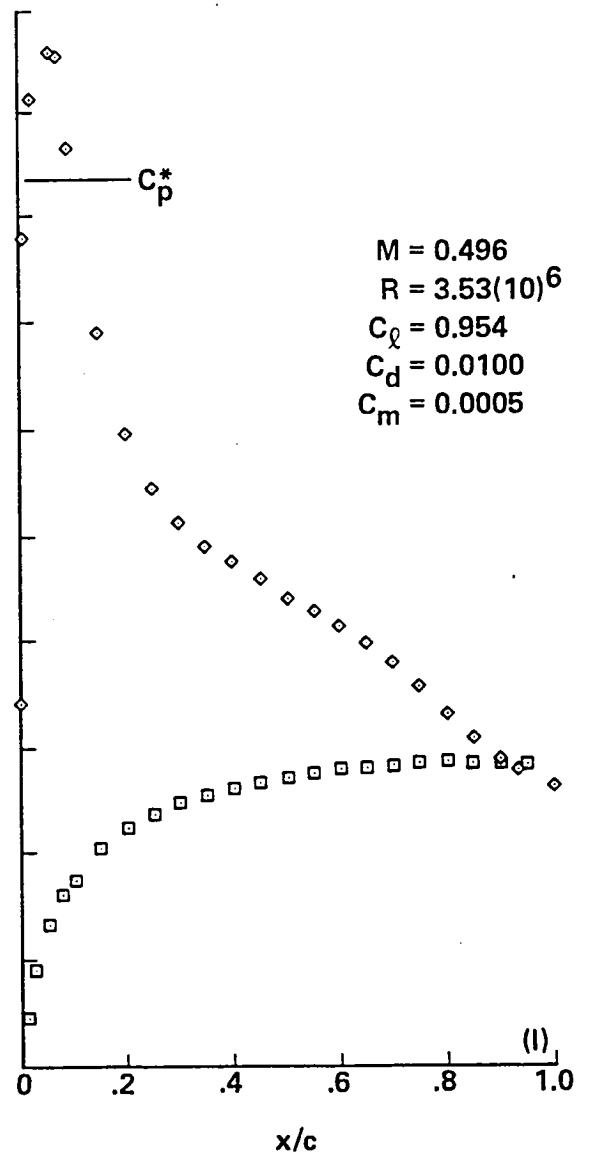
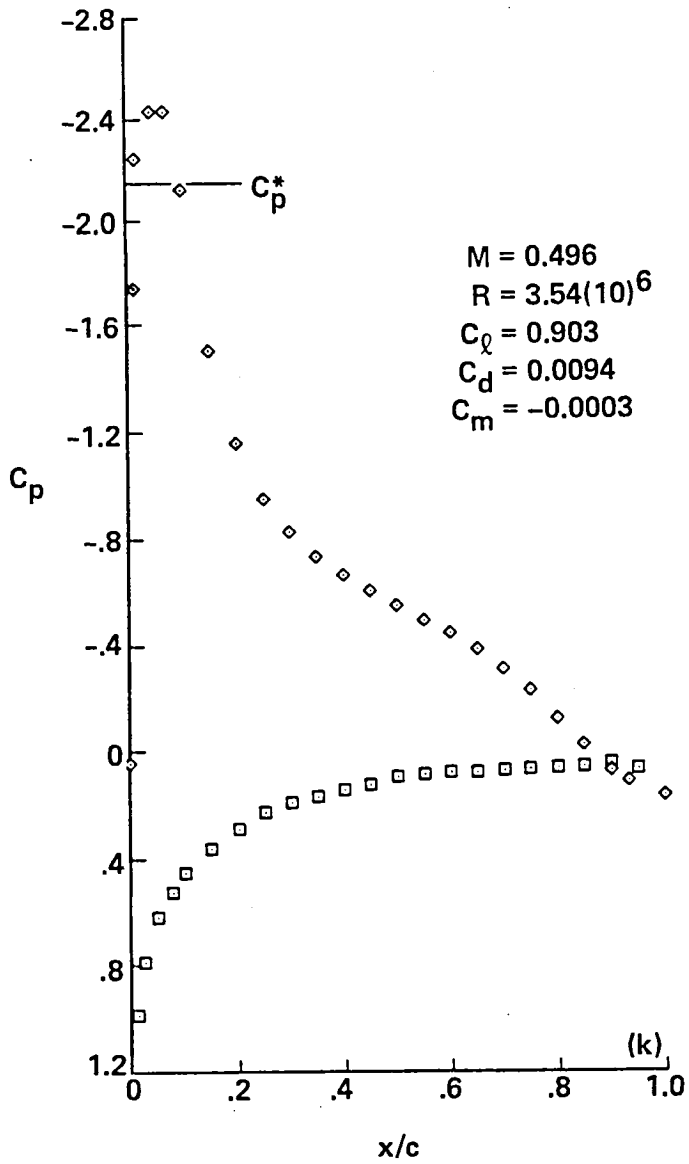


Figure 6.- Continued.

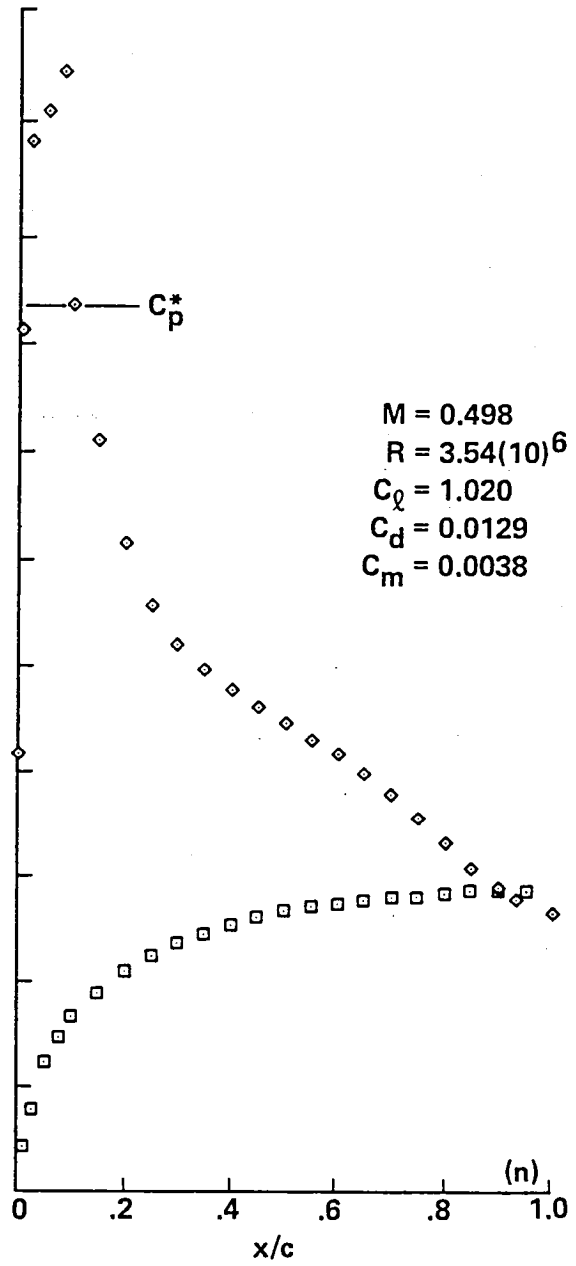
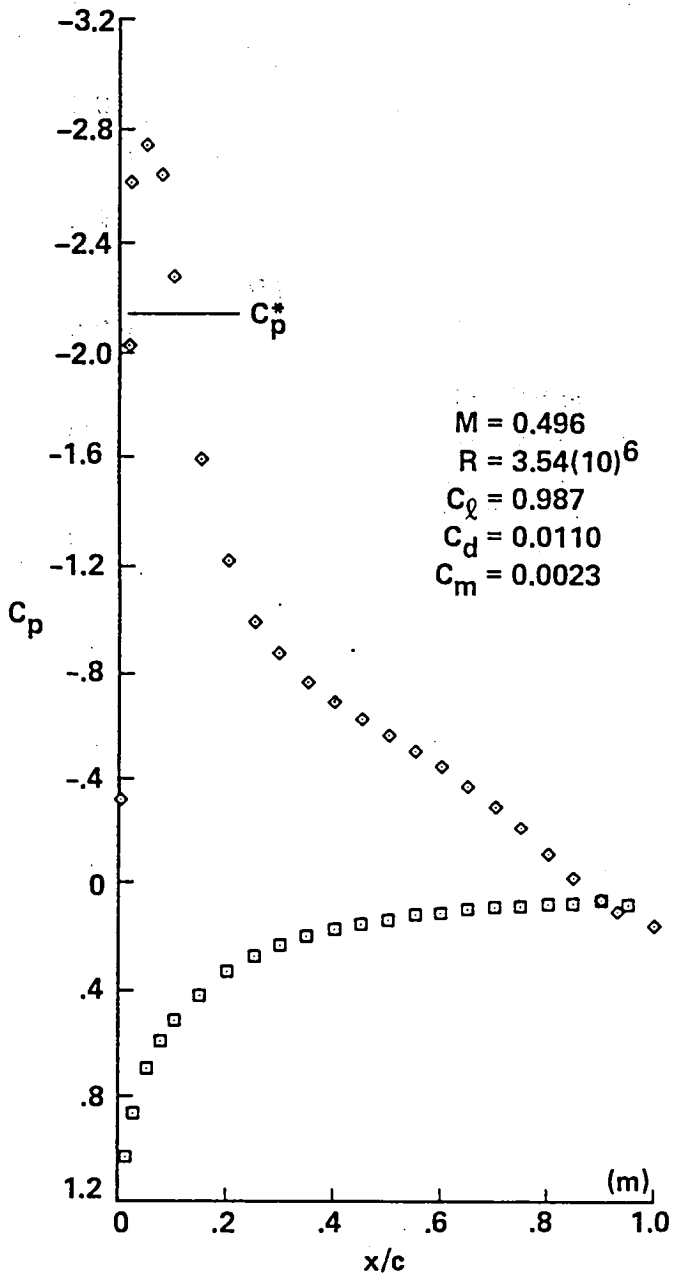


Figure 6.- Continued.

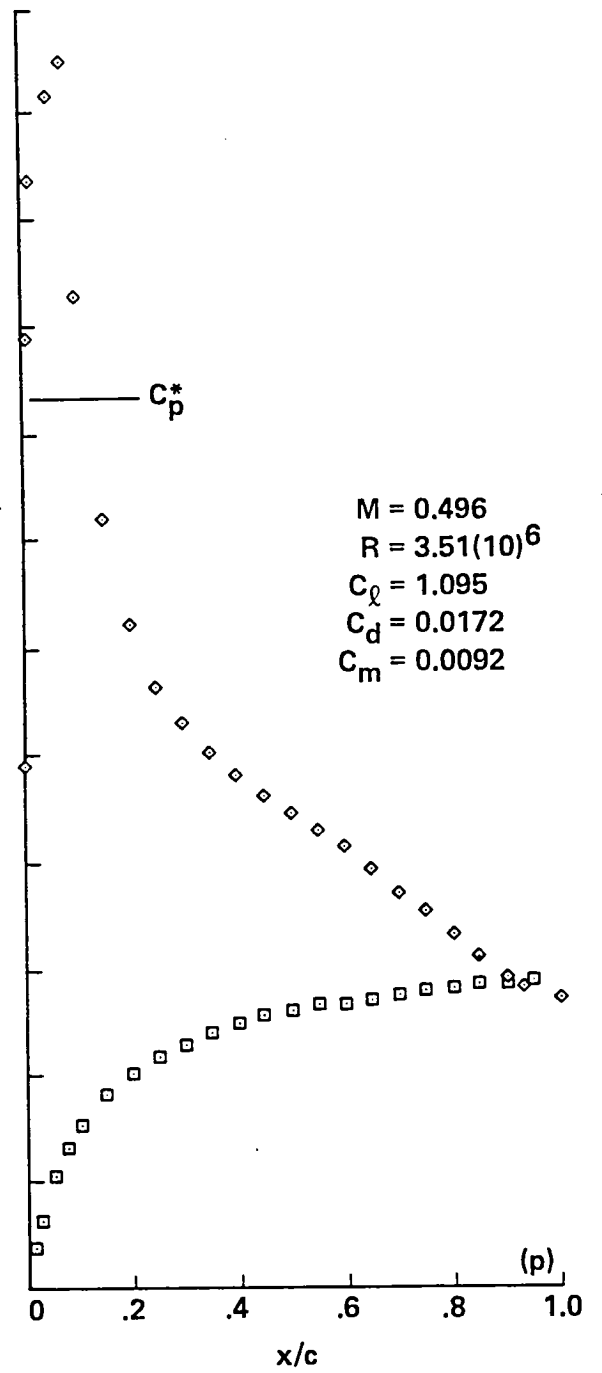
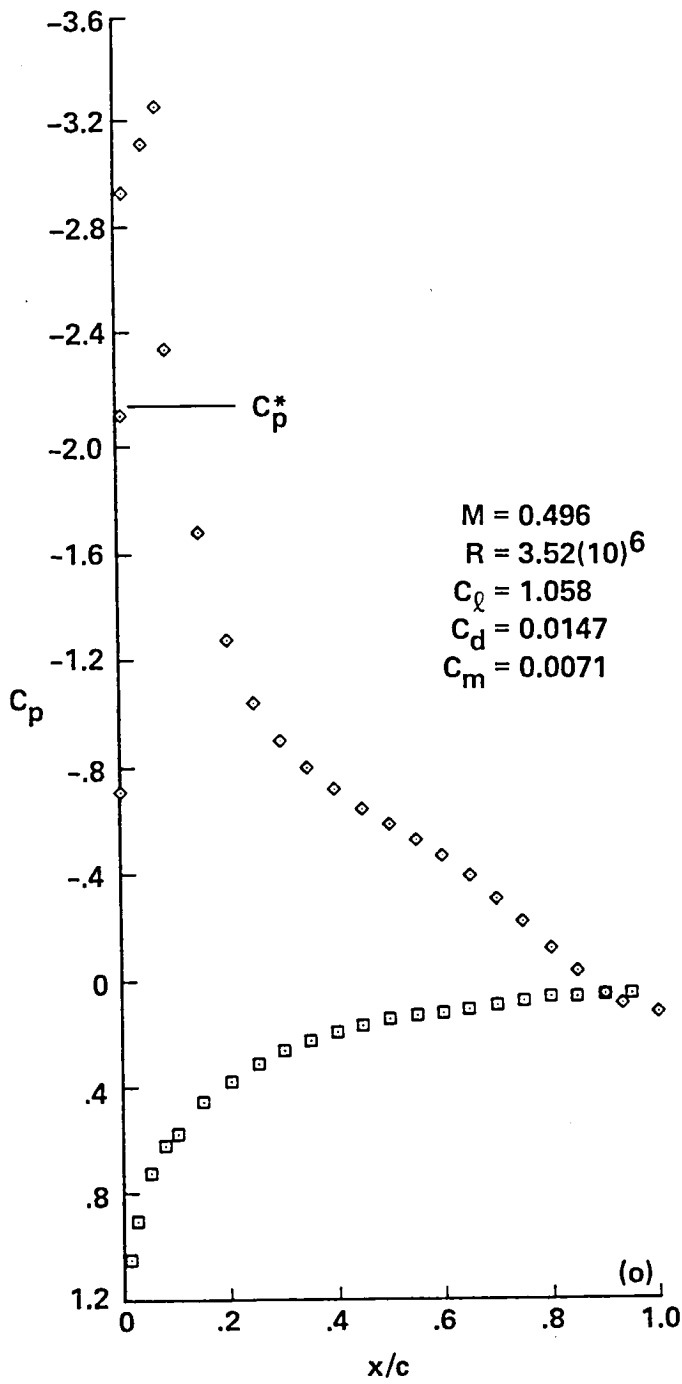


Figure 6.- Continued.

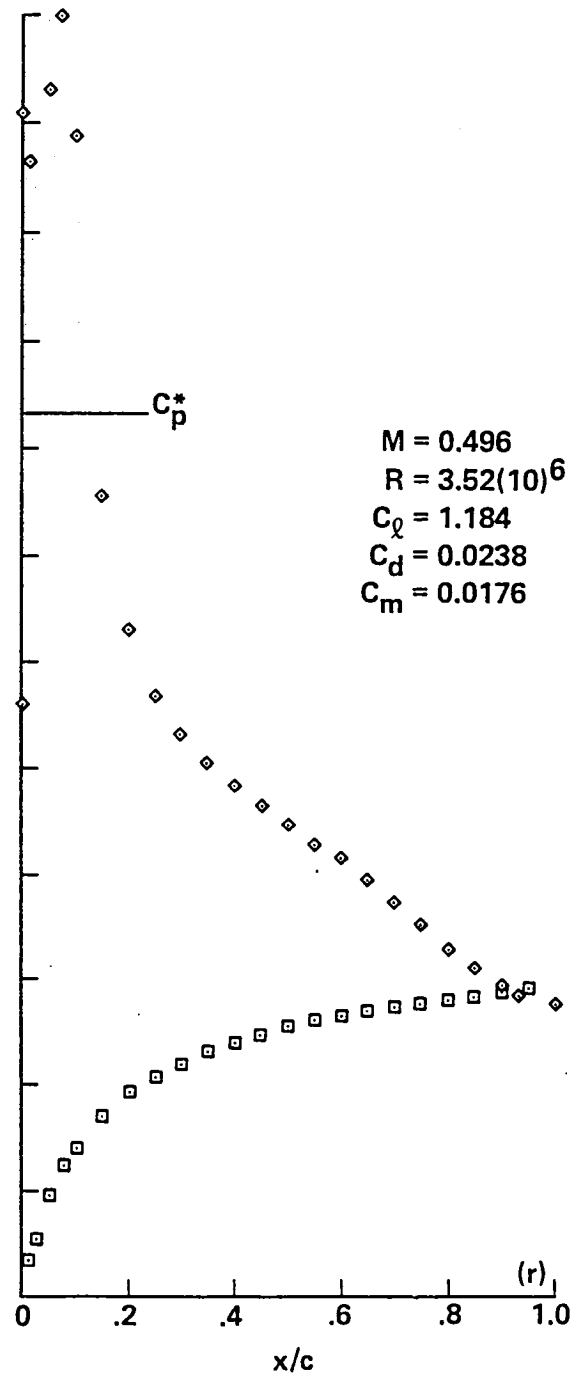
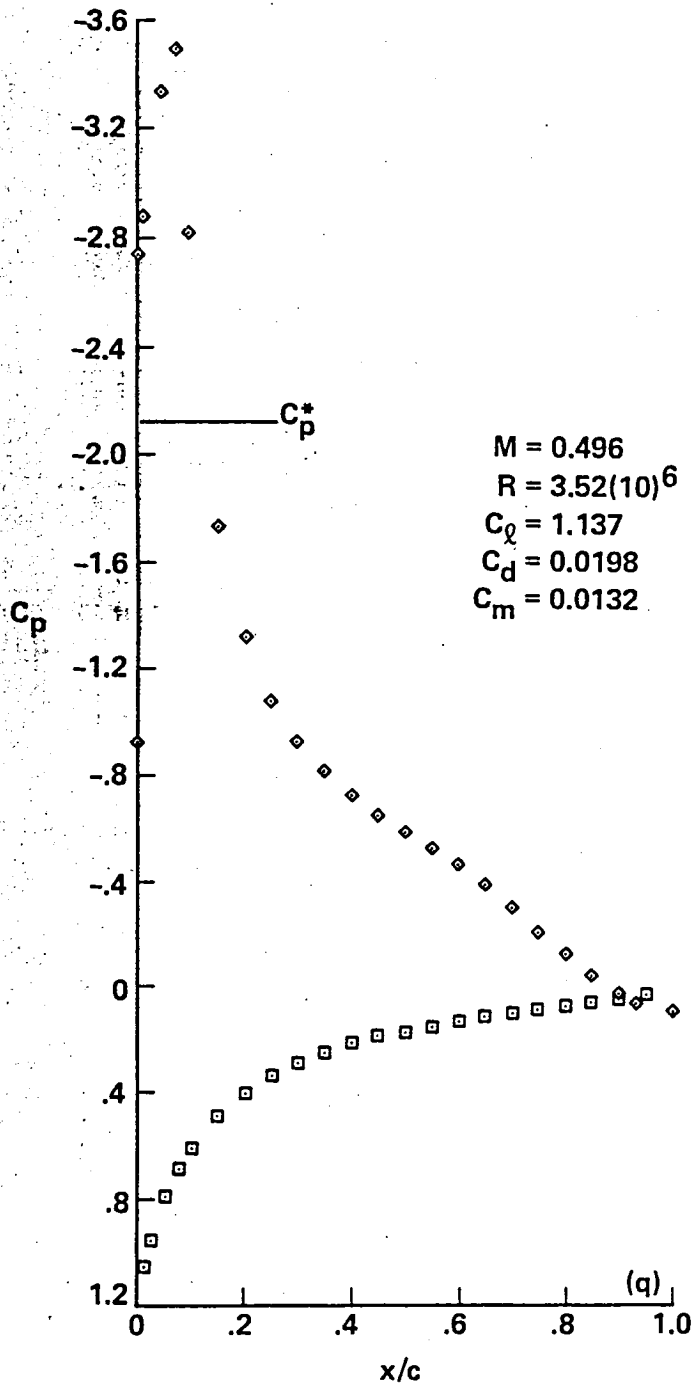


Figure 6.- Continued.

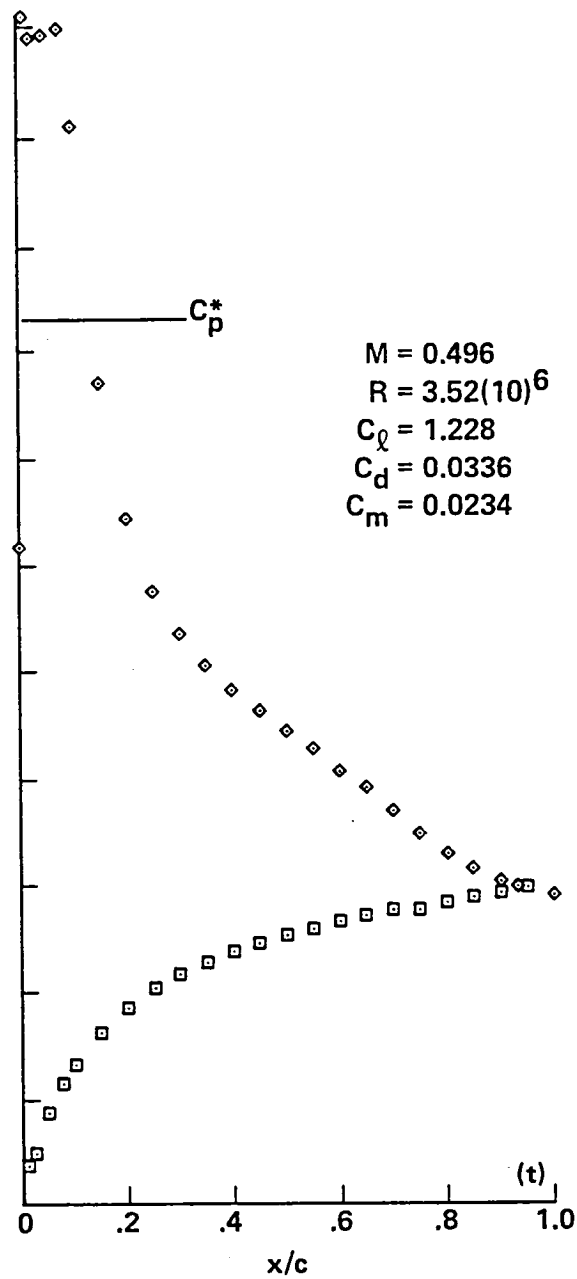
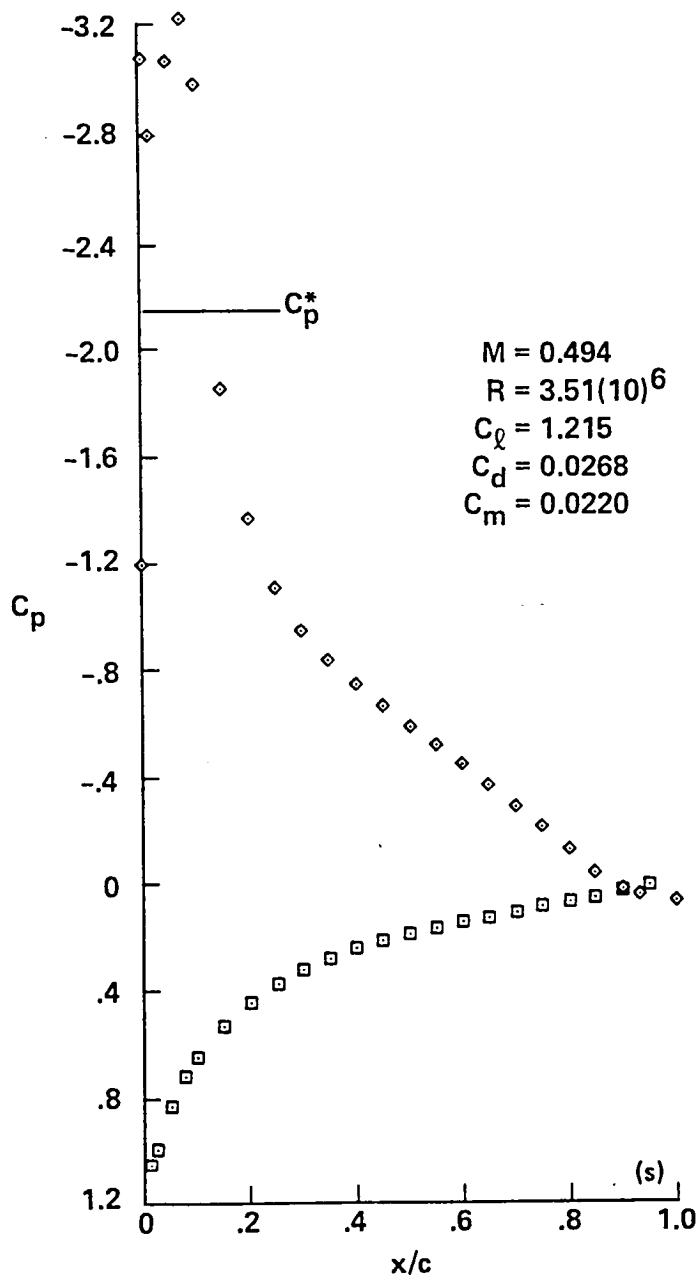


Figure 6.- Continued.

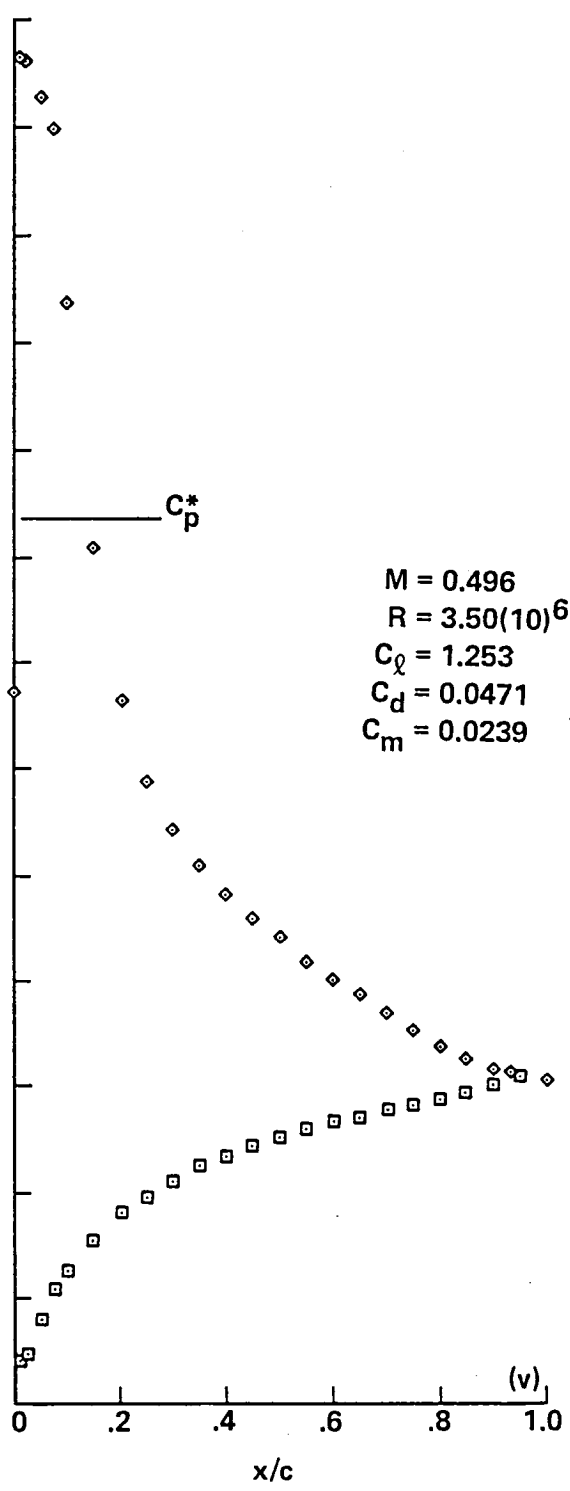
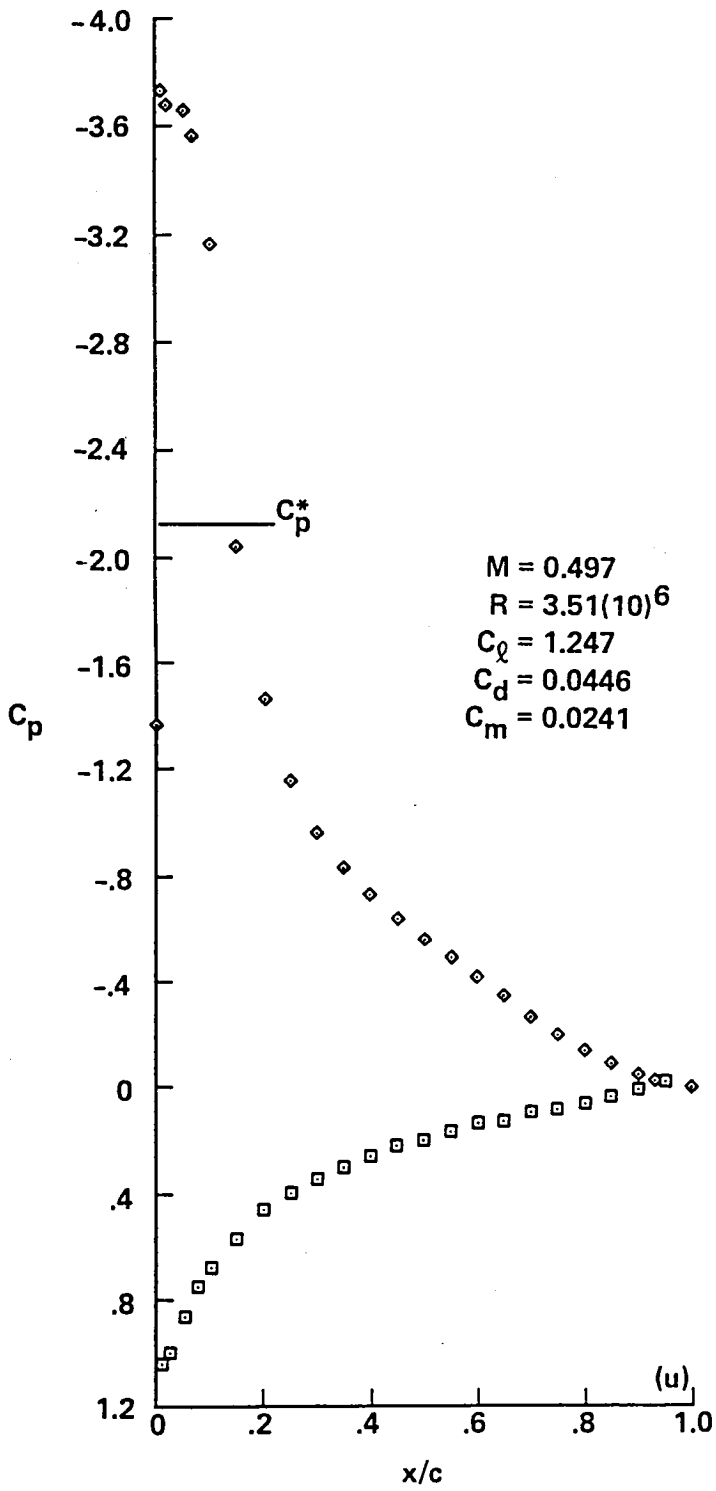


Figure 6.- Continued.

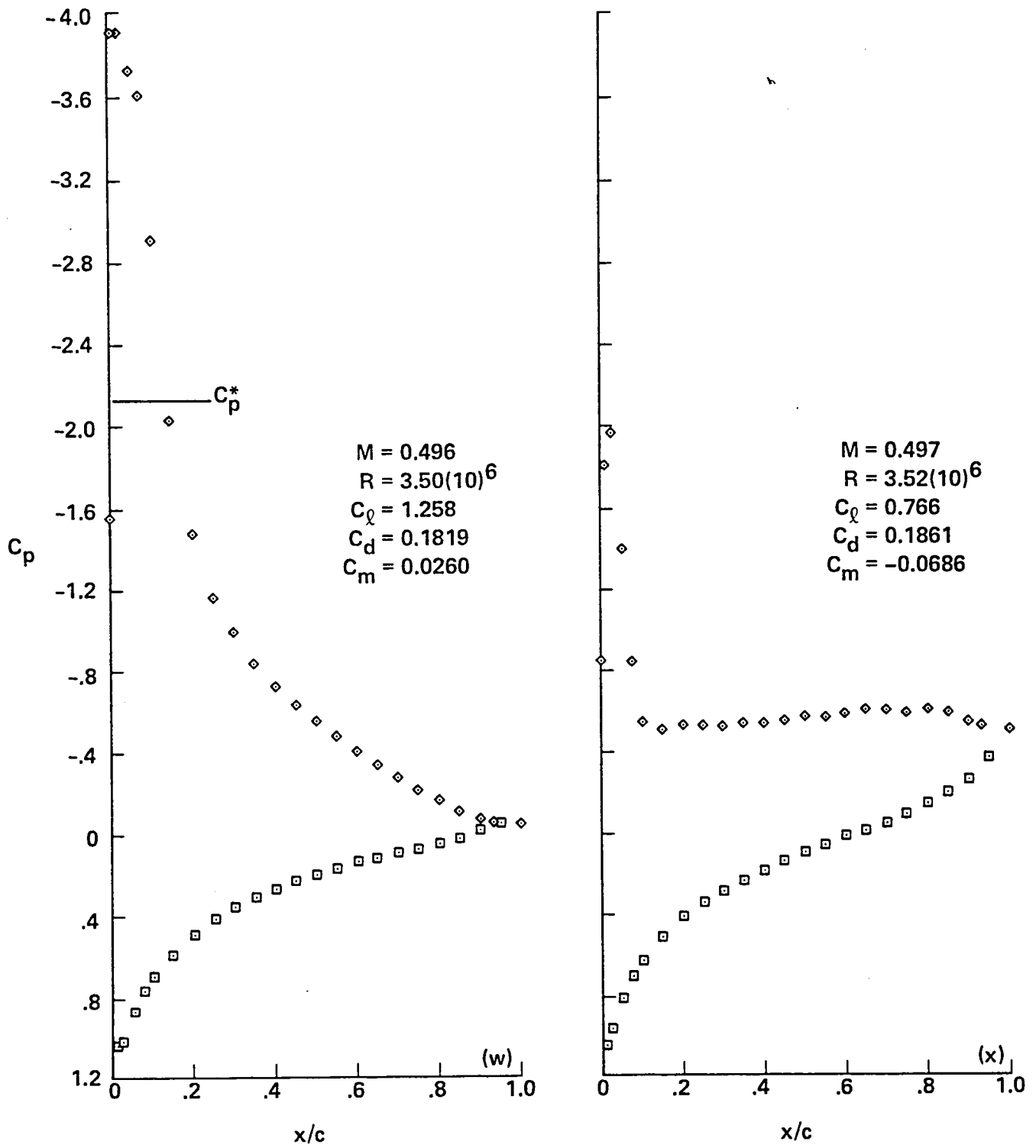


Figure 6.- Concluded.

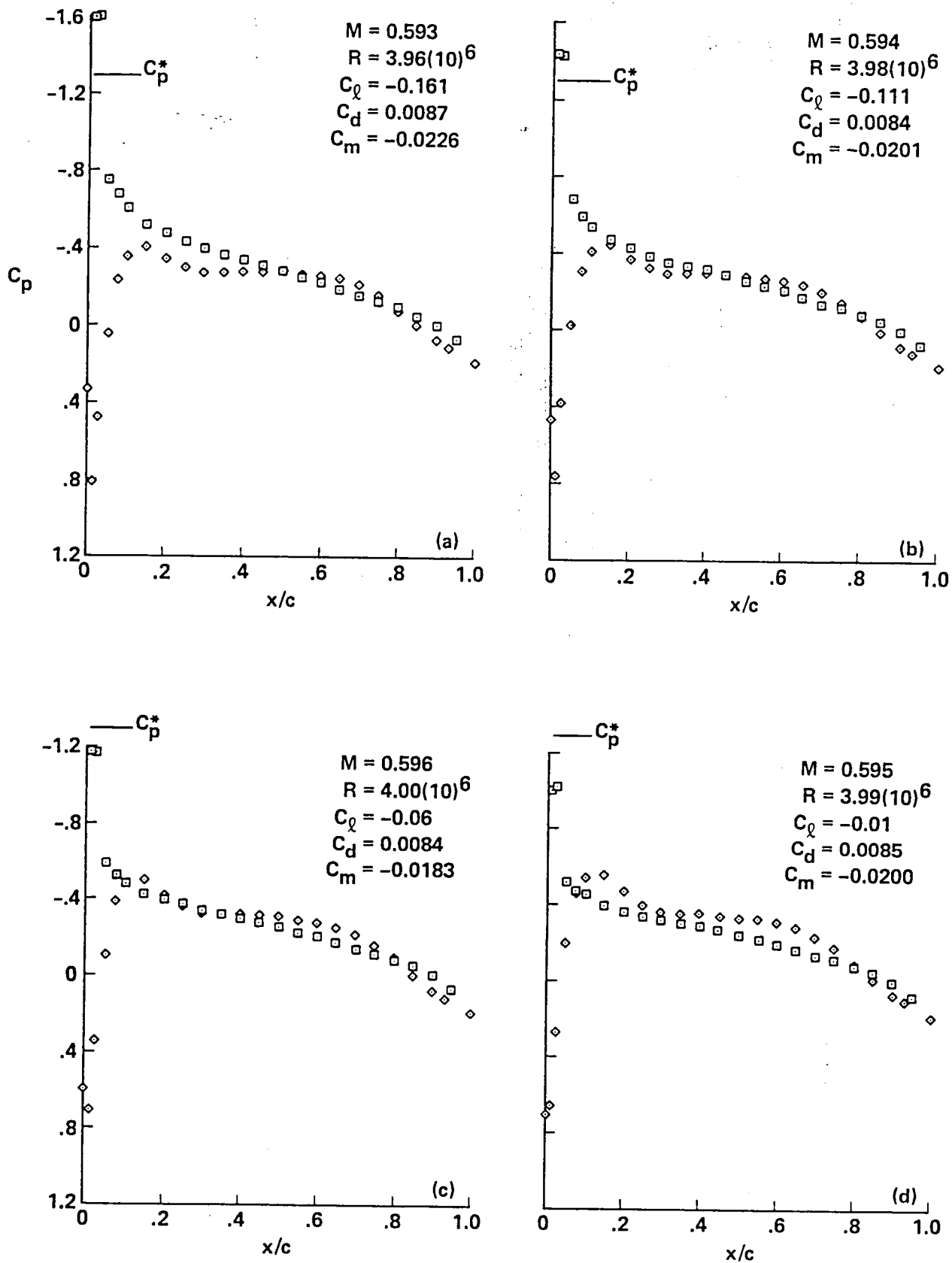


Figure 7.- Pressure distributions for A-1 airfoil, $M_{set} = 0.6$.

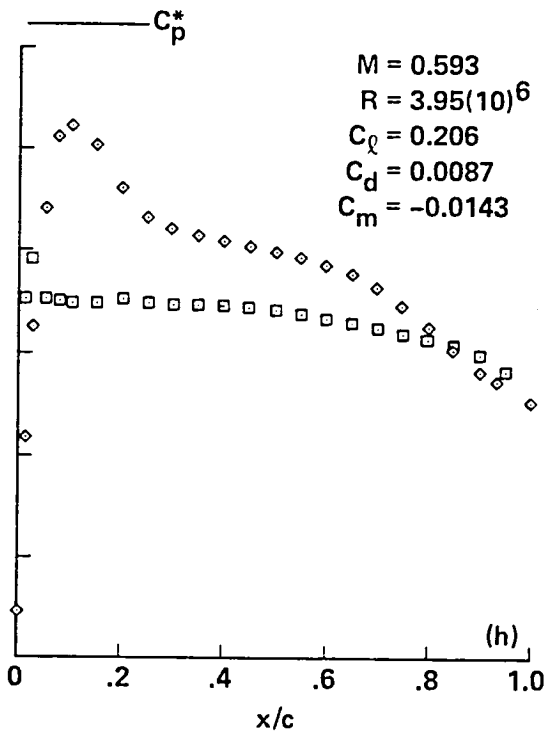
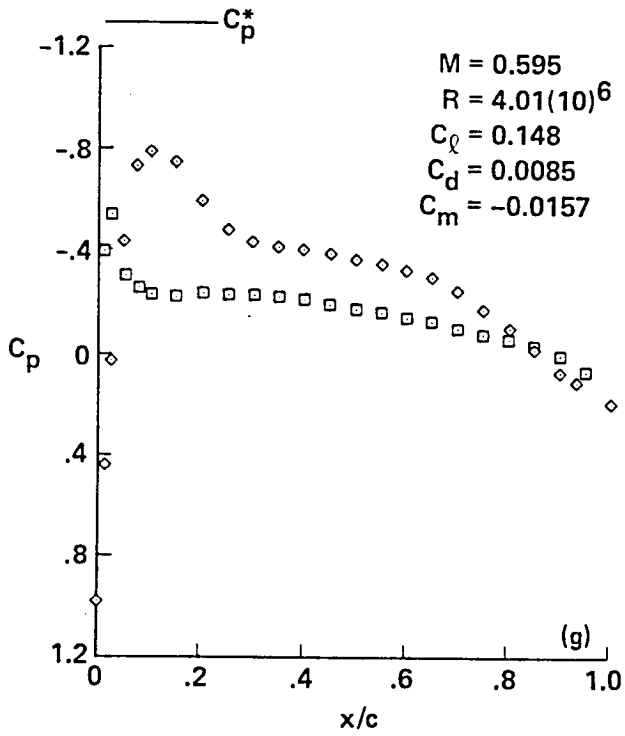
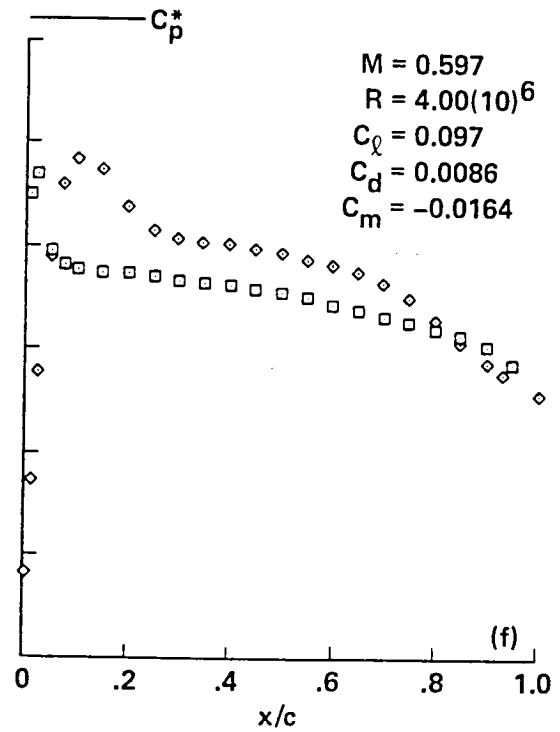
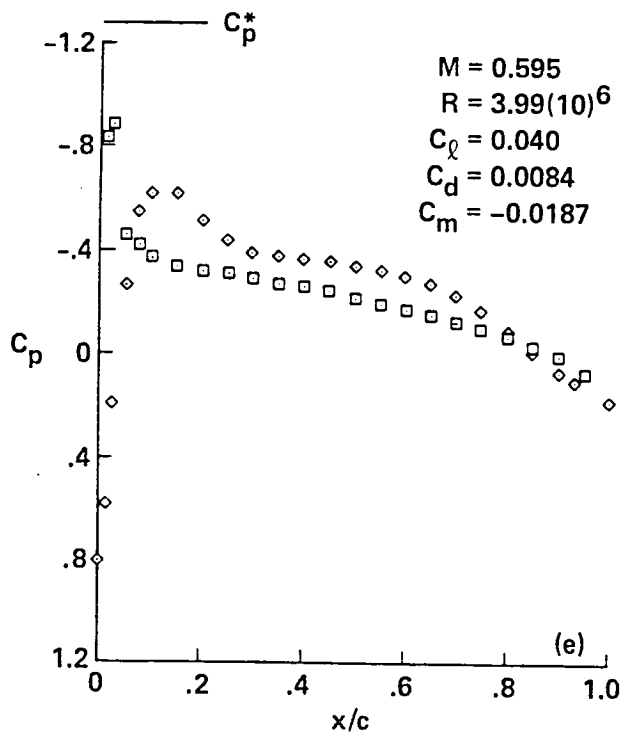


Figure 7.- Continued.

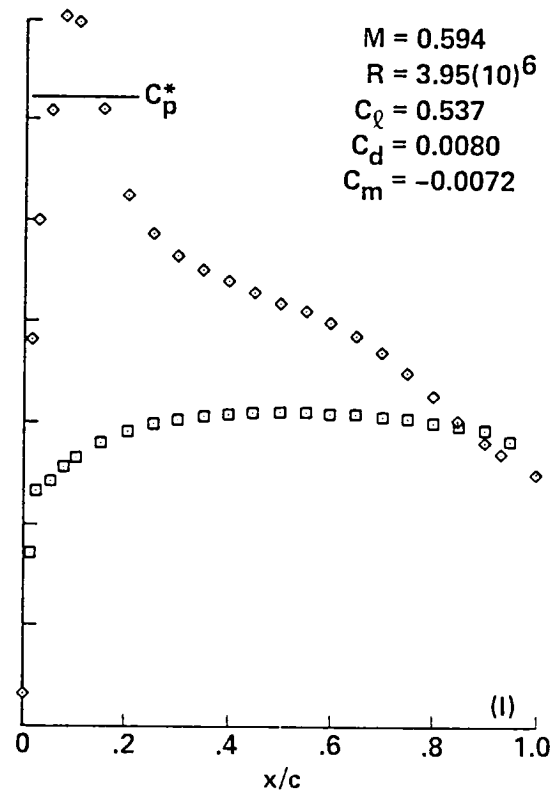
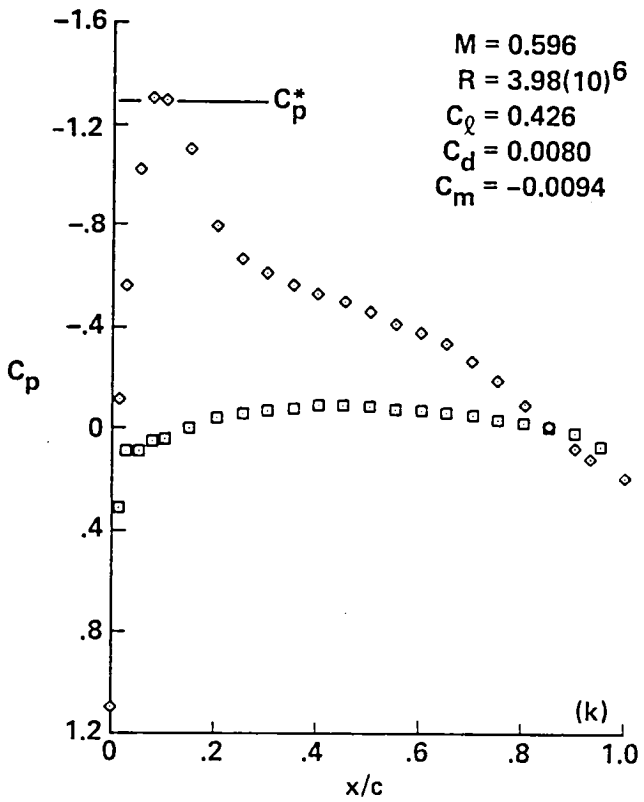
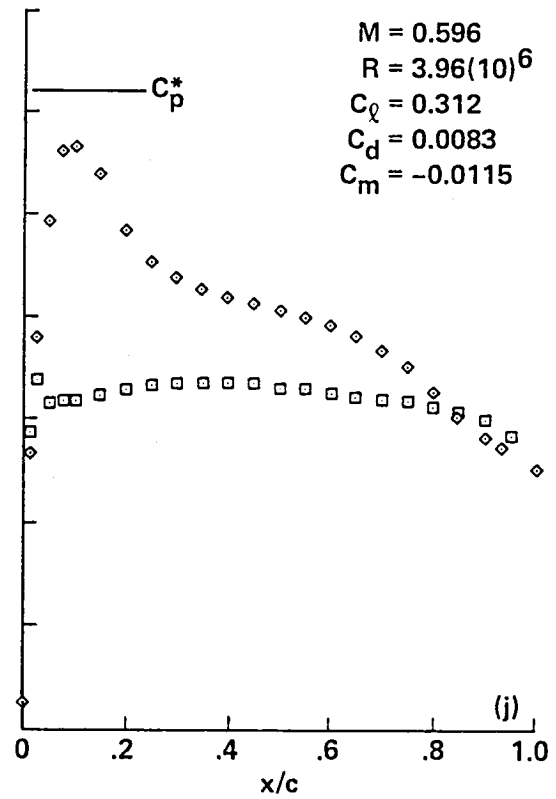
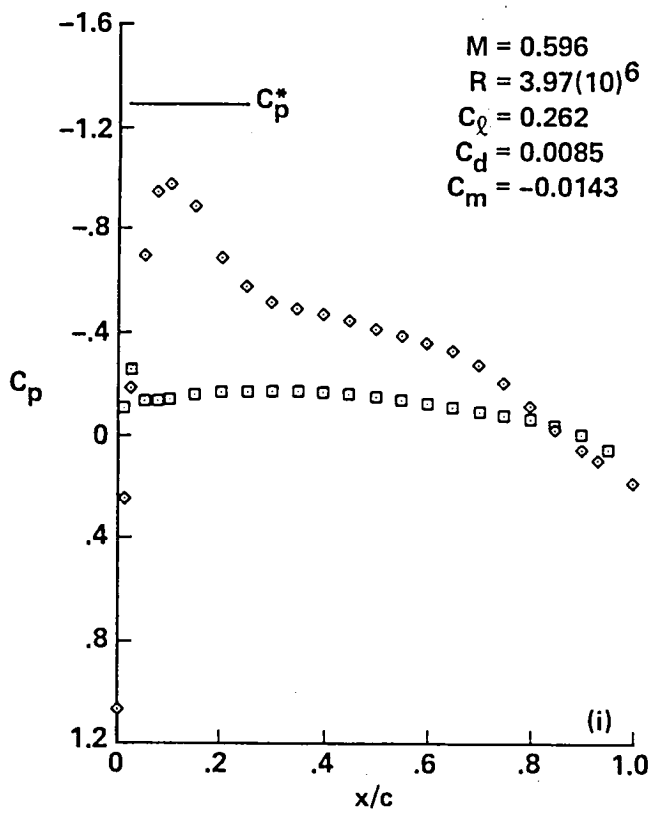


Figure 7.- Continued.

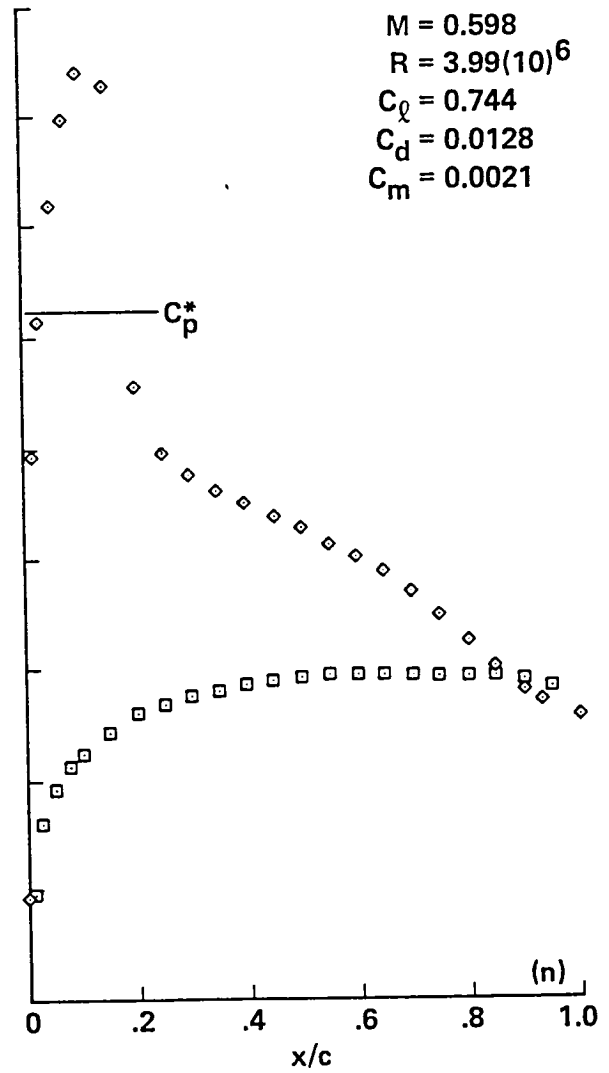
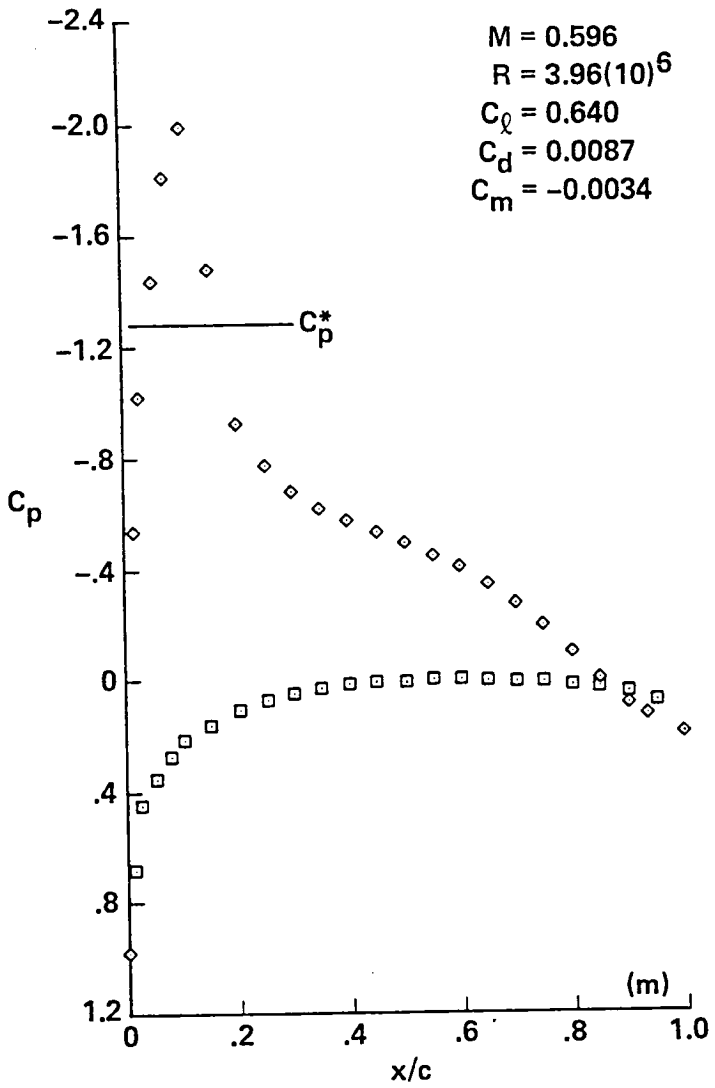


Figure 7.- Continued.

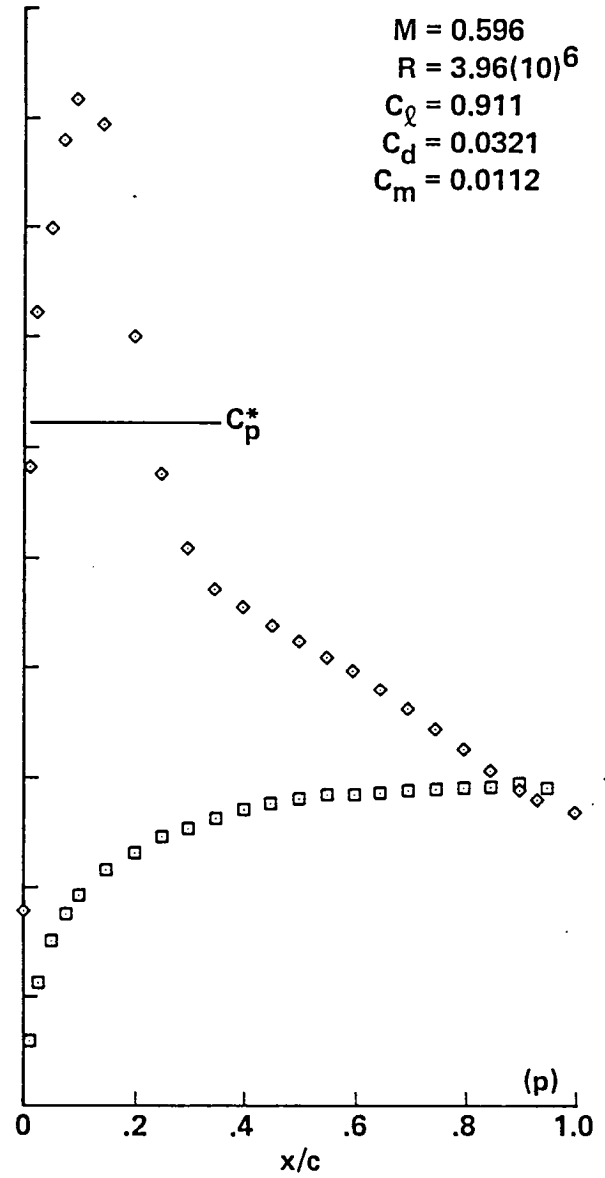
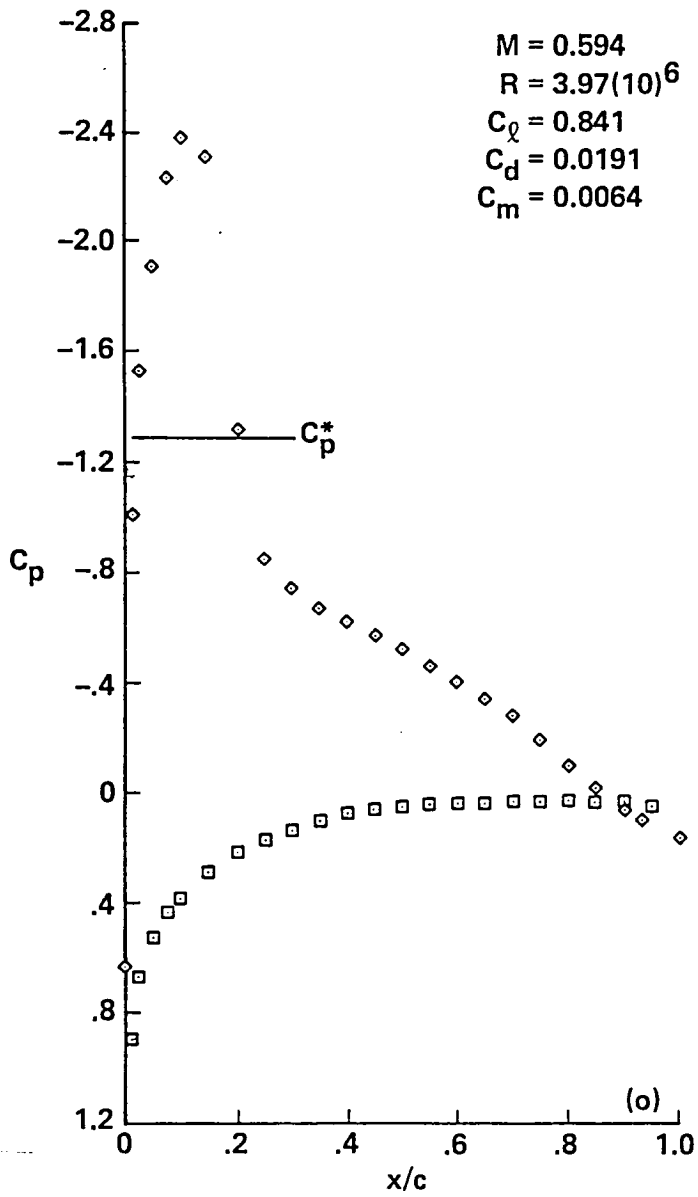


Figure 7.- Continued.

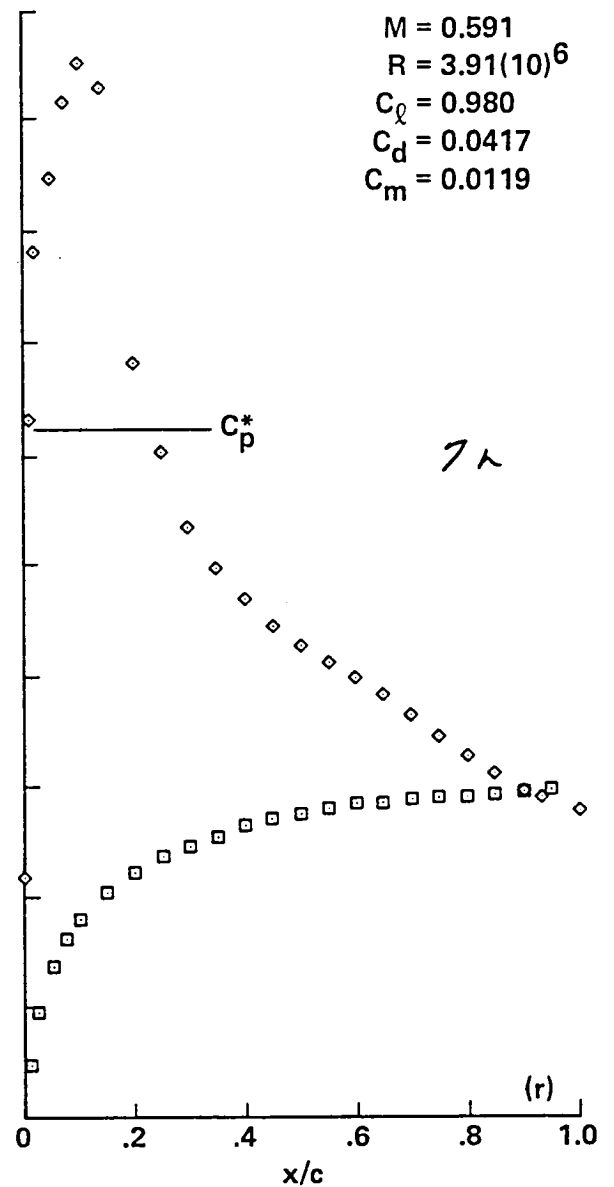
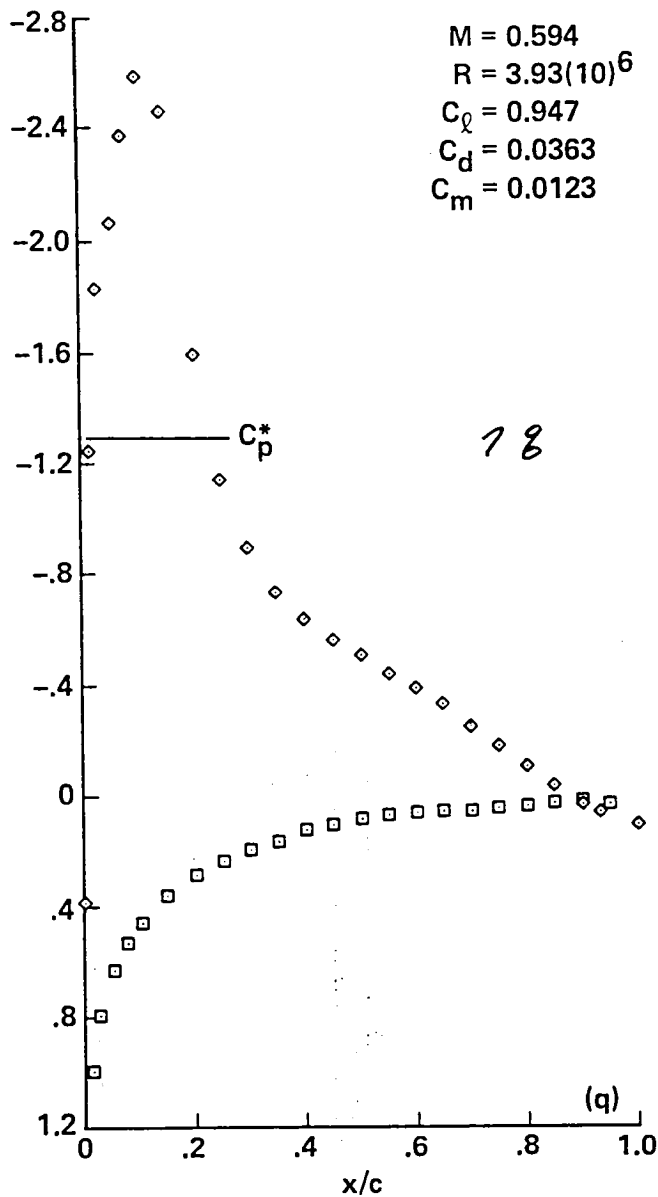


Figure 7.- Continued.

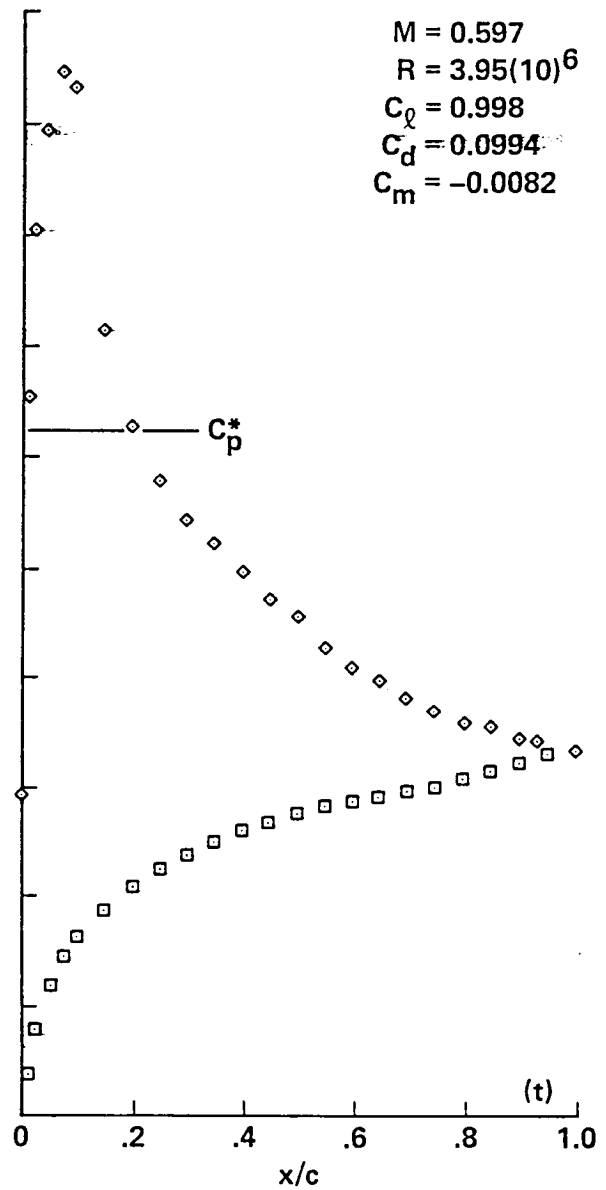
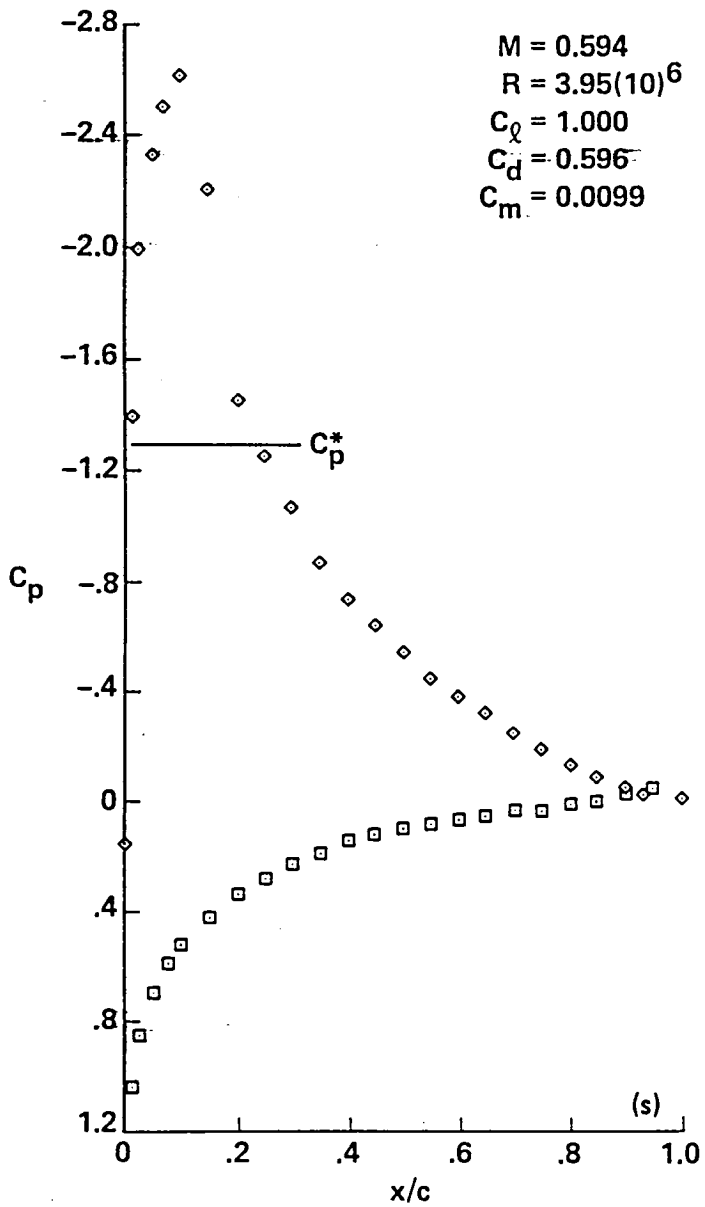


Figure 7.- Continued.

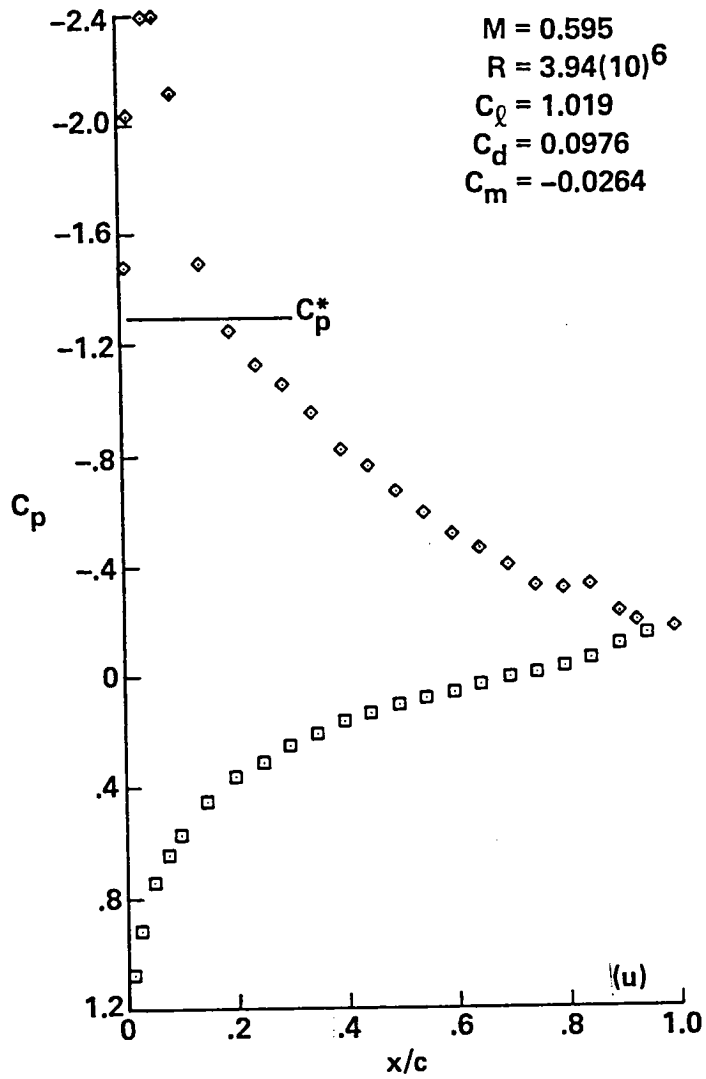


Figure 7.- Concluded.

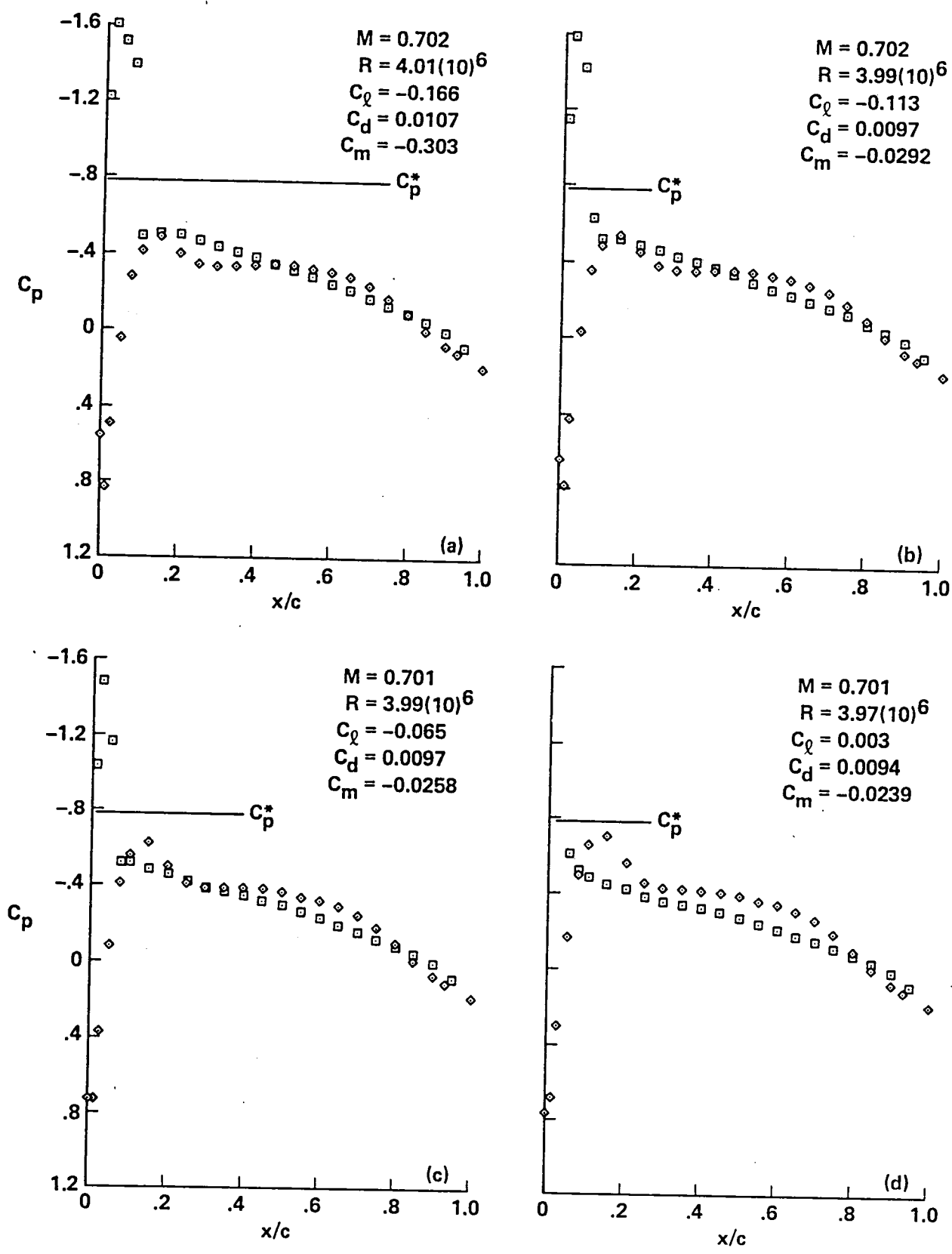


Figure 8.- Pressure distributions for A-1 airfoil, $M_{set} = 0.7$.

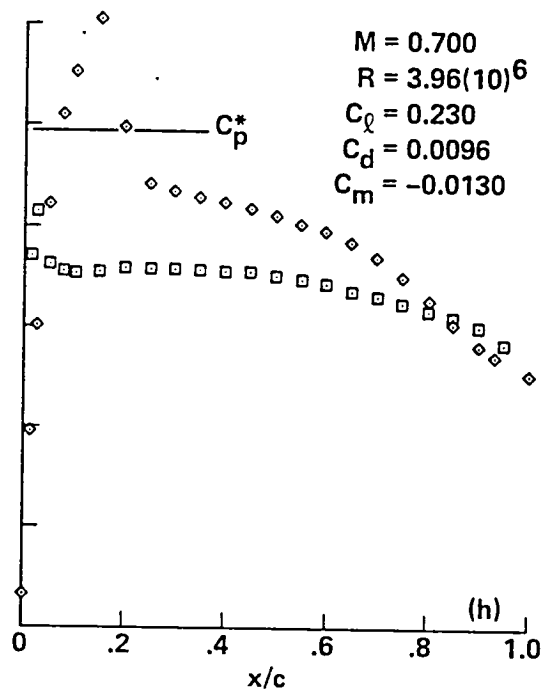
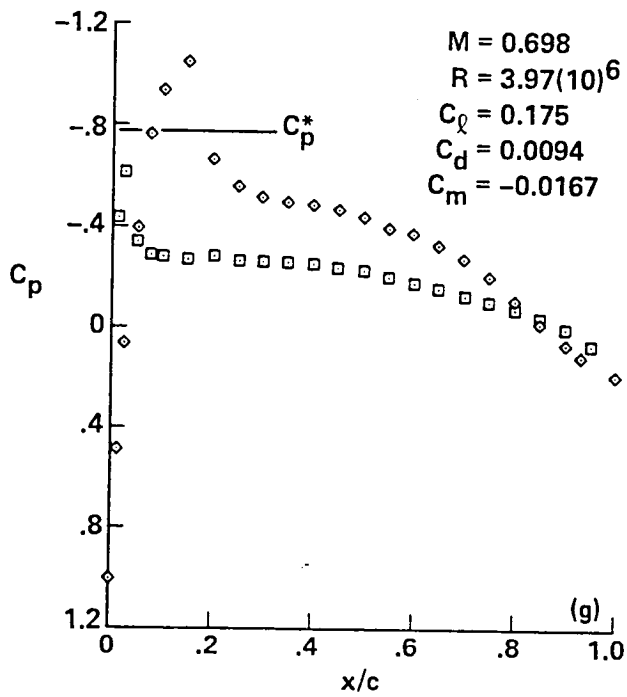
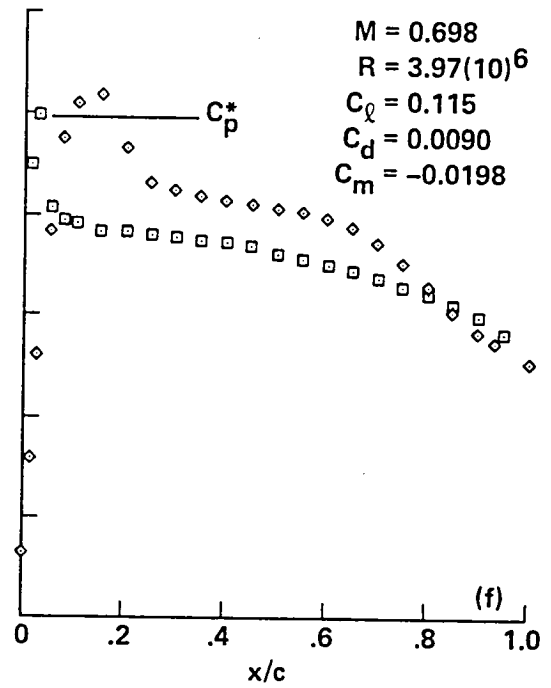
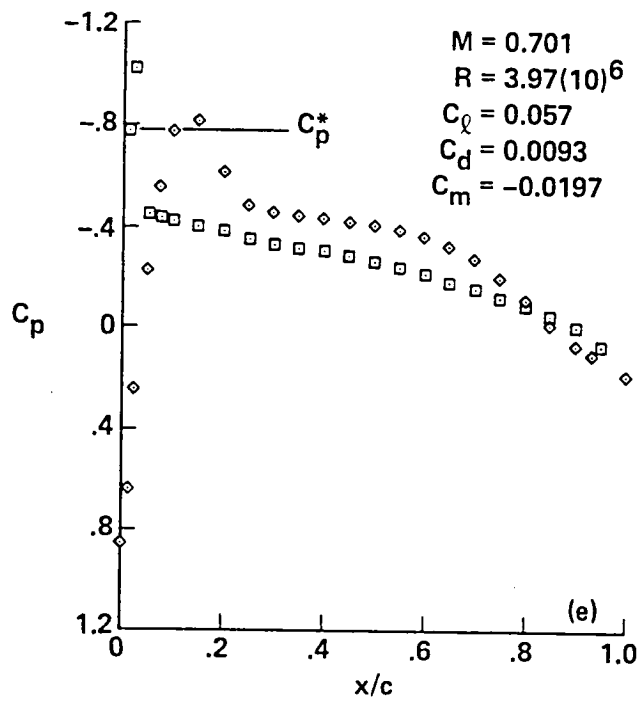


Figure 8.- Continued.

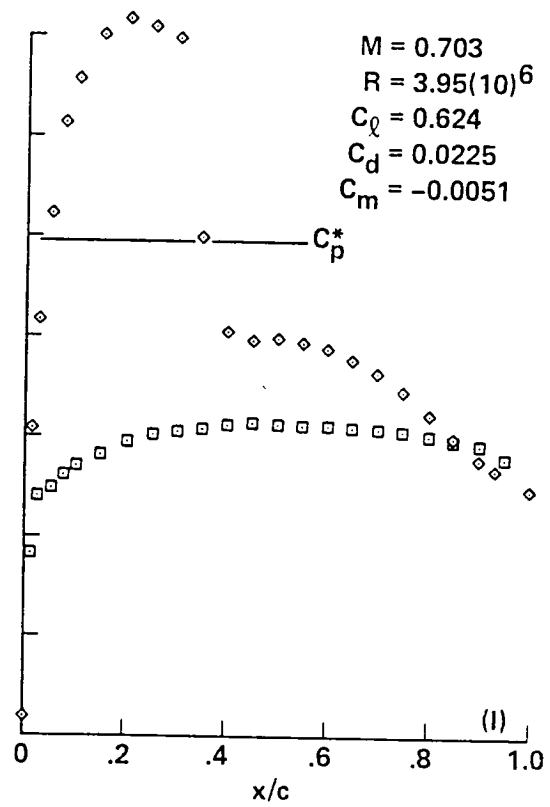
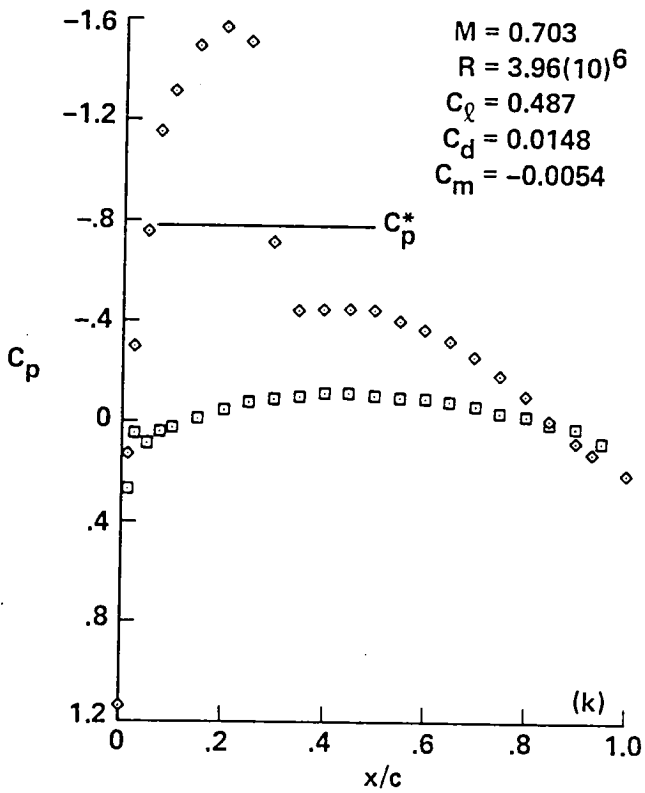
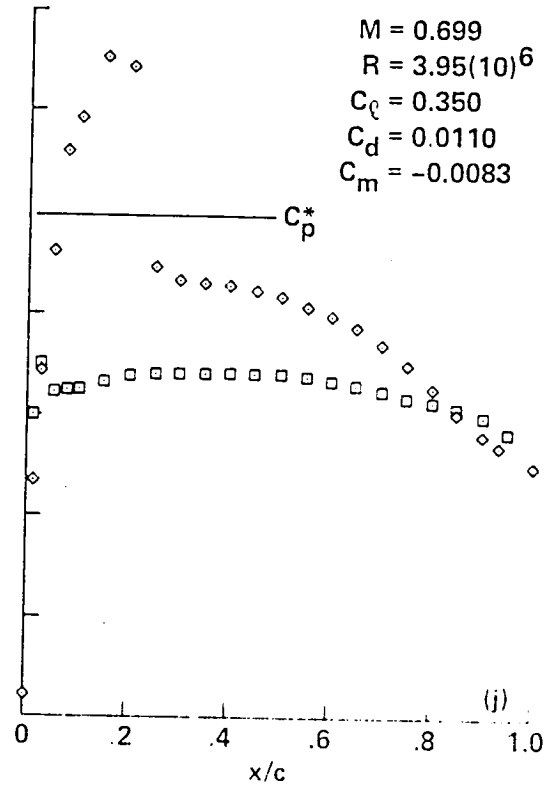
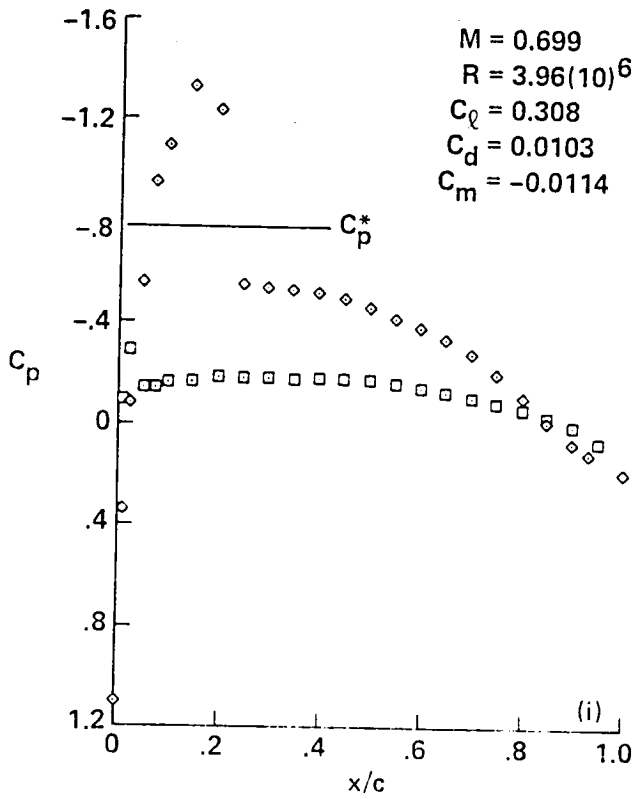


Figure 8.- Continued.

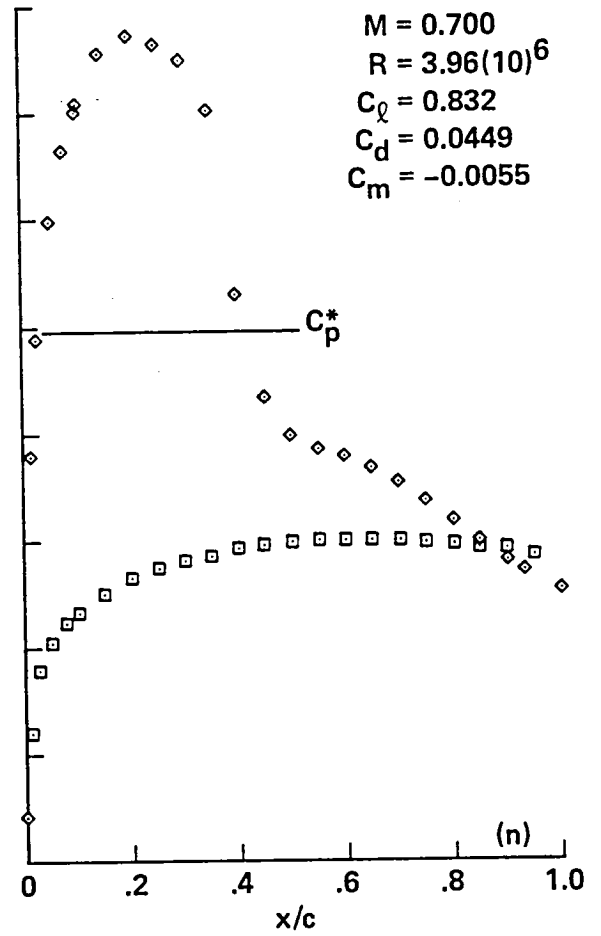
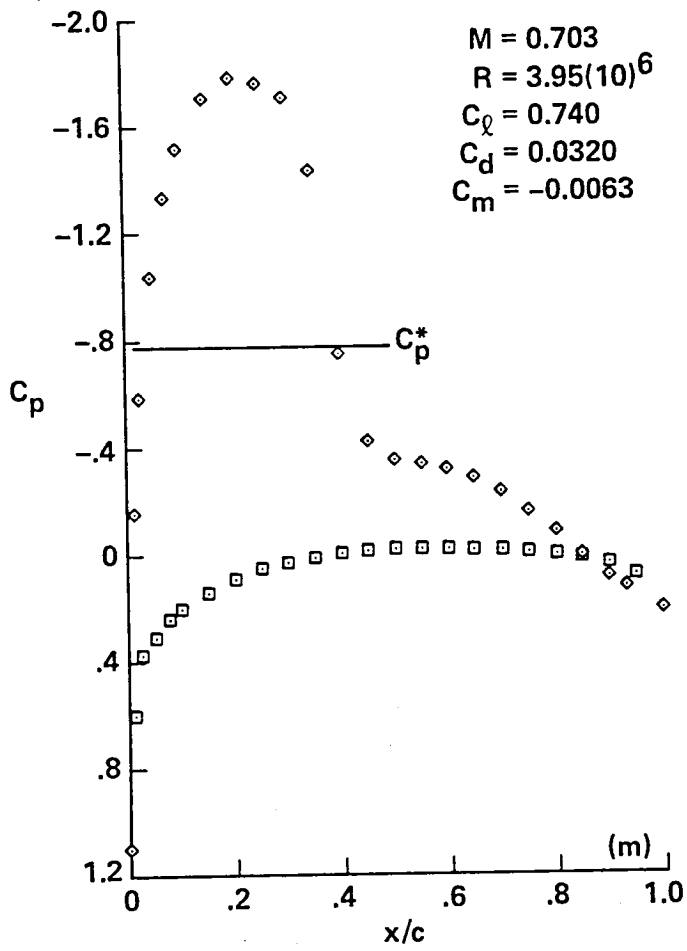


Figure 8.- Continued.

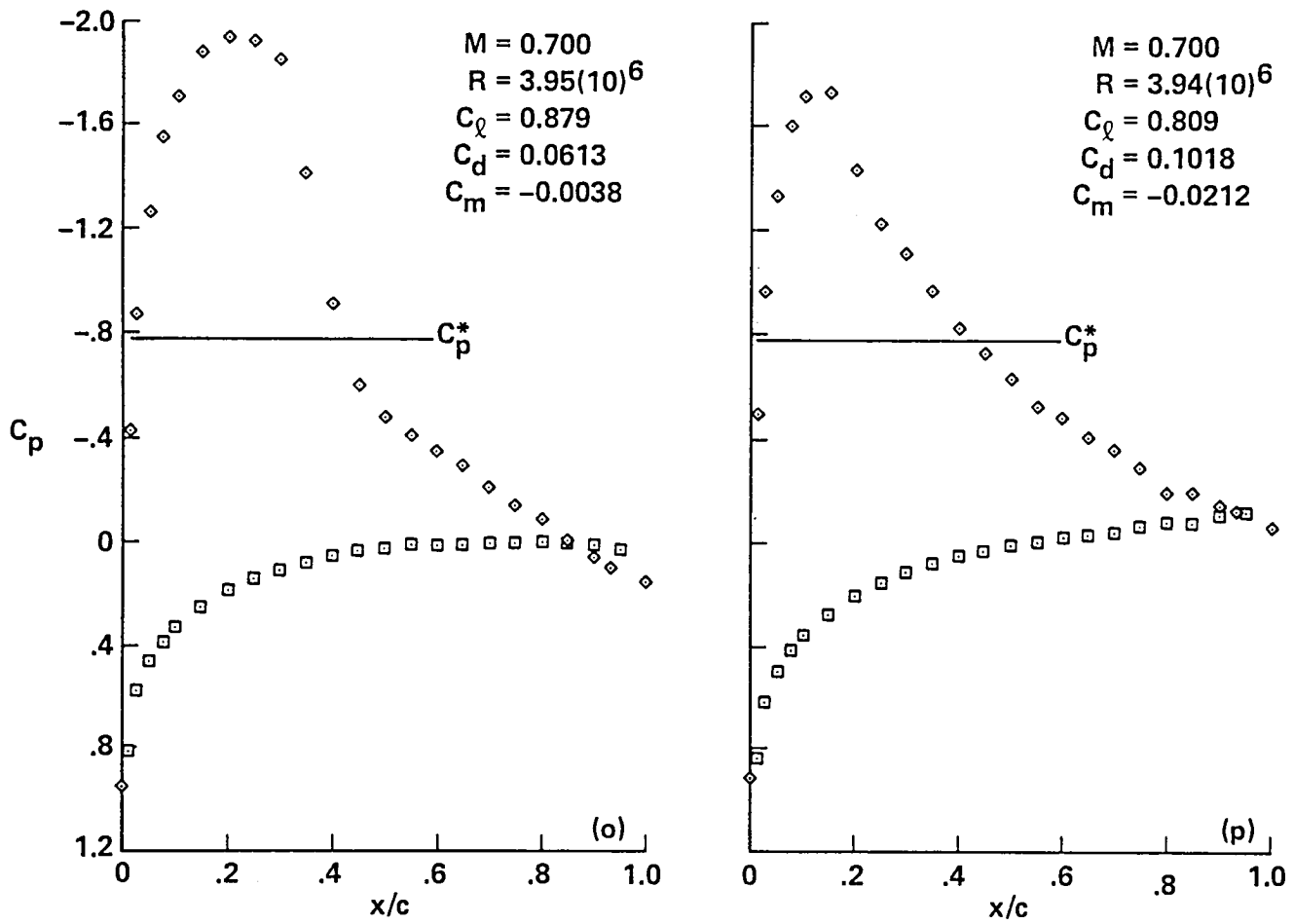


Figure 8.- Concluded.

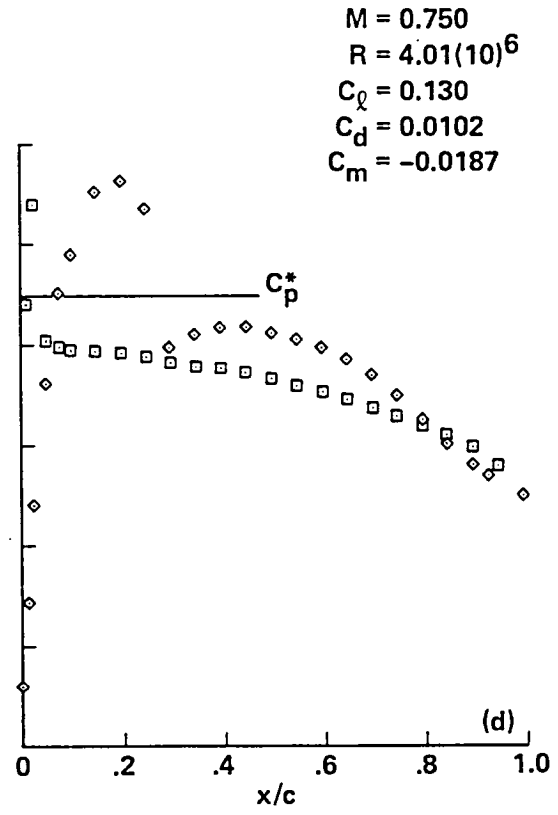
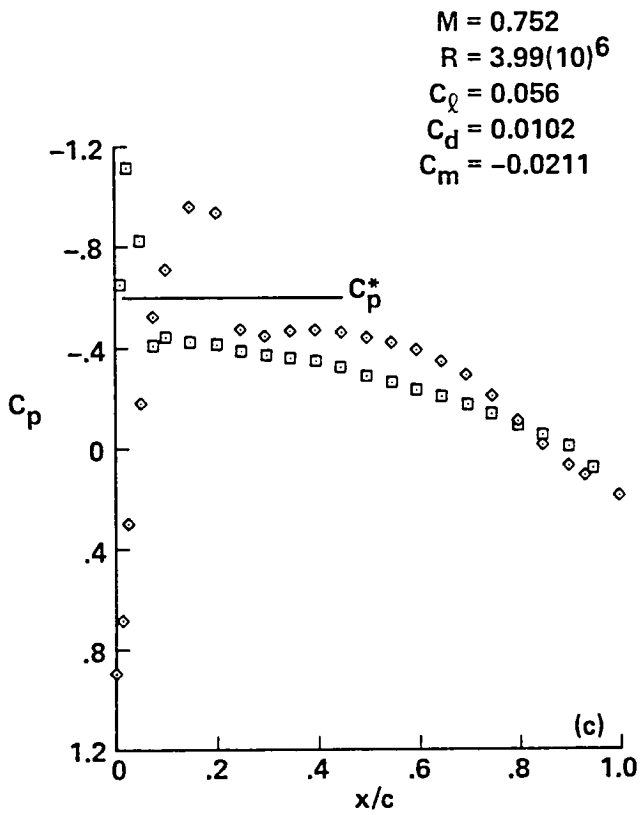
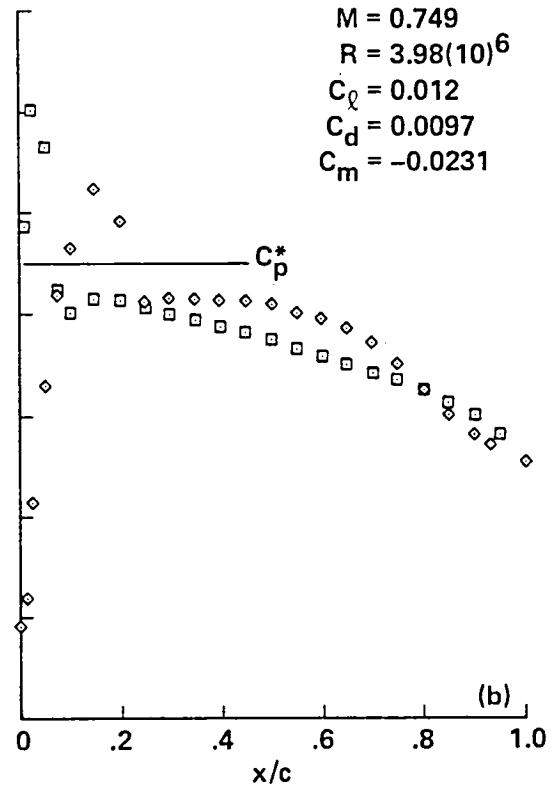
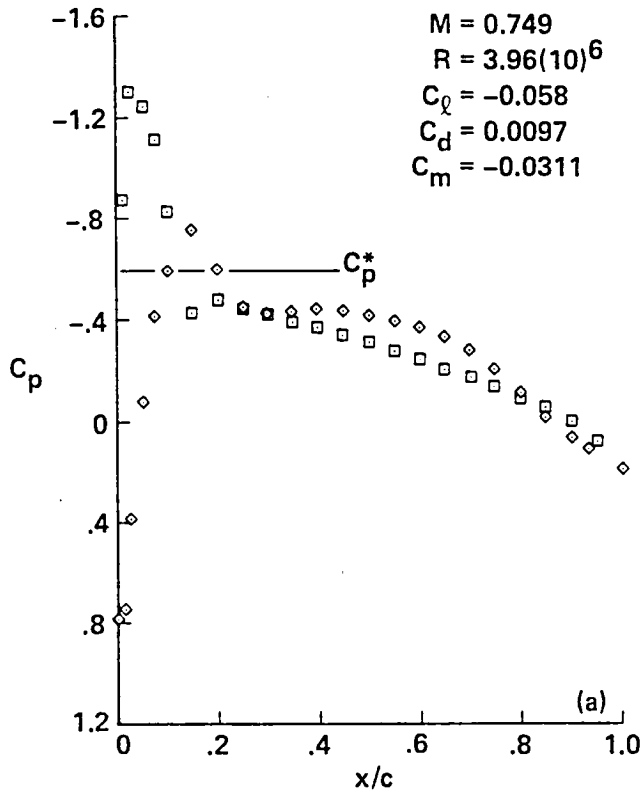


Figure 9.- Pressure distributions for A-1 airfoil, $M_{set} = 0.75$.

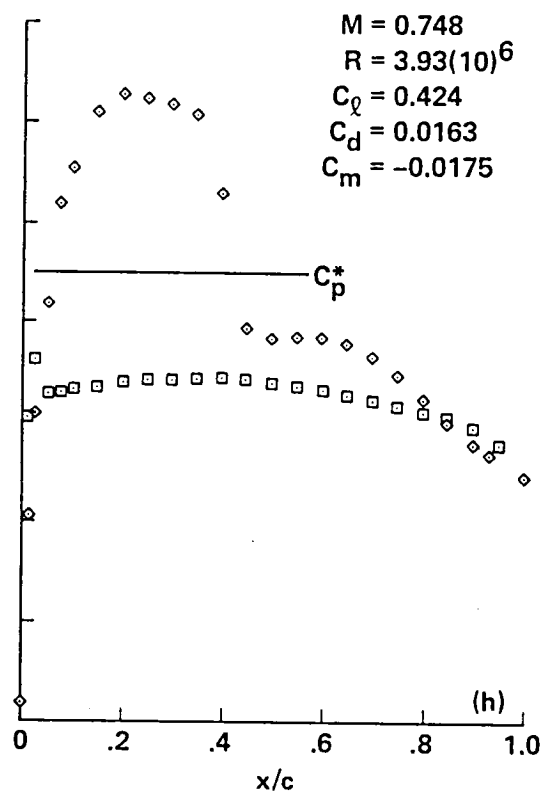
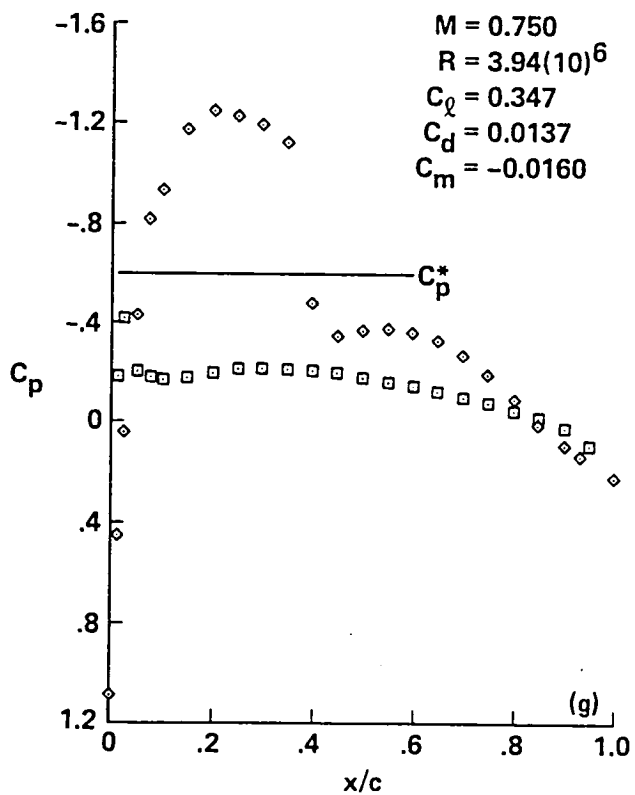
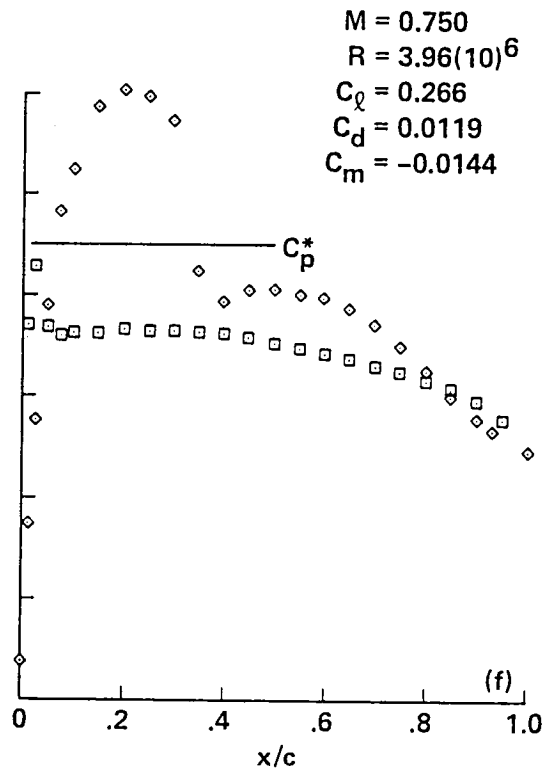
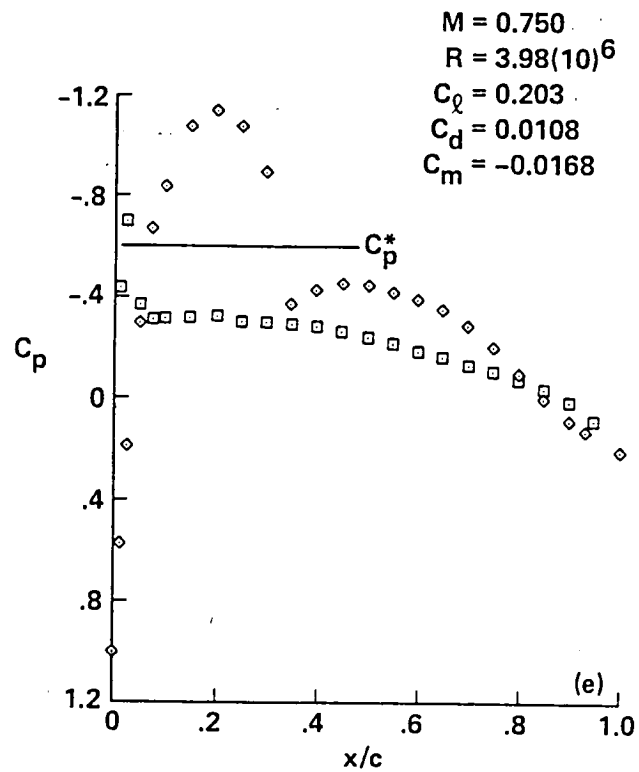


Figure 9.- Continued.

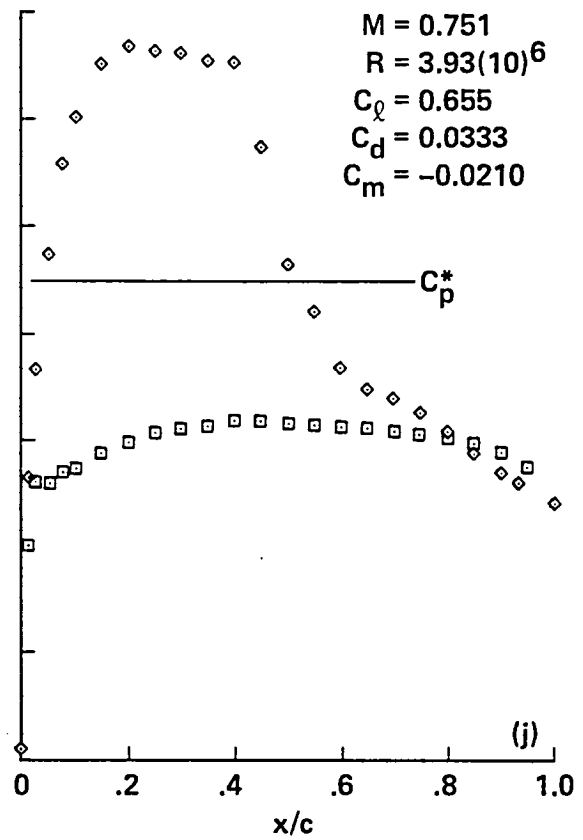
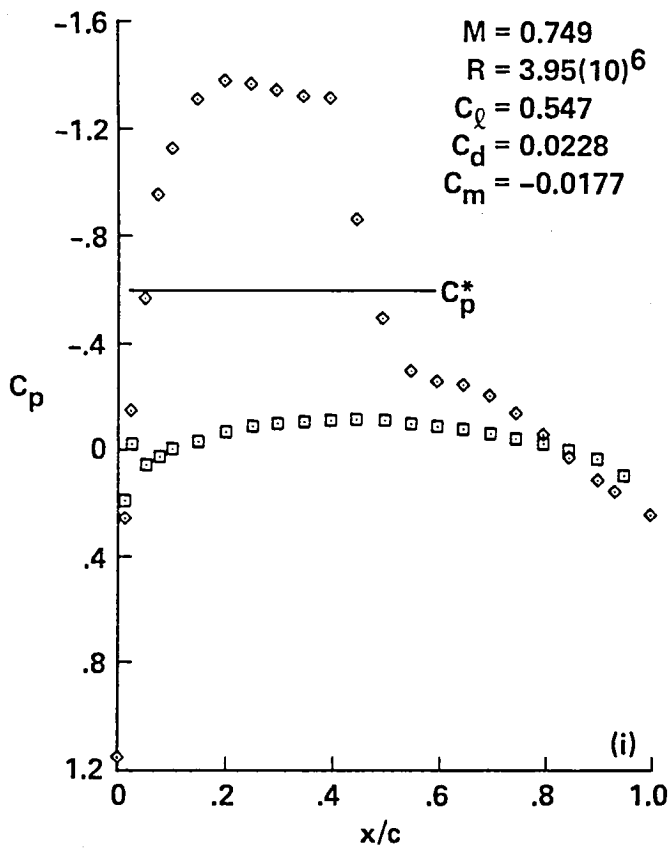


Figure 9.- Continued.

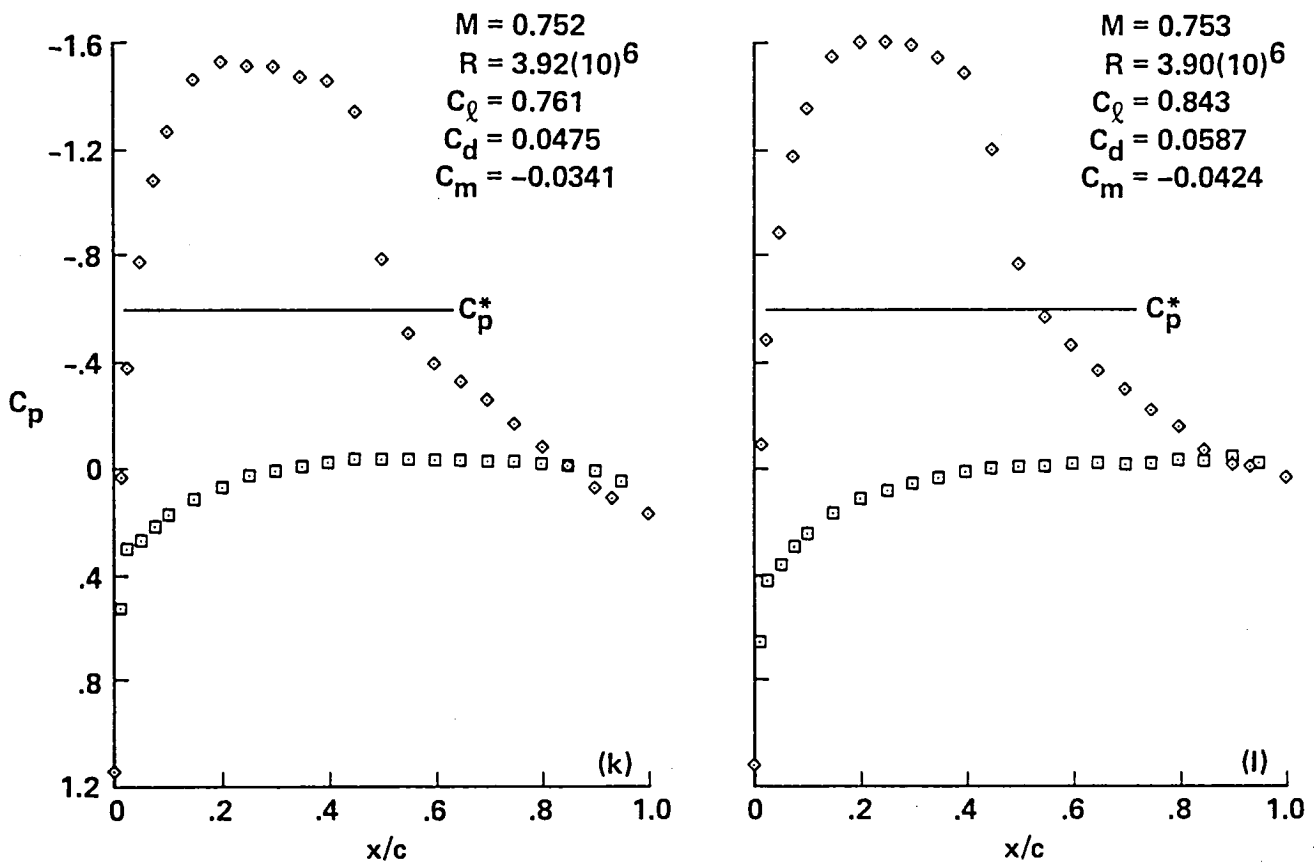


Figure 9.- Continued.

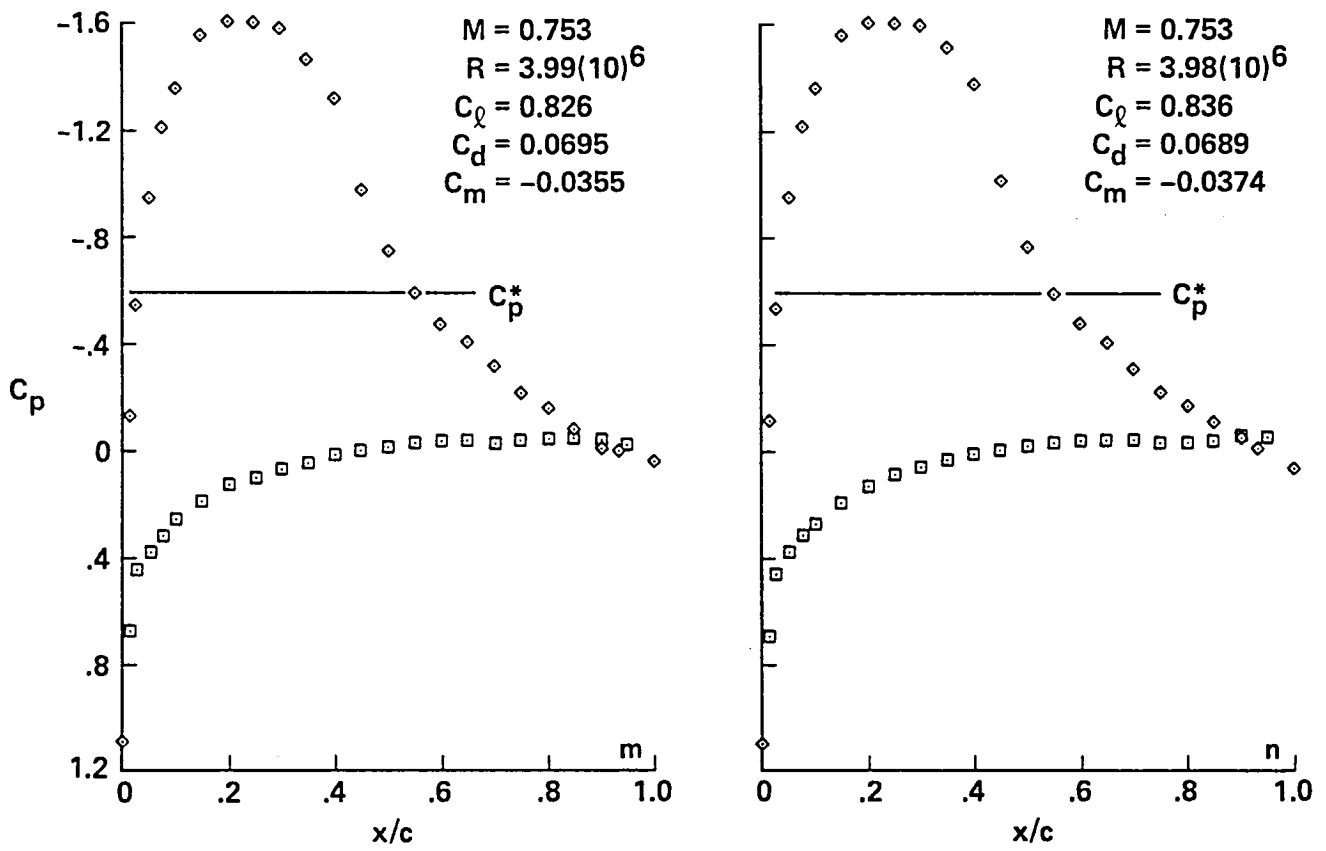


Figure 9.- Concluded.

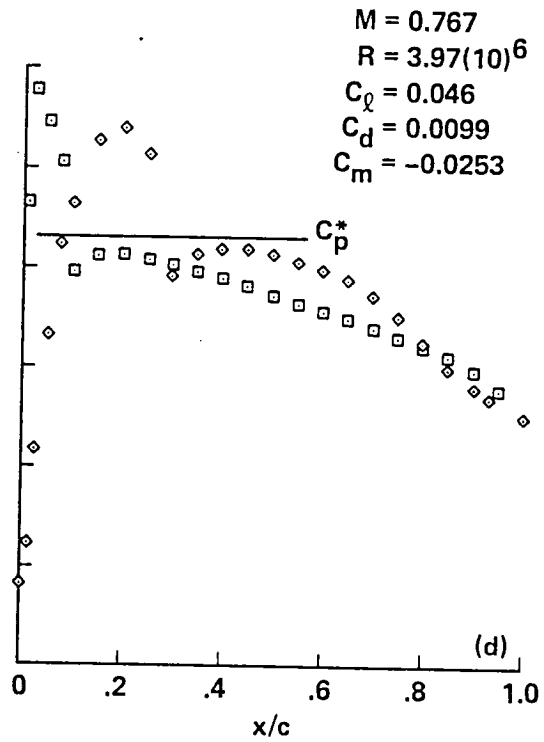
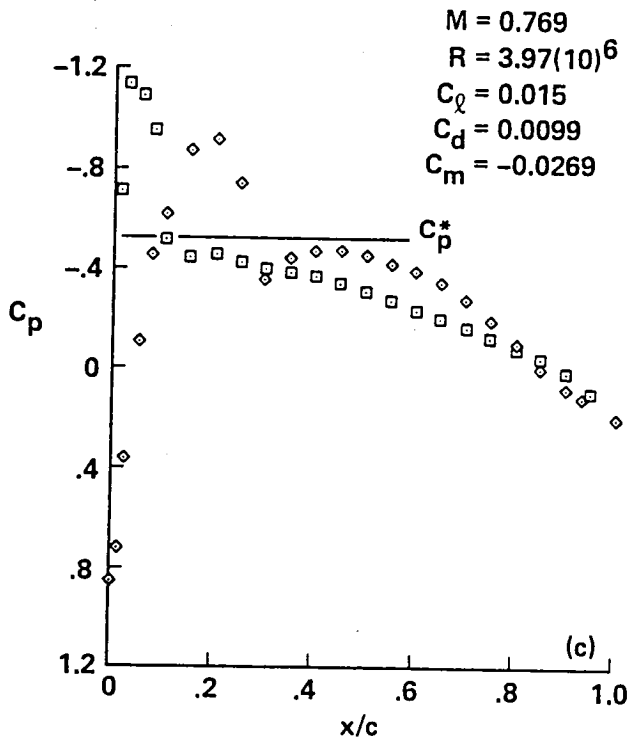
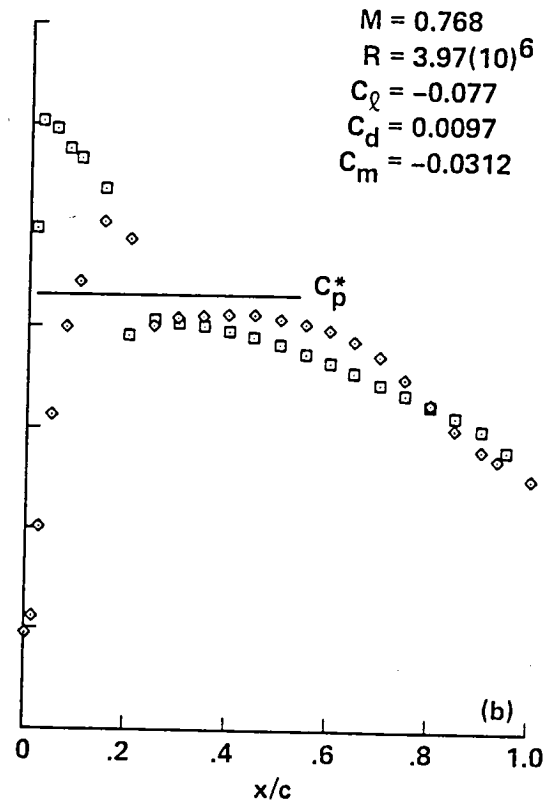
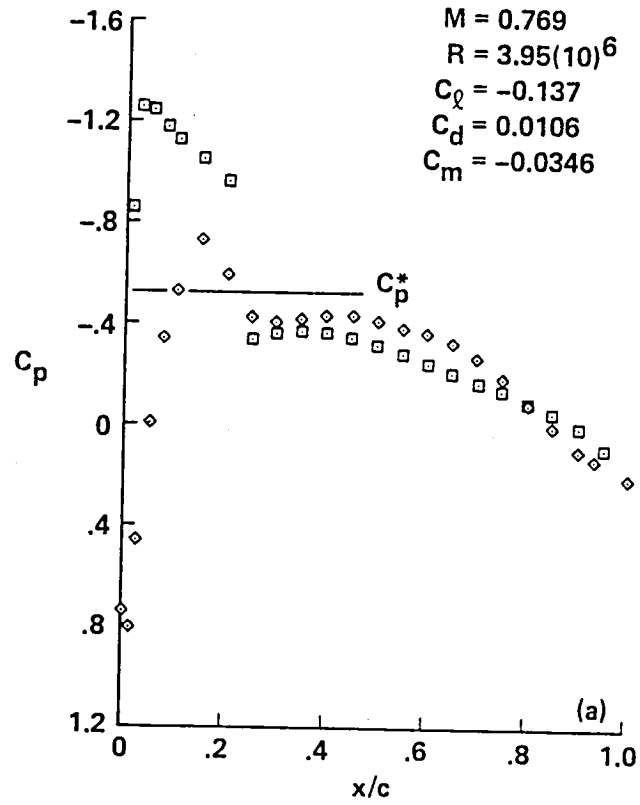


Figure 10.- Pressure distributions for A-1 airfoil, $M_{set} = 0.77$.

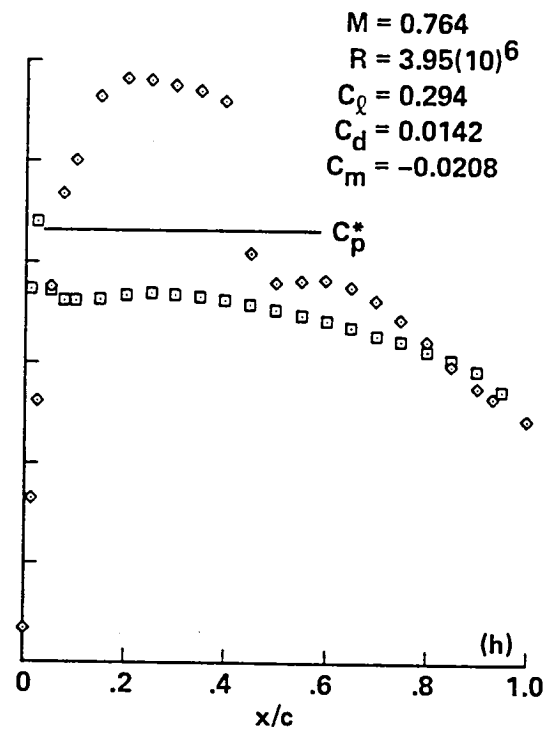
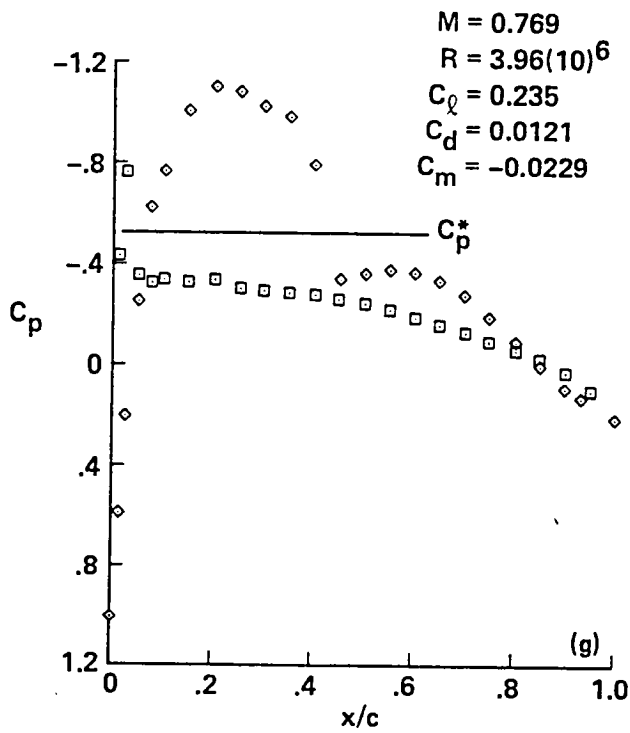
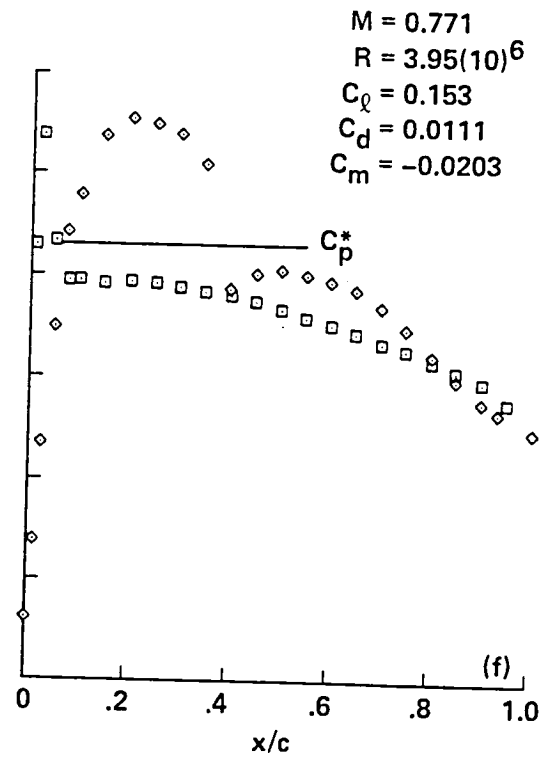
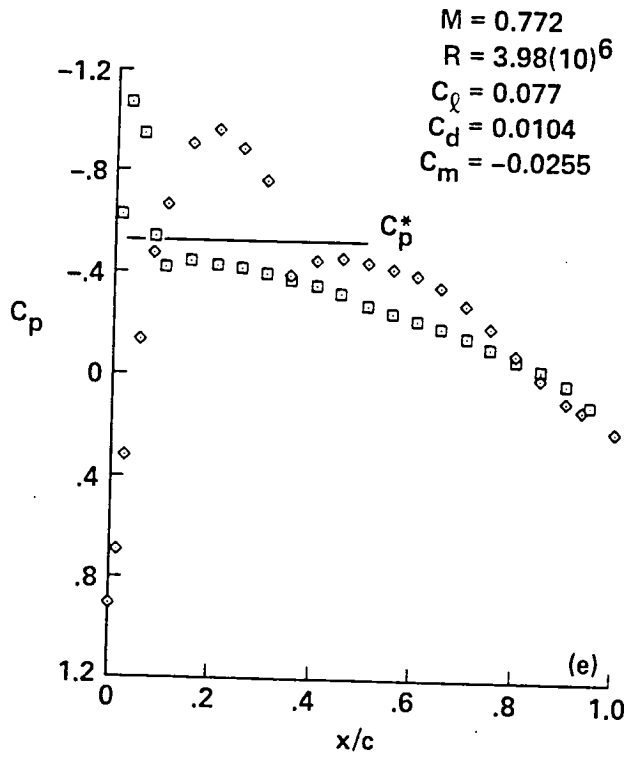


Figure 10.- Continued.

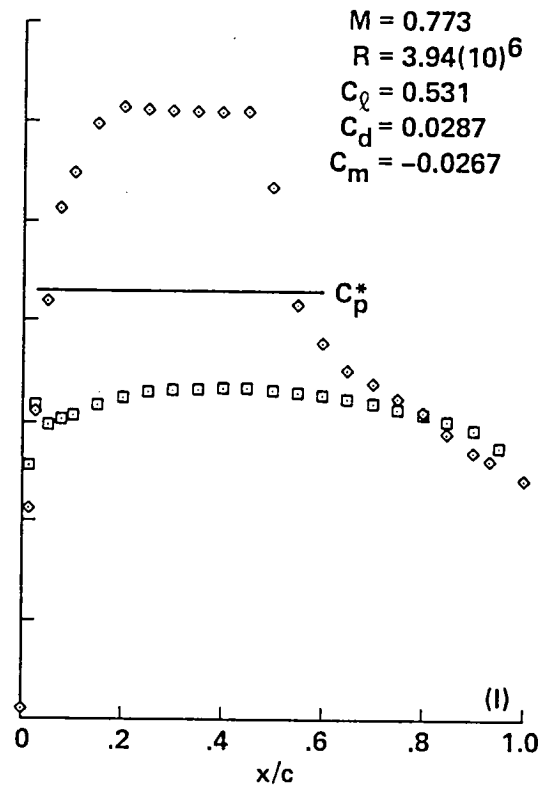
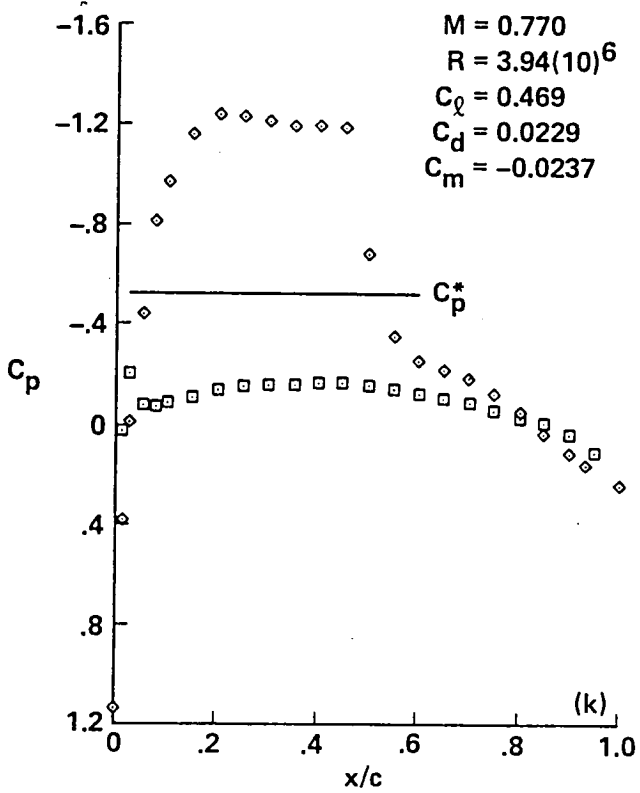
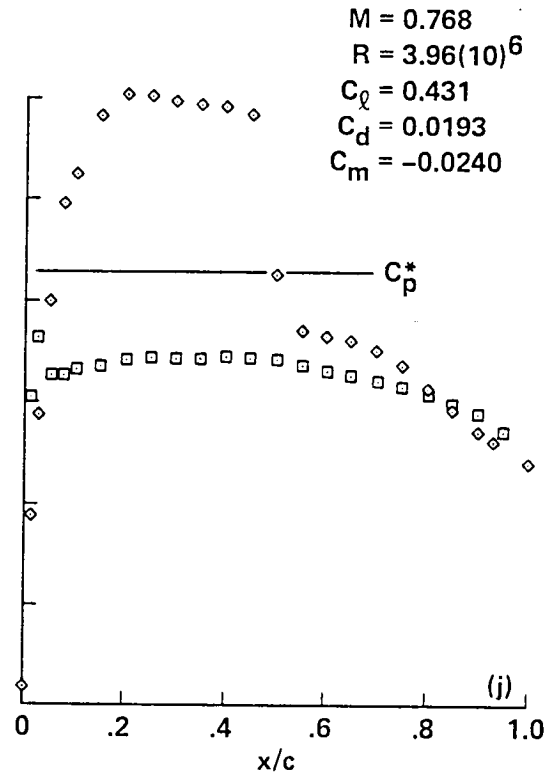
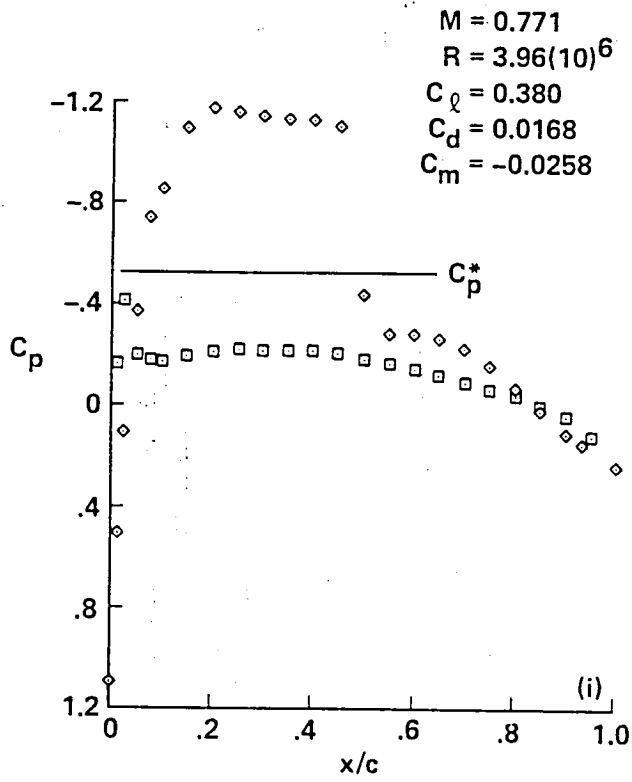


Figure 10.- Continued.

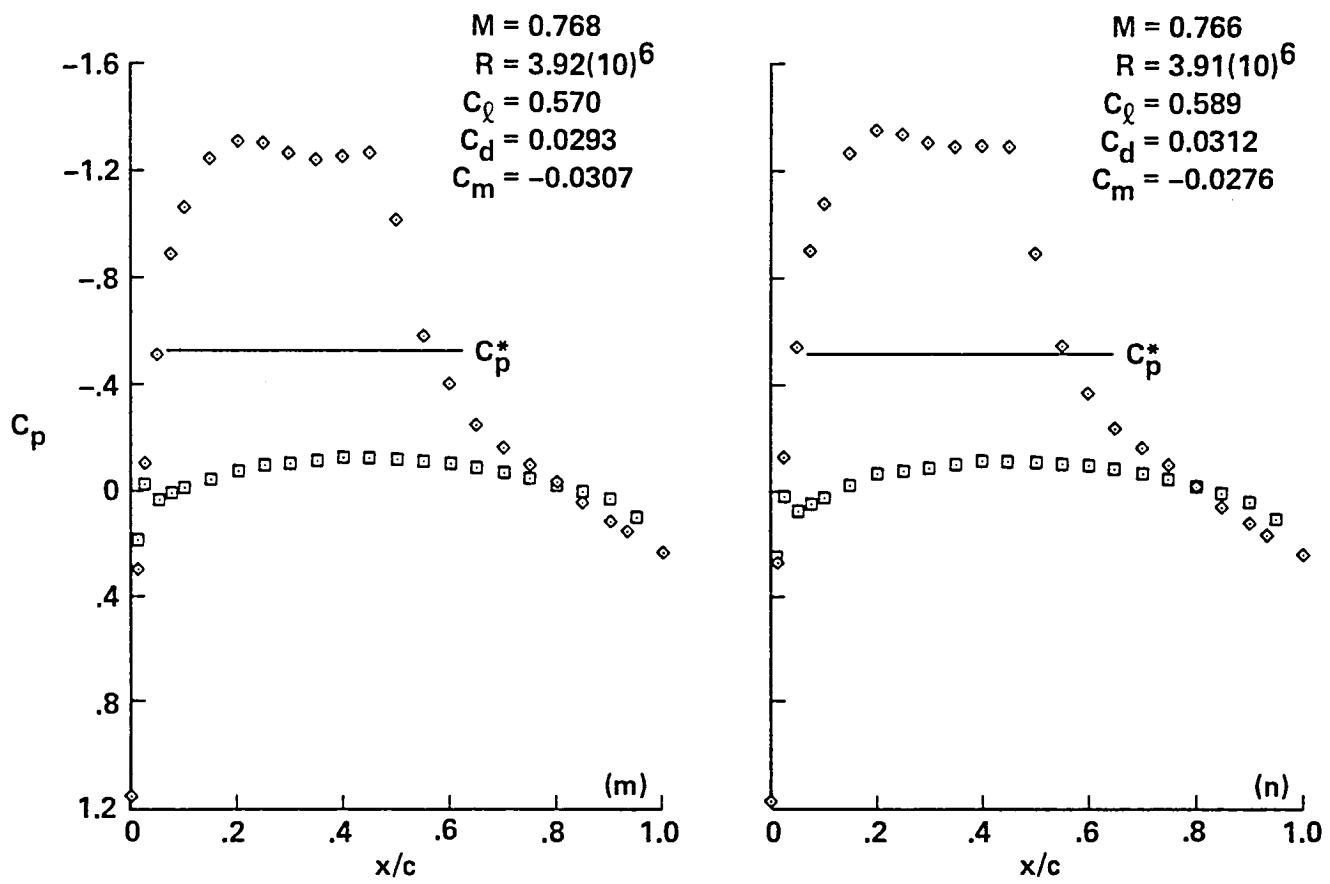


Figure 10.- Continued.

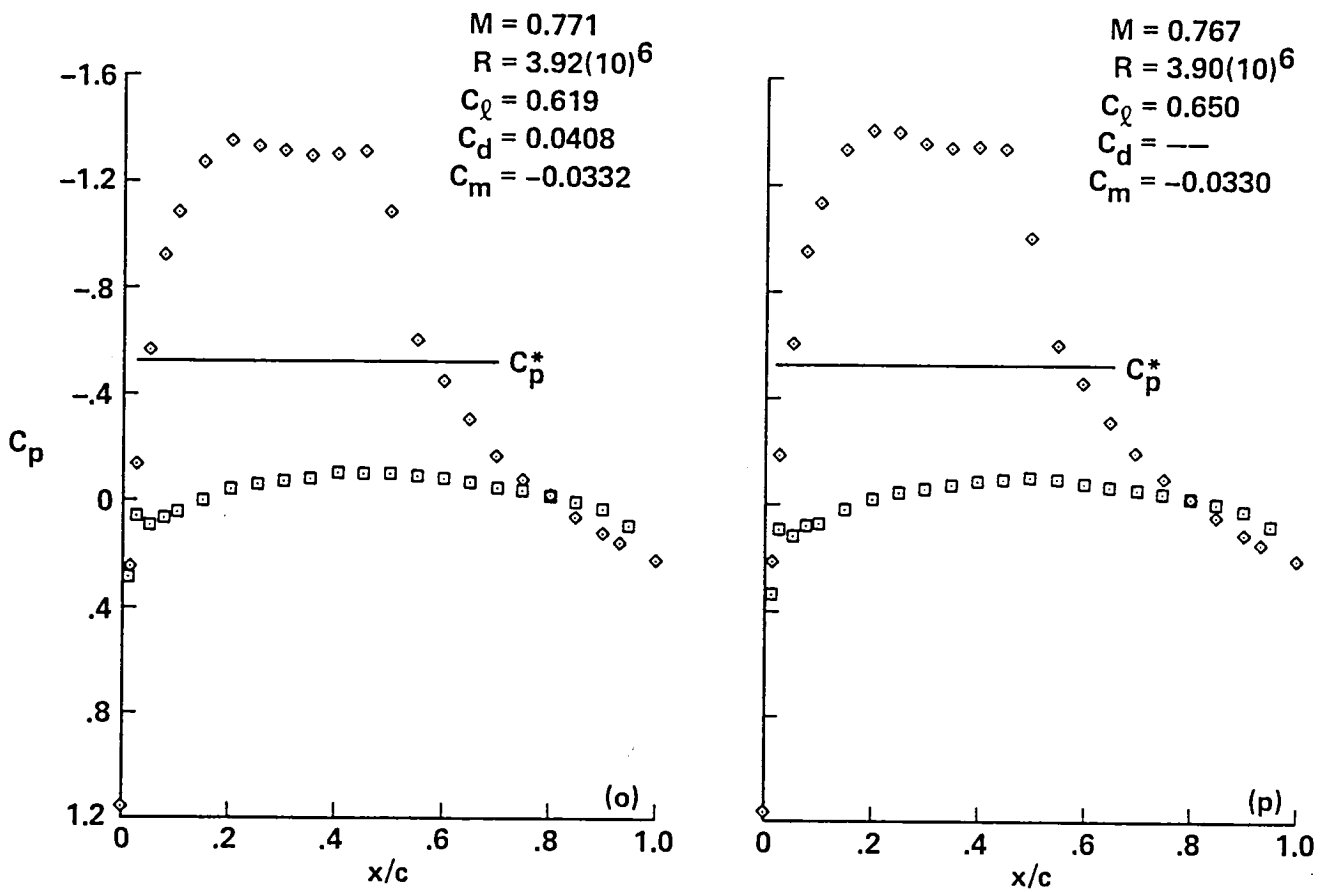


Figure 10.- Continued.

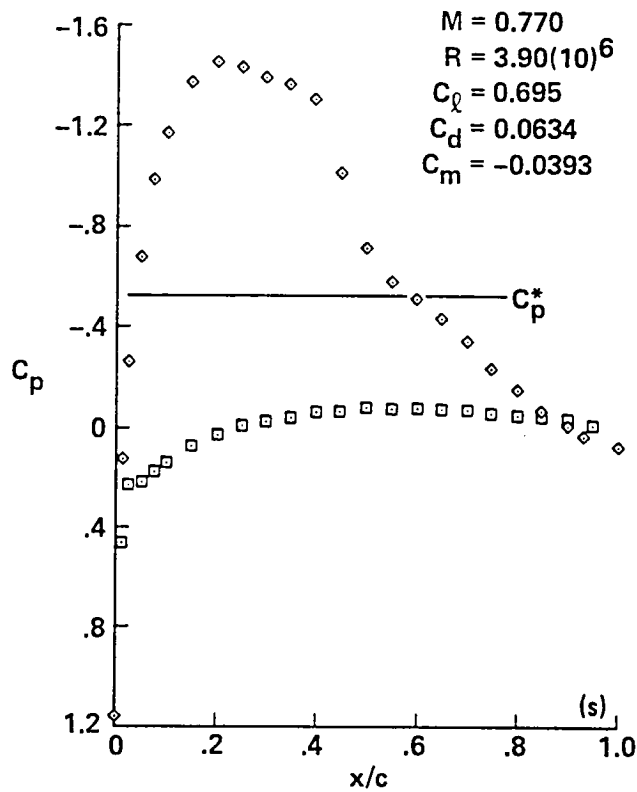
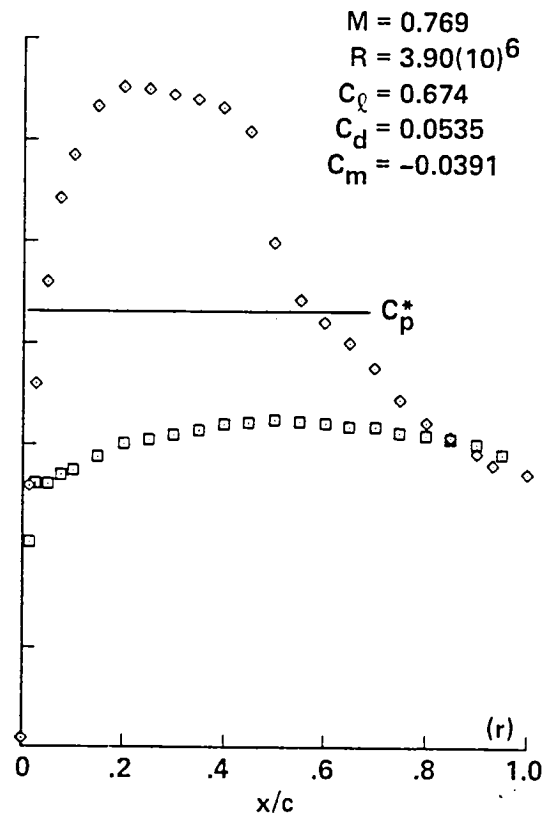
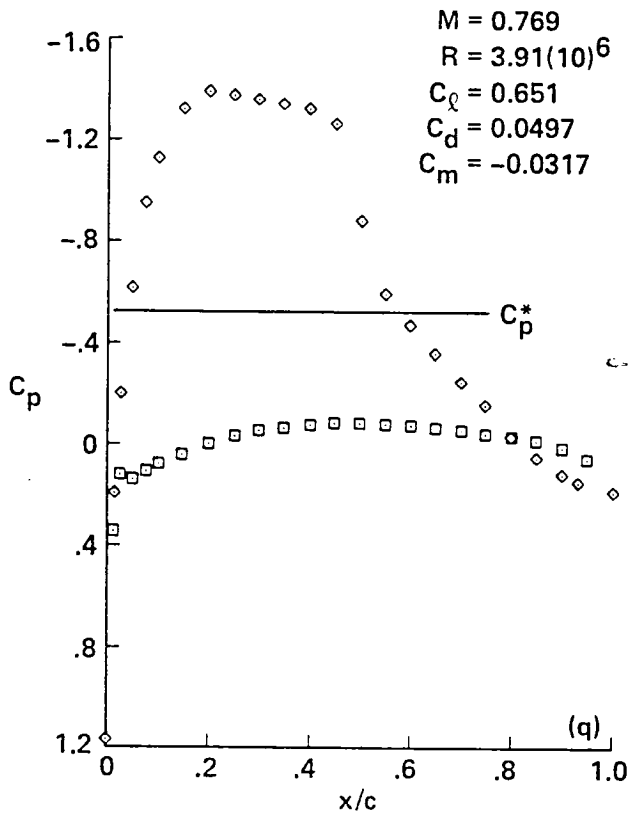


Figure 10.- Concluded.

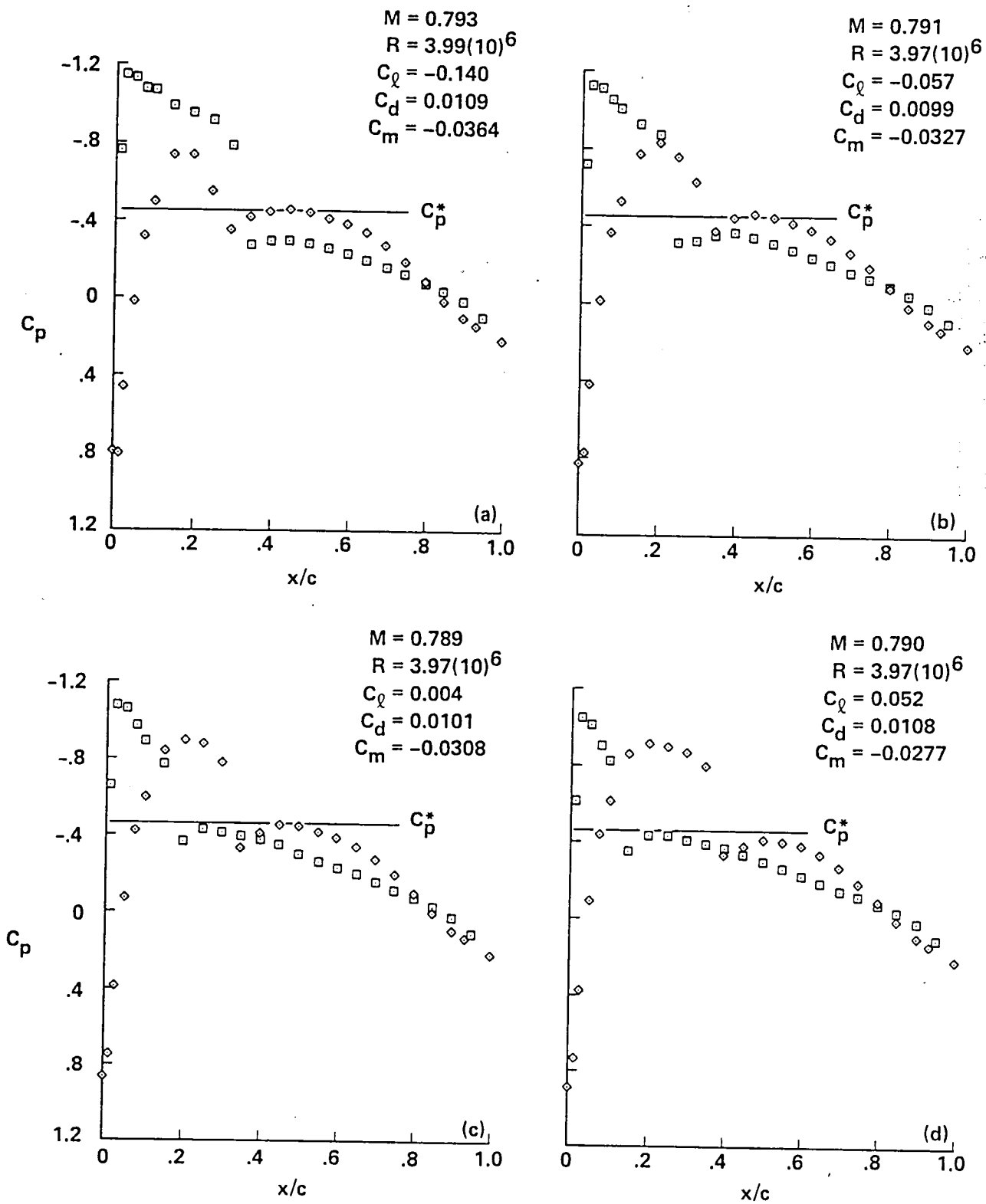


Figure 11.- Pressure distributions for A-1 airfoil, $M_{set} = 0.79$.

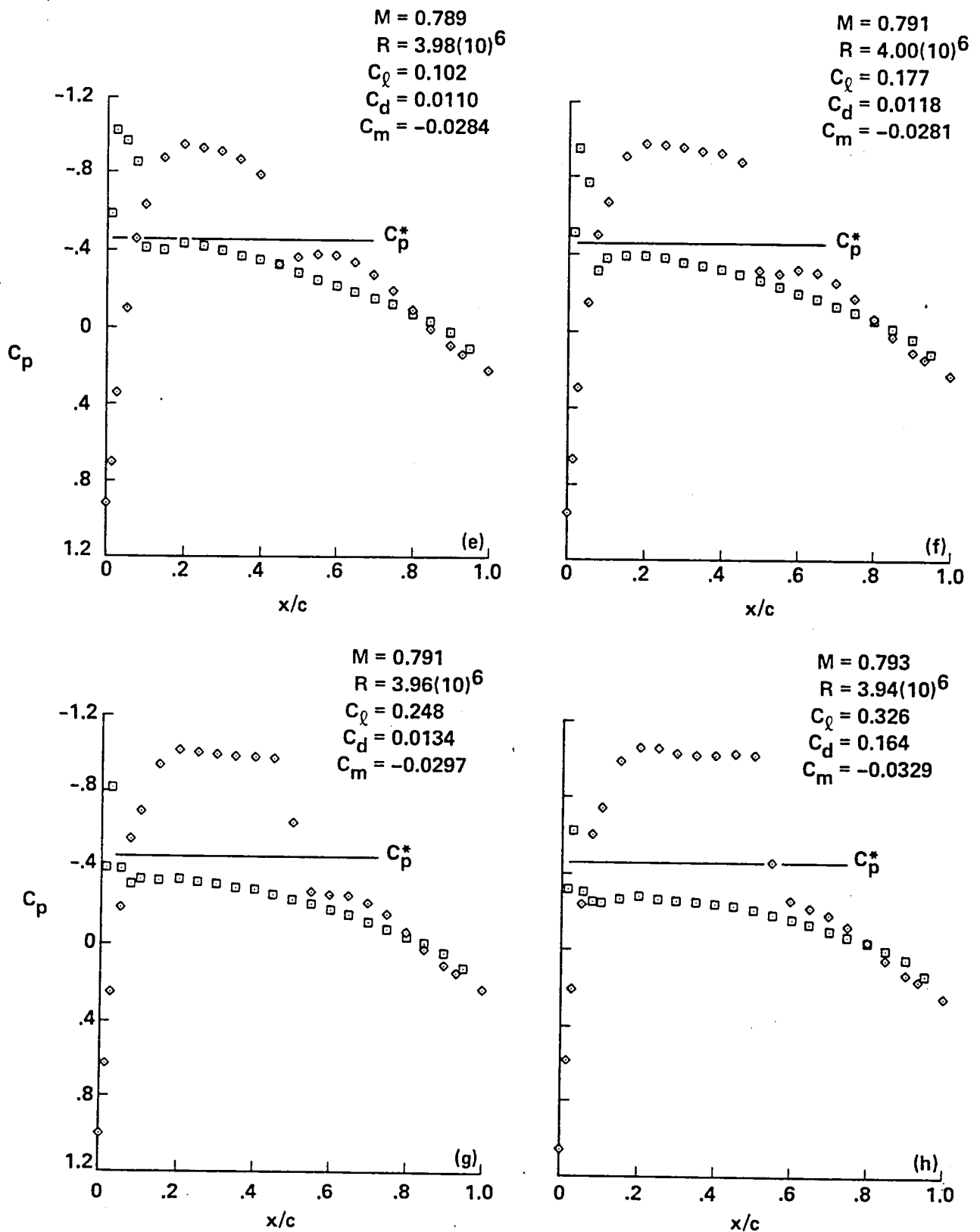


Figure 11.- Continued.

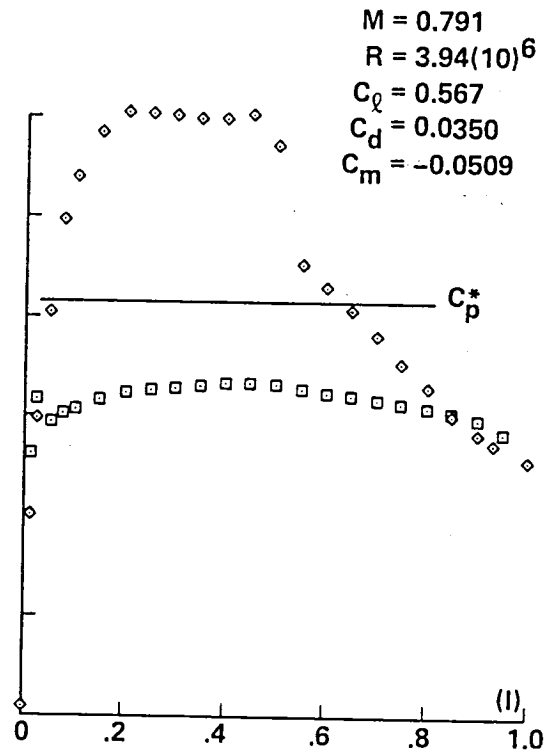
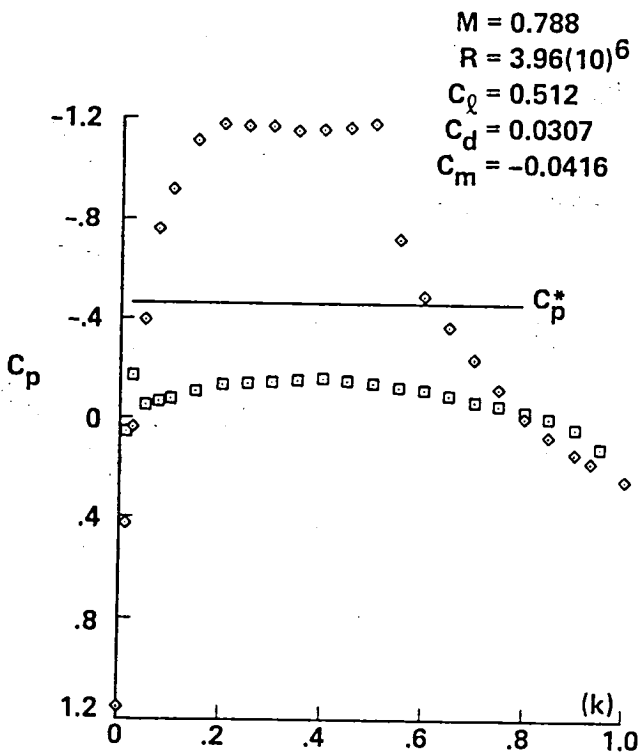
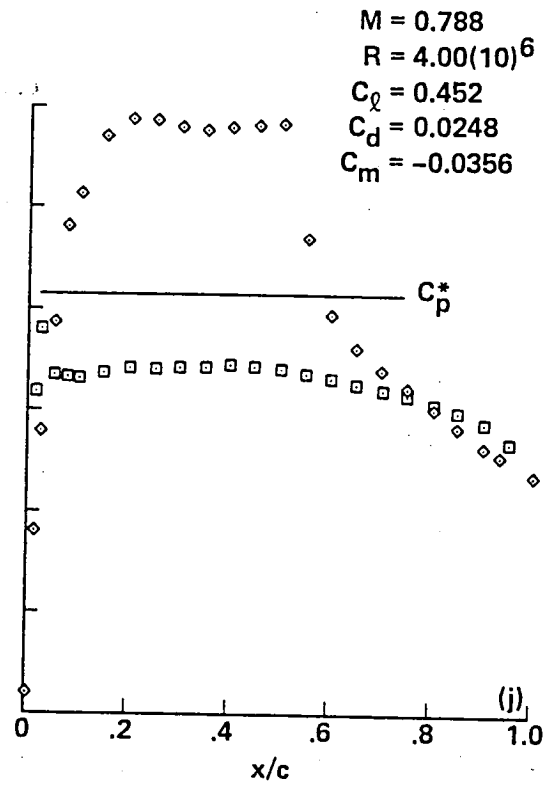
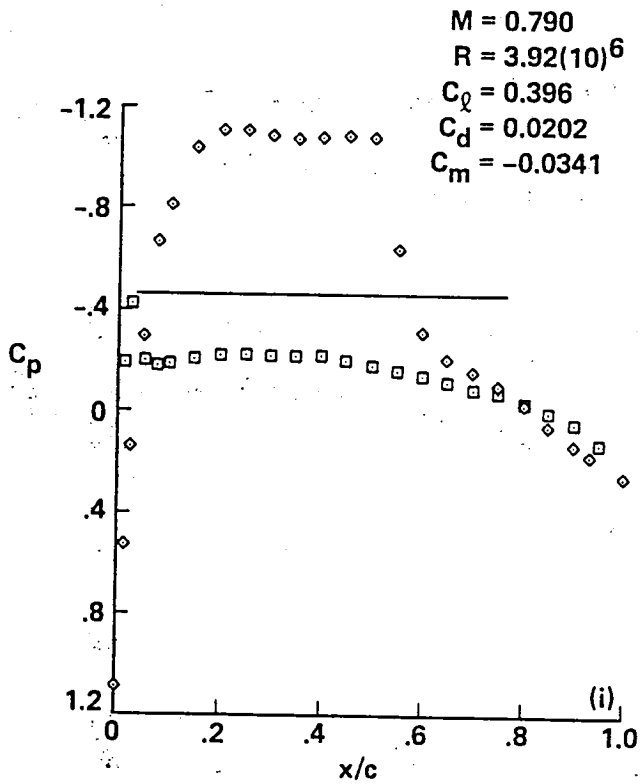


Figure 11.- Continued.

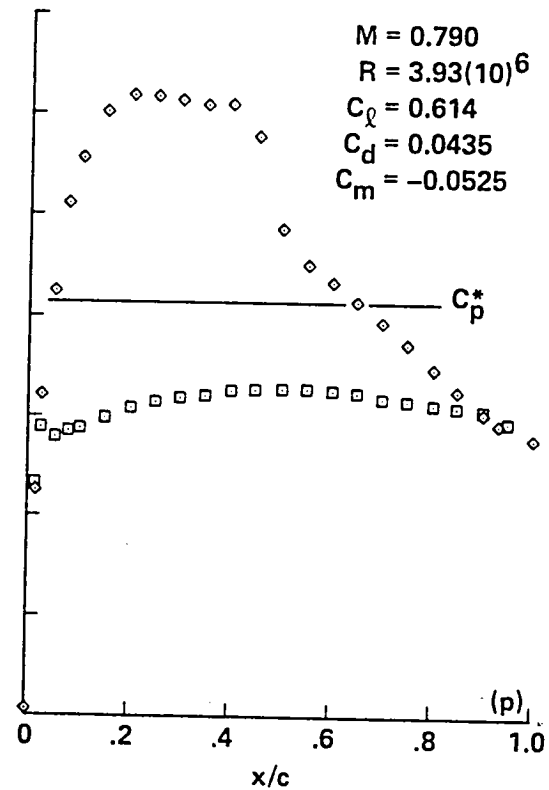
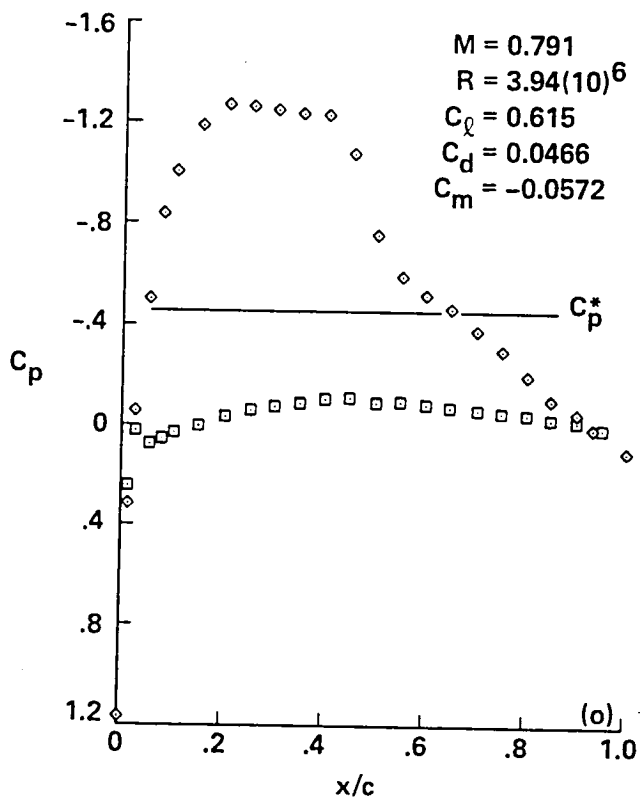
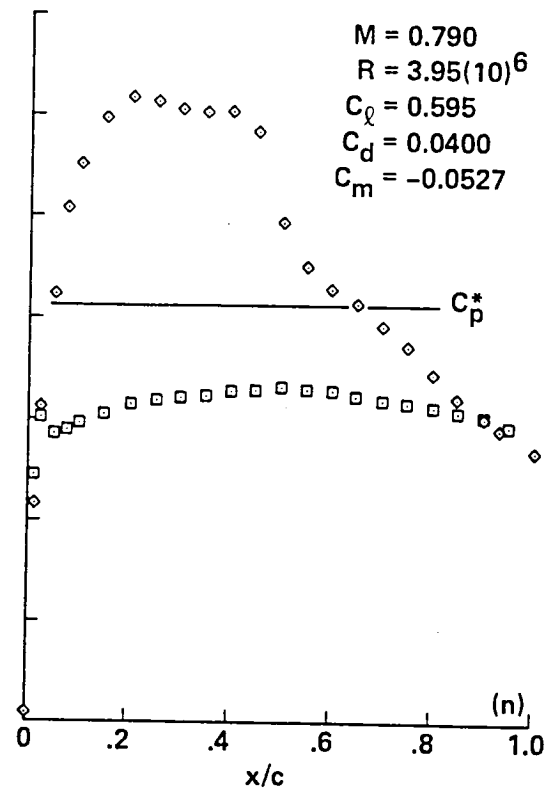
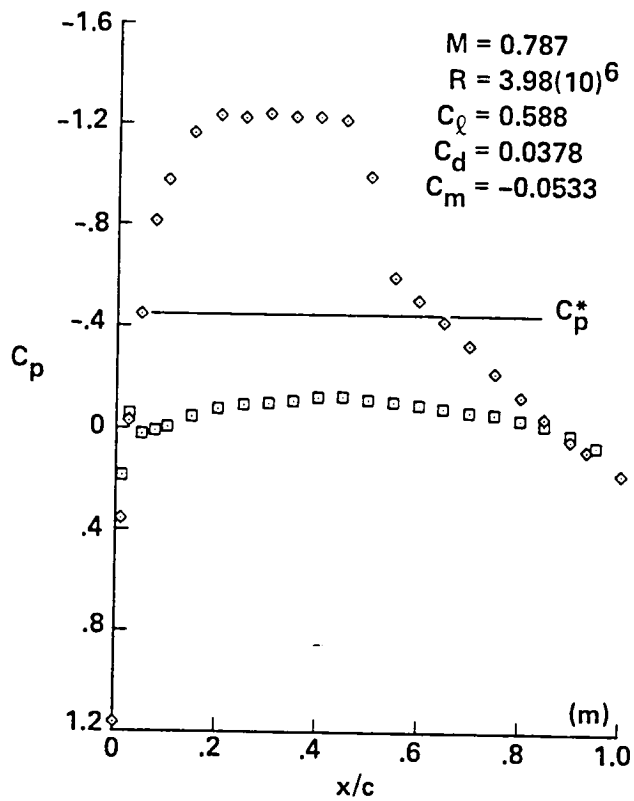


Figure 11.- Continued.

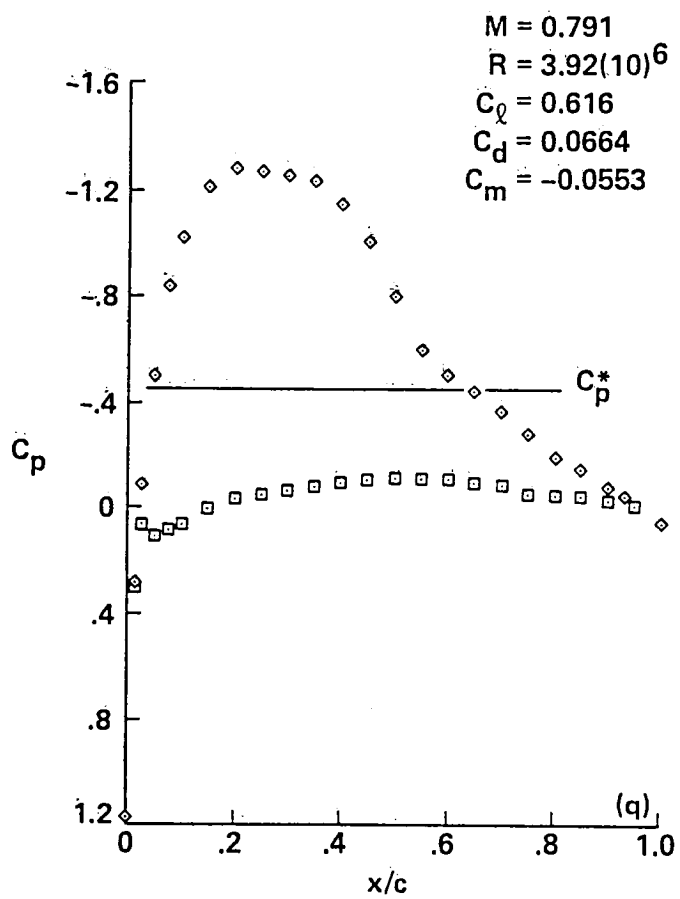


Figure 11.- Concluded.

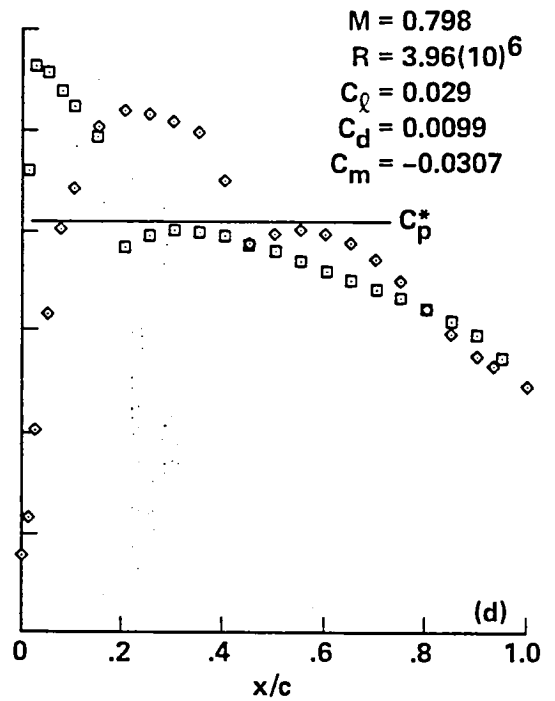
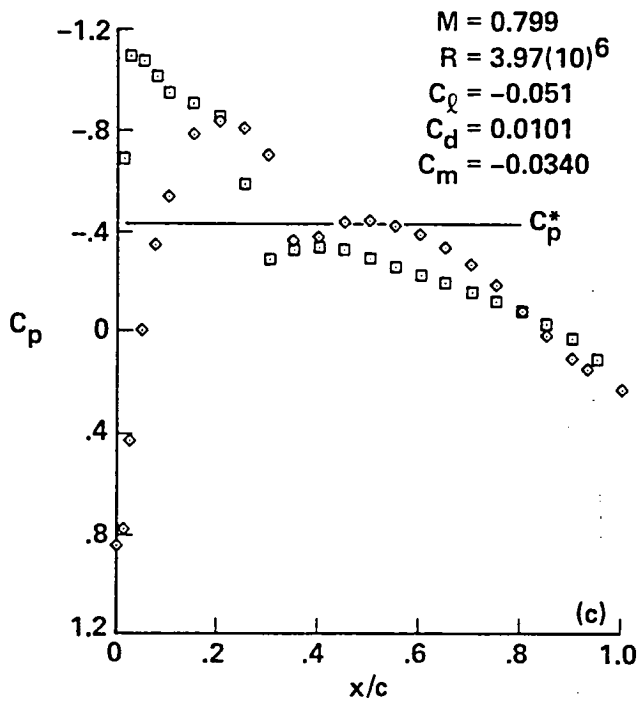
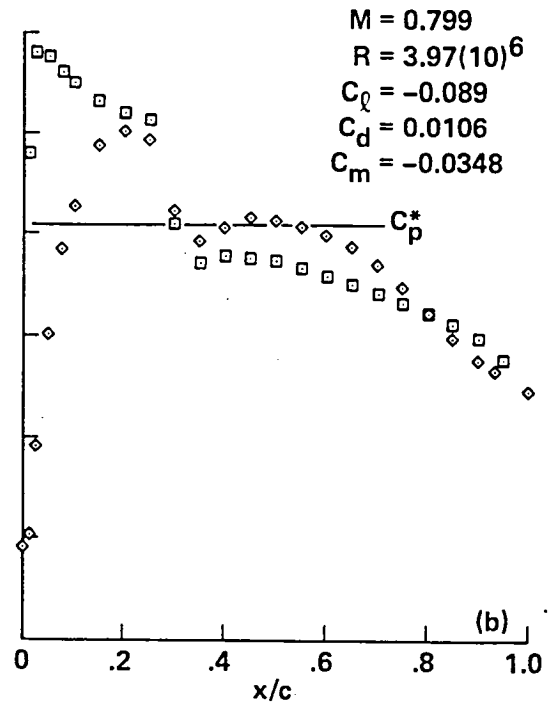
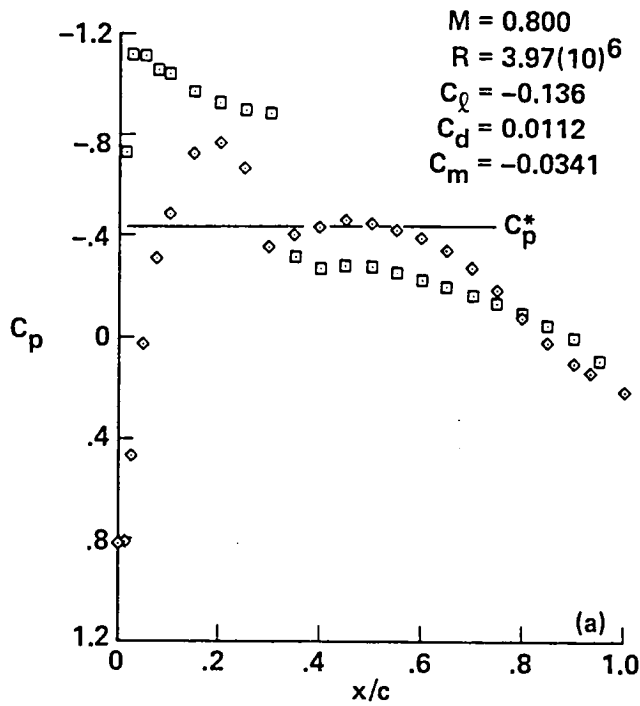


Figure 12.- Pressure distributions for A-1 airfoil, $M_{set} = 0.8$.

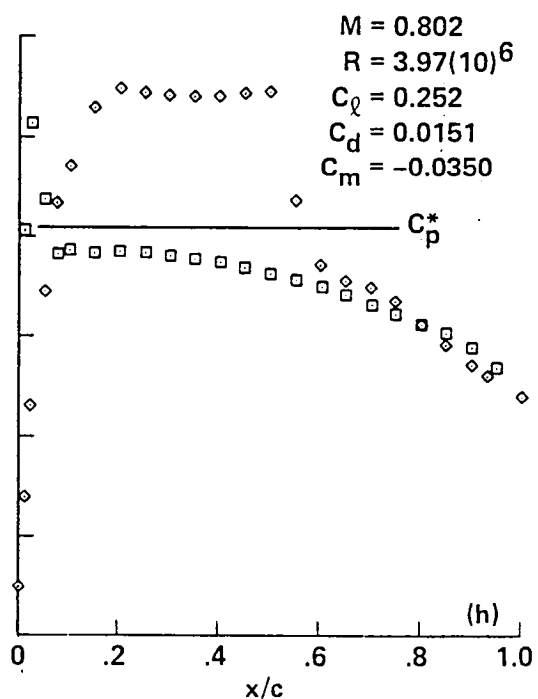
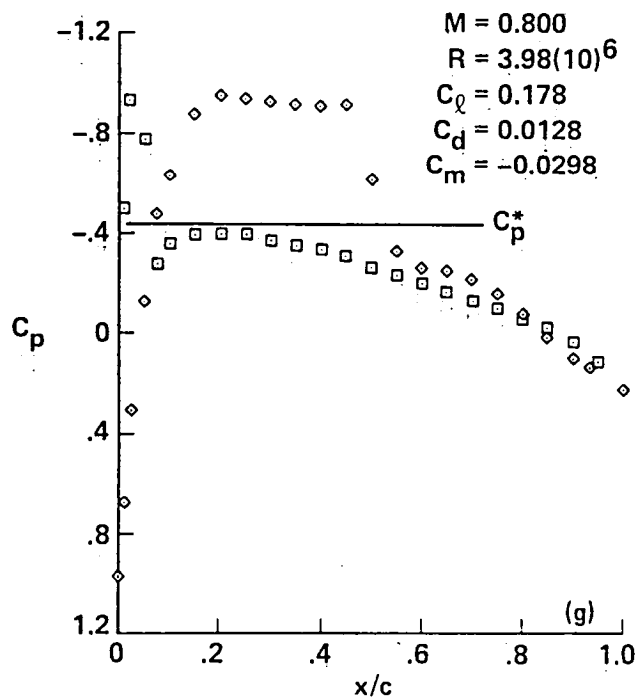
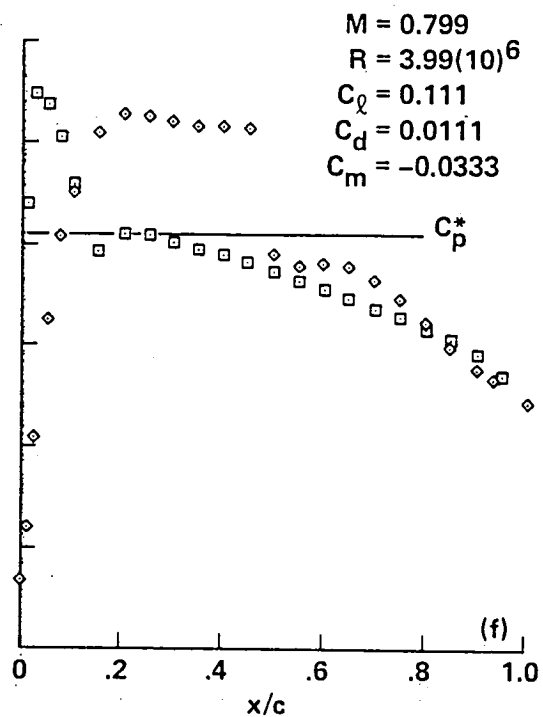
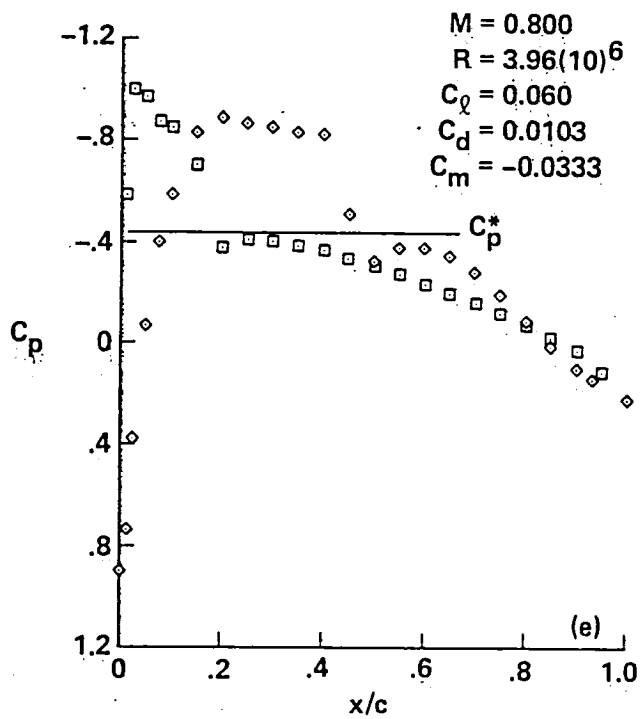


Figure 12.- Continued.

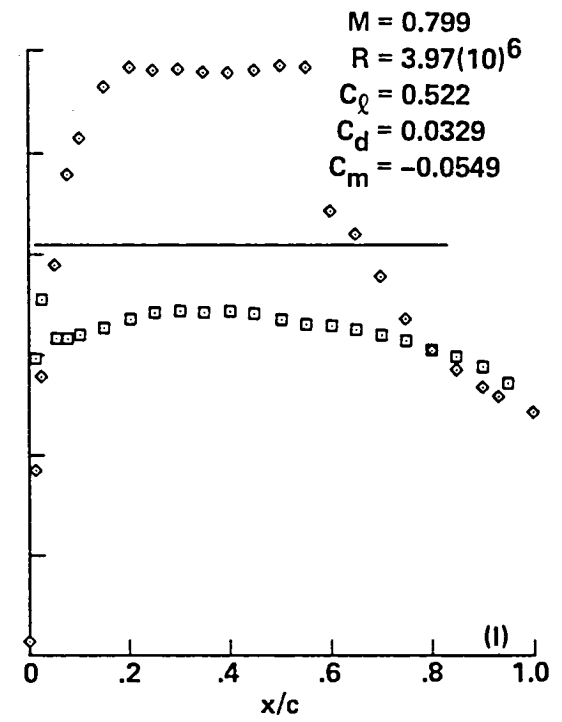
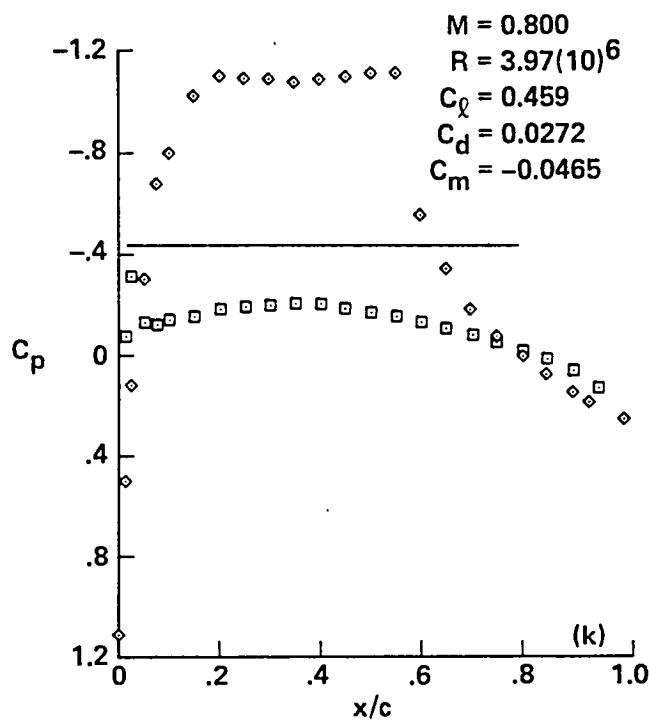
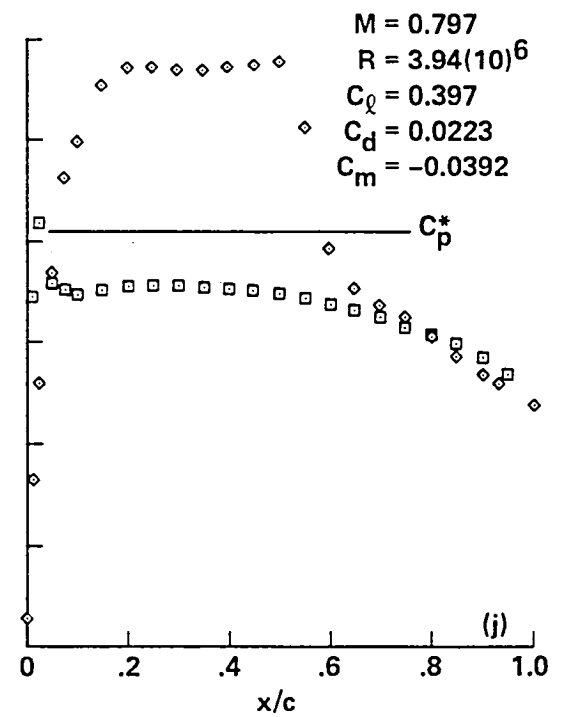
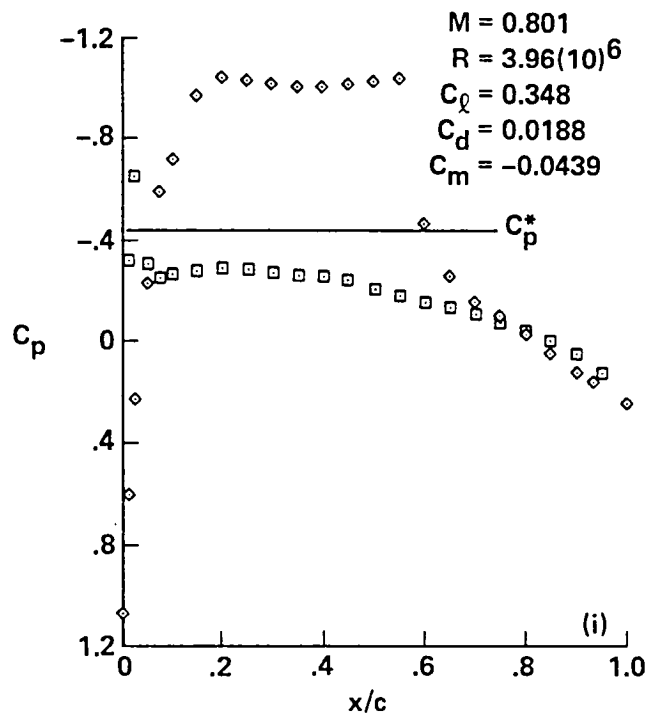


Figure 12.- Continued.

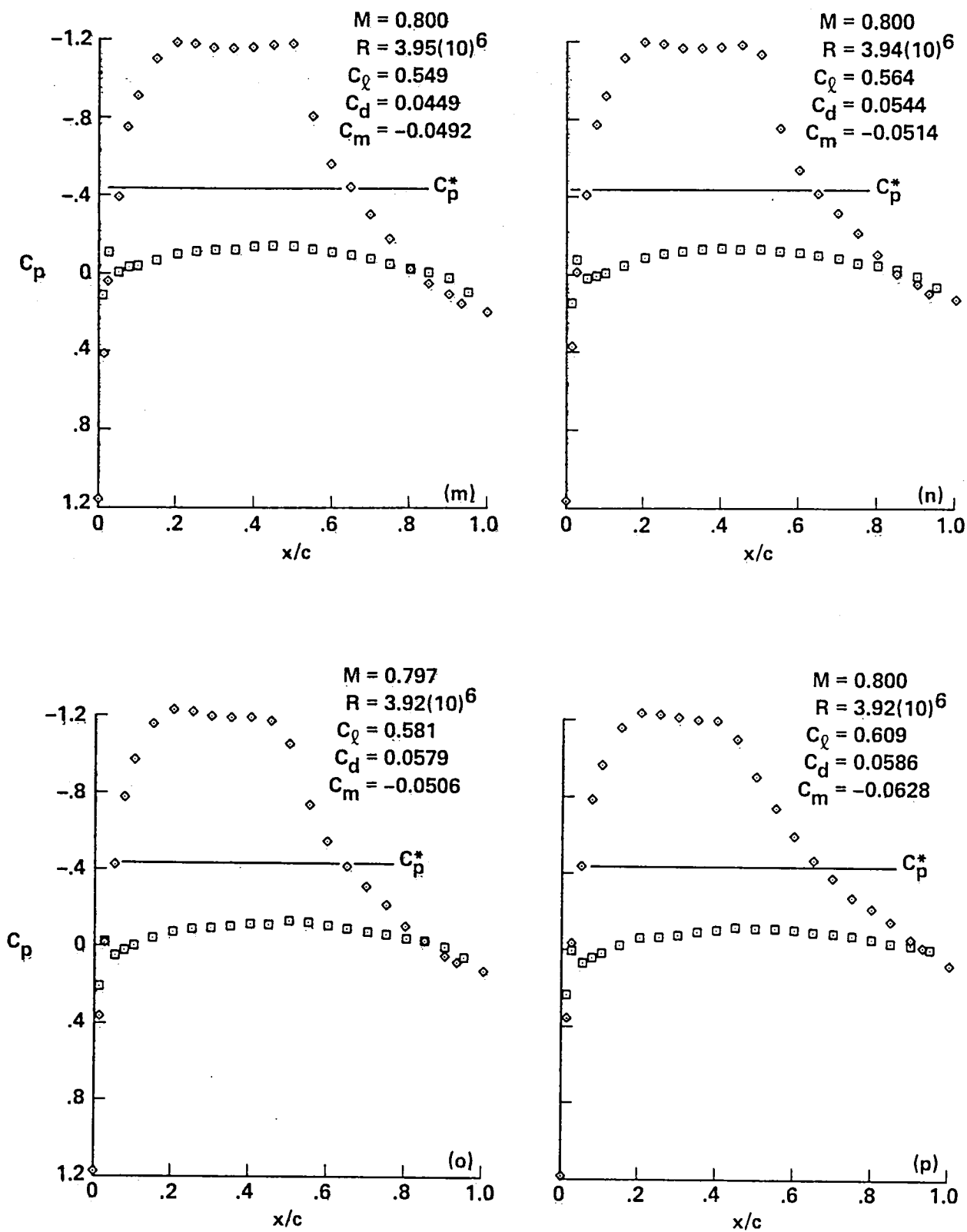


Figure 12.- Concluded.

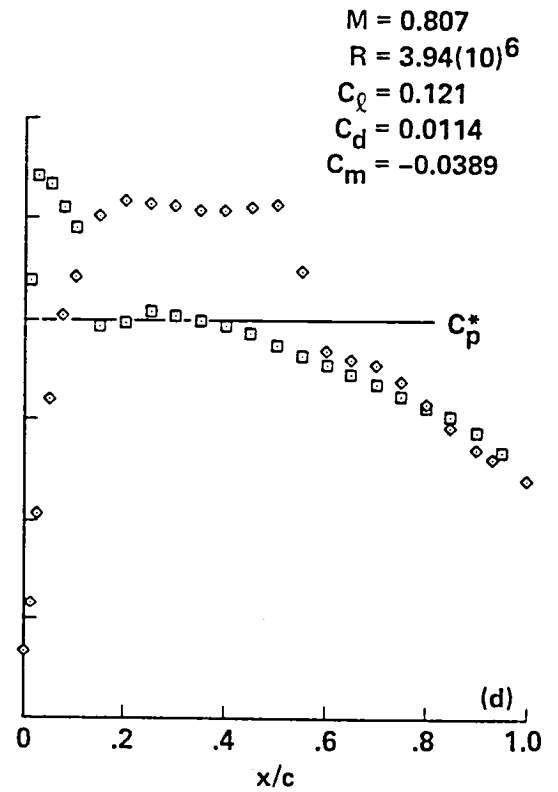
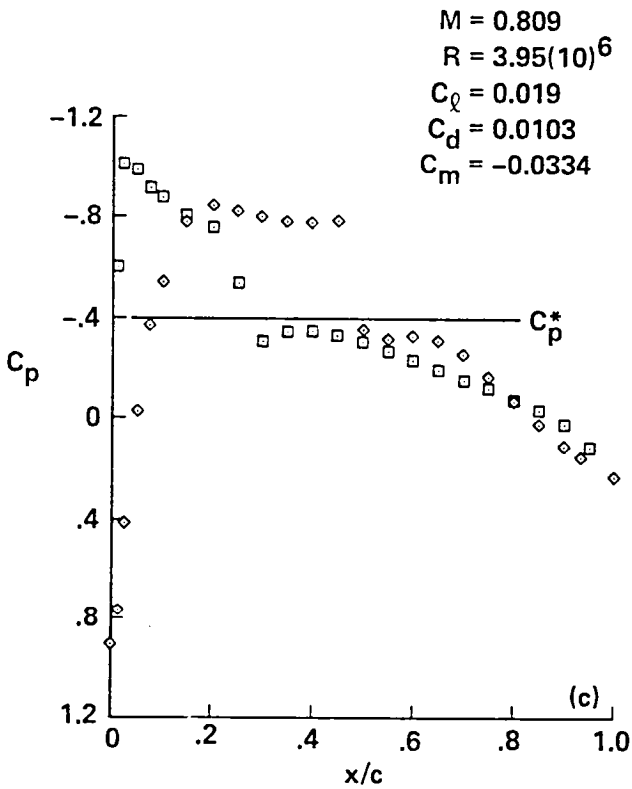
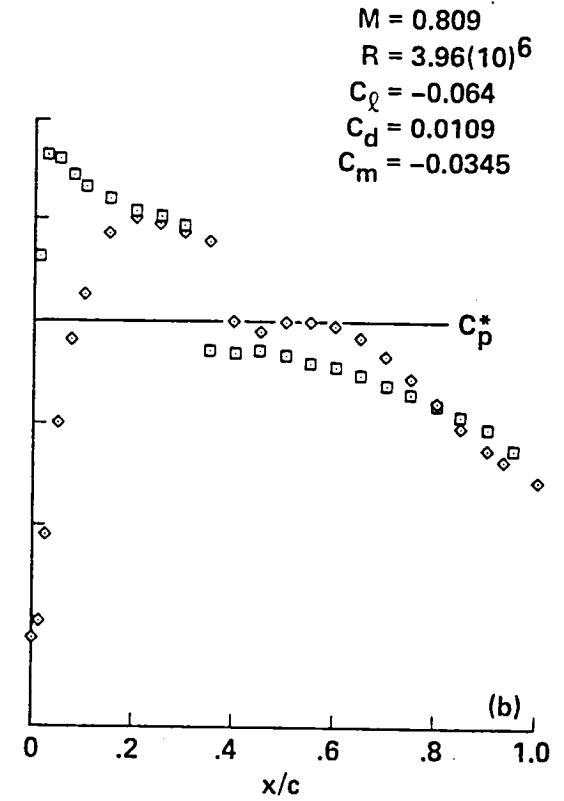
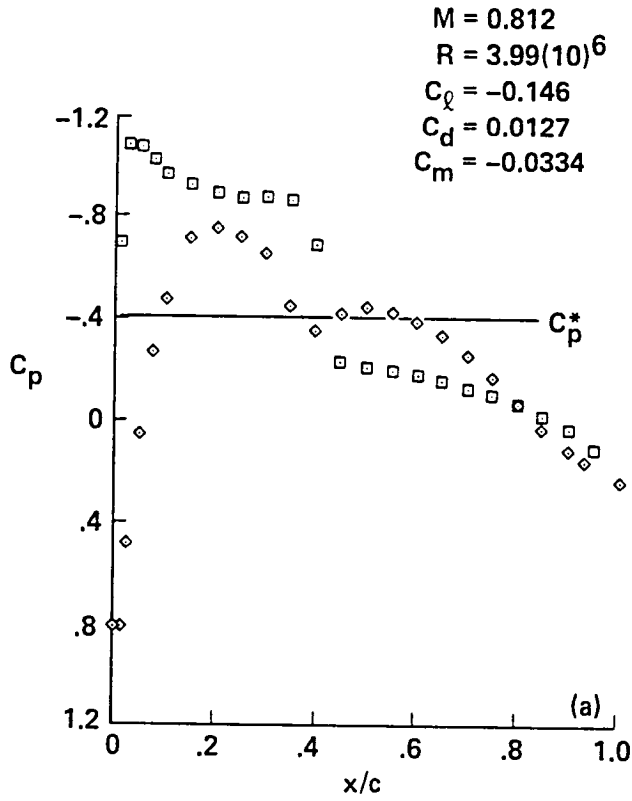


Figure 13.- Pressure distributions for A-1 airfoil, $M_{set} = 0.81$.

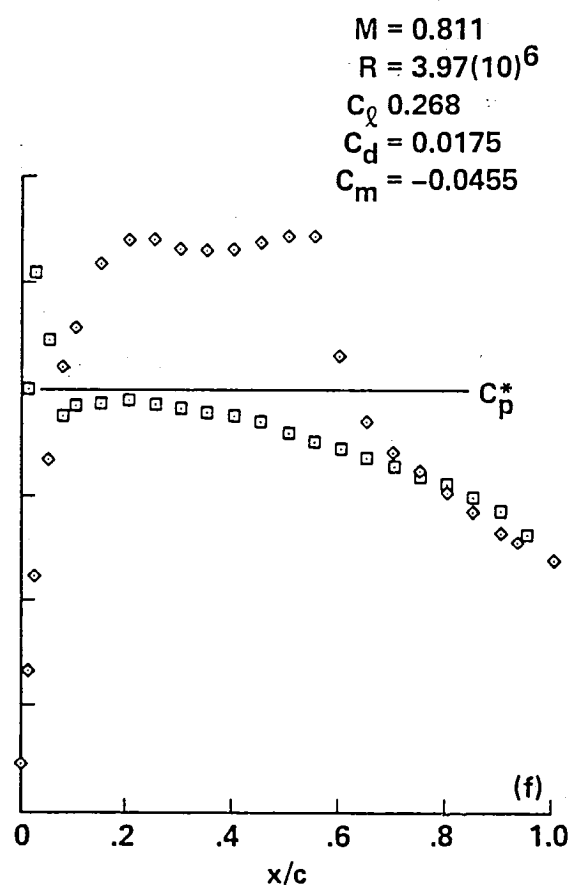
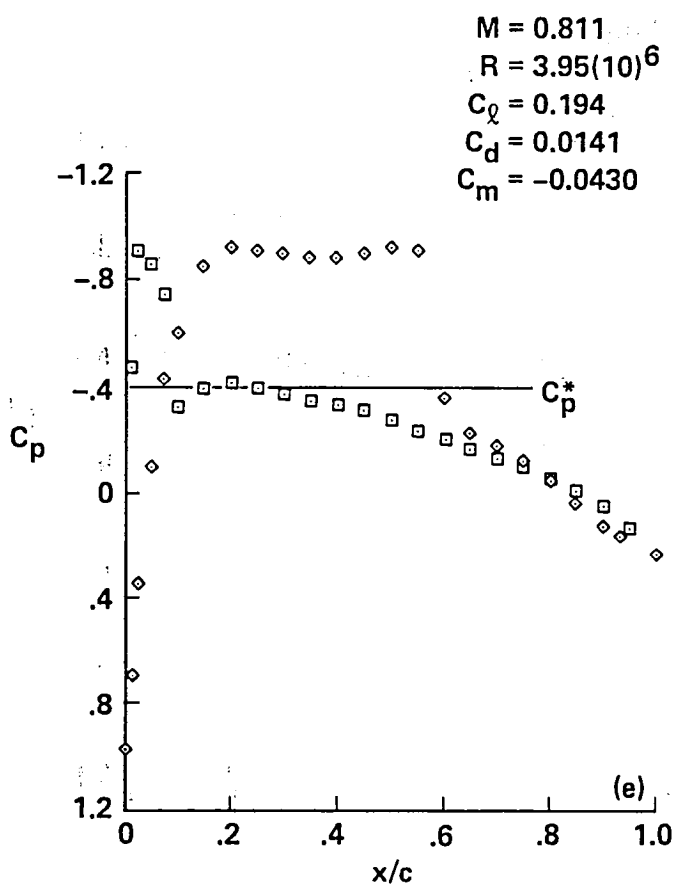


Figure 13.- Continued.

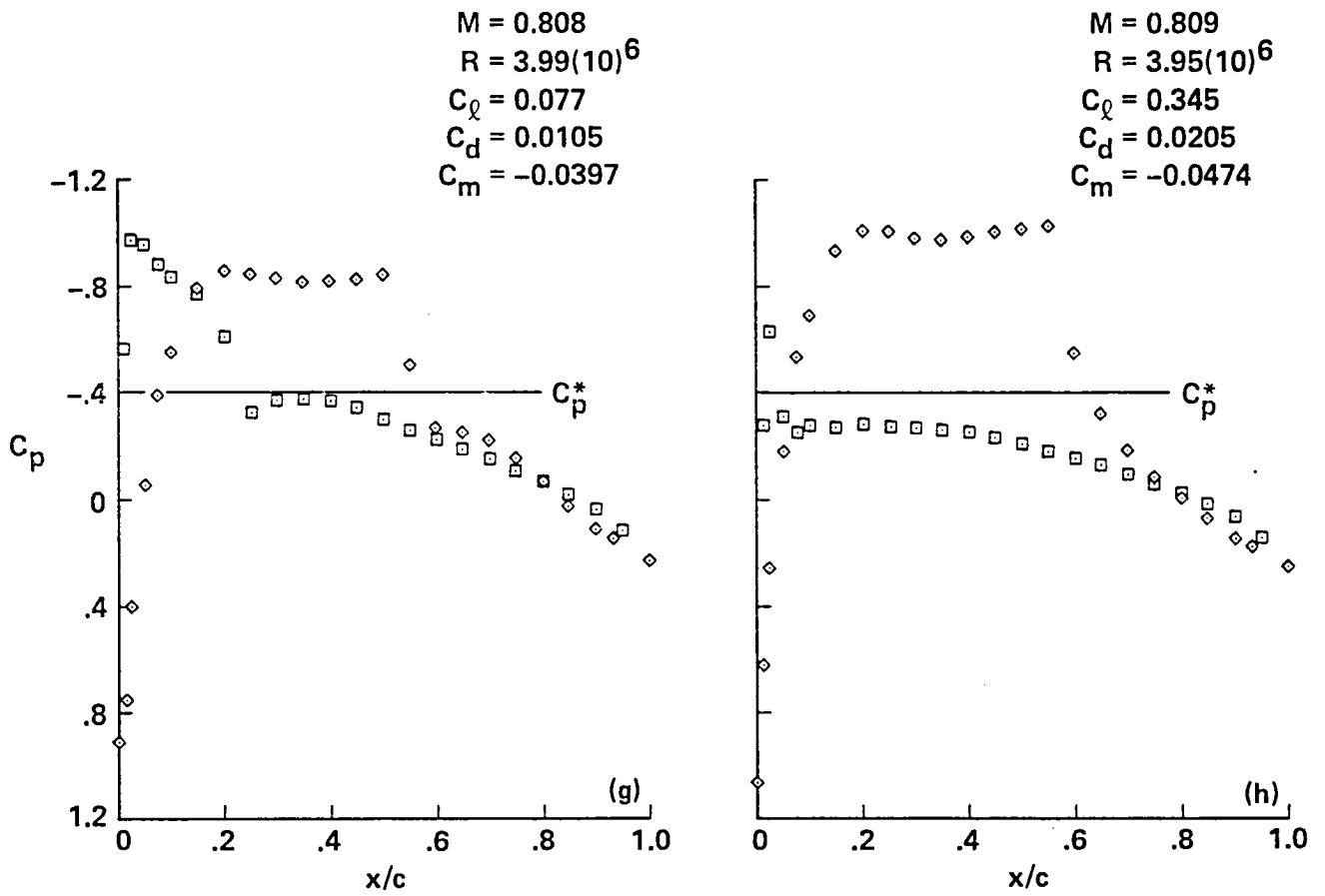


Figure 13.- Continued.

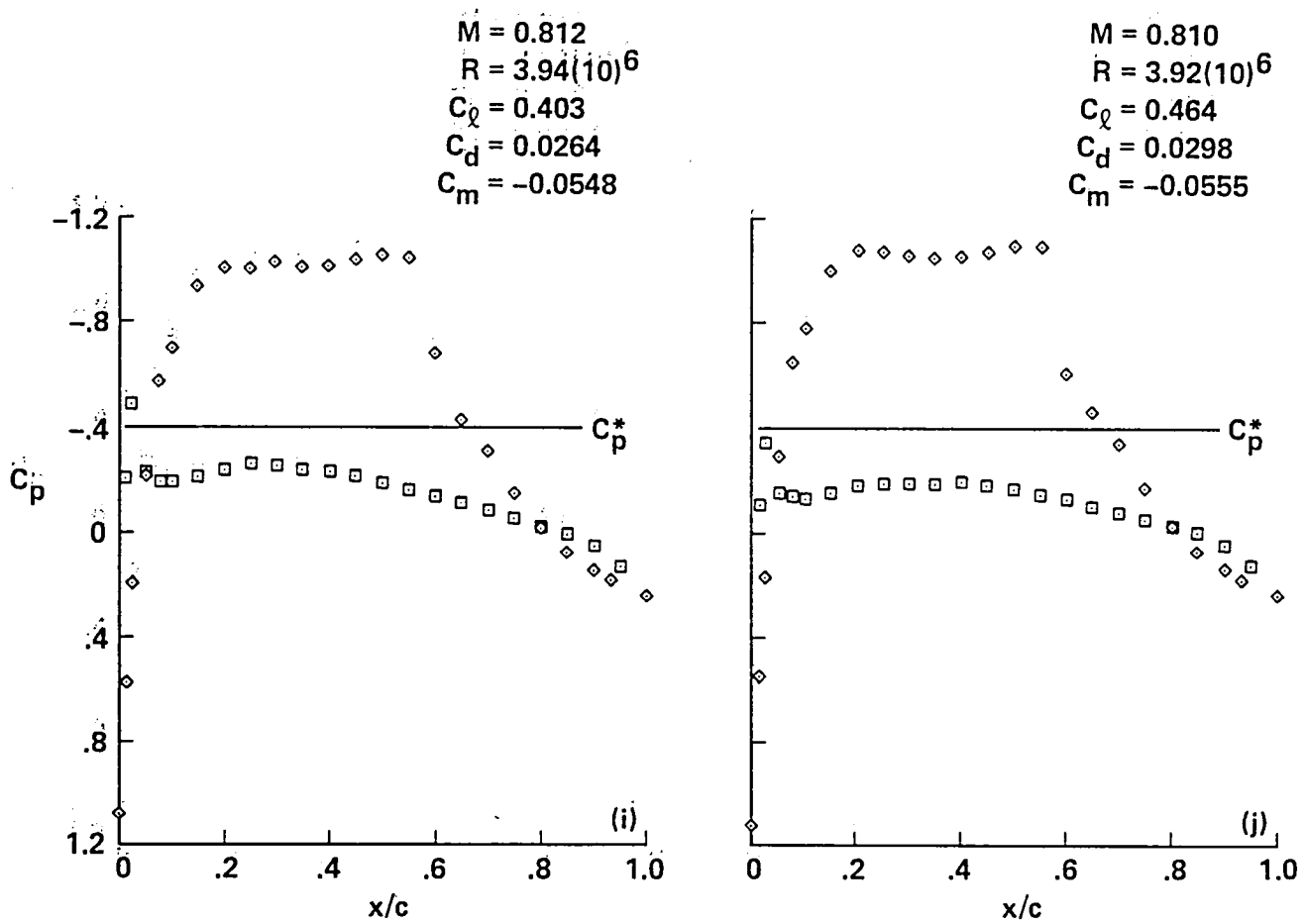


Figure 13.- Continued.

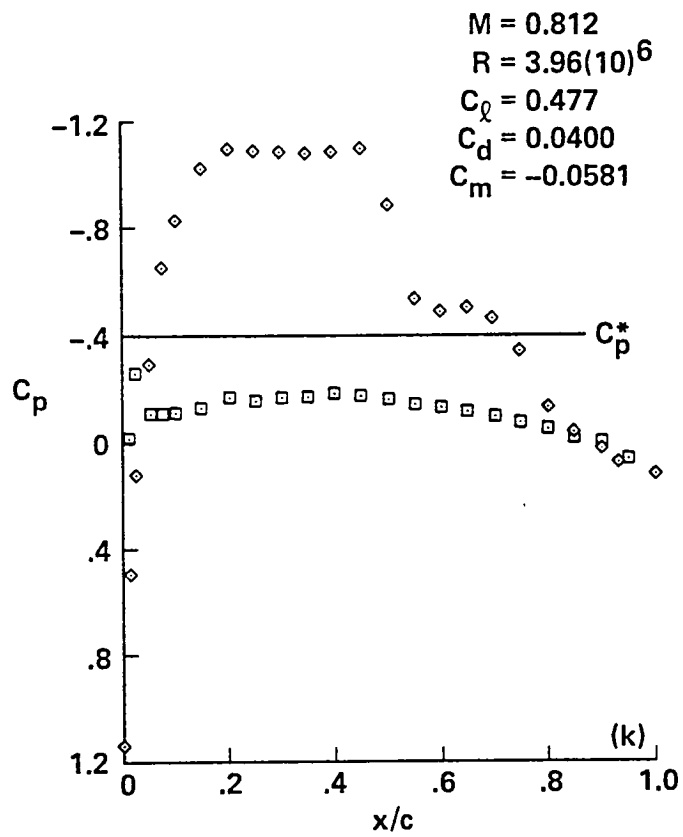


Figure 13.- Concluded.

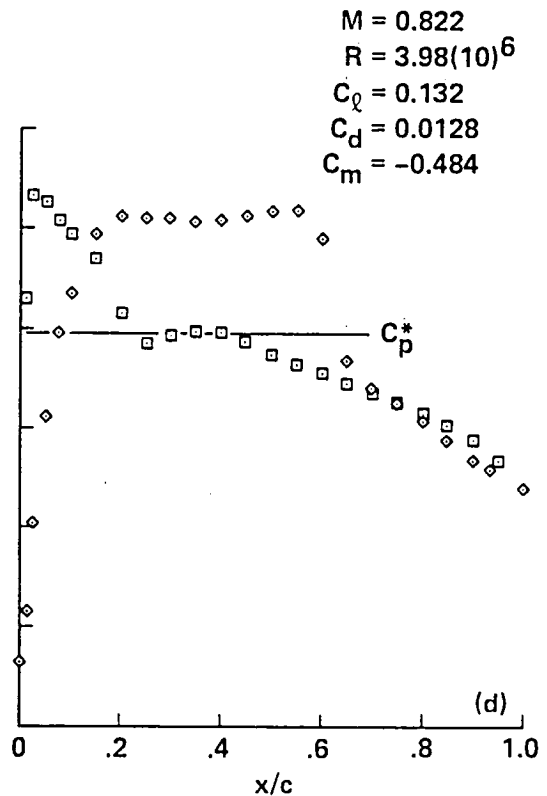
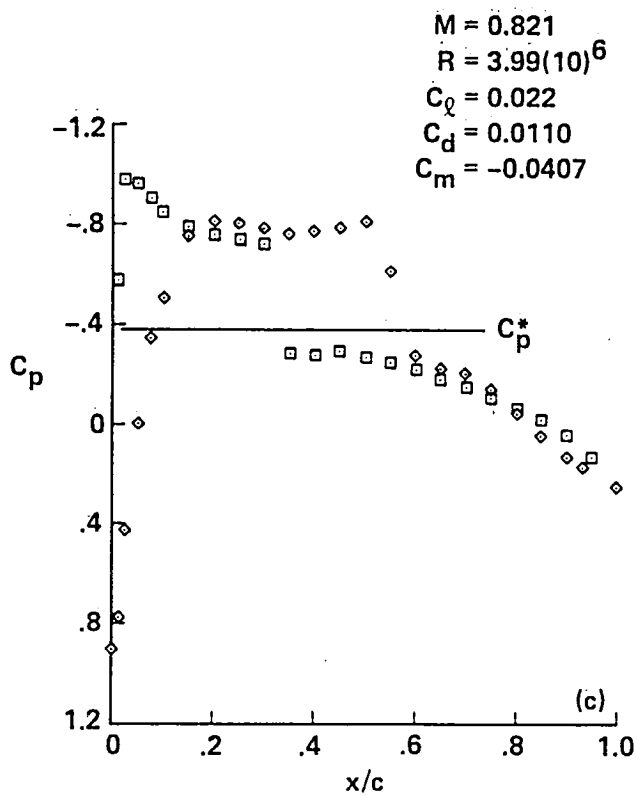
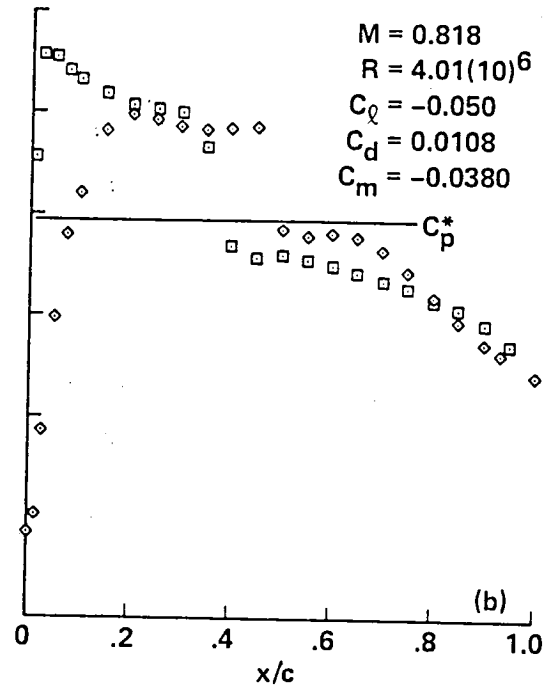
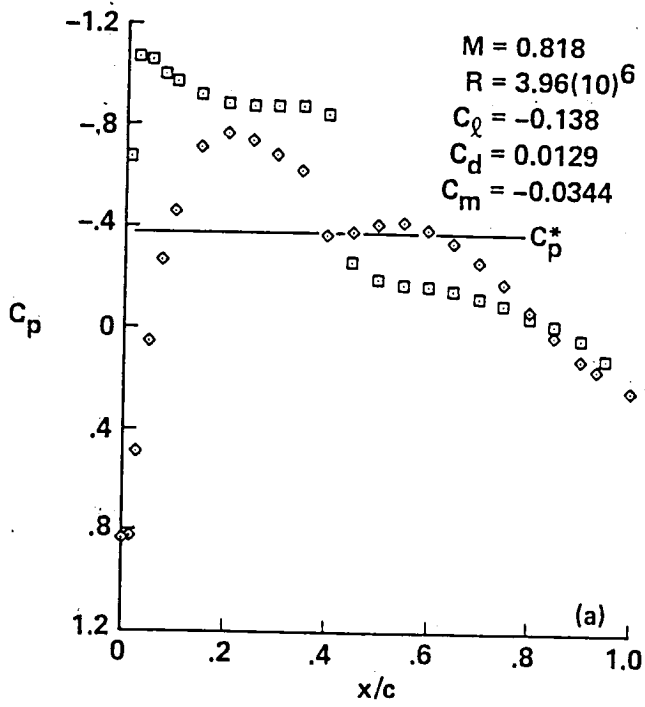


Figure 14.- Pressure distribution for A-1 airfoil, $M_{set} = 0.82$.

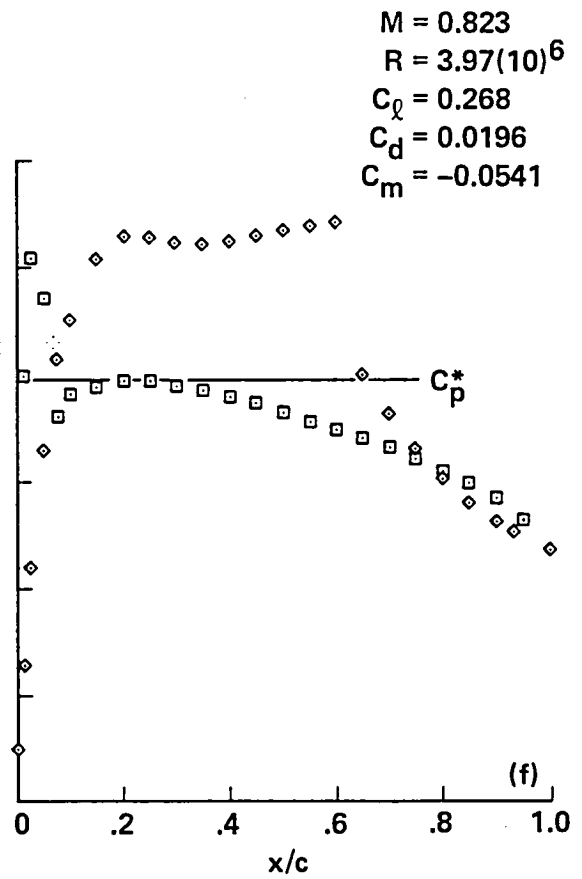
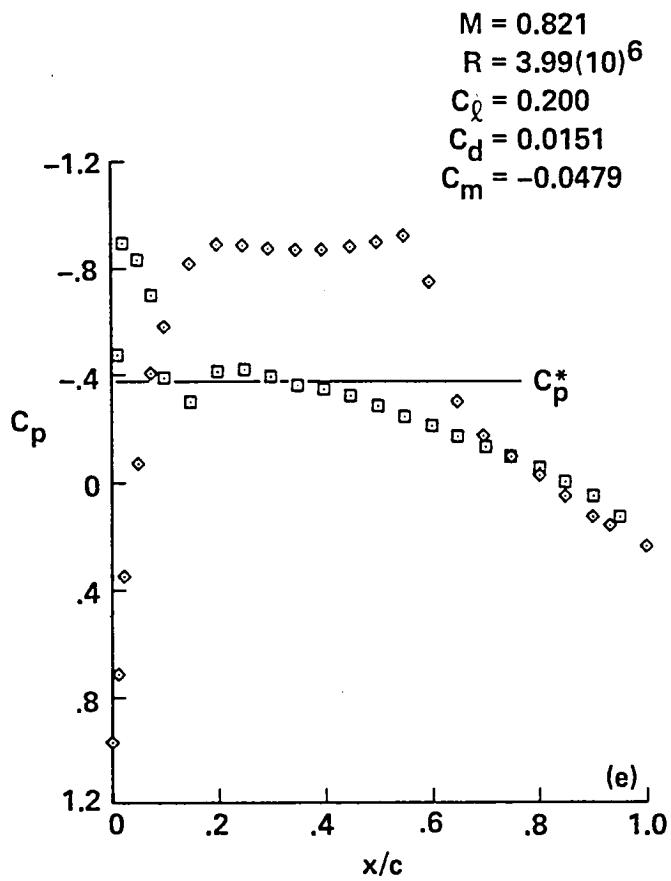


Figure 14.- Continued.

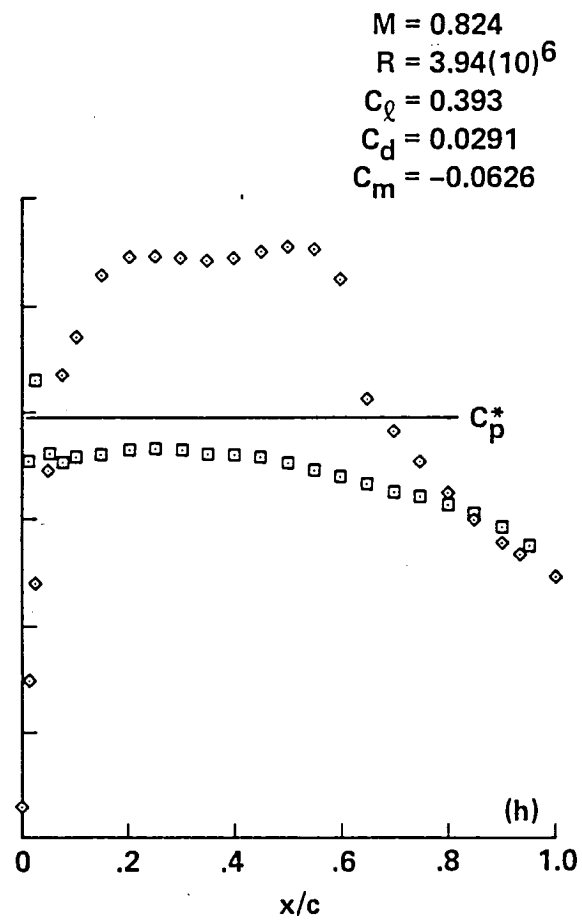
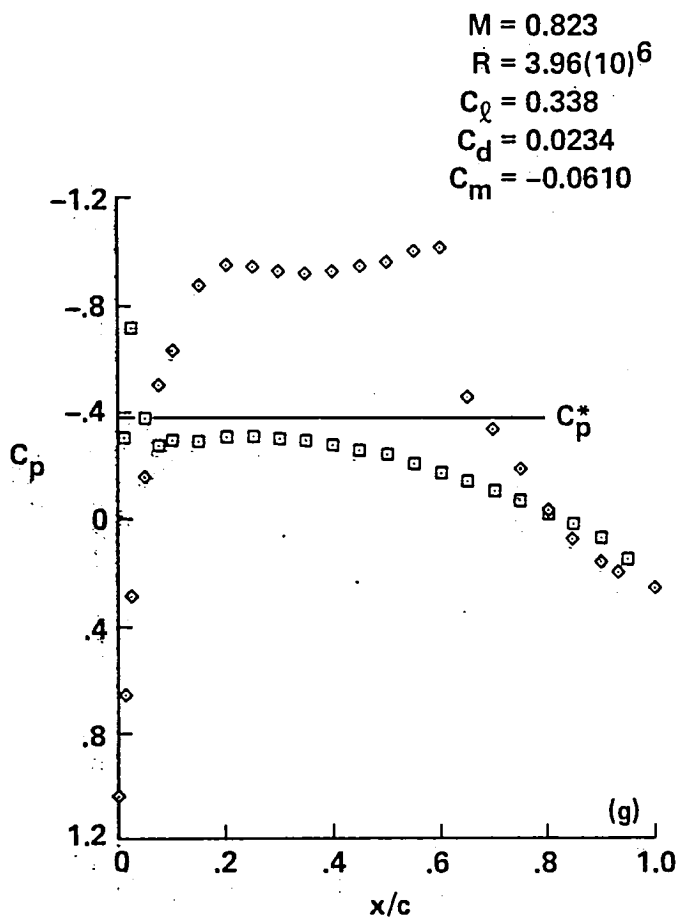


Figure 14.- Continued.

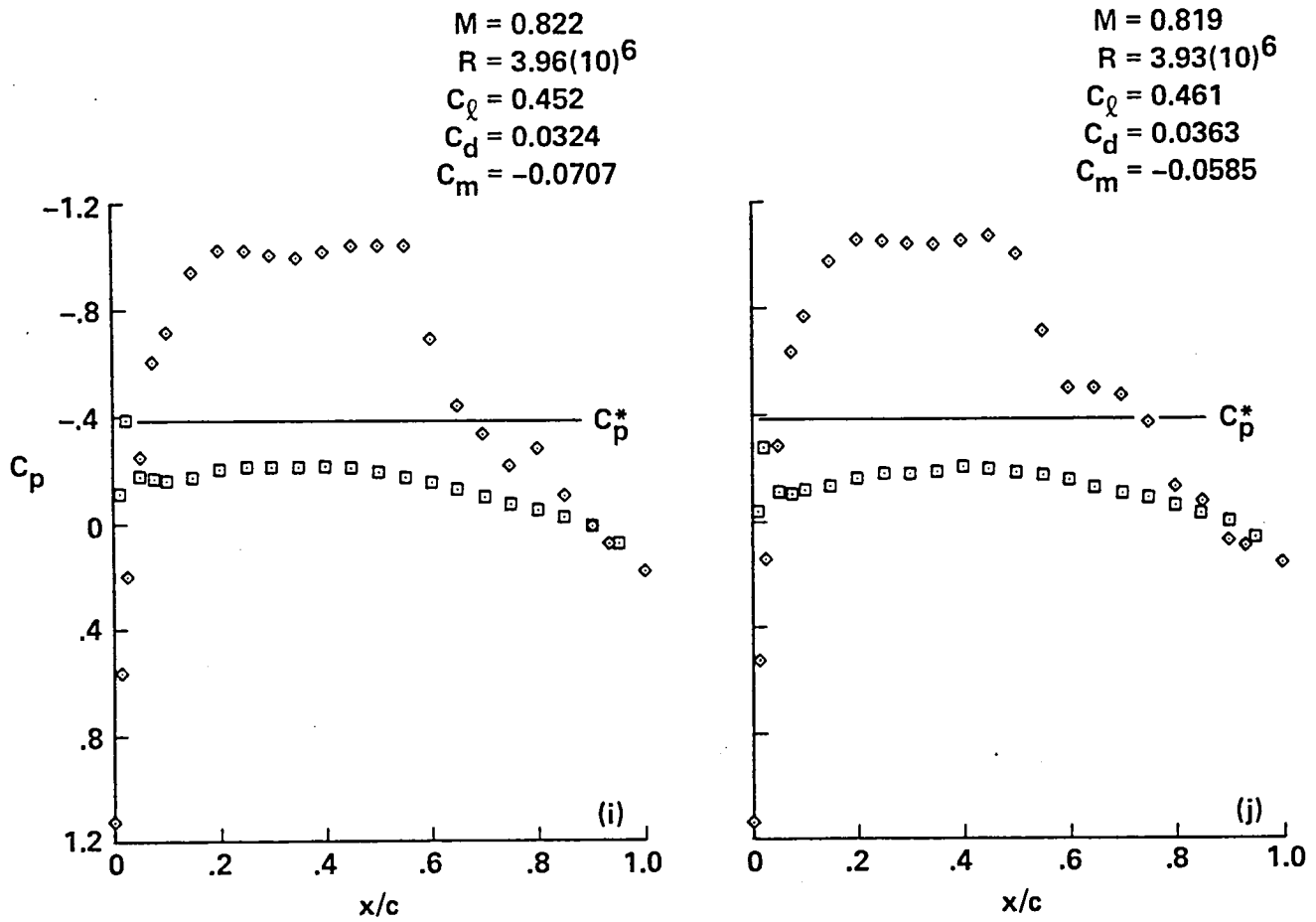


Figure 14.- Concluded.

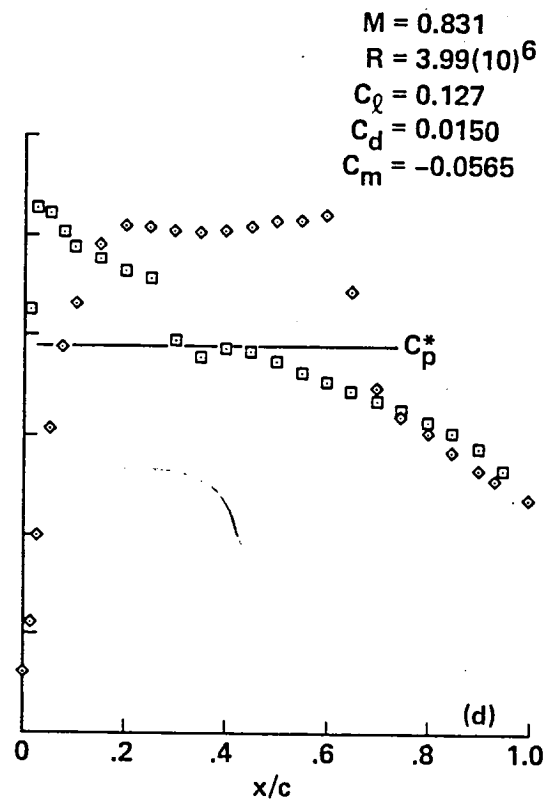
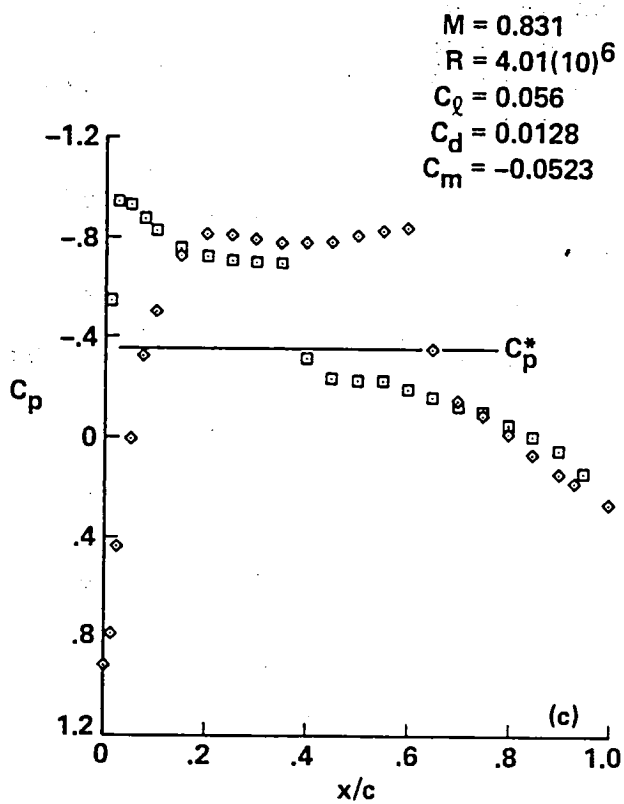
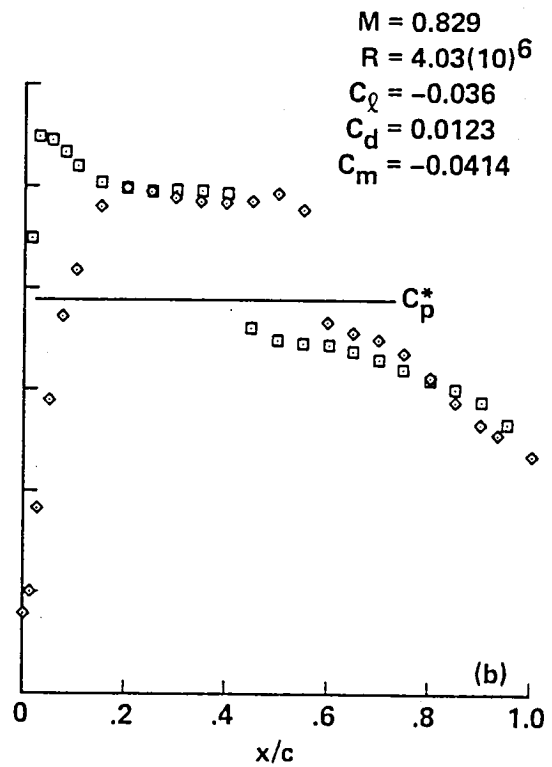
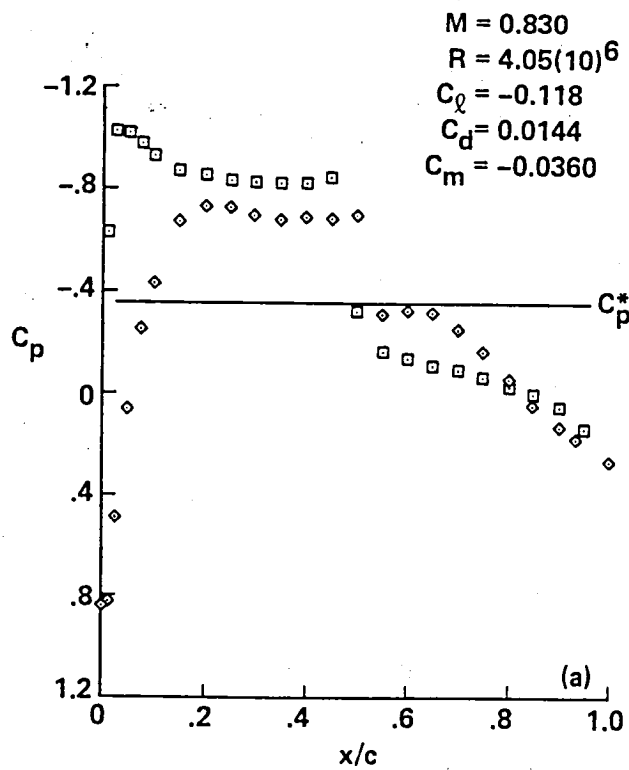


Figure 15.- Pressure distributions for A-1 airfoil, $M_{set} = 0.83$.

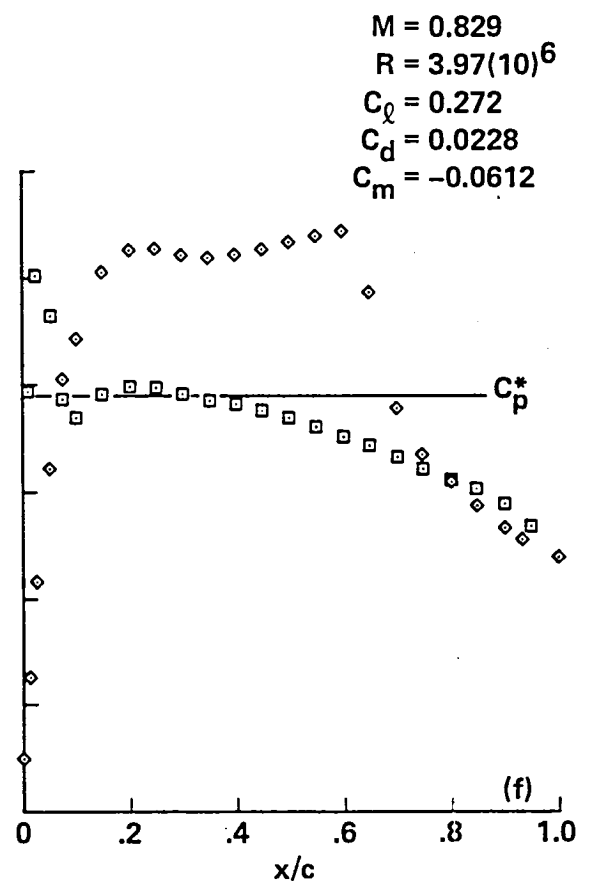
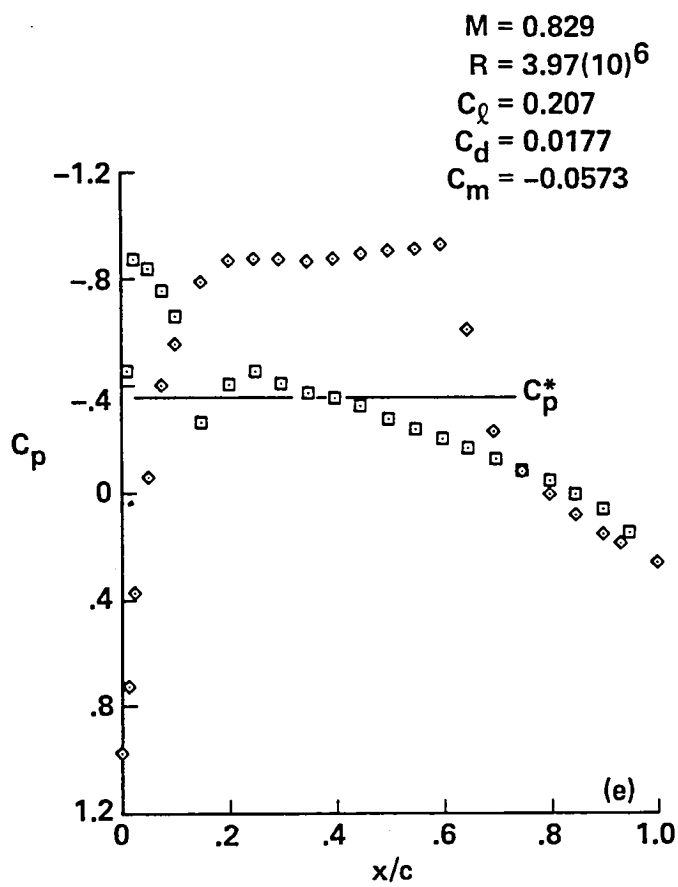


Figure 15.- Continued.

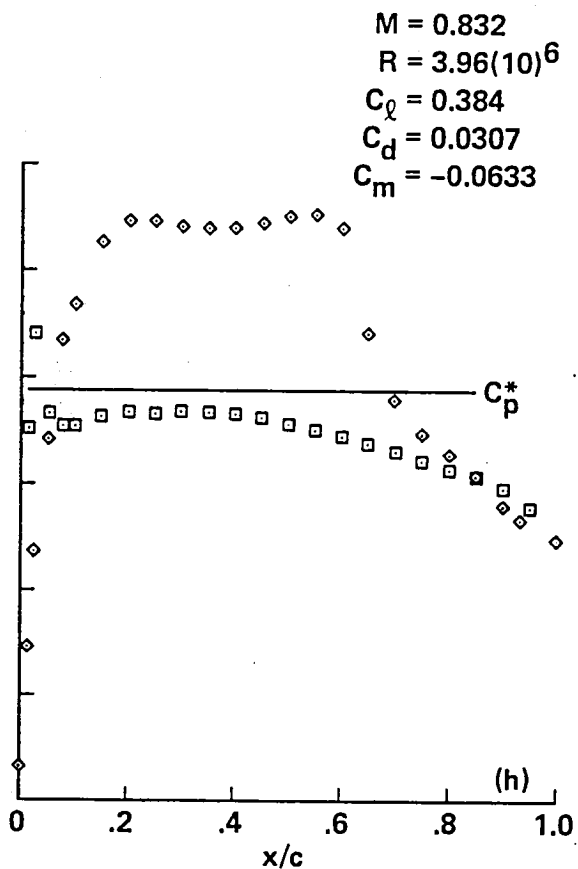
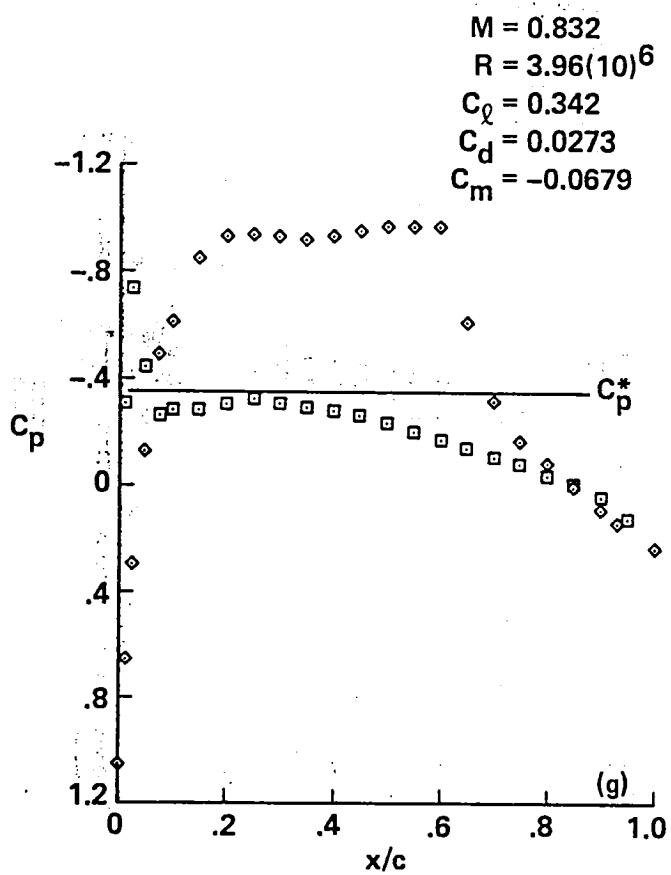


Figure 15.- Concluded.

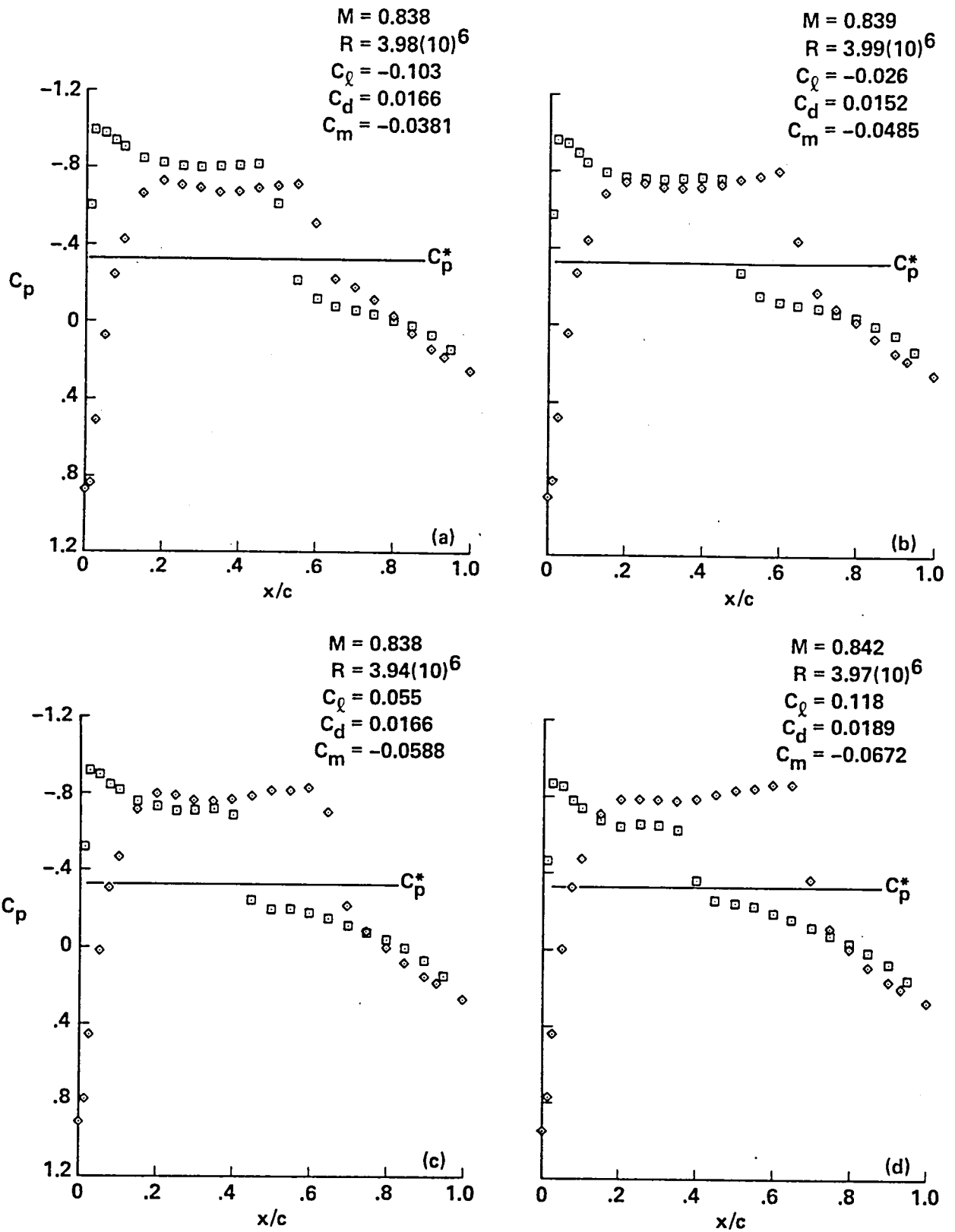


Figure 16.- Pressure distributions for A-1 airfoil, $M_{set} = 0.84$.

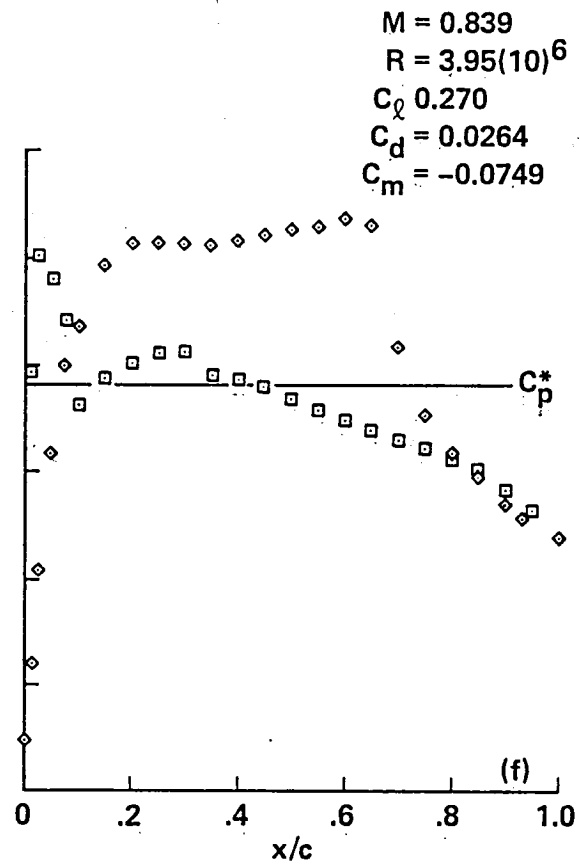
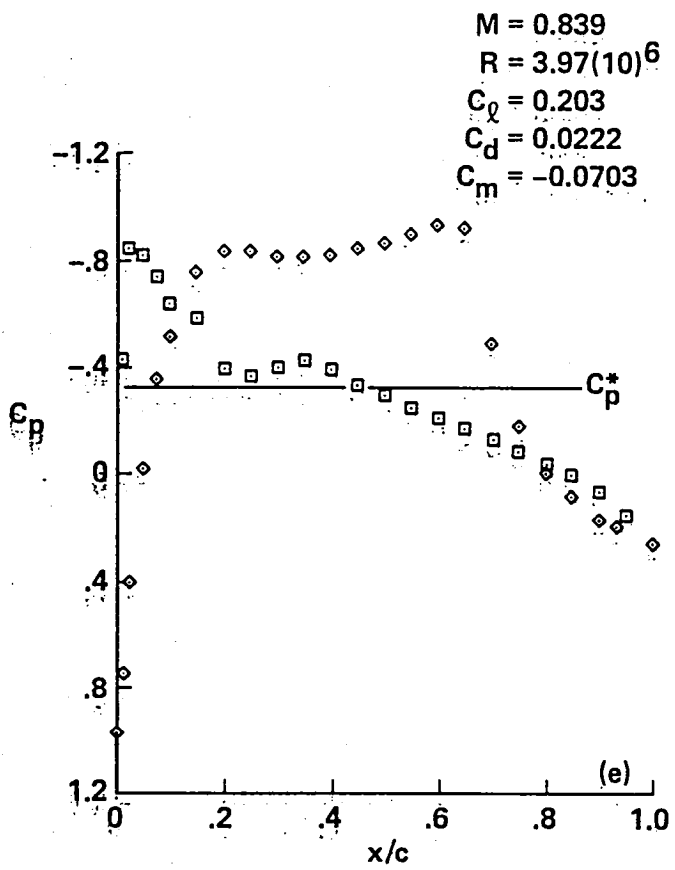


Figure 16.- Continued.

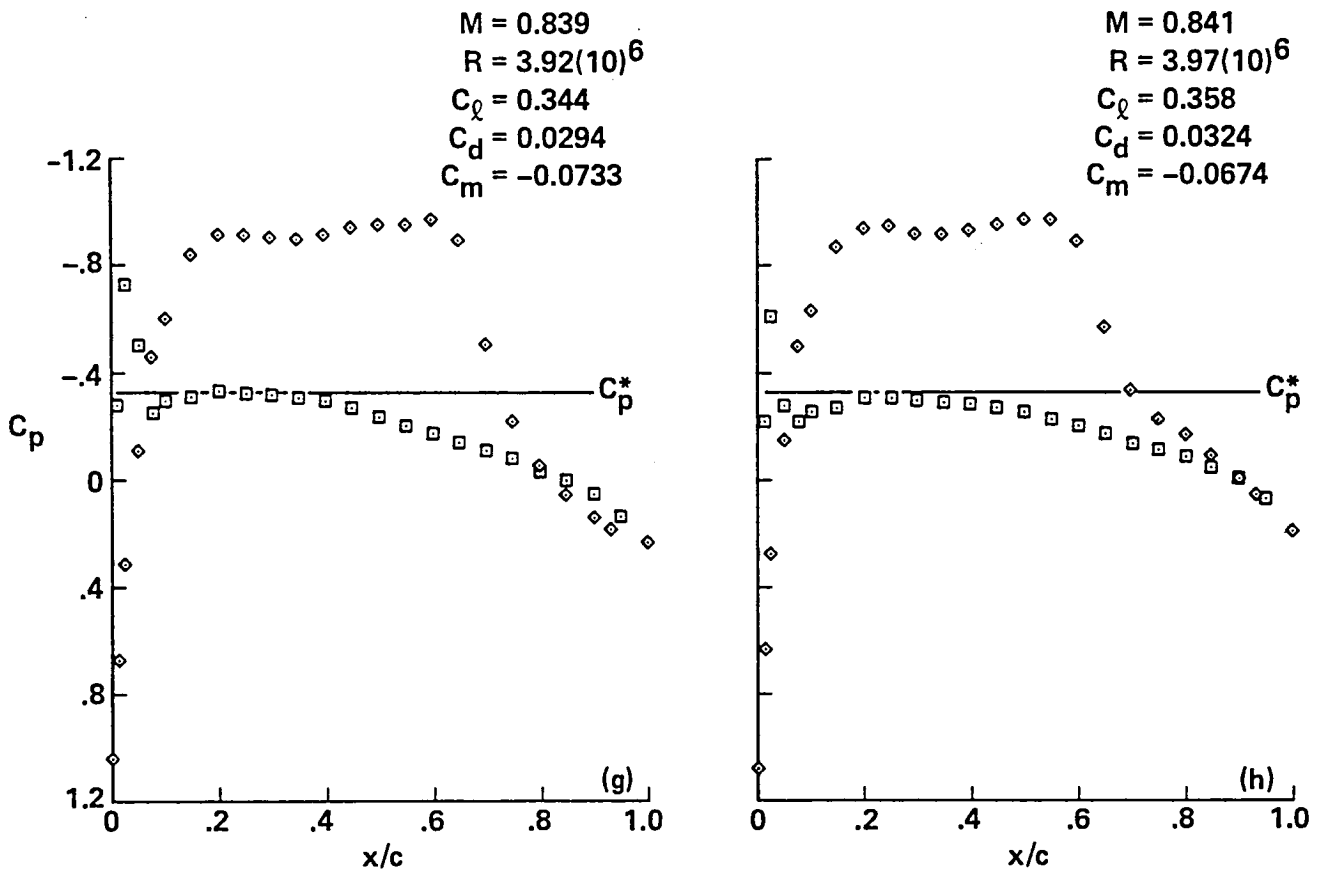


Figure 16.- Concluded.

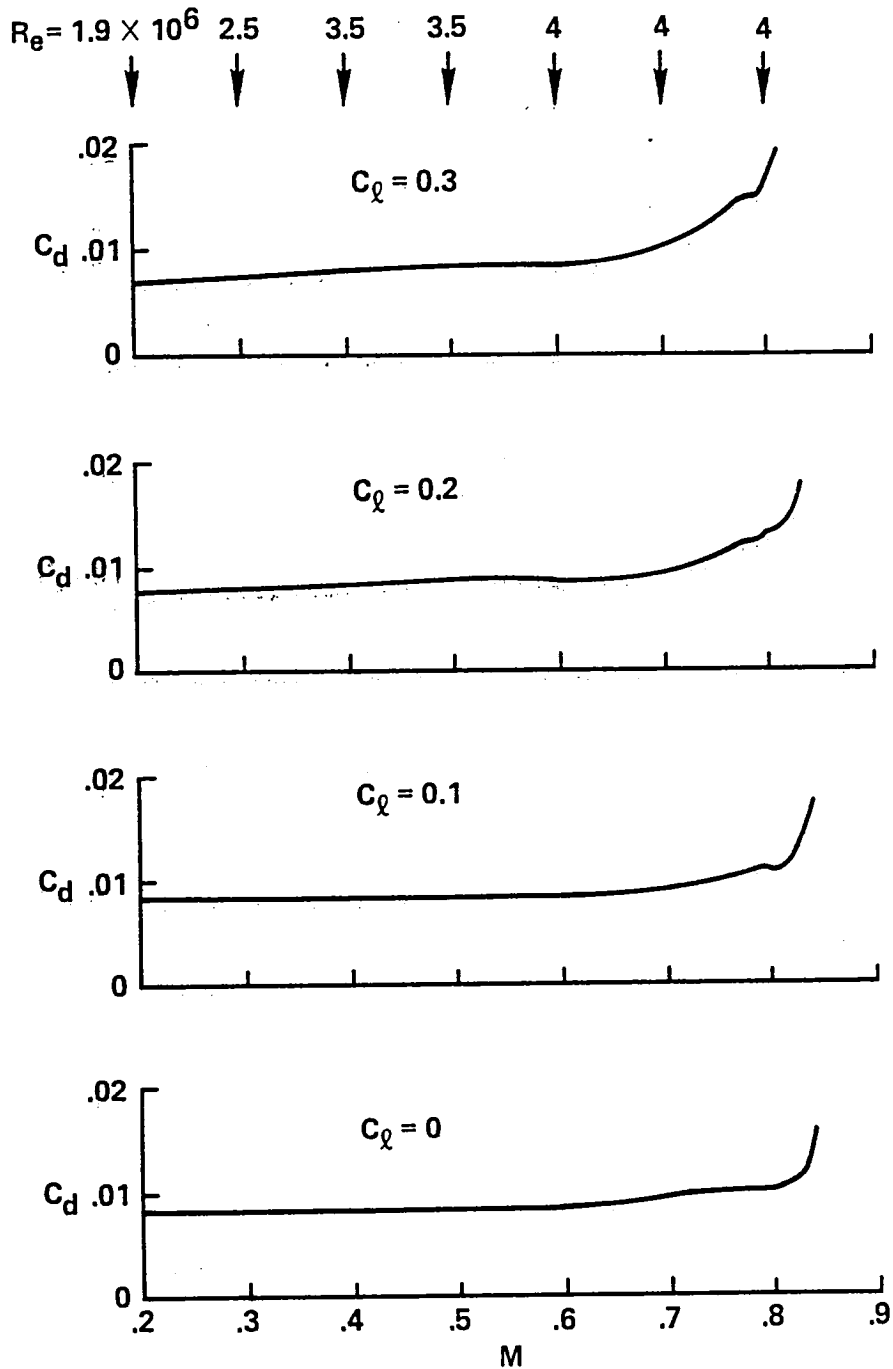


Figure 17.- Variation of section drag coefficient with Mach member for the A-1 airfoil, transition free.

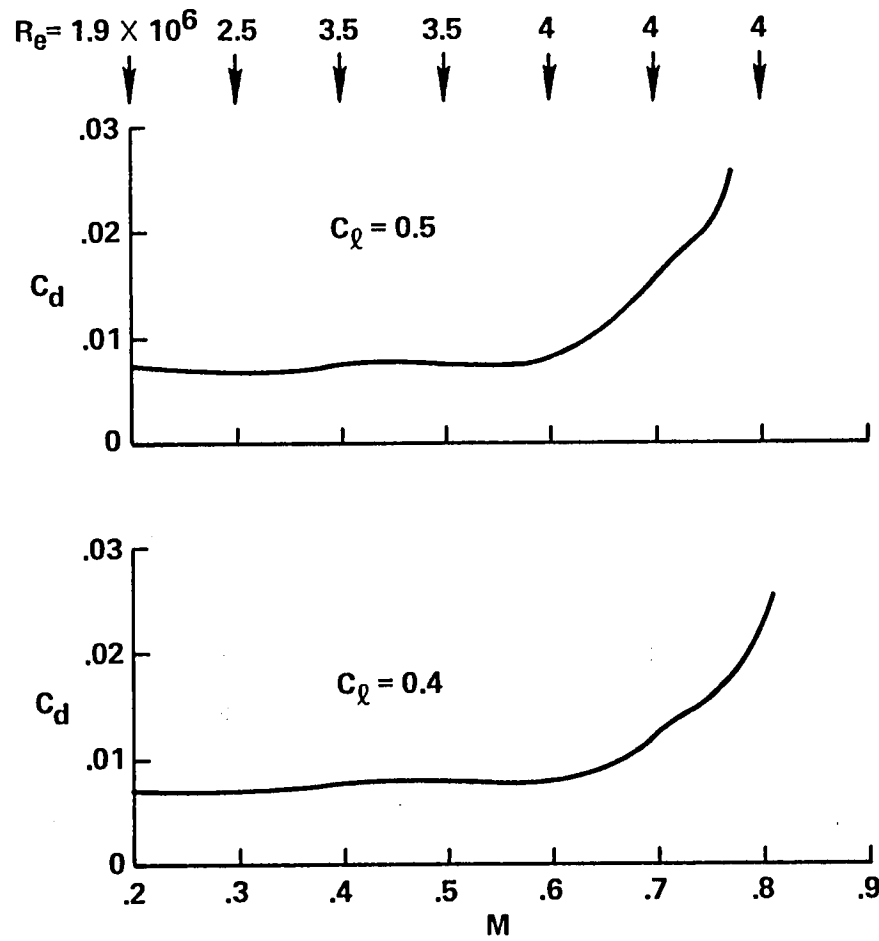


Figure 17.- Concluded.

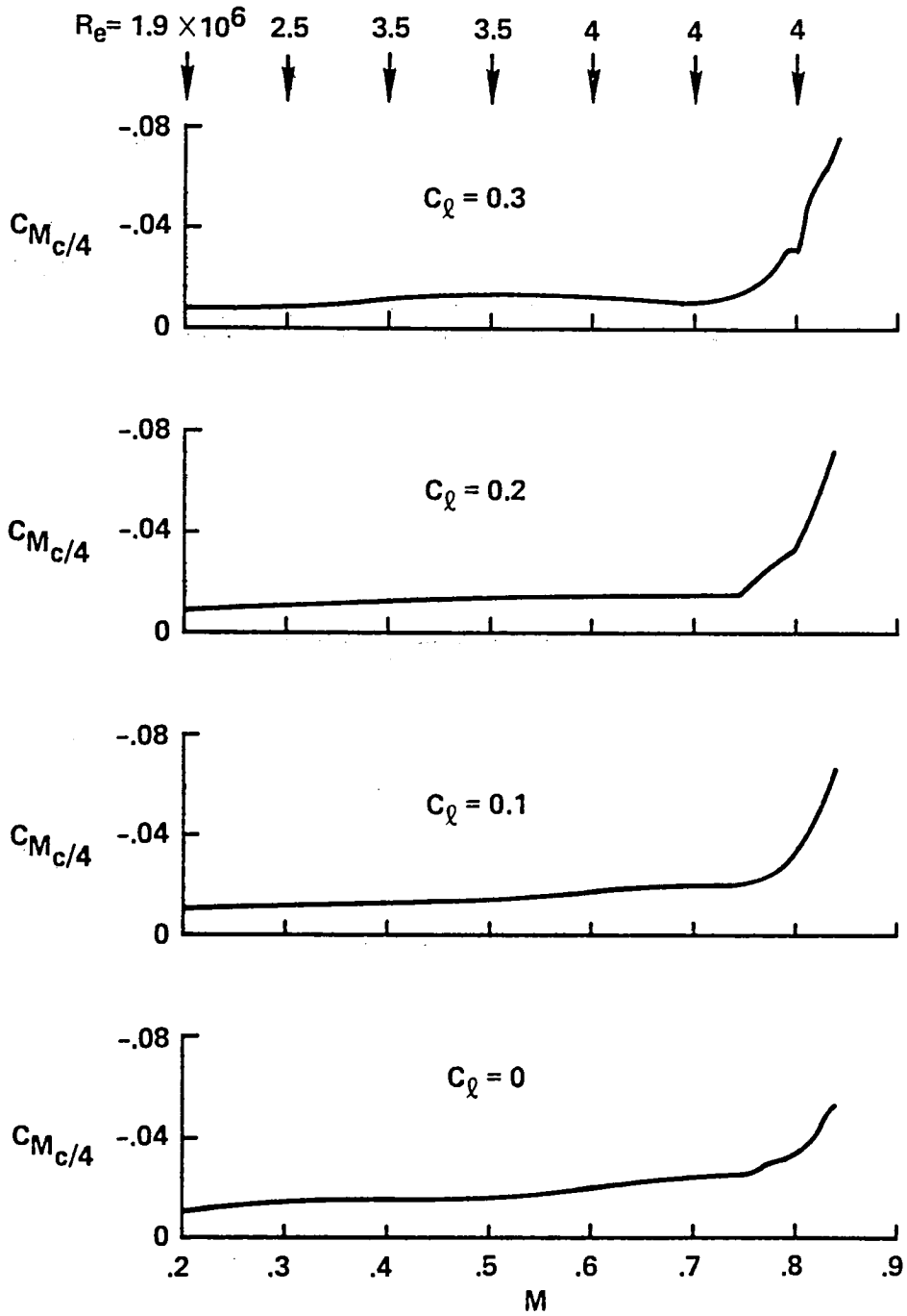


Figure 18.- Variation of section pitching-moment coefficient with Mach number for the A-1 airfoil, transition free.

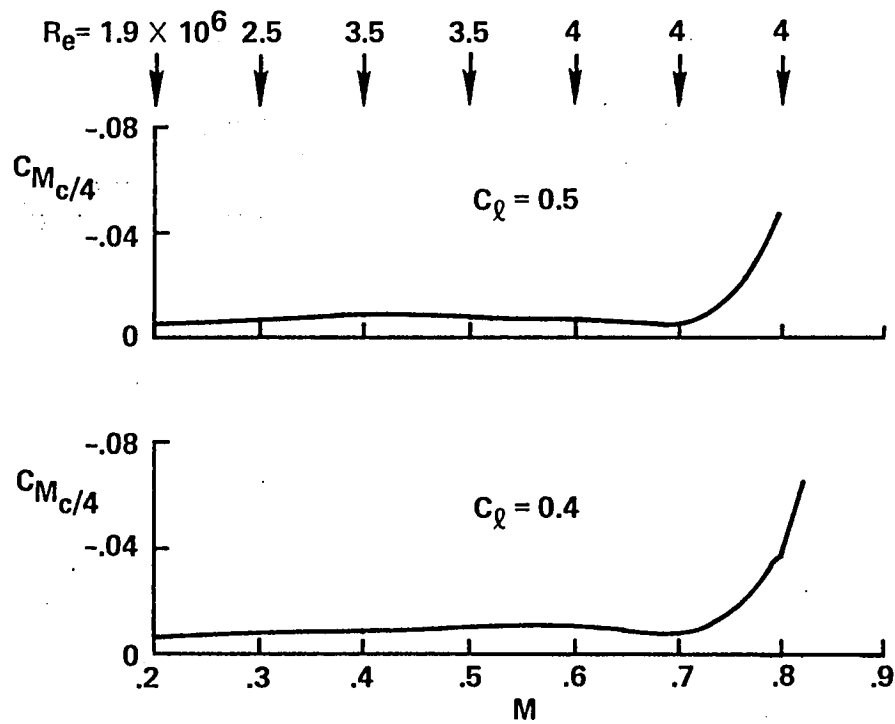


Figure 18.- Concluded.

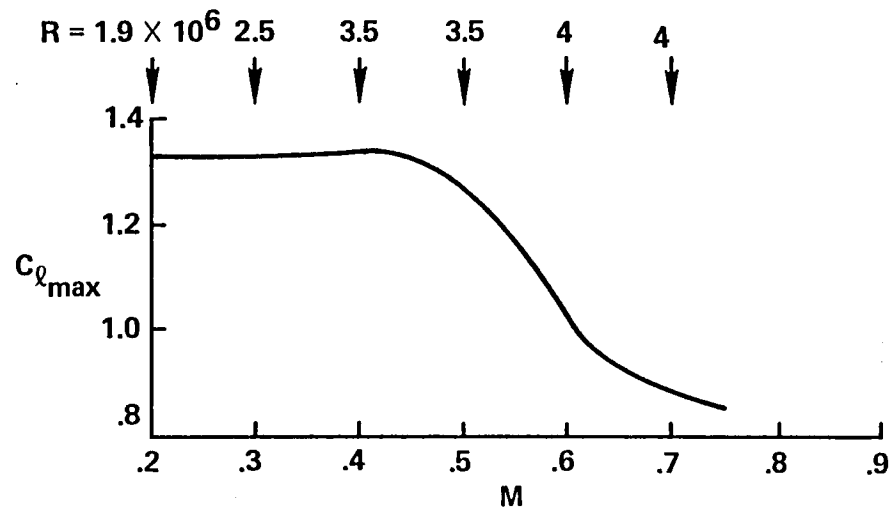
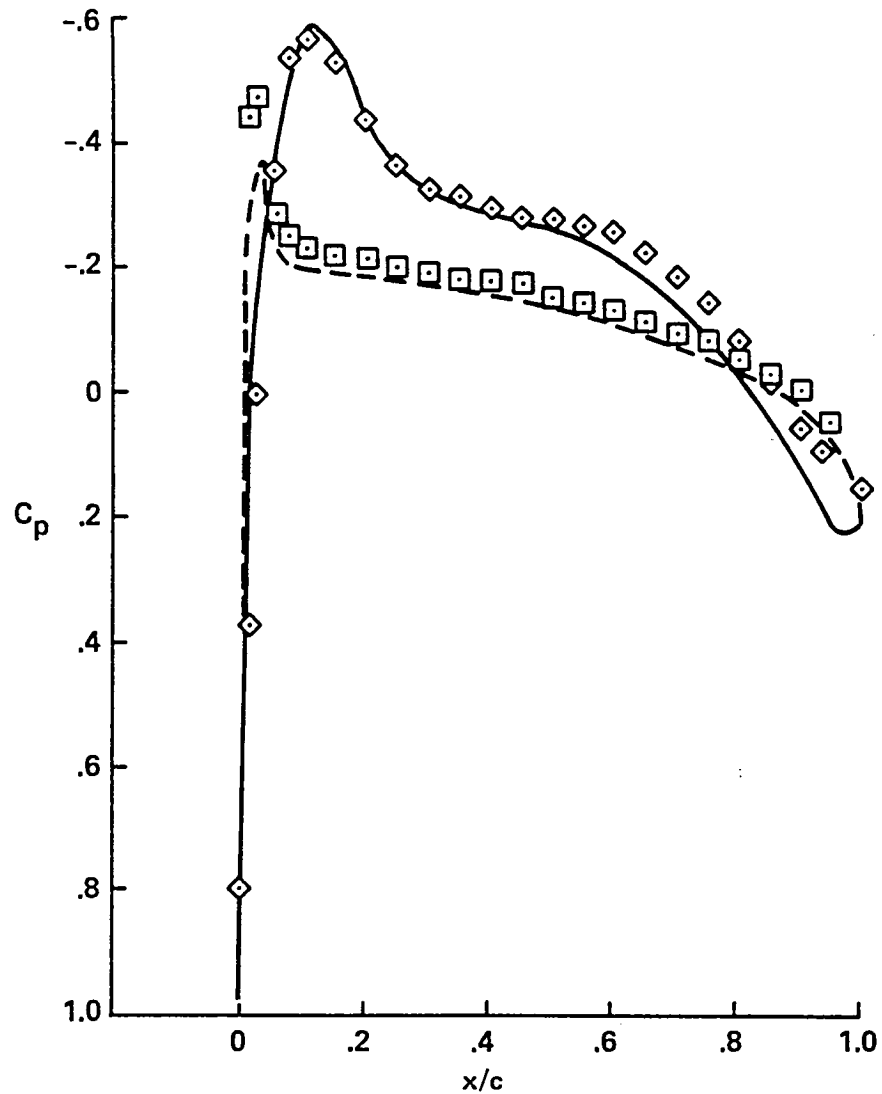


Figure 19.- Variation of section maximum-lift coefficient with Mach number for the A-1 airfoil, transition free.

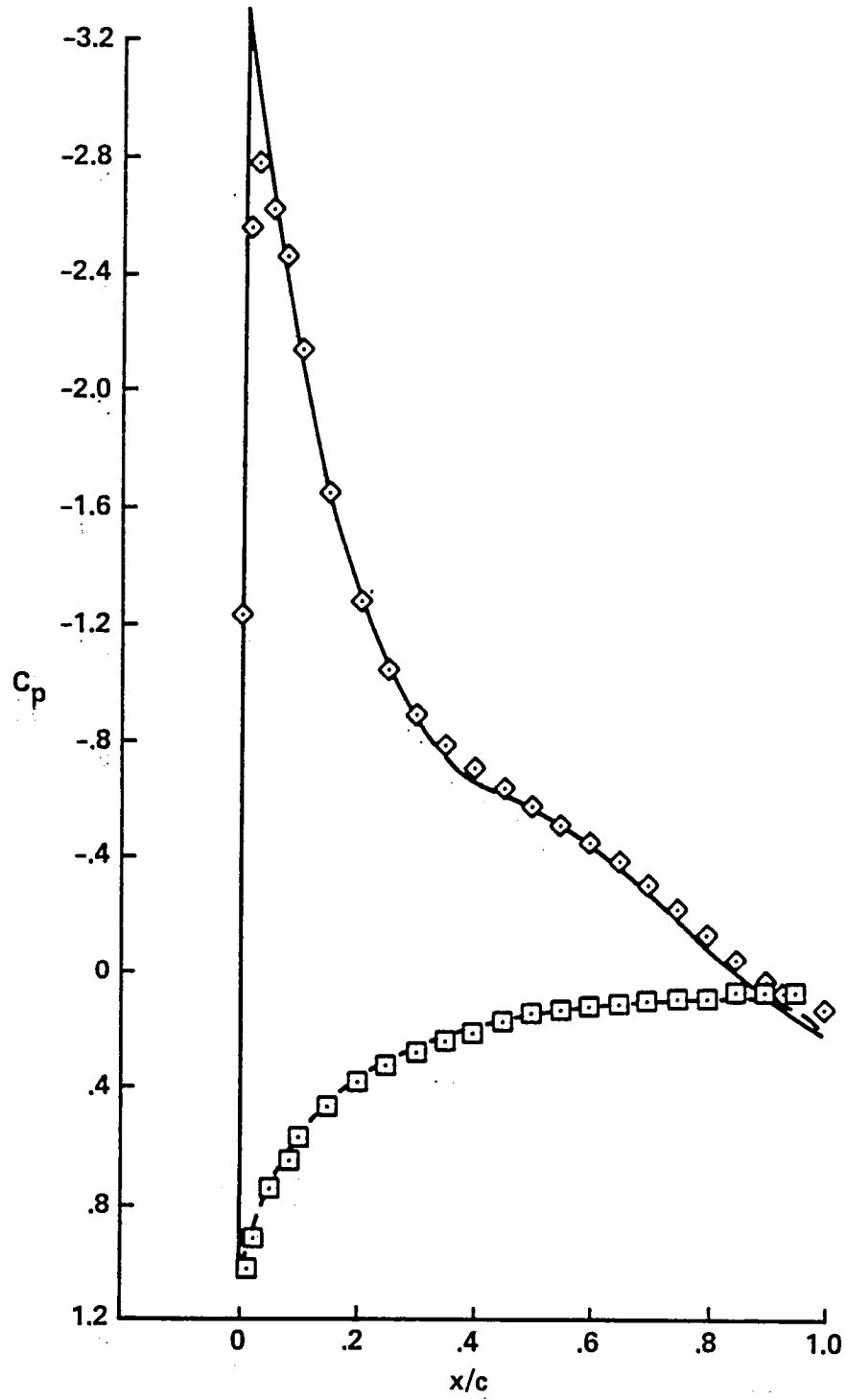
	C_l	C_d	C_m
— THEORY UPPER SURFACE			
- - - THEORY LOWER SURFACE	0.083	0.0091	0.0033
◇ EXPERIMENT UPPER SURFACE			
□ EXPERIMENT LOWER SURFACE	0.083	0.0086	-0.0106



(a) $M_{set} = 0.2$, $R = 1.88 \times 10^6$.

Figure 20.- Experiment-theory comparison A-1 airfoil.

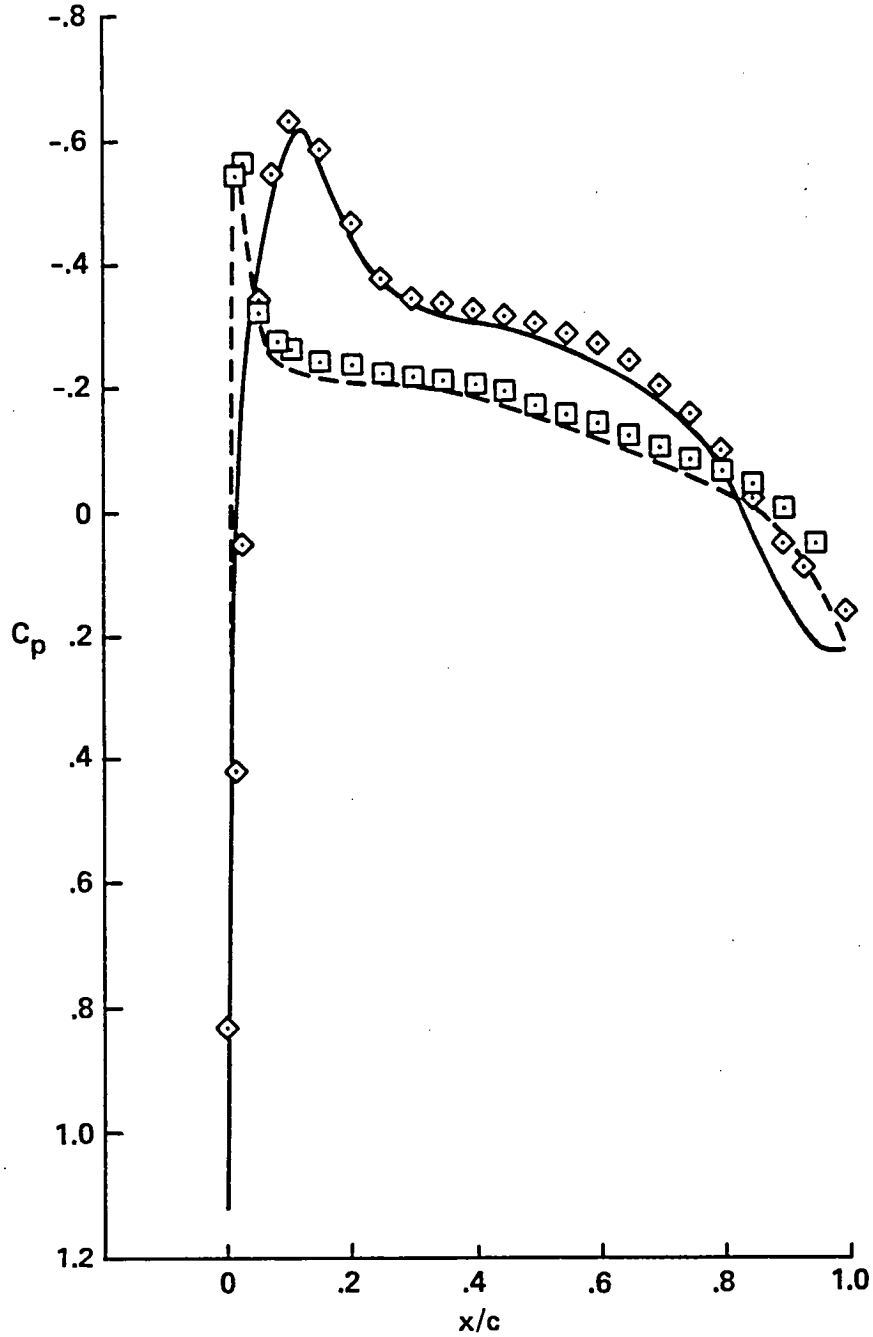
	C_l	C_d	C_m
— THEORY UPPER SURFACE			
- - - THEORY LOWER SURFACE	1.028	0.0120	0.0150
◇ EXPERIMENT UPPER SURFACE			
□ EXPERIMENT LOWER SURFACE	1.034	0.0118	-0.0027



(b) $M_{set} = 0.2$, $R = 1.87 \times 10^6$.

Figure 20.- Continued.

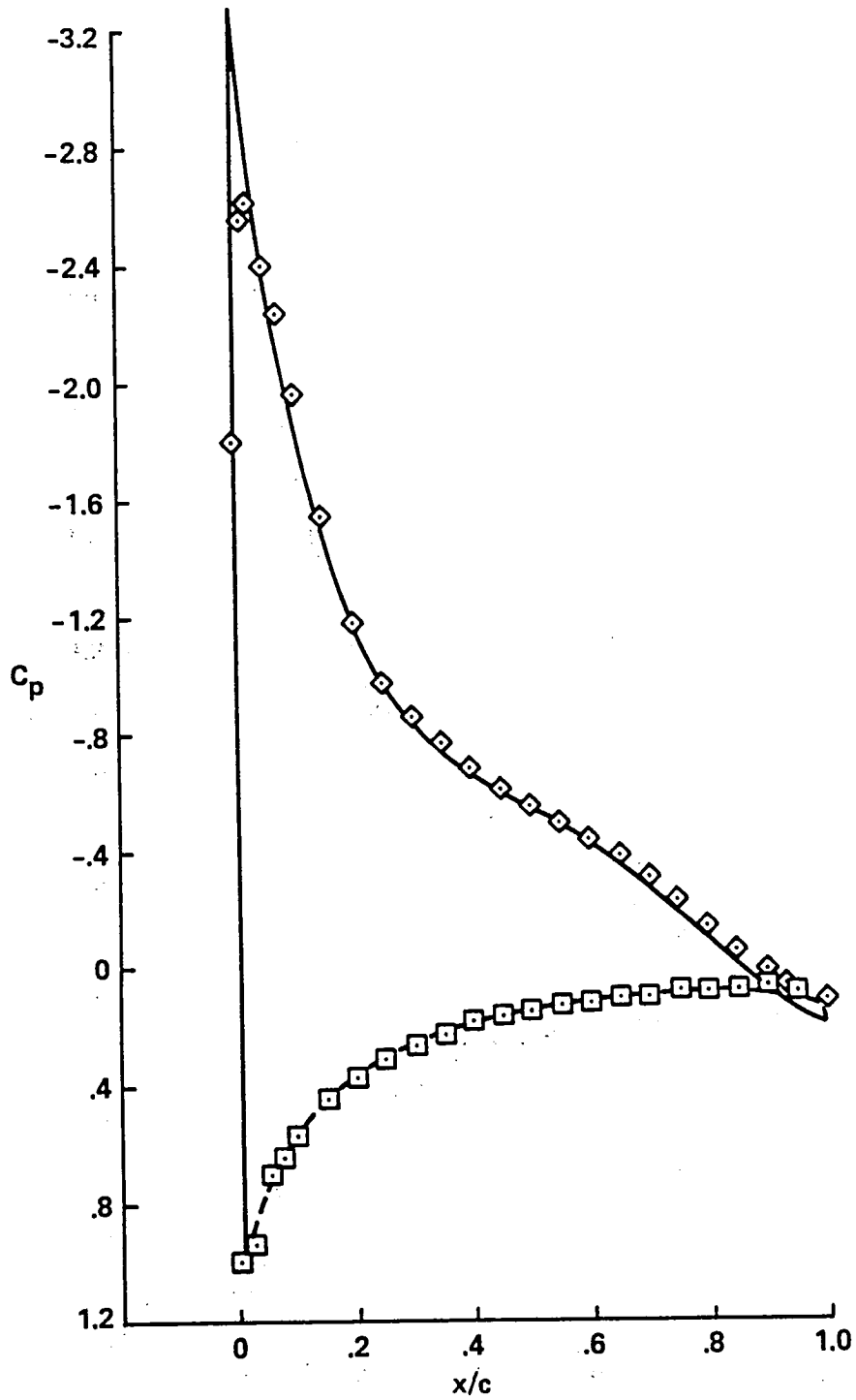
—	THEORY UPPER SURFACE	γ_l	γ_d	γ_m
- - -	THEORY LOWER SURFACE	0.083	0.0081	-0.0052
◇	EXPERIMENT UPPER SURFACE			
□	EXPERIMENT LOWER SURFACE	0.083	0.0087	-0.0134



(c) $M_{set} = 0.4$, $R = 3.49 \times 10^6$.

Figure 20.- Continued.

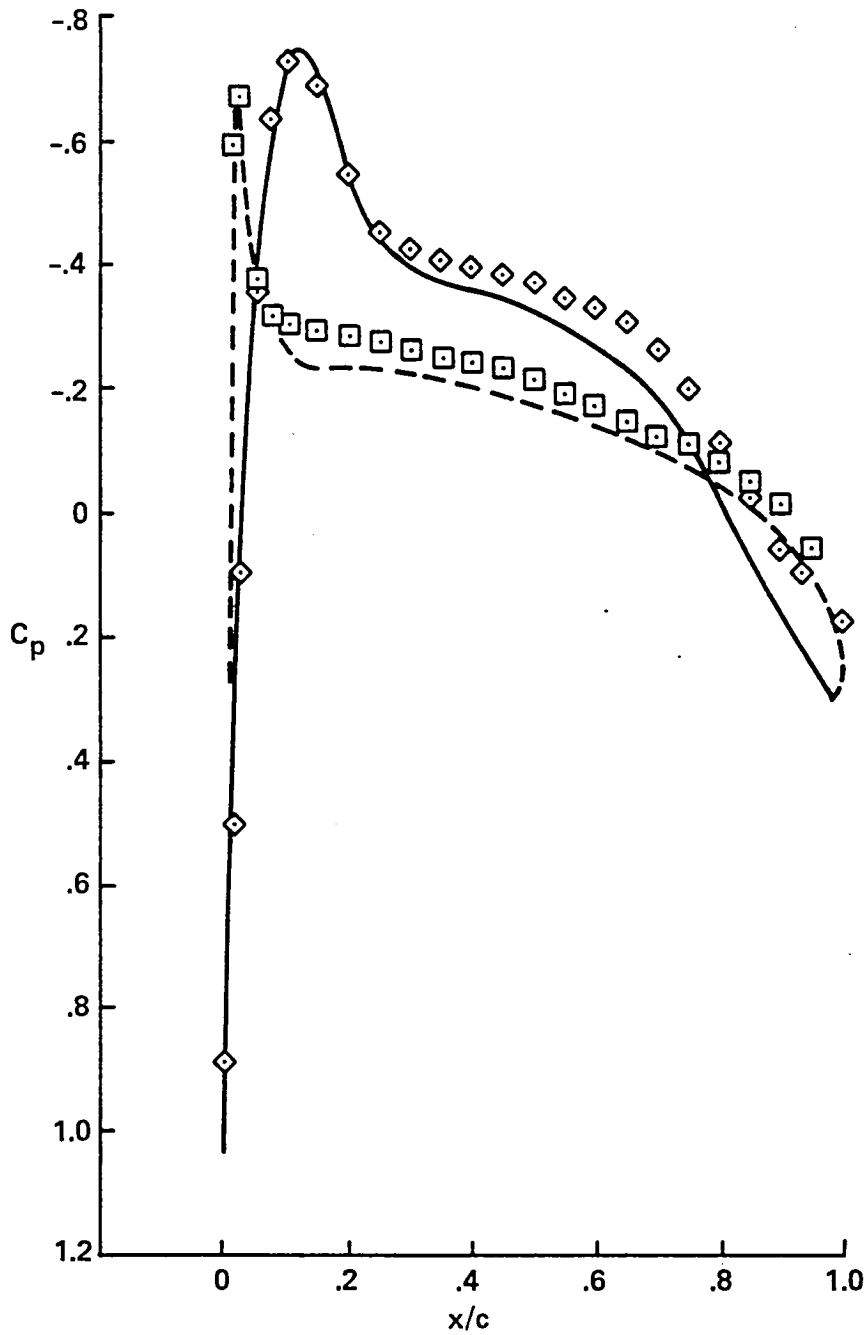
	C_l	C_d	C_m
— THEORY UPPER SURFACE			
- - - THEORY LOWER SURFACE	0.992	0.0106	0.0092
◇ EXPERIMENT UPPER SURFACE			
□ EXPERIMENT LOWER SURFACE	0.999	0.0122	-0.0083



(d) $M_{set} = 0.4$, $R = 3.47 \times 10^6$.

Figure 20.- Continued.

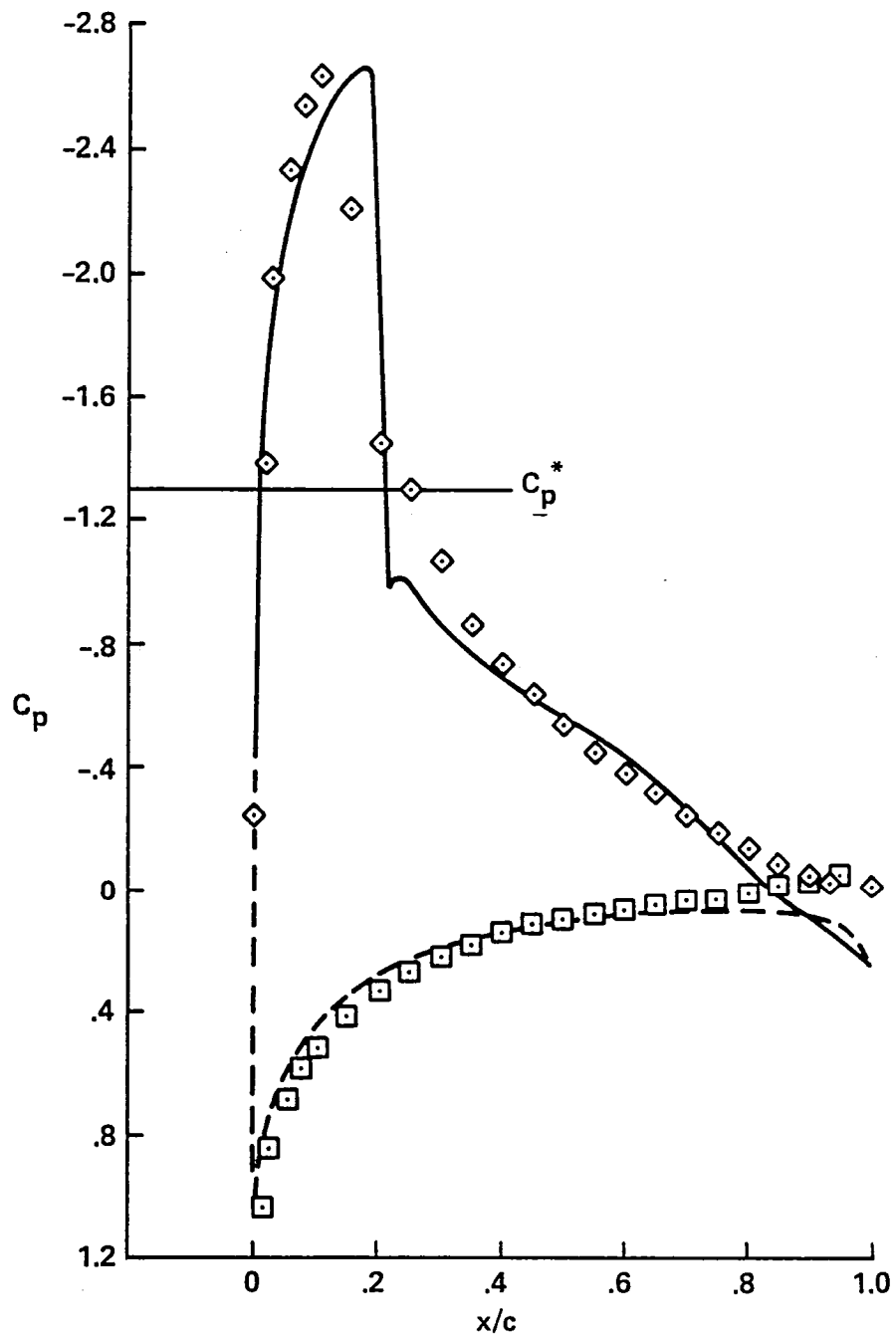
	C_l	C_d	C_m
— THEORY UPPER SURFACE			
- - - THEORY LOWER SURFACE	0.097	0.0089	0.0025
◇ EXPERIMENT UPPER SURFACE			
□ EXPERIMENT LOWER SURFACE	0.097	0.0086	-0.0164



(e) $M_{set} = 0.6$, $R = 4.00 \times 10^6$.

Figure 20.- Continued.

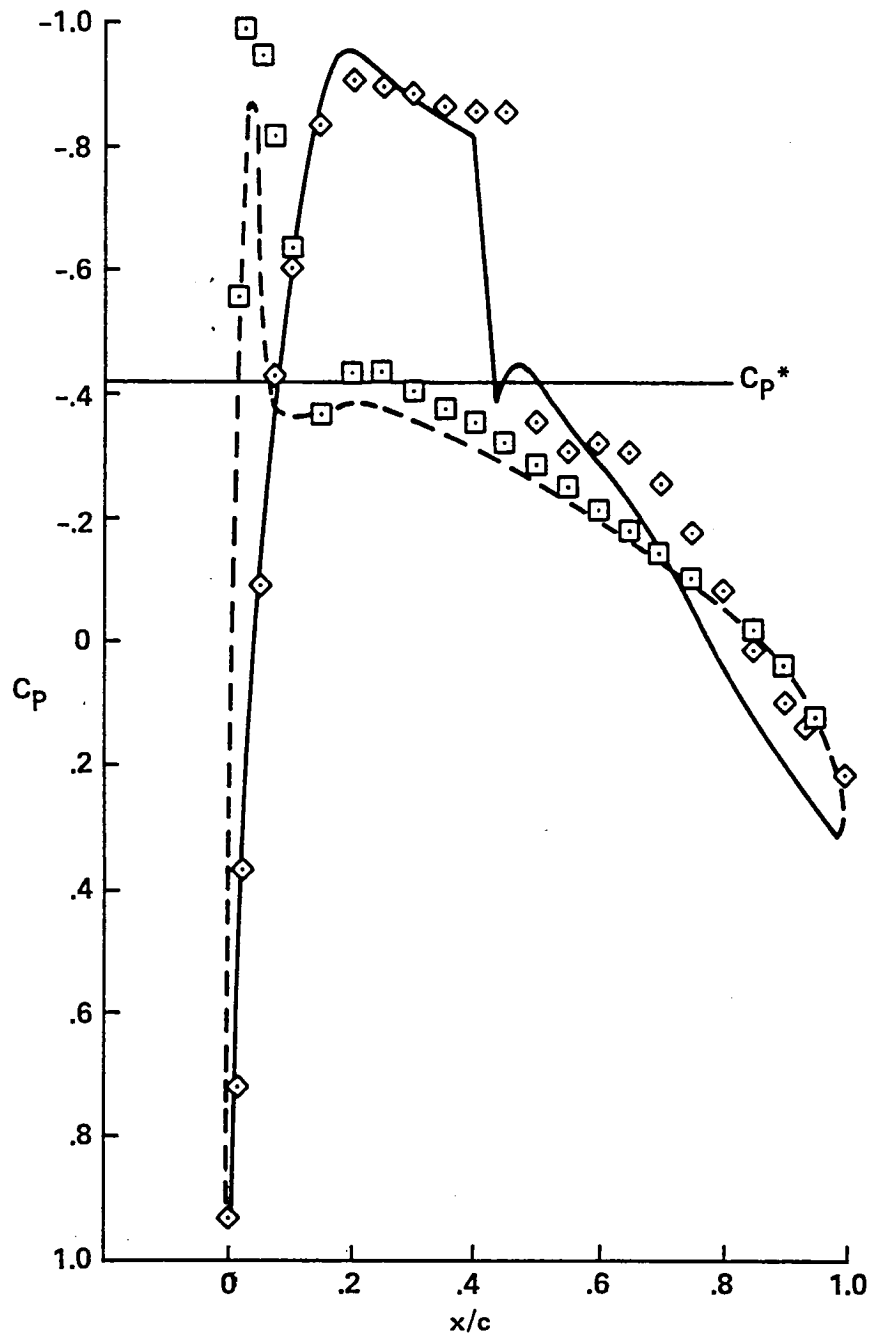
	C_l	C_d	C_m
— THEORY UPPER SURFACE			
- - - THEORY LOWER SURFACE	0.991	0.0196	0.0200
◇ EXPERIMENT UPPER SURFACE			
□ EXPERIMENT LOWER SURFACE	1.000	0.0596	0.0099



(f) $M_{set} = 0.6$, $R = 3.95 \times 10^6$.

Figure 20.- Continued.

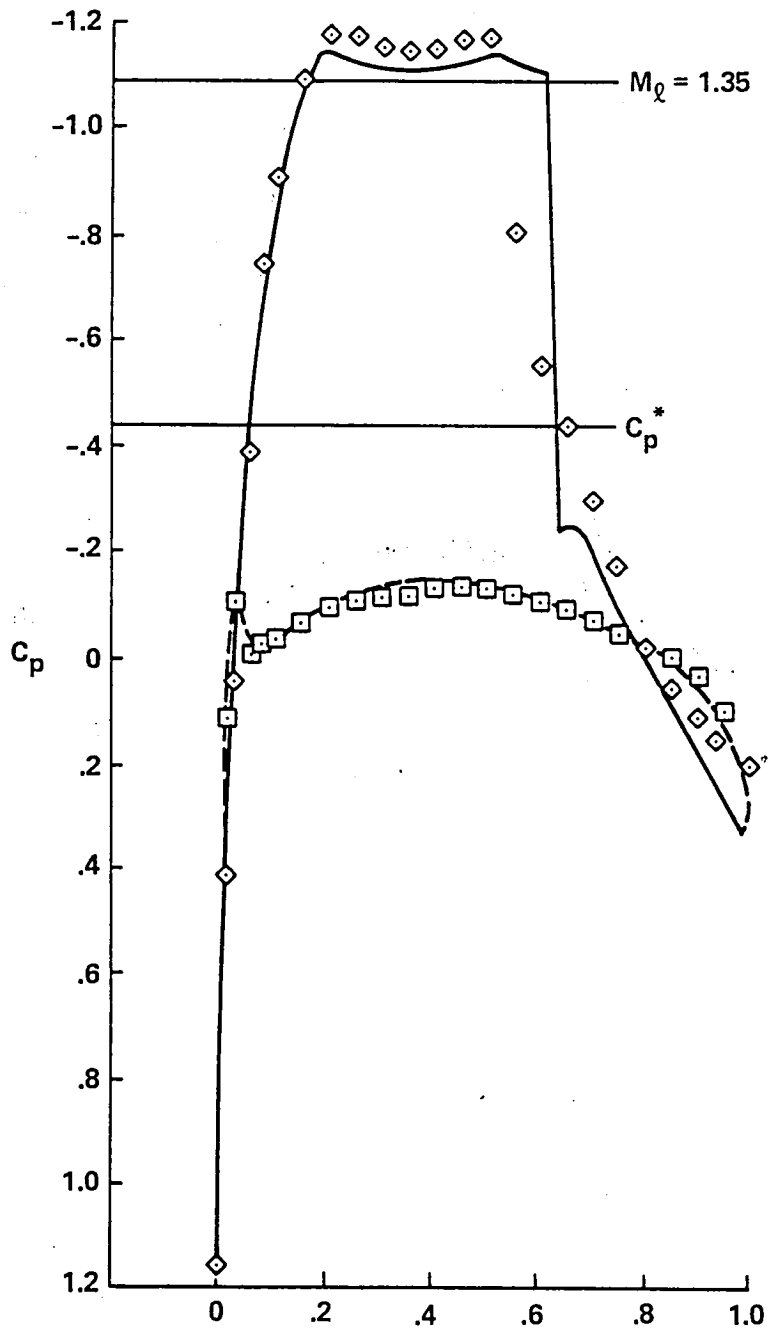
	C_l	C_d	C_m
— THEORY UPPER SURFACE			
- - - THEORY LOWER SURFACE	0.111	0.0128	0.0004
◇ EXPERIMENT UPPER SURFACE			
□ EXPERIMENT LOWER SURFACE	0.111	0.0111	-0.0333



(g) $M_{set} = 0.8$, $R = 3.99 \times 10^6$.

Figure 20.- Continued.

	C_l	C_d	C_m
— THEORY UPPER SURFACE			
- - - THEORY LOWER SURFACE	0.538	0.0326	-0.0453
◇ EXPERIMENT UPPER SURFACE			
□ EXPERIMENT LOWER SURFACE	0.549	0.0449	-0.0492



(h) $M_{set} = 0.800$, $R = 3.95 \times 10^6$.

Figure 20.- Concluded.

1. Report No. NASA TM-78622 AVRADCOM Tech. Rep. 79-44		2. Government Accession No.		3. Recipient's Catalog No.	
4. Title and Subtitle AN EXPERIMENTAL EVALUATION OF A HELICOPTER ROTOR SECTION DESIGNED BY NUMERICAL OPTIMIZATION				5. Report Date	
				6. Performing Organization Code	
7. Author(s) R. M. Hicks and W. J. McCroskey				8. Performing Organization Report No. A-7956	
9. Performing Organization Name and Address Ames Research Center, NASA, and AVRADCOM Research and Technology Laboratories Moffett Field, Calif. 94035				10. Work Unit No. 505-06-51-03-00	
				11. Contract or Grant No.	
12. Sponsoring Agency Name and Address National Aeronautics and Space Administration, Washington, D. C. 20546, and U.S. Army Aviation Research and Development Command, St. Louis, MO 93166				13. Type of Report and Period Covered Technical Memorandum	
				14. Sponsoring Agency Code	
15. Supplementary Notes					
16. Abstract A 10-percent thick helicopter rotor section designed by numerical optimization has been tested at Mach numbers from 0.2 to 0.84 with Reynolds numbers ranging from 1.9×10^6 at Mach 0.2 to 4×10^6 at Mach numbers above 0.5. The airfoil section exhibited maximum lift coefficients greater than 1.3 at Mach numbers below 0.45 and a drag divergence Mach number of 0.82 for lift coefficients near 0. A moderate "drag creep" was observed at low lift coefficients for Mach numbers greater than 0.6.					
17. Key Words (Suggested by Author(s)) Airfoil Helicopter Optimization			18. Distribution Statement Unlimited STAR Category - 02		
19. Security Classif. (of this report) Unclassified		20. Security Classif. (of this page) Unclassified		21. No. of Pages 131	22. Price* \$7.25

